Real-Time Ginzburg-Landau Theory for Bosonic Gases in Optical Lattices

Diploma Thesis
by
Tobias Daniel Graß

Main referee: Prof. Dr. Dr. h.c. mult. Hagen Kleinert

Submitted to the
Department of Physics
Freie Universität Berlin
November 2nd, 2009

Contents

1 Introduction

Since 2002 when for the first time a bosonic gas was loaded into an optical lattice [1], the interest in such systems of strongly correlated particles has immensely increased. The underlying physics is closely related to the phenomenon of superfluidity, which is a much older topic. Superfluidity was discovered in the 30s of the last century, as a property of cool ^{4}He liquids [2,3].

1.1 Helium II

Surely, one of the most curious phenomena in condensed matter physics is the behavior of ^{4}He at low temperature. Cooling it down at normal pressure, this noble gas becomes liquid only at temperatures below 6 K and never reaches a solid state, as shown in the phase diagram in Fig. 1.1(a). Instead, a more exciting phase transition takes place at a temperature about 2.2 K, which is directly observable: For temperatures above this critical value, the cold liquid looks like boiling water with the characteristic bubbles. These bubbles are due to a temperature gradient within the liquid which is caused by evaporative cooling at the surface of the liquid. As a consequence, the vapor pressure within the liquid is higher than at its surface, allowing for the formation of gas bubbles. At 2.2 K, the bubbles suddenly disappear and the liquid becomes completely calm. Evaporation still takes place, but in the new phase, called helium II, the thermal conductivity increases, allowing for an immediate heat balance and therefore a "bubblefree" evaporation only from the surface of the liquid.

Another astonishing feature can be observed, if one cools down ^{4}He in an open vessel: Against gravity a thin film of the fluid climbs up the wall of the vessel so that it flows out of it. This behavior comes along with a vanishing viscosity of the fluid. In 1938, P. Kapitza [2] as well as J. F. Allen and D. Misener [3] measured the viscosity of helium by observing the flow through thin capillaries. Below the critical temperature, the viscosity became suddenly very small, possibly zero. Therefore the name "superfluidity" was given to this new phase of helium.

An exciting effect due to this vanishing viscosity, is the so-called fountain effect or thermomechanical effect shown in Fig. 1.1(b): Heating helium II within a thin capillary which is in contact with a bath, causes a rise of the liquid within the capillary.

The first explanation for the phase transition undergone by cold helium was given in 1938 by F. London [6]. Only one decade earlier, S. N. Bose and A. Einstein had made the theoretical prediction of a new phase of matter, the so called Bose-Einstein condensation (BEC) [7,8]. Now London calculated the critical temperature T_c for the transition into the BEC-phase assuming an ideal gas of bosonic particles having the same density as liquid helium and the same particle mass as ^{4}He. His result, $T_c = 3.1$ K, agrees fairly well with the critical temperature of ^{4}He known from experiments, so London believed that BEC and the superfluid phenomena of ^{4}He are closely related.

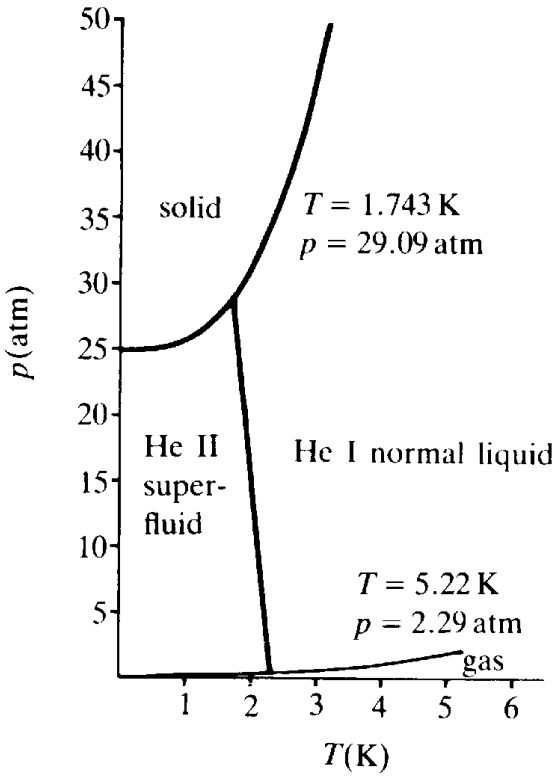

(a) Phase diagram of ^{4}He taken from [4].

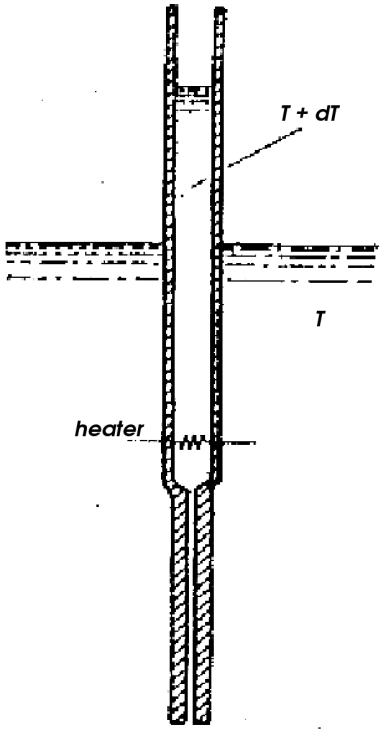

(b) Illustration of the thermomechanical effect, taken from [5].

Figure 1.1: At normal pressure, there is no solid state in the phase diagram of ^{4}He shown in (a). An interesting experiment with helium II is shown in (b): The liquid in the capillary rises when it is heated.

Shortly afterwards, L. Tisza proposed a two-fluid model [9], explaining hydrodynamic properties of superflow like the fountain effect. He therefore assumed a BE-condensed fraction of the liquid with no entropy and no viscosity and a normal fraction with finite entropy and finite viscosity. The effect shown in Fig. 1.1(b) can then be interpreted as the consequence of an osmotic pressure between the bath and the capillary. As the superfluid fraction within the capillary is destroyed by heat and the normal component has no chance to flow out of the thin capillary, the only way to equilibrate the concentration is by a flow of superfluid helium from the bath into the capillary.

The two-fluid model has been further confirmed by Andronikashvili's experiment done a few years later [10]. Instead of measuring the viscosity by the flow through a capillary, he observed the damping of a rotating disk within the liquid. What he found was a non-zero viscosity even in the superfluid phase confirming the idea of the two-fluid model: The damping is due to the normal component of the liquid which is supposed to have a finite viscosity. This experiment therefore allows for determining the temperature-dependent ratio of the normal density to the superfluid density. One result is that the whole liquid becomes superfluid if one approaches zero temperature. This does not agree with Penrose's prediction [11] of a BE-condensed fraction at $T = 0$, which is, due to interactions, less than 10% .

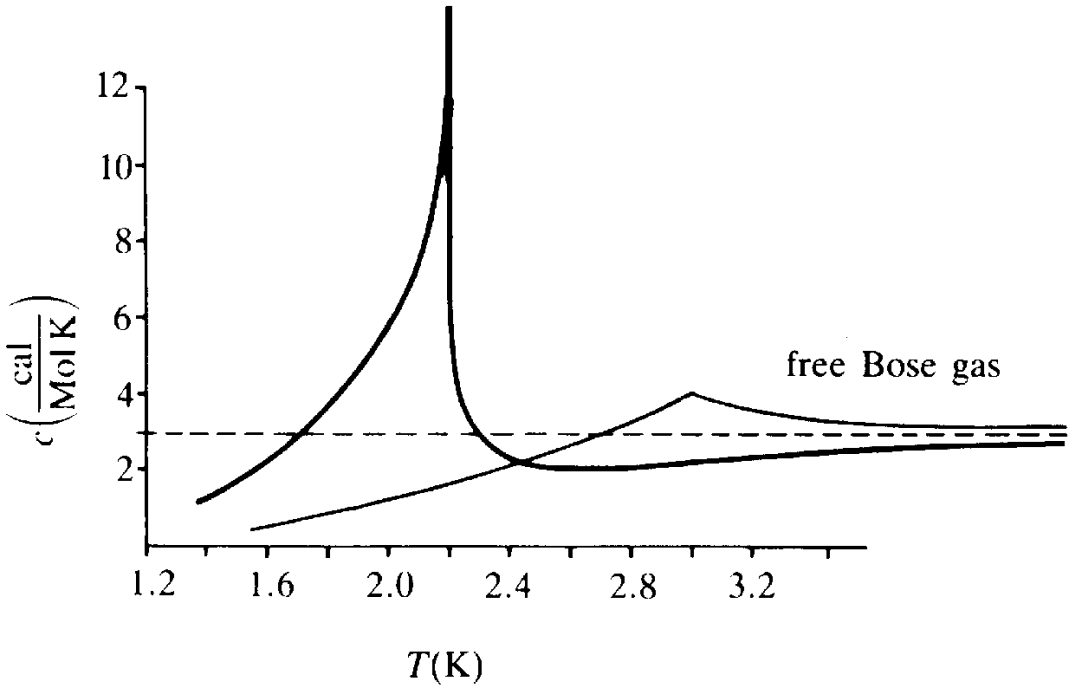

Figure 1.2: Specific heat of ^{4}He and of an ideal Bose gas with the same density and particle mass: λ-transition versus second-order phase transition. Taken from [4].

Neglecting interactions and treating a liquid as a non-interacting gas, however, did not allow for explaining all the properties of helium II. Comparing the specific heat curves of an ideal Bose gas and ^{4}He, both shown in Fig. 1.2, we can find two main differences:

- The transition from the normal helium I to the superfluid helium II shows an ostentatious logarithmic divergence resembling the Greek letter λ. Therefore it is referred to as the λ-transition. The specific heat of the ideal Bose gas, however, is finite at the critical point. This indicates that for a proper comprehension of the phase transition, interactions cannot be neglected. Strong-coupling field theory considering a Φ^4-interaction is able to give a precise explanation of the measured specific heat curve near the transition point. The universal critical exponents which have been measured with high precision by space shuttle experiments [12] agree best with the field-theoretic predictions in Refs. [13,14].

- A second difference in the specific heat of an ideal Bose gas and ^{4}He, respectively, concerns the region where the temperature approaches zero. While the specific heat of helium is proportional to T^3, like the specific heat of a solid at low temperature, the ideal gas heat obeys a different power law, being proportional to $T^{3/2}$.

In order to circumvent this latter inconsistency, L. Landau proposed another description of superfluidity [15,16]. Instead of considering the condensation of free particles into the ground-state, he assumed that helium II was made up of condensed atoms and excitations. For the latter, he postulated a dispersion relation as shown in Fig. 1.3: The energetically lowest excitations have a quasi-particle-like

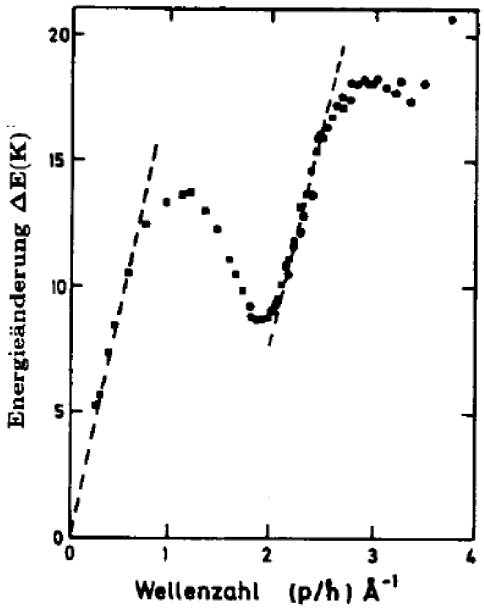

Figure 1.3: The excitation spectrum of helium II, measured via neutron scattering, confirms Landau's prediction of phonons and rotons. Taken from [17].

character like the acoustic phonons of a solid:

$$\epsilon_{\mathrm{ph}}(\boldsymbol{p}) = c|\boldsymbol{p}|, \tag{1.1}$$

where the energy ϵ_{ph} of these excitations is related to their momentum $\boldsymbol{p}$ by their velocity c. Such a dispersion relation explains the solid-like T^3-dependence of the specific heat for $T \to 0$. But other than a solid, a liquid is not expected to sustain transversal optical modes, therefore the degrees of freedom must be exhausted with other excitations. Landau postulated their dispersion relation as

$$\epsilon_{\mathrm{r}}(\boldsymbol{p}) = \Delta + \frac{\boldsymbol{p}^2}{2m}, \tag{1.2}$$

where Δ is an energy gap and m the effective mass of the excitations. These excitations are called rotons as they are considered to be the quanta of vortex motion. Both, phonons and rotons are bosonic.

What is crucial about this dispersion relation is the fact that it always has a finite group velocity $\epsilon/|\boldsymbol{p}|$. Frictionless flow can then be understood from the energy balance. Let us therefore consider superfluid helium at $T = 0$ flowing through a tube from two different reference frames. In the laboratory frame where the tube does not move all atoms flow frictionless with a velocity $\boldsymbol{v}$, each of them having the momentum $\boldsymbol{q}$. The total momentum is $\boldsymbol{Q}_0 = \sum_i \boldsymbol{q}_i$, the total energy of the system is E_0. In the rest frame of the liquid, each atom has the momentum $\boldsymbol{q}' = \boldsymbol{0}$, i.e. $\boldsymbol{Q}_0' = \boldsymbol{0}$. The total energy E_0' is related to the energy in the laboratory frame by the Galilei transform [17]:

$$E_0' = E_0 + \boldsymbol{Q}_0' \cdot \boldsymbol{v} - \frac{1}{2}M\boldsymbol{v}^2, \tag{1.3}$$

where M is the total mass. If there is friction between the wall and the liquid, there should be excitations "moving" with the wall, i.e. the total momentum in the rest frame of the liquid is non-zero, say $\boldsymbol{Q}' = \boldsymbol{p}$ for an excitation with momentum $\boldsymbol{p}$. The total energy in the rest frame of the liquid now is increased by the energy $\epsilon(\boldsymbol{p})$ of the excitation: $E' = E_0' + \epsilon(\boldsymbol{p})$. From the laboratory frame, the total energy therefore reads, according to Eq. (1.3):

$$E = E' - \boldsymbol{Q}' \cdot \boldsymbol{v} + \frac{1}{2} M \boldsymbol{v}^2 = E_0 + \epsilon(\boldsymbol{p}) - \boldsymbol{p} \cdot \boldsymbol{v}. \tag{1.4}$$

This means that the energy difference associated with an excitation is $\Delta E = E - E_0 = \epsilon(\boldsymbol{p}) - \boldsymbol{p} \cdot \boldsymbol{v}$. To be energetically favorable, i.e. $\Delta E < 0$, the excitations must fulfill the condition:

$$\frac{\epsilon(\boldsymbol{p})}{|\boldsymbol{p}|} < |\boldsymbol{v}|. \tag{1.5}$$

Because a dispersion relation like the one shown in Fig. 1.3 has the property that $\frac{\epsilon(\boldsymbol{p})}{|\boldsymbol{p}|}$ is finite for any $\boldsymbol{p}$, there exists a critical velocity $\boldsymbol{v}_\mathrm{c}$ up to which excitations are energetically unfavored and the liquid therefore flows frictionless. So Landau's theory does not only explain superfluidity from the excitation spectrum, but also predicts a critical velocity at which superfluidity breaks down. And indeed, such a critical velocity could be observed in experiments, but it turned out to be much smaller that the one predicted by Landau [18]. This deviation is due to turbulences which have not been considered in our argumentation.

The above explanation was restricted to $T = 0$, because only excitations from the ground-state are considered. But the idea can be generalized to finite temperatures by applying a two-fluid model. Other than in Tisza's model, where both the superfluid and the normal component are particle-like, Landau's model assumes a quasi-particle behavior of the normal component. This seemed to disagree with London's and Tisza's point of view relating superfluidity to BEC, but the discrepancy was solved in 1947 by N. N. Bogoliubov who gave the microscopic arguments for Landau's dispersion relation. He calculated the excitation spectrum for weakly interacting Bose gases [19] and showed that

- the depletion of the ground state can be neglected, allowing for BEC even in non-ideal gases,
- the excitations can be described by a phonon dispersion.

In this way Bogoliubov's calculation reconciles the two different points of view. The assumption of weak interaction, however, hinders a good quantitative agreement of Bogoliubov's theory with the strong interacting helium. Weakly interacting Bose gases have only been condensed since 1995 [20,21]. We will therefore further discuss Bogoliubov's theory at a later stage in this thesis.

What we have seen in this section is the important role that dispersion relations play for the understanding of superfluidity. In the following section we will shortly sketch how an experiment may test the theoretic prediction.

1.2 Bragg Spectroscopy

The dispersion relation of helium II postulated by Landau and predicted by Bogoliubov had been confirmed experimentally by neutron scattering [22]. A more precise technique which was recently

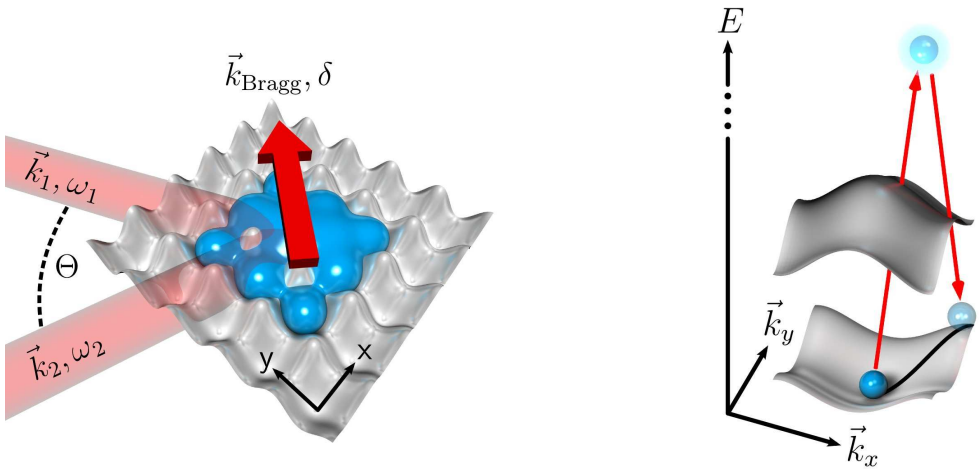

(a) (b)

Figure 1.4: The picture is taken from Ref. [25] explaining Bragg spectroscopy with bosons in an optical lattice. The two-photon transition (b) is induced by two laser beams shining on the probe (a). The angle θ between the beams and the energy difference $\hbar(\omega_1 - \omega_2)$ allow for measuring the band structure of the system.

applied to BEC [23,24] and also Bose gases in optical lattices [25,26] is Bragg spectroscopy.

It is based on a two-photon transition which is induced by two laser beams as shown in Fig. 1.4(a): The photon of one beam is absorbed and excites the system from the initial state (= the ground state) to an intermediate state. A second photon from the other beam stimulates the transition to the final state. The energy and momentum related to this excited state is known from the experimental parameters defining the lasers: their wave vectors $\boldsymbol{k}_1$ and $\boldsymbol{k}_2$ as well as their frequencies ω_1 and ω_2.

The momentum transfer of the Bragg process is $\hbar\boldsymbol{k}_{\text{Bragg}} = \hbar(\boldsymbol{k}_1 - \boldsymbol{k}_2)$. For $|\boldsymbol{k}_1| \approx |\boldsymbol{k}_2| = k$, the transferred momentum can be freely tuned by the laser angle θ:

$$\hbar\boldsymbol{k}_{\text{Bragg}} \approx 2\hbar k \sin\left(\frac{\theta}{2}\right)\left(\frac{\boldsymbol{k}_1}{|\boldsymbol{k}_1|} - \frac{\boldsymbol{k}_2}{|\boldsymbol{k}_2|}\right). \tag{1.6}$$

Thus, by varying the angle the whole Brillouin zone can be reached.

The energy balance ϵ of the two-photon process is given by the frequencies: $\epsilon = \hbar(\omega_1 - \omega_2)$. It therefore can be tuned independently from the momentum transfer by modifying one laser frequency. For a given momentum, the whole energy range can be scanned.

What is measured, is the response of the system to a given configuration, i.e. whether transitions take place or not. The probability of a Bragg process is basically given by the static structure factor $S_{\boldsymbol{k}}$ [27], which is the Fourier transform of the density correlation:

$$S_{\boldsymbol{k}} \sim \langle 0|\hat{\rho}^\dagger(\boldsymbol{k})\hat{\rho}(\boldsymbol{k})|0\rangle, \tag{1.7}$$

where $\langle 0| \cdot |0\rangle$ denotes the ground-state expectation value and $\hat{\rho}(\boldsymbol{k})$ is the Fourier transform of the density. The transitions rate $\Gamma_{\boldsymbol{k}}(\omega)$ is proportional to the dynamic structure factor $S_{\boldsymbol{k}}(\omega) = S_{\boldsymbol{k}}\delta(\hbar\omega - \epsilon_{\boldsymbol{k}})$. The peaks of this function determine the excitation spectra. The heights of the peaks are related

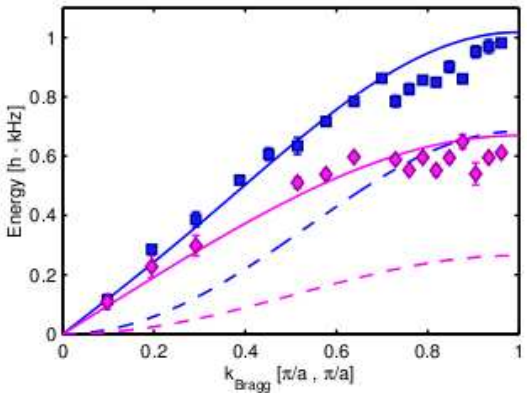

Figure 1.5: Excitation spectra of about 150.000 harmonically trapped ^{87}Rb atoms within a cubic optical lattice. The lattice depth is 7 E_{R} for the blue curve and 11 E_{R} for the purple curve. The dashed lines with the quadratic shape for small k show the single-particle band structure. The solid lines with the linear shape show the results of a Bogoliubov calculation. Obviously, the single-particle band structure does not describe well the excitations of the system. The Bogoliubov band structure, however, is quite good and fails only at the edges of the Brillouin zone.

to the spectral weights of each excitation.

All experiments [23–26] confirm the linear shape of the superfluid dispersion relation for small k. As an example Fig. 1.5 shows the recent results of Ref. [25] for a ^{87}Rb gas in a cubic optical lattice. Bosonic gases in such lattices are the topic of the present thesis which is outlined in the next section.

1.3 Outline of the Thesis

The linear dispersion relation of helium II has turned out to be crucial for the understanding of its superfluid property. In the following we want to have a close look at another system which undergoes a transition into a superfluid phase, namely bosonic atoms in optical lattices, i.e. in periodic potentials created by laser beams. The experimental data cited in the previous section suggests that a similar dispersion relation characterizes such systems. Understanding these excitation spectra theoretically might allow for interpreting them as a trademark of superfluidity. Many theories for this problem, however, are hindered by the fact that they are either good in the superfluid phase as, for instance, the weak-coupling Bogoliubov approach in Ref. [28], or in the opposite regime of an insulating system, which can be well described by a strong-coupling theory as in Ref. [29]. The goal of this thesis is to derive a theory which produces good results on both sides of the phase transition, where special attention is directed on the spectra of the system.

Common to most theoretical approaches is the Bose-Hubbard Hamiltonian, which we therefore introduce only briefly in Section 2.1. We will discuss its validity for our problem at finite temperatures and put some detail on the derivation of a useful formula for the hopping parameter.

As a guideline for our further approach, we will pick the Ginzburg-Landau theory of phase transitions in Section 2.2. One important ingredient of this theory is the spontaneous symmetry breaking discussed in Section 2.3. Then the goal will be to find an appropriate Ginzburg-Landau functional describing this effect. The proper candidate is the effective action of the system. But we will reach this only in

Chapter 6, because a lot of groundwork has to be done before.

For the prediction of excitation spectra, the dynamics of the system plays an important role, so in the first section of Chapter 3 we will introduce the quantum-mechanical time evolution. Since the effective action is the Legendre transform of the generating functional of the cumulants, which on its part is the logarithm of the generating functional of the Green's functions, we dedicate the rest of this chapter to a presentation of different Green's function formalisms. It is possible to define real-time Green's functions at zero temperature or to rotate the problem to imaginary times, which allows for a description at finite temperature, but real-time information is no longer directly accessible. After discussing both methods shortly in Sections 3.2 and 3.3, we will therefore introduce a third Green's function formalism, the so-called closed-time-contour formalism, with which we can treat the real-time problem at finite temperature. Since this will be the formalism of our choice, it will be presented in more details, and important conventions for the following chapters are made in Sections 3.4 and 3.5.

As the Hamiltonian is not exactly solvable, we have to rely on perturbation theory. In Chapter 4 we will see how the perturbative expansion works for the generating functional of the cumulants. Its peculiarity consists in treating the symmetry-breaking source terms and the kinetic part of the Hamiltonian as a perturbation. The expansion with respect to the currents may yield a functional of the typical Ginzburg-Landau form. The hopping expansion is on the one hand obvious for practical reasons, since it reduces the unperturbed part of the Hamiltonian to a simply solvable problem. On the other hand, we have good physical reasons to consider the kinetic part as a perturbation, since we know from Quantum Monte Carlo data [30] that it is small compared to the interactions in the interesting regime, where the phase transition takes place. We will furthermore argue with dimensional scaling properties of the Hamiltonian, due to which a hopping expansion solves the problem exactly in infinite dimensions. Applying the linked-cluster theorem discussed in Section 4.3, we are then able to find diagrammatic rules for our series expansion in Section 4.5. To get the desired Ginzburg-Landau functional, we would have to truncate the series in the fourth order of the source terms. But since the closed-time-contour formalism doubles the time degrees of freedom, they grow exponentially in higher-orders of our perturbation theory, and therefore we will write down the expansion only up to the second order in the currents in Section 4.6. This restricts the validity of this functional to the insulating phase, but after having seen, how to perform the Legendre transformation of this functional in Chapter 5, we will be well prepared to repeat the procedure up to the desired fourth order in Chapter 6.

One main ingredient of the Legendre transform is a resummation of the Green's functions, which we will discuss in Section 5.3. Here we will find that, although the perturbative part of the Hamiltonian has entered the expansion only in first order, some higher-order diagrams are taken into account, when we consider the effective action.

The fourth-order expansion in Chapter 6 actually demands calculating sixteen further complicated Green's functions. By proving that one of them is zero, we will find that the equations of motion depend on only four new Green's functions. Analyzing their symmetry properties reduces the computational task to only one Green's function in this order. The lengthy calculation of this function is put into the appendix. For an analytical treatment of the equations of motion, we still have to linearize these equations in Section 6.2.

After that, the theory is ready and we can apply it to get the desired results. These are presented in Chapter 7 for zero temperature. We will first discuss the phase boundary and the spectra in the insulating phase. In Section 7.2 the spectra in the superfluid phase will be found and discussed. They are compared to the Bogoliubov prediction and to the spectra obtained in the insulating phase. We are especially interested in a mapping between both regimes. In Section 7.3 the critical behavior on both sides of the phase boundary will be analyzed in the light of a scaling theory. Critical exponents for the gap and the mass of the spectra will be obtained.

In the last chapter, we will have a look at other theories in order to compare our approach with them. In Section 8.1 we will point out the relation to the Gross-Pitaevskii equation in the limit of weak interactions. In Section 8.2 we will compare our results with those obtained by a formalism which we actually consider to be equivalent for problems near equilibrium, namely a Ginzburg-Landau approach in imaginary time.

2 Models for the Problem

In this chapter we are going to prepare our later study of bosonic particles in an optical lattice by introducing and discussing the seminal Bose-Hubbard (BH) model [31,32] as the underlying Hamiltonian of the system. An interesting feature of this model is the possible phase transition from the so called Mott-insulator (MI) phase without any long-range correlations between the particles to the superfluid (SF) phase where such correlations exist. Therefore, we will also present the Ginzburg-Landau model for the free energy as a functional of an order field [14], which has turned out to be extremely useful for the description of second-order phase transitions like, for instance, the transition from a paramagnetic into a ferromagnetic phase.

At this place, however, we should stress a fundamental difference between this type of phase transition, which can be understood from a classical point of view, and the phase transition that we have to deal with: While in classical thermodynamics phase transitions are driven by thermal fluctuations of the system and the phase diagram therefore basically depends on the temperature, the MI-SF transition might occur even at zero temperature. The fluctuations establishing the long-range correlations are of quantum nature, thus it is called a quantum phase transition. Instead of thermodynamical quantities like temperature, parameters of the Hamiltonian like the coupling constant determine the criticality of the system.

In Ehrenfest's classification scheme for phase transitions, discontinuities in the free energy or in any of its derivatives with respect to temperature (cf. Ref. [33]) are considered: If a discontinuity occurs first in the nth derivative, the phase transition is said to be of $(n+1)$th order. Thus, at a second-order phase transition, the free energy of a system does not jump, but changes its shape abruptly. Adapting this scheme to quantum phase transitions, these are said to be of second order, if excitations from the ground state have no energy gap at the phase boundary [34]. One goal of this thesis is to show that the Ginzburg-Landau model originally used for describing thermal phase transitions of second order, can be applied as well to the quantum phase transition undergone by BH systems.

2.1 Bose-Hubbard Model

The investigation of bosonic particles in optical lattices is usually based on the Bose-Hubbard model [31,32]. Given a perfectly periodic external potential and a short-range interaction between two particles, e.g. a contact interaction, the model describes the situation of particles localized on lattice sites i being able to interact with other particles on the same site and to hop to neighboring sites. The simplest and most common version of the Bose-Hubbard-Hamiltonian reads:

$$\hat{\mathrm{H}}_{\mathrm{BH}} = \sum_i \left[\frac{1}{2} U \hat{\mathrm{a}}_i^\dagger \hat{\mathrm{a}}_i \left(\hat{\mathrm{a}}_i^\dagger \hat{\mathrm{a}}_i - 1 \right) - \mu \hat{\mathrm{a}}_i^\dagger \hat{\mathrm{a}}_i \right] - J \sum_{\langle i,j \rangle} \hat{\mathrm{a}}_i^\dagger \hat{\mathrm{a}}_j, \tag{2.1}$$

where $\hat{a}_i^\dagger$ and $\hat{a}_i$ are the bosonic creation and annihilation operators and the index i denotes the lattice site. The operators fulfill the usual bosonic commutation relations

$$\left[\hat{a}_i^\dagger, \hat{a}_j^\dagger\right] = [\hat{a}_i, \hat{a}_j] = 0, \qquad \left[\hat{a}_i, \hat{a}_j^\dagger\right] = \delta_{ij}. \tag{2.2}$$

The parameters U and J in Eq. (2.1) characterize the on-site interaction strength and the hopping strength, respectively. While the interaction is local, the hopping process is described by a non-local sum being proportional to the hopping strength J. The bracket $\langle\cdot,\cdot\rangle$ restricts this sum to nearest neighbor terms only, so it reflects the annihilation of one particle at a site i and its re-creation at an adjacent site j. There is a third parameter μ in Eq. (2.1) which represents the chemical potential. We need it as a grand-canonical description is chosen. This means that the system is assumed to be in contact with a huge bath allowing for an exchange of both energy and particles.

In order to relate the model parameters to the ones configuring the experiments [1], we note that the total particle number of the system N and the average particle number per site n become fixed in thermal equilibrium via a minimization of the grand-canonical free energy. The interaction parameter U can be tuned by the s-wave scattering length of the particles a_{BB} via Feshbach resonances [35]. Besides, U is influenced by the particle mass m and the lattice potential $V(\boldsymbol{x})$. These two parameters also determine the hopping strength J. This thesis is restricted to the most common case of a cubic lattice potential

$$V_{\mathrm{ext}}(\boldsymbol{x}) = \sum_{j=1}^{3} V_0 \sin^2\left(\frac{\pi}{a} x_j\right), \tag{2.3}$$

which can be realized by six counter-propagating lasers. Here V_0 denotes the intensity of the laser. The lattice constant is $a = \lambda/2$, where λ is the wavelength of the laser light.

The interaction potential is usually specified to a delta-potential describing contact interaction

$$V_{\mathrm{int}}(\boldsymbol{x}_1, \boldsymbol{x}_2) = \frac{4\pi a_{\mathrm{BB}}\hbar^2}{m}\delta(\boldsymbol{x}_1 - \boldsymbol{x}_2). \tag{2.4}$$

While the experimentalists have the convention to measure all parameters having the dimension of energies (like J, U, V_0, μ) in units of the recoil energy $E_{\mathrm{R}} = \hbar^2\pi^2/(2a^2m)$, from the theoretical point of view, it is more comfortable to use one of the model's parameters as a basic energy unit. We will mostly measure all energies in units of U.

2.1.1 Model Parameters

In order to express U and J in terms of the experimental parameters, the Bose-Hubbard Hamiltonian given by Eq. (2.1) has to be derived from the general many-body Hamiltonian, which is done, for instance, in Ref. [36]. We only present the main results here and derive an alternative formula for J.

The interaction parameter U is found to be

$$U = U_i = \frac{4\pi a_{\mathrm{BB}}\hbar^2}{m}\int \mathrm{d}^3x\ |w(\boldsymbol{x} - \boldsymbol{x}_i)|^4, \tag{2.5}$$

where $w(\boldsymbol{x} - \boldsymbol{x}_i)$ is the energetically lowest Wannier function [37]. The argument of this function

depends on the coordinates $\boldsymbol{x}_i$ of the lattice site i, where the particle is localized. The Wannier functions are also needed for defining the hopping parameter J:

$$J = J_{ij} = -\int \mathrm{d}^3x \; w^*(\boldsymbol{x} - \boldsymbol{x}_i) \left[-\frac{\hbar^2}{2m}\nabla^2 + V_{\mathrm{ext}}(\boldsymbol{x}) \right] w(\boldsymbol{x} - \boldsymbol{x}_j). \tag{2.6}$$

To derive Eqs. (2.5) and (2.6), two fundamental assumptions have to be made:

1. Other than the first-band Wannier function need not to be taken into account.

2. The overlap between neighboring Wannier functions can be neglected in the interaction term. So we end up with a local interaction. Consequently, we apply this restriction also to the kinetic term J_{ij} and restrict it to the first non-trivial contribution, which is the overlap of nearest neighbors.

We will briefly discuss the validity of these assumptions in the next subsection.

The Wannier functions, whose knowledge is required in the above expressions, come from solid-state physics. This connection is no surprise, since the situation here is basically the same as in a solid: There are particles moving in a periodic potential. Thus the Bloch theorem can be applied, which tells us that the accessible states form energy bands. The determination of the Bloch states $\Phi_{n,\boldsymbol{k}}$, where n is the band number and $\hbar\boldsymbol{k}$ the momentum, demands solving the Schrödinger equation for a single particle in a periodic potential, i.e.:

$$\left[-\frac{\hbar^2}{2m}\nabla^2 + V_0 \sum_{j=1}^{3} \sin^2\left(\frac{\pi}{a}x_j\right) \right] \Phi_{n,\boldsymbol{k}}(\boldsymbol{x}) = E_{n,\boldsymbol{k}}\Phi_{n,\boldsymbol{k}}(\boldsymbol{x}). \tag{2.7}$$

As the Bloch states describe delocalized particles in the lattice with fixed wave vector $\boldsymbol{k}$, one has to make a Fourier transformation in order to deal with localized particles, i.e. particles with fixed site index and indefinite momentum. This gives us the Wannier functions:

$$w(\boldsymbol{x} - \boldsymbol{x}_i) = N^{-1/2} \sum_{\boldsymbol{k}} \mathrm{e}^{-i\boldsymbol{k}\boldsymbol{x}_i} \Phi_{0,\boldsymbol{k}}(\boldsymbol{x}), \tag{2.8}$$

where N is the number of lattice sites and the sum runs over all $\boldsymbol{k}$'s in the first Brillouin zone. Here we have restricted ourselves to the lowest Bloch band, because there is no Pauli principle for bosons, so at low temperature the occupation of higher bands can be neglected.

In Ref. [36] a numerical approach for calculating the Wannier functions is compared with a harmonic approximation which becomes exact in the limit of an infinite strong lattice potential. In this approximation, the Wannier function of an one-dimensional system reads

$$w(x) = \left(\frac{\pi^2 V_0}{a^4 E_{\mathrm{R}}}\right)^{1/8} \exp\left[-\frac{\pi^2}{2}\sqrt{\frac{V_0}{E_{\mathrm{R}}}} \left(\frac{x}{a}\right)^2 \right]. \tag{2.9}$$

The Wannier functions in higher dimensions can easily be constructed by multiplication of one-dimensional functions. In three dimensions we therefore have:

$$w(\boldsymbol{x} - \boldsymbol{x}_i) = w(x - x_i)w(y - y_i)w(z - z_i). \tag{2.10}$$

Inserting this into Eq. (2.5) yields the on-site potential in harmonic approximation. One finds that this expression depends on the dimensionality of the lattice. In three dimension it reads

$$\frac{U}{E_\mathrm{R}} = \sqrt{8\pi}\frac{a_\mathrm{BB}}{a}\left(\frac{V_0}{E_\mathrm{R}}\right)^{3/4}. \tag{2.11}$$

Except for very small lattice potentials, this harmonic approximation produces values of U similar to the ones obtained by the numerical method.

For the hopping parameter J a useful formula can be found from the theory of Mathieu's equation which agrees better with the numerical results than the harmonic approximation (see Ref. [38]) and requires no knowledge of the Wannier functions. It reads:

$$\frac{J}{E_\mathrm{R}} = \frac{4}{\sqrt{\pi}}(V_0/E_\mathrm{R})^{3/4}\mathrm{e}^{-2\sqrt{V_0/E_\mathrm{R}}}. \tag{2.12}$$

To derive it, we first must separate the space coordinates. To this end, we insert the separation ansatz (2.10) in Eq. (2.6) and note that according to Eq. (2.3) the operator $\hat{\mathrm{h}} \equiv -\frac{\hbar^2}{2m}\nabla^2 + V_\mathrm{ext}(\boldsymbol{x})$ can be written as a sum of operators acting on one spatial coordinate only: $\hat{\mathrm{h}} = \hat{\mathrm{h}}_x + \hat{\mathrm{h}}_y + \hat{\mathrm{h}}_z$. Then Eq. (2.6) reads

$$\begin{aligned} J_{ij} = -\Bigg\{ &\int_{-\infty}^{\infty}\mathrm{d}x\; w^*(x-x_i)\hat{\mathrm{h}}_x w(x-x_j)\int_{-\infty}^{\infty}\mathrm{d}y\; w^*(y-y_i)w(y-y_j)\int_{-\infty}^{\infty}\mathrm{d}z\; w^*(z-z_i)w(z-z_j) \\ &+\int_{-\infty}^{\infty}\mathrm{d}x\; w^*(x-x_i)w(x-x_j)\int_{-\infty}^{\infty}\mathrm{d}y\; w^*(y-y_i)\hat{\mathrm{h}}_y w(y-y_j)\int_{-\infty}^{\infty}\mathrm{d}z\; w^*(z-z_i)w(z-z_j) \\ &+\int_{-\infty}^{\infty}\mathrm{d}x\; w^*(x-x_i)w(x-x_j)\int_{-\infty}^{\infty}\mathrm{d}y\; w^*(y-y_i)w(y-y_j)\int_{-\infty}^{\infty}\mathrm{d}z\; w^*(z-z_i)\hat{\mathrm{h}}_z w(z-z_j)\Bigg\}. \end{aligned} \tag{2.13}$$

In the following, we will need the orthonormality of the Wannier functions

$$\int_{-\infty}^{\infty}\mathrm{d}x\; w^*(x-x_i)w(x-x_j) = \delta(x_i - x_j). \tag{2.14}$$

Now we concentrate on the fact that J_{ij} should describe nearest neighbor hopping only, so in one spatial direction, say x, we have $x_i - x_j = a$, while in all the other directions, say y and z, the spatial distance is zero. From this we see that the hopping matrix element does not depend on the dimensionality of system. There is always only one term on the right-hand side of Eq. (2.13) which survives. The whole expression reduces to

$$J_{ij} = -\delta_{<i,j>}\int_{-\infty}^{\infty}\mathrm{d}x\; w^*(x-x_i)\hat{\mathrm{h}}_x w(x-x_j) \equiv \delta_{<i,j>}J. \tag{2.15}$$

The matrix element $\delta_{<i,j>}$ should make sure, that i and j are nearest neighbors. It is equivalent to write

$$J_{ij} = \begin{cases} J, & \text{if } i,j \text{ nearest neighbors} \\ 0, & \text{otherwise} \end{cases} \tag{2.16}$$

If we express the Wannier functions in terms of the Bloch functions by inserting Eq. (2.8), we can still use the orthogonality of the Bloch functions, i.e.:

$$\int_{-\infty}^{\infty} \mathrm{d}x\ \Phi^*_{0,\boldsymbol{k}'}(x)\ \Phi_{0,\boldsymbol{k}}(x) = \delta_{\boldsymbol{k},\boldsymbol{k}'}. \tag{2.17}$$

With this we obtain

$$J_{ij} = -\delta_{<i,j>}\frac{1}{N_x}\sum_{k_x} \mathrm{e}^{ik_x(x_i-x_j)}E_{0,k_x} = -\delta_{<i,j>}\frac{1}{N_x}\sum_{k_x} \mathrm{e}^{ik_x a}E_{0,k_x}. \tag{2.18}$$

From the Bloch theorem we know that the energy bands have the periodicity of the reciprocal lattice, i.e.

$$E_{n,k} = E_{n,k+2\pi/a}. \tag{2.19}$$

Due to the inversion symmetry of the external potential from Eq. (2.3), we furthermore have the Kramer's theorem (see e.g. Ref. [39])

$$E_{n,k} = E_{n,-k}. \tag{2.20}$$

According to Eqs. (2.19) and (2.20), all the sine-terms in the Fourier series of $E_{0,k}$ are zero:

$$E_{0,k} = \frac{e_0}{2} + \sum_{m=1}^{\infty} e_m \cos(kma), \tag{2.21}$$

with the coefficients

$$e_i = \frac{a}{\pi}\sum_{k\in 1.\mathrm{BZ}} E_{0,k}\cos(kma). \tag{2.22}$$

We insert this in Eq. (2.18) and transform the sum into an integral, according to the rule $1/N\sum_k \rightarrow \frac{L/2\pi}{L/a}\int_{-\pi/a}^{\pi/a}\mathrm{d}k$. These integrals then read

$$\int_{-\pi/a}^{\pi/a} \cos(ka)\cos(mka)\mathrm{d}k = \delta_{m,1}\frac{\pi}{a}, \tag{2.23}$$

$$\int_{-\pi/a}^{\pi/a} \sin(ka)\cos(mka)\mathrm{d}k = 0. \tag{2.24}$$

This means that J reduces to minus half of the first Fourier coefficient of $E_{0,\boldsymbol{k}}$:

$$J = -\frac{e_1}{2}. \tag{2.25}$$

Now we must relate the first Fourier coefficient to the bandwidth B of $E_{0,\boldsymbol{k}}$. Since $\cos(2n\pi) = \cos(0)$ with $n \in \mathbb{N}$, even Fourier coefficients do not contribute to the bandwidth. When we furthermore suppose that $E_{0,k}$ has a shape similar to the cosine, the third and higher Fourier coefficients have to be much smaller than the first one. Thus, the bandwidth of $E_{0,k}$ is almost identical with two times the absolute value of the first Fourier coefficient. With Eq. (2.25) we get $J = B/4$.

Now we consider the Schrödinger equation (2.7) and use the trigonometric relation $\sin^2\alpha = (1 - \cos 2\alpha)/2$ in order to transform it into the one-dimensional Mathieu equation

$$\left[-\frac{\partial^2}{\partial x'^2} + \frac{\tilde{V}_0}{2}(1 - \cos 2x')\right] \Phi_{n,k} = \tilde{E}_{n,k}\Phi_{n,k}(x'), \tag{2.26}$$

where we substituted the energies $E \to \tilde{E} \equiv E/E_\mathrm{R}$ and lengths $x \to x' \equiv (\pi/a)x$ to dimensionless variables. From the literature on this equation [40], we know that there are stable solutions for a given eigenvalue $\tilde{E}_{n,k}$ only within stability regions depending on V_0. The energetically lowest stability region has a bandwidth which is known to be given by four times the right side of Eq. (2.12) for large $\tilde{V}_0$. With the relation between J and B derived above follows Eq.(2.12).

2.1.2 Assumptions Made in the Bose-Hubbard Model

Obviously, the model Hamiltonian (2.1) idealizes the experimental situation, as it contains the following four assumptions:

1. The system is translationally invariant.
2. Only one state is considered on each lattice state.
3. No interaction between particles on distinct sites is included in the model.
4. Hopping to other than nearest neighbor sites is excluded.

To justify the first assumption, we must recognize that the system is assumed to be large compared with the lattice spacing and the trap, which is necessary to confine the gas, represents a very smooth potential. Nevertheless, there are some effects like the amplitude damping of the order parameter in collapse and revival experiments [41,42] or a visibility smaller than one even deep in the superfluid phase which cannot be understood from the point of view of an infinitely large, homogeneous system [43]. The inhomogeneity of the trap could be taken into account by letting the chemical potential depend on the lattice site, but we will not do that, because the equations of motion, that we will derive later, become local in Fourier space if spatial homogeneity is assumed.

Let's take a look on the justification of the other assumptions: The second one restricts the model to systems of only one type of particles. Furthermore, particles with degenerate spin states cannot be described by such a Hamiltonian. In many cases, however, the system is magnetically trapped, such that all spins are aligned. Then it depends basically on the temperature of the system, if we can restrict ourselves to the lowest energy band and the corresponding Wannier function $w(\boldsymbol{x} - \boldsymbol{x}_i)$, or if higher bands are important, too. In a few moments we will crudely estimate the occupation of higher bands for a realistic temperature, in order to see that higher bands do not play an important role.

The third assumption at first depends on the interaction between the particles, which must be very short-range. Whether this is the case, depends very much on the particles under consideration. For the most frequent experimental case of alkali atoms, the magnetic dipole moment is relatively small and the electric dipole moment is zero, thus in a good approximation, only contact interaction must be taken into account. This alone is still not sufficient to restrict the interaction to the form given in

Eq. (2.5), since a particle at site i, described by the nth Wannier function $w_n(\boldsymbol{x}-\boldsymbol{x}_i)$, has a finite probability to be in contact with a particle at a different site j described by $w_m(\boldsymbol{x'}-\boldsymbol{x}_j)$. However, if the second assumption is true, i.e. $n=m=0$, the overlap of the lowest nearest neighbor Wannier functions is very small [44], which then justifies the third and also the fourth assumption. Excited bands, however, are less localized, so if the second assumption fails, the others may not hold. Thus the basic question is, whether we really can restrict ourselves to the lowest single-particle band.

As we deal with finite temperatures, the goodness of the second assumption has to be put into question. By a Taylor expansion of the lattice potential (2.3), we find that in the first non-vanishing order a harmonic potential $V(\boldsymbol{x})=(\pi/a)^2V_0\boldsymbol{x}^2$ describes the system. In this approximation, the energy of the nth excited state is $E_n=(n+1/2)\hbar\sqrt{(2\pi^2V_0)/(ma^2)}=(2n+1)\sqrt{V_0E_\mathrm{R}}$, where m is the particle mass.

Taking the value for E_R from Ref. [25], which is about $1\cdot10^{-11}$ eV, and a typical value for V_0, say 20 E_R, we have $E_1\approx1,5\cdot10^{-10}$ eV while $E_0\approx0,5\cdot10^{-10}$ eV. Now we have to compare these values with the thermal energy $k_\mathrm{B}T$. As there is still no method of measuring the temperature, we rely on theoretical considerations in order to find a suitable guess of it. In Ref. [36], for instance, the temperature of the gas is calculated by comparing the theoretical with the experimental visibility where the data is taken from Ref. [25]. For $V_0=$ 20 E_R, a temperature about 600 nK is found. This gives a ratio $E_1/(k_\mathrm{B}T)$ of about 3, while $E_0/(k_\mathrm{B}T)$ is about one. Inserting this in the Bose-Einstein statistic, where the medium occupation number is given by $\langle n\rangle=1/\{\exp[E/(k_\mathrm{B}T)]-1\}$, we find $\langle n_0\rangle/\langle n_1\rangle\approx10$. So the first excited band does not play a very important role and the first assumption can be justified not only for zero but as well for more realistic temperatures. Nevertheless, there seem to be cases where the occupation of higher Bloch bands has to be considered in order to achieve a good agreement with experiments. An example are Bose-Fermi gas mixtures [45,46].

2.2 Phase Transitions

As already mentioned above, our main interest is related to the phase transition between the MI and the SF phase which may occur in a lattice filled with bosons. Experimentally, this transition becomes manifest in the time-of-flight absorption pictures of the gas taken after switching off both the trap, which has confined the system, and the optical lattice. Then the initial momenta of the atoms make the cloud expand in space, leading to a density distribution that reproduces the momenta distribution integrated in one spatial direction. Since in the superfluid phase the bosons are delocalized over the whole lattice, they have, by Heisenberg's uncertainty principle, a definite momentum. Therefore, sharp absorption peaks are measured in the SF phase while in the MIt phase the opposite is the case: Localized atoms have no definite momentum and the time-of-flight absorption pictures show a fuzzy cloud (see Figure 2.1).

In order to quantify this effect, the visibility $\mathcal{V}$ is defined as

$$\mathcal{V}\equiv\frac{n_\mathrm{max}-n_\mathrm{min}}{n_\mathrm{max}+n_\mathrm{min}}, \tag{2.27}$$

where n_max is the highest and n_min the lowest density on a circle through the first side maximum around the center peak as shown in the inset of Fig. 2.2. In this figure the data from an experiment

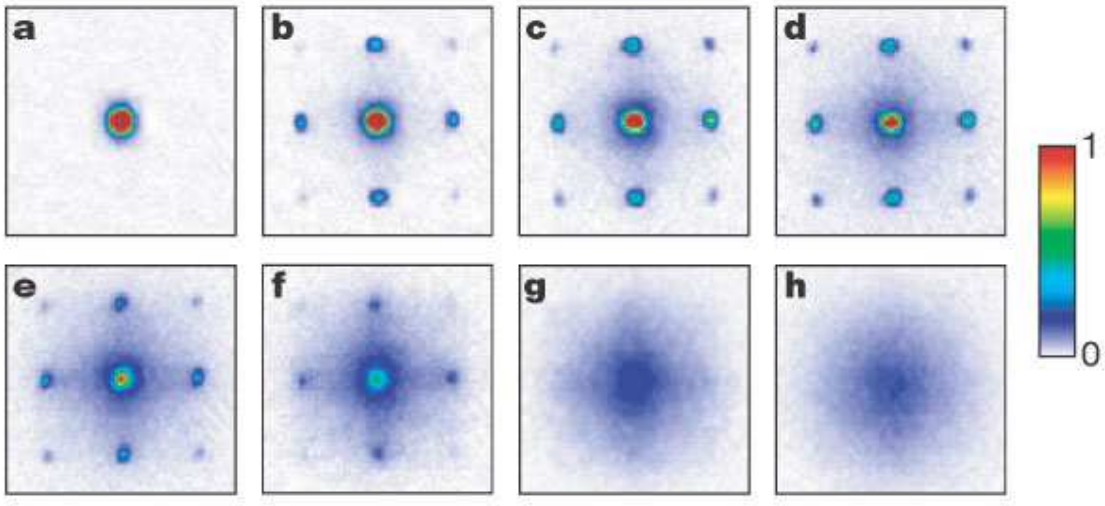

Figure 2.1: Time-of-flight absorption pictures taken from [1]: When the lattice potential is increased from zero (a) to 20 recoil energies (h), the phase coherence between the atoms on different sites gets lost. In between the system carries out a phase transition from the SF into the MI phase.

measuring the visibility is shown [47]. Although the occurrence of a phase transition is evident from Figs. 2.1 and 2.2, both figures do not allow for determining the position of the phase transition. It thus would be nice to find other criteria marking the phase transition. We will later see that the excitation spectra can do that job.

From the theoretical point of view, the Bose-Hubbard model allows for predicting this phase transition and calculating the phase boundary or even the time-of-flight absorption pictures. For understanding such a second order phase transition, we introduce now the concept of an order parameter by Ginzburg and Landau.

2.2.1 Order Field and Ginzburg-Landau Model

The basic idea related to the order parameter is that we have a quantity which vanishes on the disordered side of the transition and takes finite values on the ordered side. In the following we denote this parameter by Ψ. The dependence of the free energy $\mathcal{F}$ on this parameter is assumed to be:

$$\mathcal{F} = F_0 + (\lambda_2/2)\,|\Psi|^2 + (\lambda_4/4!)\,|\Psi|^4 + O(|\Psi|^5), \tag{2.28}$$

with λ_2 and λ_4 being phenomenological parameters to be determined. It is important not to have odd terms in this expansion, as otherwise the transition would be of first order, i.e. the energy would change discontinuously in the critical regime [14]. For systems which exhibit a second-order phase transition, characterized by the vanishing of the characteristic energy scale in the excitation spectrum [34], the existence of a cubic term is forbidden by symmetry arguments. In our case, the symmetry in consideration is the phase-rotational invariance of the Bose-Hubbard Hamiltonian (2.1).

The description in Eq. (2.28) which was invented by Landau can be generalized to the so called **Ginzburg-Landau model** by letting Ψ vary in space. The free energy $\mathcal{F}$ can then be written as a

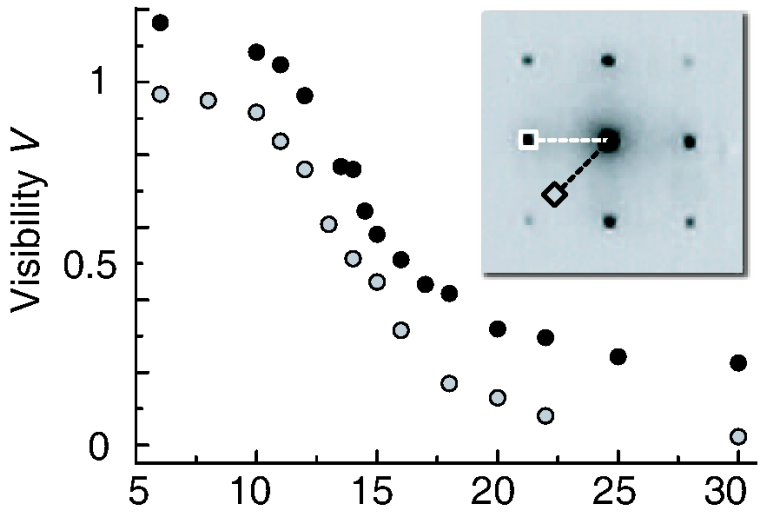

Figure 2.2: For $N = 3.6\ 10^5$ (gray circles) and $N = 5.9\ 10^5$ (black circles) ^{87}Rb atoms the visibility was measured as a function of the lattices potential by Ref. [47]. The inset marks the region of the time-of-flight pictures which were used in order to define the visibility.

functional of the order field $\Psi(\boldsymbol{x})$ and its gradient:

$$\mathcal{F}[\Psi] = \int d^3x \left(F_0(\boldsymbol{x}) + \frac{1}{2} |\nabla\Psi(\boldsymbol{x})|^2 + \frac{\lambda_2}{2} |\Psi(\boldsymbol{x})|^2 + \frac{\lambda_4}{4!} |\Psi(\boldsymbol{x})|^4 \right), \tag{2.29}$$

where $F_0(\boldsymbol{x})$ is the free energy in the disordered phase. As it depends on the sign of λ_2, whether a zero or nonzero $\Psi(\boldsymbol{x})$ minimizes $\mathcal{F}$, phase transitions are expected when the sign of λ_2 changes. Originally applied to thermal phase transitions, the Landau coefficients λ_i were supposed to depend basically on the temperature of the system. For λ_2 one has $\lambda_2 \sim \frac{T}{T_c} - 1$, where T_c is the critical temperature [14]. Our goal, however, is the description of a quantum phase transition, so we wish to find coefficients which depend on a parameter given by the Hamiltonian of the system [34]. In our system, the critical regime is determined by the relative value of the hopping parameter J to the on-site potential U.

In the theory of superfluidity [4], the transition to the superfluid phase is attended by a macroscopic occupation of the ground state. So as an order parameter or order field, a quantity should be chosen, which is proportional to the condensate amplitude. In the latter, the expectation value of the annihilation operator will define the discrete order field: $\hbar\Psi_i \equiv \langle \hat{a}_i \rangle$. We will see in the next section that a transition to non-vanishing order fields is related to a breakdown of the phase-rotational symmetry. The difference between the normal and the superfluid phase is illustrated in the plot of the free energy $\mathcal{F}[\Psi]$ (see Figure 2.3), which has a paraboloid shape in the normal phase and a wine-bottle shape in the superfluid phase. So there is only one minimum in the normal phase at $\Psi = 0$, but in the superfluid phase, for any continuous phase angle γ, the system has a global minimum at a finite Ψ_0.

2.2.2 Spontaneous Symmetry Breaking

When the Hamiltonian is invariant under a symmetry operation, but the ground state is not, it has to be degenerate [48]. The degenerate ground states are denoted by a label α which corresponds to an observable distinguishing the different states. There is no reason that a special α is preferred by

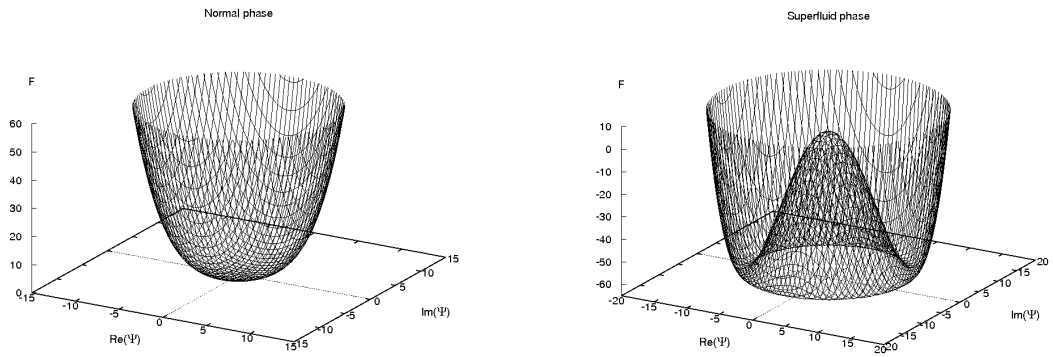

Figure 2.3: The Landau free energy $\mathcal{F}$ as a function of the order parameters: In the normal phase only one minimum exists at the origin, in the superfluid phase gauge invariance leads to infinitely many degenerate minima.

nature, so its expectation value $\langle\alpha\rangle$ should simply be the average of all possible α, which can be set zero without loss of generality.

A phase transition takes place when the invariance of the Hamiltonian breaks down and the degeneracy is lifted. Then one of the states $|\alpha\rangle$ becomes the unique ground state and $\langle\alpha\rangle$ is no longer zero. The physical reason for this is a breakdown of ergodicity [49]. It might be caused, e.g., by a potential barrier between the different states $|\alpha\rangle$, such that the system gets stuck in one arbitrary state forever.

In order to describe phase transitions, it is a useful method to add external sources to the Hamiltonian which are linearly coupled to the order field. The symmetry of the system is destroyed by these objects which besides might have no further physical meaning and be artificial.

The broken symmetry in our case of the transition to a superfluid phase is gauge invariance [4]: The Bose-Hubbard Hamiltonian (2.1) remains unchanged under a global phase rotation with a constant phase angle γ for all creation and annihilation operators, i.e. $\hat{a}_i \to \hat{a}_i e^{i\gamma}$ and $\hat{a}_i^\dagger \to \hat{a}_i^\dagger e^{-i\gamma}$. This means that the expectation value of the creation and annihilation operators must not depend on the phase angle γ, which is only possible if $\langle\hat{a}_i\rangle = \langle\hat{a}_i^\dagger\rangle = 0$. It is found that in this normal phase at $T = 0$ the occupation number $n_i = \langle\hat{a}_i^\dagger\hat{a}_i\rangle$ is pinned to integer values depending on μ/U [34].

With an increasing hopping parameter J, however, the coupling of neighboring sites becomes more important. At some critical value J/U, it occurs that states with a broken symmetry are preferred [34]. Then we are in the superfluid phase with a non-zero $\langle\hat{a}_i\rangle$. This means that from the infinitely many minima in Fig. 2.3 the system has to choose one.

As the broken symmetry is continuous, the phase of the order parameter can fluctuate without exciting it energetically. These zero-energy-excitations are called Nambu-Goldstone modes [50,51]. There is a famous theorem, the so-called Goldstone theorem, which predicts one massless excitation mode for each broken continuous symmetry. Fluctuations of the amplitude, in contrast, amongst them all the fluctuations in the normal phase, have to go "uphill" against the free energy. Thus, the coherence length of the phase fluctuations are infinite, while the amplitude fluctuations have a finite coherence length [4].

One of our later goals will be the study of the excitation spectra for bosons in optical lattices. We will find what the Goldstone theorem predicts, namely one massless mode in the superfluid phase.

3 Green's Functions Formalisms

The partition function of a quantum system, described by a time-independent Hamilton operator $\hat{\mathrm{H}}$, is given by

$$\mathcal{Z} \equiv \mathrm{Tr}\left(e^{-\beta\hat{\mathrm{H}}}\right), \tag{3.1}$$

with $\beta = 1/(k_{\mathrm{B}}T)$ being the inverse of the temperature T times the Boltzmann's constant k_{B}. It determines all thermodynamic quantities, like the free energy, the entropy or the specific heat of the system. On the other hand, no information on local properties of the system, which for instance are needed for calculating time-of-flight absorption pictures, can be extracted from this expression. This information is contained in the so called correlation functions [14]. We will soon get to know a lot of different formalisms in which correlation or Green's functions appear. So we are not going to give a precise definition yet, but only a preview of what is meant by them:

$$G(i_1, \cdots, i_n; i_{n+1}, \cdots, i_m) \sim \langle \hat{\mathrm{a}}_{i_1} \cdots \hat{\mathrm{a}}_{i_n} \hat{\mathrm{a}}^\dagger_{i_{n+1}} \cdots \hat{\mathrm{a}}^\dagger_{i_{n+m}} \rangle, \tag{3.2}$$

where $n, m \in \mathbb{N}$. The operators $\hat{\mathrm{a}}_i$ and $\hat{\mathrm{a}}^\dagger_i$ are the bosonic annihilation and creation operators which have already appeared in the definition of the Bose-Hubbard Hamiltonian (2.1) and fulfill the usual commutation relations (2.2). The meaning of the bracket $\langle \cdot \rangle$ depends on the applied formalism. In a $T \neq 0$ - theory it is defined by the following trace

$$\langle \cdot \rangle \equiv \frac{1}{\mathcal{Z}} \, \mathrm{Tr}(\cdot \, e^{-\beta\hat{\mathrm{H}}}), \tag{3.3}$$

which is the thermal average. For a pure quantum-dynamic theory at $T = 0$, however, $\langle \cdot \rangle$ means the quantum-mechanical expectation value with respect to the ground state. After a short presentation of the correlation functions in this zero-temperature formalism in Section 3.2, we will deal with finite temperatures and then always have the definition (3.3).

One feature, that is common to all the presented formalisms, is some kind of time dependence of the correlation functions. So first we have to give an introduction to the time evolution of quantum-mechanical systems.

3.1 Quantum Mechanical Pictures

As in classical physics, the time evolution of a quantum mechanical system is generated by the Hamiltonian. But while in classical physics it is clear on which objects the time evolution has to act, as no discrepancy between the observables and the corresponding functions exists, the situation in quantum theory is not that obvious. Of course, the theory has to reproduce the measurable quantities, but it deals with theoretical constructs like states and operators, which are not *per se* observable. Only some

special combinations of them, e.g. scalar products, expectation values or transition amplitudes, can be measured directly. For this reason, a freedom of choice remains: the time evolution of an observable can either be constructed by letting the states evolve with time (Schrödinger picture) or the operators (Heisenberg pictures) or both (Dirac picture).

3.1.1 Schrödinger and Heisenberg Picture

For the perturbative calculations done later in this thesis, the Dirac picture will be used. Nevertheless, a short definition of the Schrödinger and the Heisenberg pictures is helpful, since the Dirac picture is a mixture of both. Moreover, it's in the Heisenberg picture, where the definition of the correlation functions (3.2) holds as well in the time-dependent case.

There is one time, say $t = 0$, when the Schrödinger and the Heisenberg picture coincide. Then the constant Heisenberg states $|\phi\rangle_{\mathrm{H}}$, can be identified with the Schrödinger states $|\phi(0)\rangle_{\mathrm{S}}$:

$$|\phi(0)\rangle_{\mathrm{S}} \equiv |\phi\rangle_{\mathrm{H}}. \tag{3.4}$$

The time evolution of the Schrödinger states is generated by the total Hamiltonian $\hat{\mathrm{H}}_{\mathrm{S}}(t)$. This operator, although in the Schrödinger picture, might have an explicit time dependence, e.g. because of a time-dependent potential. By solving the time-dependent Schrödinger equation

$$i\hbar\frac{\partial}{\partial t}|\phi(t)\rangle_{\mathrm{S}} = \hat{\mathrm{H}}_{\mathrm{S}}(t)|\phi(t)\rangle_{\mathrm{S}} \tag{3.5}$$

we can find out how a state evolves with time [48]:

$$|\phi(t)\rangle_{\mathrm{S}} = \hat{\mathrm{T}}\left\{e^{-\frac{i}{\hbar}\int_0^t dt'\hat{\mathrm{H}}_{\mathrm{S}}(t')}\right\}|\phi(0)\rangle_{\mathrm{S}}. \tag{3.6}$$

Here the time-ordering operator $\hat{\mathrm{T}}$ is introduced. It acts on an operator product by bringing it into chronological order from the right to the left. Eq. (3.6) holds for the most general case. Simplifications are possible, if $\hat{\mathrm{H}}_{\mathrm{S}}(t)$ has no explicit time-dependence or if Hamiltonians at different time arguments commute, i.e. $[\hat{\mathrm{H}}_{\mathrm{S}}(t), \hat{\mathrm{H}}_{\mathrm{S}}(t')] = 0$. In the latter case, one can drop the time-ordering operator in Eq. (3.6), in the first case the integration in the exponent yields trivially $\exp\left(-\frac{i}{\hbar}\hat{\mathrm{H}}_{\mathrm{S}}t\right)$.

In contrast to the states, the operators $\hat{\mathrm{O}}$, if not explicitly time-dependent, are constant in the Schrödinger picture. The opposite is the case in the Heisenberg picture where the states are constant. As the expectation values have to be the same in both pictures, the relation between Heisenberg and Schrödinger operators is found to be:

$$\hat{\mathrm{O}}_{\mathrm{H}}(t) \equiv \hat{\mathrm{T}}\left[e^{\frac{i}{\hbar}\int_0^t dt'\hat{\mathrm{H}}_{\mathrm{S}}(t')}\right]\hat{\mathrm{O}}_{\mathrm{S}}(t)\hat{\mathrm{T}}\left[e^{-\frac{i}{\hbar}\int_0^t dt'\hat{\mathrm{H}}_{\mathrm{S}}(t')}\right]. \tag{3.7}$$

From this, we find the famous Heisenberg equation of motion by differentiation:

$$\frac{\mathrm{d}\hat{\mathrm{O}}_{\mathrm{H}}(t)}{\mathrm{d}t} = \frac{i}{\hbar}\left[\hat{\mathrm{H}}_{\mathrm{H}}(t), \hat{\mathrm{O}}_{\mathrm{H}}(t)\right] + \left(\frac{\partial\hat{\mathrm{O}}_{\mathrm{S}}(t)}{\partial t}\right)_{\mathrm{H}}. \tag{3.8}$$

3.1.2 Dirac Picture

The Dirac picture will be introduced now in a little bit more detail, as the perturbation theory that we will perform later works in this picture. The idea is to split the Hamiltonian in a "free" part $\hat{\mathrm{H}}_0$ that can be solved exactly and a small perturbative term $\lambda\hat{\mathrm{H}}_1(t)$ whose influence on the system is to be calculated in a power series of λ. So λ might be only a formal device which can be set to 1 at the end. Usually $\hat{\mathrm{H}}_0$ is chosen to be time-independent, while explicit time-dependencies of the Hamilton operator appear as the perturbation. Although it is not essential, let us take such a splitting for convenience.

The Dirac states $|\phi(t)\rangle_\mathrm{D}$ and operators $\hat{\mathrm{O}}_\mathrm{D}(t)$ are defined by the following relations to their equivalents in the Schrödinger picture [48,49]:

$$|\phi(t)\rangle_\mathrm{D} \equiv \exp\left(\frac{i}{\hbar}\hat{\mathrm{H}}_{0\mathrm{S}}t\right)|\phi(t)\rangle_\mathrm{S}, \tag{3.9}$$

$$\hat{\mathrm{O}}_\mathrm{D}(t) \equiv \exp\left(\frac{i}{\hbar}\hat{\mathrm{H}}_{0\mathrm{S}}t\right)\hat{\mathrm{O}}_\mathrm{S}(t)\exp\left(-\frac{i}{\hbar}\hat{\mathrm{H}}_{0\mathrm{S}}t\right). \tag{3.10}$$

It is important to note that for the unperturbed system, where $\hat{\mathrm{H}}_0$ is the full Hamiltonian, the Dirac picture coincides with the Heisenberg picture.

By inserting Eq. (3.9) into the Schrödinger equation Eq. (3.5), we get a Schrödinger-like equation for the time evolution of the Dirac states, which is driven by $\hat{\mathrm{H}}_{1\mathrm{D}}(t)$. Correspondingly, we obtain from (3.10) a Heisenberg-like equation of motion for the time evolution of the Dirac operators, which is driven by $\hat{\mathrm{H}}_{0\mathrm{S}} = \hat{\mathrm{H}}_{0\mathrm{D}} \equiv \hat{\mathrm{H}}_0$:

$$i\hbar\frac{\partial}{\partial t}|\phi(t)\rangle_\mathrm{D} = \hat{\mathrm{H}}_{1\mathrm{D}}(t)|\phi(t)\rangle_\mathrm{D}, \tag{3.11}$$

$$\frac{\mathrm{d}}{\mathrm{d}t}\hat{\mathrm{O}}_\mathrm{D}(t) = \frac{i}{\hbar}\left[\hat{\mathrm{H}}_0, \hat{\mathrm{O}}_\mathrm{D}\right] + \left(\frac{\partial\hat{\mathrm{O}}_\mathrm{H}(t)}{\partial t}\right)_\mathrm{D}. \tag{3.12}$$

We define a unitary operator $\hat{\mathrm{U}}(t, t_0)$, called evolution operator, with the property:

$$|\phi(t)\rangle_\mathrm{D} = \hat{\mathrm{U}}(t, t_0)|\phi(t_0)\rangle_\mathrm{D}. \tag{3.13}$$

Then we get from Eq. (3.11)

$$i\hbar\frac{\partial}{\partial t}\hat{\mathrm{U}}(t, t_0) = \hat{\mathrm{H}}_{1\mathrm{D}}(t)\hat{\mathrm{U}}(t, t_0), \tag{3.14}$$

which has to be solved with the initial condition

$$\hat{\mathrm{U}}(t_0, t_0) = \mathbb{1}. \tag{3.15}$$

Integrating Eq. (3.14) with Eq. (3.15) iteratively, yields a formal solution for the time-evolution

operator [49]:

$$\hat{\mathrm{U}}(t,t_0) = 1 + \left(\frac{-i}{\hbar}\right)\int_{t_0}^{t} dt_1\ \hat{\mathrm{H}}_{1\mathrm{D}}(t_1) + \left(\frac{-i}{\hbar}\right)^2 \int_{t_0}^{t} dt_1 \int_{t_0}^{t_1} dt_2\ \hat{\mathrm{H}}_{1\mathrm{D}}(t_1)\hat{\mathrm{H}}_{1\mathrm{D}}(t_2) + \cdots + \\ + (\frac{-i}{\hbar})^n \int_{t_0}^{t} dt_1 \cdots \int_{t_0}^{t_{n-1}} dt_n \hat{\mathrm{H}}_{1\mathrm{D}}(t_1)\cdots\hat{\mathrm{H}}_{1\mathrm{D}}(t_n) + \cdots . \tag{3.16}$$

This expression is called **Dyson series**. With the help of the time-ordering operator $\hat{\mathrm{T}}$ it can be written more compactly according to:

$$\hat{\mathrm{U}}(t,t_0) = \sum_{n=0}^{\infty} \frac{(-i/\hbar)^n}{n!} \int_{t_0}^{t} dt_1 \cdots \int_{t_0}^{t} dt_n \hat{\mathrm{T}}\left\{\hat{\mathrm{H}}_{1\mathrm{D}}(t_1)\cdots\hat{\mathrm{H}}_{1\mathrm{D}}(t_n)\right\}, \tag{3.17}$$

where the factor $1/n!$ arises from the fact that there are exactly $n!$ permutations in the expression on the right side. Noting that this is the power expansion of the exponential function, Eq. (3.17) reduces to:

$$\hat{\mathrm{U}}(t,t_0) = \hat{\mathrm{T}}\exp\left(\frac{-i}{\hbar}\int_{t_0}^{t} \mathrm{d}t_1 \hat{\mathrm{H}}_{1\mathrm{D}}(t_1)\right). \tag{3.18}$$

By comparing Eqs. (3.7), (3.10), and (3.18), we find the following useful relation between the Heisenberg and the Dirac operators:

$$\hat{\mathrm{O}}_{\mathrm{H}}(t) = \hat{\mathrm{U}}(t_0,t)\hat{\mathrm{O}}_{\mathrm{D}}(t)\hat{\mathrm{U}}(t,t_0). \tag{3.19}$$

3.2 Correlation Functions at $T = 0$

Now that the time evolution is defined, we can adapt the definition (3.2) of the correlation functions to the time-dependent case. All we have to do is to include a time-ordering operator $\hat{\mathrm{T}}$ and write down the operators in the Heisenberg picture [49]:

$$G(x_1,\cdots,x_n;x_{n+1},\cdots,x_{n+m}) \equiv \left\langle \hat{\mathrm{T}}\left(\hat{\mathrm{a}}_{\mathrm{H}}(x_1)\cdots\hat{\mathrm{a}}_{\mathrm{H}}(x_n)\hat{\mathrm{a}}^{\dagger}_{\mathrm{H}}(x_{n+1})\cdots\hat{\mathrm{a}}^{\dagger}_{\mathrm{H}}(x_{n+m})\right)\right\rangle. \tag{3.20}$$

Here the collective index $x_j \equiv \{i_j, t_j\}$ contains the time variable as well as the spatial coordinates, i.e. site indices. It still might be useful to take prefactors into the definition, but we will struggle with them later. Remember that in this definition the brackets mean the expectation value with respect to the full ground-state $|\Omega\rangle$. For $T \neq 0$, we will have to modify the definition by introducing a thermal averaging. This leads either to the imaginary-time formalism (ITF) or to the closed-time-path formalism (CTPF) being introduced later.

But let us first sketch the manipulations that can be performed on Eq. (3.20) in order to derive an expression appropriate for a perturbative expansion. Using Eq. (3.19) we can switch to the Dirac picture. This leaves us with evolution operators between all the operators in (3.20). Because of the time-ordering operator in front of them and the group property of $\hat{\mathrm{U}}$, i.e. $\hat{\mathrm{U}}(t,t')\hat{\mathrm{U}}(t',t'') = \hat{\mathrm{U}}(t,t'')$, they can be combined. Then the Gell-Mann-Low theorem [52] states that the ground state of the perturbed system $|\Omega\rangle$ is, up to a possible phase which is canceled by a denominator, related to the ground state of the unperturbed system $|0\rangle$ by a time evolution from the infinite past, where the perturbation was

completely switched off, to a finite time when the perturbation is completely switched on. Analogously, a time evolution to the infinite future relates $\langle\Omega|$ to $\langle 0|$. So instead of taking the expectation value with respect to the full ground state, we can take it with respect to the unperturbed ground state $|0\rangle$ only, if we simultaneously extend the time evolution to times in the infinite past and future. This allows for calculating the whole correlation function by a straight time evolution from $-\infty$ to ∞. For the 2-point correlation function at $T = 0$, one gets for example [49]:

$$G(x_1; x_2) = \langle\Omega|\hat{\mathrm{T}}\left\{\hat{\mathrm{a}}_{\mathrm{H}}(x_1)\hat{\mathrm{a}}^{\dagger}_{\mathrm{H}}(x_2)\right\}|\Omega\rangle = \lim_{t\to\infty}\frac{\langle 0|\hat{\mathrm{T}}\left\{\hat{\mathrm{a}}_{\mathrm{D}}(x_1)\hat{\mathrm{a}}^{\dagger}_{\mathrm{D}}(x_2)\hat{\mathrm{U}}(t,-t)\right\}|0\rangle}{\langle 0|\hat{\mathrm{U}}(t,-t)|0\rangle}. \tag{3.21}$$

This expression paths the way for a perturbative calculation in which $\hat{\mathrm{U}}$ is replaced by the Dyson series (3.16). This formalism, however, does not hold for finite temperature. Therefore, we refer to it as zero-temperature formalism (ZTF). For finite temperatures a thermal average, i.e. a trace over all states, must replace the ground state expectation value. But then the Gell-Mann-Low theorem cannot be applied any longer. We will see in the next section how to circumvent this by rotating the problem to imaginary times.

3.3 Wick Rotation and Thermal Green's Functions

For problems in thermal equilibrium a connection between quantum dynamics to statistical mechanics can be exploited, which stems from the formal similarity between time evolution and thermal averaging. To see this relation, we assume a Hamiltonian without any explicit time dependence. Then the Dirac picture evolution operator (3.18) is found to be given in terms of Schrödinger operators:

$$\hat{\mathrm{U}}(t,0) = \mathrm{e}^{\frac{i}{\hbar}\hat{\mathrm{H}}_0 t}\mathrm{e}^{-\frac{i}{\hbar}\hat{\mathrm{H}}_{\mathrm{S}} t}. \tag{3.22}$$

Comparing this with the partition function (3.1), we write down the following equation and notice that it becomes true for $\tilde{\tau} = -i\hbar\beta$:

$$\mathcal{Z} = \mathrm{Tr}\left\{e^{-\beta\hat{\mathrm{H}}_0}\hat{\mathrm{U}}(\tilde{\tau},0)\right\} = \mathcal{Z}^{(0)}\langle\hat{\mathrm{U}}(\tilde{\tau},0)\rangle_0, \tag{3.23}$$

where $\langle\cdot\rangle_0$ is the thermal average with respect to $\hat{\mathrm{H}}_0$ according to definition (3.3), and $\mathcal{Z}^{(0)} = \mathrm{Tr}\mathrm{e}^{-\beta\hat{\mathrm{H}}_0}$ is the partition function of the unperturbed system. Note that the operator $\hat{\mathrm{H}}_0$ is the same in the Dirac as in the Schrödinger picture.

This analytical continuation to a complex time variable is called **Wick rotation** [53]. The factor i appearing in the new "time" variable $\tilde{\tau}$ can be absorbed by the i which comes along with the time evolution. This delivers a time evolution without any i's. The Wick rotated time evolution operator in the Dirac picture then reads:

$$\hat{\mathrm{U}}(\tau,\tau_0) = \hat{\mathrm{T}}\exp\left(-\frac{1}{\hbar}\int_{\tau_0}^{\tau} d\tau_1\hat{\mathrm{H}}_{1\mathrm{D}}(\tau_1)\right), \tag{3.24}$$

where τ is a real number, though it is often called imaginary time.

What has been said about evolution in real time, remains true in the ITF. In the Dirac picture we have for the evolution of the states:

$$|\phi(\tau)\rangle_{\mathrm{D}} = \hat{\mathrm{U}}(\tau,\tau_0)|\phi(\tau_0)\rangle_{\mathrm{D}}. \tag{3.25}$$

The relation between time-independent Schrödinger operators and Dirac operators depending on imaginary time is in analogy to Eq. (3.10):

$$\hat{\mathrm{O}}_{\mathrm{D}}(\tau) \equiv \mathrm{e}^{\hat{\mathrm{H}}_0\tau/\hbar}\hat{\mathrm{O}}_{\mathrm{S}}\mathrm{e}^{-\hat{\mathrm{H}}_0\tau/\hbar}. \tag{3.26}$$

Correspondingly, instead of Eq. (3.19) we find for the Heisenberg operators:

$$\hat{\mathrm{O}}_{\mathrm{H}}(\tau) = \hat{\mathrm{U}}(\tau_0,\tau)\hat{\mathrm{O}}_{\mathrm{D}}(\tau)\hat{\mathrm{U}}(\tau,\tau_0). \tag{3.27}$$

We can now take the definition of the correlation functions (3.20) and modify it by letting the operators depend on imaginary time instead of real time. We still replace the quantum mechanical expectation value by a thermal average. We then get functions which are usually referred to as thermal or imaginary-time Green's functions or, in order to stress the number N of operators, N-point functions:

$$G(x_1,\cdots,x_n;x_{n+1},\cdots,x_{n+m}) \equiv \frac{\mathrm{Tr}\left\{\mathrm{e}^{-\beta\hat{\mathrm{H}}}\hat{\mathrm{T}}\left(\hat{\mathrm{a}}_{\mathrm{H}}(x_1)\cdots\hat{\mathrm{a}}_{\mathrm{H}}(x_n)\hat{\mathrm{a}}^{\dagger}_{\mathrm{H}}(x_{n+1})\cdots\hat{\mathrm{a}}^{\dagger}_{\mathrm{H}}(x_{n+m})\right)\right\}}{\mathrm{Tr}\left\{\mathrm{e}^{-\beta\hat{\mathrm{H}}}\right\}}. \tag{3.28}$$

We now have defined the collective variable $x \equiv \{i,\tau\}$. Most often, the number of annihilators equals the number of creators, i.e. $n = m$ and $N = 2n$.

Definition (3.28) can be brought to a form similar to Eq. (3.21). To this end we have to transform the Heisenberg operators in the Dirac picture using Eq. (3.27) and note that taking the thermal average with respect to the total Hamiltonian (which does not depend on real time) is the same as an evolution in imaginary time from 0 to $\hbar\beta$ given by Eq. (3.24) and taking the thermal average with respect to the unperturbed Hamiltonian $\hat{\mathrm{H}}_0$. To this end we rewrite Eq. (3.22) as

$$e^{-\beta\hat{\mathrm{H}}} = e^{-\beta\hat{\mathrm{H}}_0}\hat{\mathrm{U}}(\hbar\beta,0). \tag{3.29}$$

We then find:

$$G(x_1,\cdots,x_n;x_{n+1},\cdots,x_{n+m}) = \frac{\mathrm{Tr}\left\{\mathrm{e}^{-\beta\hat{\mathrm{H}}_0}\hat{\mathrm{U}}(\hbar\beta,0)\hat{\mathrm{T}}\left(\hat{\mathrm{a}}_{\mathrm{D}}(x_1)\cdots\hat{\mathrm{a}}_{\mathrm{D}}(x_n)\hat{\mathrm{a}}^{\dagger}_{\mathrm{D}}(x_{n+1})\cdots\hat{\mathrm{a}}^{\dagger}_{\mathrm{D}}(x_{n+m})\right)\right\}}{\mathrm{Tr}\left\{\mathrm{e}^{-\beta\hat{\mathrm{H}}_0}\hat{\mathrm{U}}(\hbar\beta,0)\right\}}. \tag{3.30}$$

Despite of many analogies between evolution in real time and in imaginary time, two differences should be mentioned here. The first one is quite a formal one: Whereas the real-time evolution operator $\hat{\mathrm{U}}(t,t_0)$ defined in Eq. (3.18) is unitary, i.e. $\hat{\mathrm{U}}(t,t_0)\hat{\mathrm{U}}^{\dagger}(t,t_0) = \mathbb{1}$, its imaginary-time analog $\hat{\mathrm{U}}(\tau,\tau_0)$ from Eq. (3.24) is not. This would mean that $\hat{\mathrm{O}}^{\dagger}(\tau) \neq \left(\hat{\mathrm{O}}(\tau)\right)^{\dagger}$. To bypass this inconsistency, we have to remind that τ should be treated like an imaginary variable, i.e. apart from acting on the operator itself, complex conjugation should also change the sign of τ. Thus instead of $\hat{\mathrm{U}}^{\dagger}(\tau,\tau_0)$, we

take as the complex conjugated imaginary-time evolution operator:

$$\overline{\hat{\mathrm{U}}(\tau,\tau_0)} \equiv \hat{\mathrm{U}}^\dagger(-\tau,-\tau_0). \tag{3.31}$$

With this definition, $\hat{\mathrm{U}}$ is unitary even in the ITF.

The second and very important difference between real and imaginary time comes along with the interpretation of the imaginary time as something like an inverse temperature. Thus, the evolution along the imaginary-time axis makes sense only in the interval $[0,\hbar\beta]$. As Eq. (3.28) is a function of imaginary-time differences, all of its time arguments lie within the interval $[-\hbar\beta,\hbar\beta]$. In Ref. [54] it is shown for the 2-point function $G(\tau_1,\tau_2)$ that it can be interpreted as a function $\tilde{G}(\tau)$ of one time variable $\tau=\tau_1-\tau_2$ with the property

$$\tilde{G}(\tau) = \pm\tilde{G}(\tau+\hbar\beta), \tag{3.32}$$

where the upper sign holds for bosonic particles whereas for fermions the anti-commutation relations imply a minus sign. Respecting this property, we can periodically extend the imaginary-time functions to times of any absolute value. This $\hbar\beta$-periodicity (anti-periodicity) becomes especially important when one transforms the functions into frequency space. While the real-time correlation functions depend on continuous frequencies, their imaginary-times analogs depend on discrete frequencies called Matsubara frequencies

$$\omega_n = \frac{n\pi}{\hbar\beta}, \tag{3.33}$$

where n is an integer. Eq. (3.32) implies that for bosons only frequencies with even n can survive in the Fourier transformation, while for fermions n has to be odd.

3.4 Closed-Time-Path Formalism (CTPF)

When using imaginary times, no effects appearing in real time like excitation spectra can be described, unless one re-rotates back to the real-time axis. This is usually done in frequency space, where the real-time functions appear as functions of continuous frequencies, while the imaginary-time functions transform into functions of a discrete set of Matsubara frequencies lying on the imaginary axis. Therefore, an analytic continuation from imaginary time to real time is uniquely possible only under the additional condition that we have infinitely many coinciding points with a limit point in the region of analyticity. In Ref. [54] it is shown how this procedure works for the 2-point function by replacing $i\omega_n \to -\omega \pm i\epsilon$. For more complicated functions depending on more than one frequency, however, this analytic continuation becomes very difficult. For the 3-point and 4-point functions, this problem is discussed in detail in Refs. [55–57].

If the Hamiltonian has an explicit dependence on real times, then the ITF is not applicable any longer, since it performs no time evolution along the real-time axis.

Therefore we would like to have a formalism keeping real times, but since our system is very large, the thermodynamic limit should also be taken into account, i.e. it should not be restricted to zero

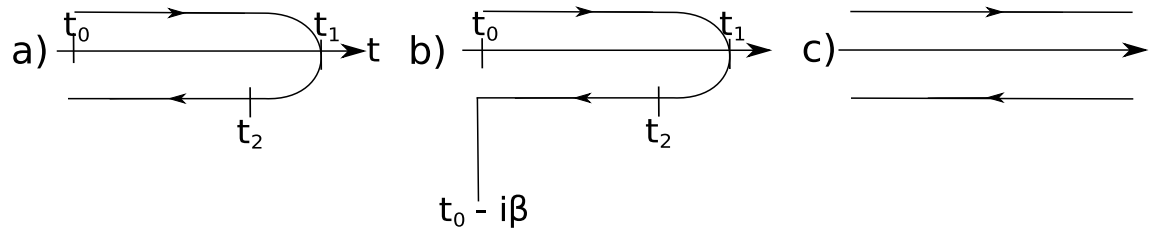

Figure 3.1: Contours of time evolution: a) Schwinger contour, b) interaction contour, c) Keldysh contour.

temperature. The CTPF presented now promises a description at both real time and finite temperature.

The Green's functions, which we want to calculate now, are again thermal averages with respect to a given initial density matrix $\hat{\rho}$, but now of a product of real-time-dependent Heisenberg operators. Instead of directly giving the definition, it is useful to see where it comes from. So let's have a look at the following operator product which has not any time-ordering:

$$\langle \hat{\mathrm{a}}_{\mathrm{H}}(t_1)\hat{\mathrm{a}}^{\dagger}_{\mathrm{H}}(t_2)\rangle_{\rho} \equiv \frac{\mathrm{Tr}\left\{\hat{\rho}\hat{\mathrm{a}}_{\mathrm{H}}(t_1)\hat{\mathrm{a}}^{\dagger}_{\mathrm{H}}(t_2)\right\}}{\mathrm{Tr}\left\{\hat{\rho}\right\}}. \tag{3.34}$$

We have suppressed spatial coordinates here. Inserting the relation (3.19) between the Heisenberg and the Dirac picture yields

$$\langle \hat{\mathrm{a}}_{\mathrm{H}}(t_1)\hat{\mathrm{a}}^{\dagger}_{\mathrm{H}}(t_2)\rangle_{\rho} = \frac{\mathrm{Tr}\left\{\hat{\rho}\ \hat{\mathrm{U}}(t_0,t_1)\hat{\mathrm{a}}_{\mathrm{D}}(t_1)\hat{\mathrm{U}}(t_1,t_2)\hat{\mathrm{a}}^{\dagger}_{\mathrm{D}}(t_2)\hat{\mathrm{U}}(t_2,t_0)\right\}}{\mathrm{Tr}\left\{\hat{\rho}\right\}}, \tag{3.35}$$

where $\hat{\mathrm{U}}$ is the Dirac time evolution operator defined in Eq. (3.18). We see that the time evolution goes forward from an initial time t_0 to the largest time (t_1 or t_2) and back to t_0, i.e. the time evolves along a closed path. Such a contour, which is shown in Fig. 3.1a), is sometimes called Schwinger contour as he first introduced it [58].

But we still have to consider the procedure of thermal averaging: If the system is initially in equilibrium, the density matrix in Eq. (3.35) reads

$$\hat{\rho} = \mathrm{e}^{-\beta\hat{\mathrm{H}}} = \sum_{X} \mathrm{e}^{-\beta E_X}|X\rangle\langle X| \tag{3.36}$$

with $|X\rangle$ being an eigenbasis to $\hat{\mathrm{H}}$ with eigenvalues E_X. The formalism, however, is not necessarily restricted to such a special initial condition.

Since we have no eigenbasis for the full Hamiltonian $\hat{\mathrm{H}}$, we are not able to calculate the Green's function in Eq. (3.35) perturbatively by only expanding the real-time evolution operator $\hat{\mathrm{U}}$. A possible way out would therefore be a mix between evolution in real *and* imaginary time [59]. This would lead to a contour shown in Fig. 3.1b). Instead we can also push the starting point of our time evolution in the infinite past. Then the part of the contour from t_0 to $t_0 - i\hbar\beta$ is infinitely far away from anything happening at finite times, so that it should make no difference, if the system was perturbed or unperturbed at the beginning. This means that we can substitute $\hat{\rho}$ by the density matrix $\hat{\rho}_0$ of the unperturbed system [60,61]. This density matrix will cause no difficulties, as a diagonal basis for

the unperturbed problem should be known. Since the time-evolution operator is unitary, we can also extend the contour from the largest time t_1 to the infinite future and end up with contour in Fig. 3.1c), which was first introduced by L. V. Keldysh [62]. Instead of Eq. (3.35), we now have correlations like

$$\langle \hat{a}_H(t_1)\hat{a}_H^\dagger(t_2)\rangle_0 \equiv \frac{\mathrm{Tr}\left\{e^{-\beta\hat{H}_0}\hat{a}_H(t_1)\hat{a}_H^\dagger(t_2)\right\}}{\mathrm{Tr}\left\{e^{-\beta\hat{H}_0}\right\}}, \tag{3.37}$$

which yields, when translated into the Dirac picture,

$$\langle \hat{a}_H(t_1)\hat{a}_H^\dagger(t_2)\rangle_0 = \frac{\mathrm{Tr}\left\{e^{-\beta\hat{H}_0}\hat{U}(-\infty,t_1)\hat{a}_D(t_1)\hat{U}(t_1,t_2)\hat{a}_D^\dagger(t_2)\hat{U}(t_2,-\infty)\right\}}{\mathrm{Tr}\left\{e^{-\beta\hat{H}_0}\right\}}. \tag{3.38}$$

The index 0 at the bracket means a thermal averaging with respect to the unperturbed Hamiltonian $\hat{H}_0$. Note that this does not mean that it is the correlation of the unperturbed system, because the influence of the perturbation is included in the time evolution.

We will now try to collect the different pieces of the time evolution into a single operator which performs a time evolution along the contour indicated in Fig. 3.1c). For this purpose, we introduce the identity $\mathbb{1} = \hat{U}(t_2,\infty)\hat{U}(\infty,t_2)$ in front of the second operator if $t_1 > t_2$ or the identity $\mathbb{1} = \hat{U}(t_1,\infty)\hat{U}(\infty,t_1)$ behind the first operator if $t_1 < t_2$. We find for $t_1 > t_2$:

$$\langle \hat{a}_H(t_1)\hat{a}_H^\dagger(t_2)\rangle_0 = \frac{\mathrm{Tr}\left\{e^{-\beta\hat{H}_0}\left(\hat{U}(-\infty,t_1)\hat{a}_D(t_1)\hat{U}(t_1,t_2)\hat{U}(t_2,\infty)\right)\left(\hat{U}(\infty,t_2)\hat{a}_D^\dagger(t_2)\hat{U}(t_2,-\infty)\right)\right\}}{\mathrm{Tr}\left\{e^{-\beta\hat{H}_0}\right\}}, \tag{3.39}$$

and for $t_1 < t_2$:

$$\langle \hat{a}_H(t_1)\hat{a}_H^\dagger(t_2)\rangle_0 = \frac{\mathrm{Tr}\left\{e^{-\beta\hat{H}_0}\left(\hat{U}(-\infty,t_1)\hat{a}_D(t_1)\hat{U}(t_1,\infty)\right)\left(\hat{U}(\infty,t_1)\hat{U}(t_1,t_2)\hat{a}_D^\dagger(t_2)\hat{U}(t_2,-\infty)\right)\right\}}{\mathrm{Tr}\left\{e^{-\beta\hat{H}_0}\right\}}. \tag{3.40}$$

In both equations the parentheses signalize that the operator product can be split into two parts. The right part can be interpreted as a time evolution from $-\infty$ to ∞ with the operator $\hat{a}_D^\dagger(t_2)$ appearing during the evolution, while the part on the left side evolves back from ∞ to $-\infty$ with $\hat{a}_D(t_1)$ lying on this path. We can write the evolution in the forward direction compactly by introducing the time-ordering operator $\hat{T}$. For the backward path the direction is inverted requiring the anti-time-ordering operator $\hat{\tilde{T}}$ for a compact writing. This allows for reducing both Eq. (3.39) and Eq. (3.40) to:

$$\langle \hat{a}_H(t_1)\hat{a}_H^\dagger(t_2)\rangle_0 = \frac{\mathrm{Tr}\left\{e^{-\beta\hat{H}_0}\hat{\tilde{T}}\left(\hat{U}(-\infty,\infty)\hat{a}_D(t_1)\right)\hat{T}\left(\hat{U}(\infty,-\infty)\hat{a}_D^\dagger(t_2)\right)\right\}}{\mathrm{Tr}\left\{e^{-\beta\hat{H}_0}\right\}}. \tag{3.41}$$

Now we define an operator $\hat{S}^\dagger\hat{S}$ where $\hat{S} \equiv \hat{U}(\infty,-\infty)$, which performs a time evolution along the

contour of Fig. 3.1c), i.e.

$$\hat{\mathrm{S}}^{\dagger}\hat{\mathrm{S}} = \exp\left\{-\frac{i}{\hbar}\int_{\mathrm{c}} \mathrm{d}t\ \hat{\mathrm{H}}_{1\mathrm{D}}(t)\right\}, \tag{3.42}$$

and a contour-ordering operator $\hat{\mathrm{T}}_{\mathrm{c}}$ collocating first the operators on the forward path in time-order while the backward ones are placed further left and brought to anti-time-order. This, however, requires that each operator is provided with an additional information about its path. Therefore we will denote operators that should appear on the forward path by the index + and the operators on the backward path with the index -. This enables us to transform the contour integration in (3.42) into a single integration from $t = -\infty$ to ∞. We only need to change the sign of the operators on the backward path, e.g.:

$$\hat{\mathrm{S}}^{\dagger}\hat{\mathrm{S}} = \exp\left\{-\frac{i}{\hbar}\int_{-\infty}^{\infty} \mathrm{d}t\left[\hat{\mathrm{H}}_{1+\mathrm{D}}(t) - \hat{\mathrm{H}}_{1-\mathrm{D}}(t)\right]\right\}. \tag{3.43}$$

The advantage of introducing path indices should become clear by using (3.42) in order to re-write Eq. (3.41). We simply get

$$\langle \hat{\mathrm{a}}_{\mathrm{H}}(t_1)\hat{\mathrm{a}}^{\dagger}_{\mathrm{H}}(t_2)\rangle_0 = \frac{\mathrm{Tr}\left\{\mathrm{e}^{-\beta\hat{\mathrm{H}}_0}\hat{\mathrm{T}}_{\mathrm{c}}\left(\hat{\mathrm{S}}^{\dagger}\hat{\mathrm{S}}\hat{\mathrm{a}}_{-\mathrm{D}}(t_1)\hat{\mathrm{a}}^{\dagger}_{+\mathrm{D}}(t_2)\right)\right\}}{\mathrm{Tr}\left\{\mathrm{e}^{-\beta\hat{\mathrm{H}}_0}\right\}}. \tag{3.44}$$

This shows us that the considered correlation $\langle \hat{\mathrm{a}}_{\mathrm{H}}(t_1)\hat{\mathrm{a}}^{\dagger}_{\mathrm{H}}(t_2)\rangle_0$ can be calculated by going into the Dirac picture and performing a time evolution along a closed path with the second operator lying on the forward and the first operator lying on the backward part of the contour. We will discuss other path-orderings of two operators in the next section. We will find that any physically relevant 2-point correlation can be expressed in terms of path-ordered Green's functions. This motivates us to generalize the definition to higher orders. We therefore define the CTPF Green's functions as thermal averages (with respect to $\hat{\mathrm{H}}_0$) of *path-ordered* operators in the Dirac picture. Furthermore, we multiply with the convenient prefactor i^{n+m-1}. Then we have with the abbreviation $x \equiv \{i, t\}$:

$$\begin{aligned} &G^{\pm\cdots\pm}(x_1, \cdots, x_n; x_{n+1}, \cdots, x_{n+m}) \\ &\equiv i^{n+m-1}\left\langle \hat{\mathrm{T}}_{\mathrm{c}}\left\{\hat{\mathrm{S}}^{\dagger}\hat{\mathrm{S}}\hat{\mathrm{a}}_{\pm\mathrm{D}}(x_1)\cdots\hat{\mathrm{a}}_{\pm\mathrm{D}}(x_n)\hat{\mathrm{a}}^{\dagger}_{\pm\mathrm{D}}(x_{n+1})\cdots\hat{\mathrm{a}}^{\dagger}_{\pm\mathrm{D}}(x_{n+m})\right\}\right\rangle_0. \end{aligned} \tag{3.45}$$

These 2^{n+m} functions for any n, m represent the basis of our further considerations.

3.5 Keldysh Rotation

Since the path index introduced in the section above doubles the time degrees of freedom, the CTPF Green's functions rapidly become very complex. A helpful simplification is the Keldysh rotation presented in this section. To this end we will first examine the easiest Green's functions of only one annihilation and one creation operator. By rotating them we find how to extract useful information out of them. The same can and will be done later for higher Green's functions. Taking the definition

(3.45) and translating back into the Heisenberg picture, we find the following four 2-point functions:

$$\begin{aligned}
G_{ij}^{++}(t,t') &= i\Big\langle \hat{\mathrm{T}}\left\{\hat{\mathrm{a}}_{i,\mathrm{H}}(t)\hat{\mathrm{a}}_{j,\mathrm{H}}^{\dagger}(t')\right\}\Big\rangle_0,\\
G_{ij}^{+-}(t,t') &= i\Big\langle \hat{\mathrm{a}}_{j,\mathrm{H}}^{\dagger}(t')\hat{\mathrm{a}}_{i,\mathrm{H}}(t)\Big\rangle_0,\\
G_{ij}^{-+}(t,t') &= i\Big\langle \hat{\mathrm{a}}_{i,\mathrm{H}}(t)\hat{\mathrm{a}}_{j,\mathrm{H}}^{\dagger}(t')\Big\rangle_0,\\
G_{ij}^{--}(t,t') &= i\Big\langle \hat{\tilde{\mathrm{T}}}\left\{\hat{\mathrm{a}}_{i,\mathrm{H}}(t)\hat{\mathrm{a}}_{j,\mathrm{H}}^{\dagger}(t')\right\}\Big\rangle_0.
\end{aligned} \tag{3.46}$$

These are the time-ordered Green's function, two Green's functions with a fixed order and the anti-time-ordered Green's function. They can be used to form a 2x2 matrix

$$\tilde{\boldsymbol{G}}_{ij}(t,t') \equiv \begin{pmatrix} G_{ij}^{++}(t,t') & G_{ij}^{+-}(t,t') \\ G_{ij}^{-+}(t,t') & G_{ij}^{--}(t,t') \end{pmatrix}. \tag{3.47}$$

Later we will recognize the meaning of the matrix (3.47) as a bilinear form acting on two currents, where each of them is a two-component vector.

For the concrete calculation of these functions we will have to apply a perturbative expansion. Therefore the functions in Eq. (3.46) will be expressed in the Dirac picture which allows for a power series expansion of the evolution operator (3.42) in a small parameter. To any expansion order n, we will find corrections to the Green's functions of the unperturbed system $G_{ij}^{(0)\pm\pm}(t,t')$ where $\hat{\mathrm{a}}_{\mathrm{D}}(t) = \hat{\mathrm{a}}_{\mathrm{H}}(t)$. These corrected Green's functions will be denoted by $G_{ij}^{(n)\pm\pm}(t,t')$. This perturbative procedure will be discussed in detail in the next chapter. But we should be aware of the fact that the relations between the different path-ordered Green's functions, which will be discussed now, do not only hold for the unperturbed or the full Green's functions, but also for any order of the later perturbative expansion [63].

If we use the the Heaviside step function $\theta(t)$, the time-ordered and the anti-time-ordered Green's functions defined in Eq. (3.46) can be expressed in terms of the other two functions:

$$G_{ij}^{++}(t,t') = \theta(t-t')G_{ij}^{-+}(t,t') + \theta(t'-t)G_{ij}^{+-}(t,t'), \tag{3.48}$$

$$G_{ij}^{--}(t,t') = \theta(t-t')G_{ij}^{+-}(t,t') + \theta(t'-t)G_{ij}^{-+}(t,t'). \tag{3.49}$$

From this follows the important equation

$$G_{ij}^{++}(t,t') + G_{ij}^{--}(t,t') = G_{ij}^{+-}(t,t') + G_{ij}^{-+}(t,t'). \tag{3.50}$$

This means that, without making use of the Heaviside function, we can always eliminate one of the four functions in Eq. (3.46) by expressing it in terms of the others. Therefore, the matrix (3.47) can be rotated in such a way that one matrix element vanishes. A rotation matrix which does this is:

$$Q \equiv \frac{1}{\sqrt{2}}\begin{pmatrix} 1 & 1 \\ 1 & -1 \end{pmatrix}. \tag{3.51}$$

This is called the **Keldysh rotation** which will be very useful for all our calculations. Note that

$QQ^{-1} = \mathbb{1}$. Let us still see what the rotation does on a vector:

$$Q \begin{pmatrix} A \\ B \end{pmatrix} = \frac{1}{\sqrt{2}} \begin{pmatrix} A+B \\ A-B \end{pmatrix}. \tag{3.52}$$

If the upper component of the original vector represents a quantity which depends on a time lying on the forward time path, while the lower component represents the same quantity at the same time but on the backward time path, the components of the rotated vector are called *classical* and *quantum* component:

$$O_{\mathrm{cl}}(t) \equiv \frac{1}{\sqrt{2}} \left[O_+(t) + O_-(t) \right], \qquad O_{\mathrm{q}}(t) \equiv \frac{1}{\sqrt{2}} \left[O_+(t) - O_-(t) \right]. \tag{3.53}$$

There are other choices of a convenient basis to handle the doubled time degrees of freedom in the CTPF. A discussion of them can be found in Ref. [64]. But let us stay in the Keldysh basis and see what happens to the Green's function matrix (3.47) when we rotate it: The non-vanishing elements are the following combinations:

$$\begin{aligned}
\frac{1}{2}\left(G_{ij}^{++}(t,t') - G_{ij}^{+-}(t,t') + G_{ij}^{-+}(t,t') - G_{ij}^{--}(t,t') \right) &= i\theta(t-t') \left\langle \left[\hat{\mathrm{a}}_{i,\mathrm{H}}(t), \hat{\mathrm{a}}_{j,\mathrm{H}}^\dagger(t') \right] \right\rangle_0 \equiv G_{ij}^{\mathrm{R}}(t,t'), \\
\frac{1}{2}\left(G_{ij}^{++}(t,t') - G_{ij}^{-+}(t,t') + G_{ij}^{+-}(t,t') - G_{ij}^{--}(t,t') \right) &= -i\theta(t'-t) \left\langle \left[\hat{\mathrm{a}}_{i,\mathrm{H}}(t), \hat{\mathrm{a}}_{j,\mathrm{H}}^\dagger(t') \right] \right\rangle_0 \equiv G_{ij}^{\mathrm{A}}(t,t'), \\
\frac{1}{2}\left(G_{ij}^{++}(t,t') + G_{ij}^{--}(t,t') + G_{ij}^{-+}(t,t') + G_{ij}^{+-}(t,t') \right) &= i \left\langle \left[\hat{\mathrm{a}}_{i,\mathrm{H}}(t), \hat{\mathrm{a}}_{j,\mathrm{H}}^\dagger(t') \right]_+ \right\rangle_0 \equiv A_{ij}(t,t').
\end{aligned} \tag{3.54}$$

We were able to write down two elements of the rotated matrix as a Heaviside step function times the thermal average of a commutator. The third non-vanishing element is the expectation value of an anticommutator $[\cdot,\cdot]_+$. We find that these commutator functions $G^{\mathrm{R,A}}$ are the retarded/advanced Green's functions [65,66]. They appear, e.g., in linear response theory, where the influence of a small time-dependent perturbation on a system in equilibrium is given by the retarded Green's function G^{R} of the *unperturbed* system.

The rotated matrix reads

$$\boldsymbol{G}_{ij}(t,t') \equiv Q \tilde{\boldsymbol{G}}_{ij}(t,t') Q^{-1} = \begin{pmatrix} A_{ij}(t,t') & G_{ij}^{\mathrm{R}}(t,t') \\ G_{ij}^{\mathrm{A}}(t,t') & 0 \end{pmatrix}. \tag{3.55}$$

In the following we refer to the structure of the matrix in Eq. (3.55) as the Keldysh structure. We will later explicitly see that the first hopping-corrected matrix turns out to have the same structure.

3.6 Generating Functionals

For all formalisms presented in the above section, there exist corresponding generating functionals from which the Green's functions can be derived. Their definition is quite similar to the partition function $\mathcal{Z}$ from Eq. (3.1) in equilibrium. In the ITF which deals with equilibrium system it is basically the same. The only difference is the inclusion of a so called source term in the Hamiltonian. It consists

of auxiliary external fields $j_i(t)$ and $j_i^*(t)$ coupled to a creation or annihilation operator. For bosonic systems, the $j_i(t)$'s and $j_i^*(t)$'s are complex functions called currents [67]. Of course, the currents in the ITF depend on imaginary time instead of real time. But from now on, let's specialize on the CTPF.

In the Heisenberg picture the source term $\hat{\mathrm{H}}_{\mathrm{Q}}(t)$ which is coupled to the Hamiltonian $\hat{\mathrm{H}}$ of the original system explicitly reads

$$\hat{\mathrm{H}}_{\mathrm{Q,H}}(t) = \sum_i \left[j_i(t)\hat{\mathrm{a}}_{i,\mathrm{H}}^\dagger(t) + j_i^*(t)\hat{\mathrm{a}}_{i,\mathrm{H}}(t) \right]. \tag{3.56}$$

Since the actual physical situation is described when the currents are set to zero, one may ask what it is needed for. Actually, there are two answers: First, this term allows for the construction of the Green's functions by taking functional derivatives with respect to the sources. We will see how this works in a few moments. Second we should remember from Chapter 2 that phase transitions involve symmetry breaking. Since a linear term in the Ginzburg-Landau free energy (2.29) destroys its symmetrical behavior (see Fig. 2.3), a standard method to deal with phase transitions is to add a so called conjugate or symmetry breaking field which is linearly coupled to the variable whose expectation value is taken as an order field [67]. So the physical reason for introducing currents is to break the symmetry of the Hamiltonian. Note that for an infinitely large system it remains broken even if we set the currents equal zero at the end.

In the CTPF the generating functional $\mathcal{Z}[j, j^*]$ for the Green's functions is usually defined in the Dirac picture, since the contour has been defined via the Dirac evolution operator $\hat{\mathrm{S}}^\dagger\hat{\mathrm{S}}$ from Eq. (3.42). Then the definition reads

$$\mathcal{Z}[j, j^*] \equiv \left\langle \hat{\mathrm{T}}_{\mathrm{c}} \left\{ \hat{\mathrm{S}}^\dagger \hat{\mathrm{S}} \mathrm{e}^{-\frac{i}{\hbar}\int_{\mathrm{c}} \mathrm{d}t \hat{\mathrm{H}}_{\mathrm{Q,D}}(t)} \right\} \right\rangle_0 = \left\langle \hat{\mathrm{T}}_{\mathrm{c}} \left\{ \hat{\mathrm{S}}^\dagger\hat{\mathrm{S}} \ \exp\Big[-\frac{i}{\hbar}\int_{-\infty}^{\infty} \mathrm{d}t \ \sum_i \Big(j_{i,+}(t)\hat{\mathrm{a}}_{i+,\mathrm{D}}^\dagger(t) \right. \right. \tag{3.57}$$

$$\left. \left. + j_{i,+}^*(t)\hat{\mathrm{a}}_{i+,\mathrm{D}}(t) - j_{i,-}(t)\hat{\mathrm{a}}_{i-,\mathrm{D}}^\dagger(t) - j_{i,-}^*(t)\hat{\mathrm{a}}_{i-,\mathrm{D}}(t) \Big) \Big] \right\} \right\rangle_0 .$$

As mentioned above, we can derive the contour-ordered Green's functions from $\mathcal{Z}[j, j^*]$. To this end we must take the functional derivatives with respect to the currents and set the currents to zero:

$$G^{\pm\cdots\pm}(i_1t_1, \cdots, i_{2n}t_{2n}) \sim \frac{\delta}{\delta j_{i_1,\pm}^*(t_1)} \cdots \frac{\delta}{\delta j_{i_n,\pm}^*(t_n)} \frac{\delta}{\delta j_{i_{n+1},\pm}(t_{n+1})} \cdots \frac{\delta}{\delta j_{i_{2n},\pm}(t_{2n})} \mathcal{Z}[j, j^*]\Big|_{j=j^*=0}. \tag{3.58}$$

To see that this is true we only have to compare the result of the functional derivatives with the definitions of the Green's functions in the Dirac picture given by Eq. (3.45). If we take care with the prefactor, we can exchange the proportionality sign in Eq. (3.58) by an equality sign: Each derivative with respect to j_+, j_+^* gives a factor $-i/\hbar$, while the derivatives with respect to j_-, j_-^* give a factor $+i/\hbar$.

With the generating functional of the Green's functions defined, we can now go a step further and construct the generating functional of the connected Green's functions. This is achieved by taking the logarithm of $\mathcal{Z}[j, j^*]$ and multiplying this with a convenient prefactor:

$$\mathcal{F}[j, j^*] \equiv -i \ln \mathcal{Z}[j, j^*]. \tag{3.59}$$

This functional is called $\mathcal{F}$ as in the ITF it is equal to the free energy, when the currents are set to zero. What is meant by *connected* Green's functions will get clearer in the next section, when we present a method to perturbatively calculate the quantity $\mathcal{F}[j, j^*]$.

A third generating functional that is to be mentioned is the Legendre transform of $\mathcal{F}[j, j^*]$ with respect to the currents. This functional is called the effective action and our final goal is to find an explicit expression for it. The effective action will no longer be a functional of the currents, but of its conjugates, the order fields. For this reason, it is an appropriate candidate for the Ginzburg-Landau description of the phase transition. Yet, we do not give a detailed definition of this functional, as we will extensively discuss it later.

At first we have to find a way how to calculate the generating functional $\mathcal{Z}$, which we cannot do exactly, since the Bose-Hubbard Hamiltonian from Eq. (2.1) cannot be diagonalized. Thus we rely on perturbation theory in order to be able to proceed.

4 Perturbation Expansion

Summarizing our previous considerations, we found three different time-dependent formalisms in which Green's functions or correlation functions are used to describe the system. As we would like to include both temperature and real-time dynamics in the description, we concentrate on the CTPF. Within this formalism we would like to derive the effective action as a Ginzburg-Landau functional, but to this end we first must have expressions for the functionals $\mathcal{Z}[j, j^*]$ from Eq. (3.57) and $\mathcal{F}[j, j^*]$ from Eq. (3.59). If we knew the Green's functions of the system, we could expand $\mathcal{Z}[j, j^*]$ in terms of them. But we have no basis in which the full Hamiltonian $\hat{\mathrm{H}}_{\mathrm{BH}}$ is diagonal, so it's not possible to calculate the Green's functions straightforwardly. With the introduction of the Dirac picture, however, we have already prepared the method which will allow for approximating them. To this end we must expand Eq. (3.57) not only in the currents, but also in the time evolution operator $\hat{\mathrm{S}}^\dagger\hat{\mathrm{S}}$.

4.1 Specifying the Perturbation

To proceed, we now must become more concrete and decide how to split the Bose-Hubbard Hamiltonian $\hat{\mathrm{H}}_{\mathrm{BH}}$ from Eq. (2.1). It is natural to take the local interaction as the solved part and the non-local hopping as a perturbation. With the definition of the occupation number operator $\hat{\mathrm{n}}_i \equiv \hat{\mathrm{a}}_i^\dagger\hat{\mathrm{a}}_i$, the local Hamiltonian $\hat{\mathrm{H}}_0$ can be written as

$$\hat{\mathrm{H}}_0 \equiv \sum_i \hat{\mathrm{H}}_i \equiv \sum_i \left(\frac{U}{2}\hat{\mathrm{n}}_i\left(\hat{\mathrm{n}}_i - 1\right) - \mu\hat{\mathrm{n}}_i \right). \tag{4.1}$$

This means that the Fock states $|N; n_1, \cdots, n_i, \cdots\rangle$ from second quantization provide a diagonal basis for $\hat{\mathrm{H}}_0$, i.e. they solve the $\hat{\mathrm{H}}_0$ eigenvalue problem. Here N represents the total particle number and n_i denotes an eigenvalue for $\hat{\mathrm{n}}_i$, i.e. the number of particles on site i.

Note that in our treatment, we can even generalize the local Hamiltonian to any Hamiltonian being a function f of $\hat{\mathrm{n}}_i$. So we could also write:

$$\hat{\mathrm{H}}_0 \equiv \sum_i f_i(\hat{\mathrm{n}}_i). \tag{4.2}$$

Such a generalization would be important if an external trap is considered. In our simple model, however, $\hat{\mathrm{H}}_i$ does not depend on the site index and on each lattice site we have:

$$\hat{\mathrm{H}}_i|N; n_1, \cdots, n_i, \cdots\rangle = E_{n_i}|N; n_1, \cdots, n_i, \cdots\rangle, \tag{4.3}$$

with the energy eigenvalues given by

$$E_{n_i} = \frac{U}{2} n_i(n_i - 1) - \mu n_i. \tag{4.4}$$

In the ground-state, all sites are occupied by the same number of particles. We refer to such a state in the short-hand notation $|n\rangle$ with eigenenergy E_n per site.

In the definition of $\mathcal{Z}$ in Eq. (3.57), a source term is coupled to the system. Although these source terms are local, we cannot include them in $\hat{\mathrm{H}}_0$, because they are linear in the creation or annihilation operators, so the Fock basis doesn't diagonalize them. We therefore include them in the perturbation. The whole perturbative part then reads in the Dirac picture:

$$\hat{\mathrm{H}}_1(t) \equiv \sum_{\mathrm{P}=\pm} \mathrm{P} \left[\sum_i \int_{-\infty}^{\infty} \mathrm{d}t \left(j_{i,\mathrm{P}}(t) \hat{\mathrm{a}}^\dagger_{i,\mathrm{P}}(t) + j^*_{i,\mathrm{P}}(t) \hat{\mathrm{a}}_{i,\mathrm{P}}(t) - \sum_j J_{ij} \hat{\mathrm{a}}^\dagger_{i,\mathrm{P}}(t) \hat{\mathrm{a}}_{j,\mathrm{P}}(t) \right) \right]. \tag{4.5}$$

Here and in the following the index D has been dropped as we will exclusively work within the Dirac picture. Then the evolution operator $\hat{\mathrm{S}}^\dagger \hat{\mathrm{S}}$ is defined by inserting Eq. (4.5) into Eq. (3.42). With that definition, we can write:

$$\mathcal{Z}[j, j^*] = \langle \hat{\mathrm{T}}_\mathrm{c} \hat{\mathrm{S}}^\dagger \hat{\mathrm{S}} \rangle_0. \tag{4.6}$$

This equation formally deviates from Eq. (3.57), because we now have included the source terms into the perturbative part.

We should note that the splitting introduced in Eq. (4.5) differs from the common one in quantum field theory, where the non-interacting particles are taken as the solved problem and the interaction as a perturbation. This will have consequences, since the usually applied Wick theorem holds only for systems where $\hat{\mathrm{H}}_0$ is quadratic in the creation and annihilation operators $\hat{\mathrm{a}}^\dagger_i$ and $\hat{\mathrm{a}}_i$. In the following sections we will see how to tackle this problem, but before we should discuss the validity of our ansatz.

Up to now, we have justified our choice of the perturbation by practical reasons. But we can only expect good results if the Fock states approximate well the real physical states. This should be true, as long as the off-diagonal parts that we have thrown in the perturbation Hamiltonian $\hat{\mathrm{H}}_1(t)$ from Eq. (4.5) are small compared with $\hat{\mathrm{H}}_0$ from Eq. (4.1). The source term, though at first only a technical tool, will gain importance after transforming from the currents to the order parameter in the next chapter. As discussed in Section 2.2, the order parameter must be a quantity which vanishes in the normal phase, thus at the onset of superfluidity it is small. However, to be able to describe symmetry-breaking, we will have to take into account all orders up to the fourth one.

Considering the kinetic part as a perturbation seems to be more problematic, since we want to describe a long-range correlation effect. But we should note that according to well accepted Monte-Carlo data [30], in a three-dimensional lattice the transition from the MI phase to the SF phase takes place at a critical value $J/U \approx 0.03$ or even lower, depending on the value of μ/U. Thus a hopping-expansion suggests itself. We can still go one step further and consider the scaling of the Bose-Hubbard Hamiltonian with dimension [31,68]. Ref. [68] argues that one must distinguish between non-condensed bosons sitting on one site and being able to hop to an adjacent site, and condensed bosons, which are

not localized anymore. For the energy to remain finite, the hopping matrix element has to be scaled with $J \to J/\sqrt{z}$, if there is no condensate, while in the presence of condensed bosons the scaling $J \to J/z$ must be applied. Here $z = 2d$ is the number of nearest neighbors in the d-dimensional lattice. Under this scaling rule, however, a hopping expansion without loops, i.e. without two simultaneous hopping processes between adjacent sites, becomes exact in the limit $z \to \infty$. To see that, we must recognize that there are z possibilities for a hopping from one given site to another, thus the energy for a single hopping process must be multiplied with z. This cancels the denominator from the scaled hopping strength J/z. For a loop from one given site to another and back, there are still only z possibilities, but since there are two hopping processes, we now have z^2 in the denominator. Thus for $z \to \infty$ the loop contribution to the total energy vanishes.

In high dimensions (like $d = 3$), our choice of the perturbative part in Eq. (4.5) is thus not only a practical one, but also physically justified.

4.2 Dyson Series

The following perturbative approach is based on a Taylor expansion of the generating functional $\mathcal{F}[j, j^*]$ defined in Eq. (3.59) with respect to the currents and to the hopping parameter. For temporal and spatial constant order parameters at $T = 0$, this has been done in Ref. [69]. In Ref. [70], this procedure has been applied within the ITF.

It seems to be helpful to postpone the expansion of $\mathcal{F}[j, j^*]$ and first take a look at the expansion of $\mathcal{Z}[j, j^*]$. This expansion can be done straightforwardly, but it leads, as we will see, to large and confusing formulas. But when we understand the differences between the generating functionals $\mathcal{Z}[j, j^*]$ and $\mathcal{F}[j, j^*]$, we find the expansion of the latter functional by selecting special terms from the expansion of $\mathcal{Z}[j, j^*]$, which can be done in an easy graphical way.

From Eq. (4.6) we see that $\mathcal{Z}[j, j^*]$ is nothing else than the thermal average of the time evolution operator along the whole contour, so we take a look back to the derivation of a compact expression for $\hat{\mathrm{U}}(t, t')$ in Eqs. (3.16), (3.17), and (3.18). Now we can do the opposite: Having a closed formula for the CTPF evolution operator, i.e. $\hat{\mathrm{T}}_\mathrm{c}\hat{\mathrm{S}}^\dagger\hat{\mathrm{S}}$, we expand it by taking the derivatives with respect to the currents and the hopping parameter. In Eq. (3.58) we have already seen that the derivatives of $\mathcal{Z}[j, j^*]$ with respect to the currents, evaluated at $j = j^* = 0$, are the Green's functions (times $\pm i/\hbar$). So we have:

$$\mathcal{Z}[j, j^*](J) = \sum_{m=0,m'=0}^{\infty} \frac{1}{(m!)(m'!)} \sum_{i_1,\cdots,i_{m+m'} \in \{\text{site indices}\}} \sum_{P_1,\cdots,P_{m+m'}=\pm} \int_{-\infty}^{\infty} \mathrm{d}t_{i_1} \cdots \int_{-\infty}^{\infty} \mathrm{d}t_{i_{m+m'}}$$
$$\alpha^{(m+m')}_{i_1,\mathrm{P}_1;\cdots;i_{m+m'},\mathrm{P}_{m+m'}}(J) j_{i_1,\mathrm{P}_1}(t_{i_1}) \cdots j_{i_m,\mathrm{P}_m}(t_{i_m}) j^*_{i_{m+1},\mathrm{P}_{m+1}}(t_{i_{m+1}}) \cdots j^*_{i_{m+m'},\mathrm{P}_{m+m'}}(t_{i_{m+m'}}) \tag{4.7}$$

with the expansion coefficients

$$\alpha^{(m+m')}_{i_1,\mathrm{P}_1;\cdots;i_{m+m'},\mathrm{P}_{m+m'}}(J) \equiv \tag{4.8}$$
$$\left. \frac{\delta^{m+m'} \mathcal{Z}[j, j^*](J)}{\delta j_{i_1,\mathrm{P}_1}(t_{i_1}) \cdots \delta j_{i_m,\mathrm{P}_m}(t_{i_n}) \delta j^*_{i_{m+1},\mathrm{P}_{m+1}}(t_{i_{m+1}}) \cdots \delta j^*_{i_{m+m'},\mathrm{P}_{m+m'}}(t_{i_{m+m'}})} \right|_{j=j^*=0} =$$

$$= \left\langle \hat{\mathrm{T}}_{\mathrm{c}} \left\{ \hat{\mathrm{a}}^{\dagger}_{i_1,\mathrm{P}_1}(t_{i_1}) \cdots \hat{\mathrm{a}}^{\dagger}_{i_m,\mathrm{P}_m}(t_{i_m}) \hat{\mathrm{a}}_{i_{m+1},\mathrm{P}_{m+1}}(t_{i_{m+1}}) \cdots \hat{\mathrm{a}}_{i_{m+m'},\mathrm{P}_{m+m'}}(t_{i_{m+m'}}) \right.\right.$$
$$\left.\left. \times \exp\left[\frac{i}{\hbar} \sum_{ij} \sum_{\mathrm{P}=\pm} \mathrm{P} \int_{-\infty}^{\infty} J_{ij} \hat{\mathrm{a}}^{\dagger}_{i,\mathrm{P}}(t) \hat{\mathrm{a}}_{j,\mathrm{P}}(t) \mathrm{d}t \right] \right\} \right\rangle_0 (-\frac{i}{\hbar}\mathrm{P}_1) \cdots (-\frac{i}{\hbar}\mathrm{P}_{m+m'}).$$

Up to now we have only expanded the source term in the evolution operator, so we still have to perform an expansion of these coefficients with respect to J around $J = 0$:

$$\alpha^{(m+m')}_{i_1,\mathrm{P}_1;\cdots;i_{m+m'},\mathrm{P}_{m+m'}}(J) = \tag{4.9}$$
$$\sum_{n=0}^{\infty} \frac{1}{n!} \sum_{k_1 \cdots k_{2n}} \left(\frac{\partial^n}{\partial J_{k_1 k_{n+1}} \cdots \partial J_{k_n k_{2n}}} \alpha^{(m+m')}_{i_1,\mathrm{P}_1;\cdots;i_{m+m'},\mathrm{P}_{m+m'}}(J) \Big|_{J=0} \right) J_{k_1 k_{n+1}} \cdots J_{k_n k_{2n}} = \sum_{n=0}^{\infty} \frac{1}{n!} \sum_{k_1 \cdots k_{2n}}$$
$$\times \sum_{\mathrm{P}_{k_1} \cdots \mathrm{P}_{k_n} = \pm} \int_{-\infty}^{\infty} \mathrm{d}t_{k_1} \cdots \int_{-\infty}^{\infty} \mathrm{d}t_{k_n} J_{k_1 k_{n+1}} \cdots J_{k_n k_{2n}} (\frac{i}{\hbar}\mathrm{P}_{k_1}) \cdots (\frac{i}{\hbar}\mathrm{P}_{k_n}) (-\frac{i}{\hbar}\mathrm{P}_1) \cdots (-\frac{i}{\hbar}\mathrm{P}_{m+m'})$$
$$\left\langle \hat{\mathrm{T}}_{\mathrm{c}} \left\{ \hat{\mathrm{a}}^{\dagger}_{i_1,\mathrm{P}_{i_1}}(t_{i_1}) \cdots \hat{\mathrm{a}}_{i_{m+m'},\mathrm{P}_{i_{m+m'}}}(t_{i_{m+m'}}) \hat{\mathrm{a}}^{\dagger}_{k_1,\mathrm{P}_{k_1}}(t_{k_1}) \hat{\mathrm{a}}_{k_{n+1},\mathrm{P}_{k_1}}(t_{k_1}) \cdots \hat{\mathrm{a}}^{\dagger}_{k_n,\mathrm{P}_{k_n}}(t_{k_n}) \hat{\mathrm{a}}_{k_{2n},\mathrm{P}_{k_n}}(t_{k_n}) \right\} \right\rangle_0 .$$

Note that the thermal averages in this expression are the *unperturbed* Green's functions as the operators are defined in the Dirac picture. They can be easily calculated in the Fock basis. We immediately recognize that all the terms in the sum vanish where the numbers of annihilation operators on each site does not equal the number of creation operators. This automatically implies $m = m'$ and restricts the sum over the originally $2m + 2n$ site indices in each term to a sum over only $m + n$ indices, e.g. those belonging to creation operators, plus all the permutations that can be done to the other $m + n$ indices. We finally get

$$\mathcal{Z}[j, j^*](J) = \sum_{m,n=0}^{\infty} \frac{1}{(m!)^2 n!} \sum_{k_1 \cdots k_n, i_1 \cdots i_m} \sum_{\{k_{n+1} \cdots k_{2n}, i_{m+1} \cdots i_{2m}\} \in \{k_1 \cdots k_n, i_1 \cdots i_m\}} \sum_{\mathrm{P}_{k_1} \cdots \mathrm{P}_{k_n}, \mathrm{P}_{i_1} \cdots \mathrm{P}_{i_{2m}} = \pm}$$
$$\int_{-\infty}^{\infty} \mathrm{d}t_{i_1} \cdots \int_{-\infty}^{\infty} \mathrm{d}t_{2n} \int_{-\infty}^{\infty} \mathrm{d}t_{k_1} \cdots \int_{-\infty}^{\infty} \mathrm{d}t_{k_m} (\frac{i}{\hbar}\mathrm{P}_{k_1}) \cdots (\frac{i}{\hbar}\mathrm{P}_{k_n}) (-\frac{i}{\hbar}\mathrm{P}_{i_1}) \cdots (-\frac{i}{\hbar}\mathrm{P}_{i_{2m}})$$
$$\times \left\langle \hat{\mathrm{T}}_{\mathrm{c}} \left\{ \hat{\mathrm{a}}^{\dagger}_{i_1,\mathrm{P}_{i_1}}(t_{i_1}) \cdots \hat{\mathrm{a}}_{i_{2m},\mathrm{P}_{i_{2m}}}(t_{i_{2m}}) \hat{\mathrm{a}}^{\dagger}_{k_1,\mathrm{P}_{k_1}}(t_{k_1}) \hat{\mathrm{a}}_{k_{n+1},\mathrm{P}_{k_1}}(t_{k_1}) \cdots \hat{\mathrm{a}}^{\dagger}_{k_n,\mathrm{P}_{k_n}}(t_{k_n}) \hat{\mathrm{a}}_{k_{2n},\mathrm{P}_{k_n}}(t_{k_n}) \right\} \right\rangle_0$$
$$\times j_{i_1,\mathrm{P}_{i_1}}(t_{i_1}) \cdots j_{i_m,\mathrm{P}_{i_m}}(t_{i_m}) j^*_{i_{m+1},\mathrm{P}_{i_{m+1}}}(t_{i_{m+1}}) \cdots j^*_{i_{2m},\mathrm{P}_{i_{2m}}}(t_{i_{2m}}) J_{k_1 k_{n+1}} \cdots J_{k_n k_{2n}}. \tag{4.10}$$

As this formula looks very confusing, it would be nice to find diagrammatic rules instead. The usual way to do this is to apply Wick's theorem for a decomposition of the Green's functions. But as already mentioned above, the requirements of this theorem are not complied. So another technique is necessary in order to treat the problem diagrammatically. With the help of the linked-cluster theorem, we can reduce the number of terms to only those made up of connected Green's functions or cumulants [67,71]. It is possible to decompose them into local cumulants which was done some time ago for the Fermi-Hubbard model [72] and recently adopted to the Bose-Hubbard model [73]. We will see how this works in the following sections.

4.3 Linked-Cluster Theorem

The cumulant decomposition is based on the idea to expand $\mathcal{F}[j, j^*]$ rather than $\mathcal{Z}[j, j^*]$. As our final goal will be the derivation of the effective action, we don't even need $\mathcal{Z}[j, j^*]$. The big advantage that we have when we expand $\mathcal{F}[j, j^*]$, is the fact that the linked-cluster theorem can be applied [67].

To understand the meaning of this theorem, first a definition of what a cluster is seems advisable: Associated with a cluster C is a cluster Hamiltonian $\hat{\mathrm{H}}_\mathrm{C}$ which consists of some parts of the total Hamiltonian $\hat{\mathrm{H}} = \hat{\mathrm{H}}_0 + \hat{\mathrm{H}}_1$. All terms in the perturbative expansion of a physical quantity O which are given only by this cluster Hamiltonian build a cluster C. Each cluster contributes a unique weight $W(C)$ to the expansion of O.

Now we call a cluster "linked", if there are no disjoint hoppings and if all source terms are connected by hopping terms. On the other hand, a disconnected cluster is a cluster that can be written as the disjoint union of nonempty sub-clusters, e.g. A and B with the cluster Hamiltonians $\hat{\mathrm{H}}_\mathrm{A}$ and $\hat{\mathrm{H}}_\mathrm{B}$, respectively. Denoting the Hilbert spaces of these Hamiltonian by ε_A and ε_B, $C \equiv A \bigcup B$ is a disconnected cluster if there are at least two nonempty sub-clusters with $\varepsilon_\mathrm{A} \bigcap \varepsilon_\mathrm{B} = \emptyset$.

Let's be more concrete: In our case the Hamiltonian contains sums over all site indices. If we take only parts of these sums, e.g. if we restrict the Hamiltonian to only a few site indices and make the same expansion as done before in Eq. (4.10) with the whole Hamiltonian, then we get a cluster contribution to $\mathcal{Z}[j, j^*]$. If we take only one single site i, we get a cluster of currents flowing in and out of site i. It is, per definition, linked. If we add a next neighbor site j to the expansion, the expansion would include the same terms as before, with currents on one site, but also terms with currents on both sites i *and* j. These sub-clusters can appear either accompanied by (at least) a hopping between both sites, which means they are linked, or without a hopping, which means they are unlinked.

The linked-cluster theorem now states that because of the uniqueness of the weights $W(C)$ and the additivity property of extensive quantities the weights of disconnected clusters in the expansion of an extensive quantity have to be zero [71]. From thermodynamics we know that the free energy is extensive (because of the logarithm) while the partition function is not (because of the exponential). This holds as well in our case with the generalization of those thermodynamical quantities to generating functionals, because their mathematical structure is the same.

Therefore we can, with the help of this statement, expand the free-energy-like functional $\mathcal{F}[j, j^*] \equiv -i \ln \mathcal{Z}[j, j^*]$ by taking the expansion of $\mathcal{Z}[j, j^*]$ from Eq. (4.10) and sorting out unlinked terms. In the remaining terms we have to substitute the Green's function by the so called *connected* Green's functions or cumulants. We will see how to do this in the next section.

4.4 Cumulant Decomposition

To see the relation between the connected Green's functions and the Green's functions, we first consider a system without hopping. In this case, we find out that $\ln \mathcal{Z}[j,j^*]|_{J=0}$ is a sum of local quantities:

$$\begin{aligned} -i \ln \mathcal{Z}[j,j^*]\Big|_{J=0} &= -i \ln \left\langle \hat{\mathrm{T}}_\mathrm{c} \exp\left\{ -i \sum_{\mathrm{P}=\pm} \mathrm{P} \int_{-\infty}^{\infty} \mathrm{d}t \sum_i \left[j_{i,\mathrm{P}}(t) \hat{\mathrm{a}}^\dagger_{i,\mathrm{P}}(t) + j^*_{i,\mathrm{P}}(t) \hat{\mathrm{a}}_{i,\mathrm{P}}(t) \right] \right\} \right\rangle_0 \\ &= -i \sum_i \ln \left\langle \hat{\mathrm{T}}_\mathrm{c} \exp\left\{ -i \sum_{\mathrm{P}=\pm} \mathrm{P} \int_{-\infty}^{\infty} \mathrm{d}t \left[j_{i,\mathrm{P}}(t) \hat{\mathrm{a}}^\dagger_{i,\mathrm{P}}(t) + j^*_{i,\mathrm{P}}(t) \hat{\mathrm{a}}_{i,\mathrm{P}}(t) \right] \right\} \right\rangle_0 . \end{aligned} \tag{4.11}$$

From this we can directly see what the linked-cluster theorem states: The expansion of this functional consists only of linked clusters, which in this case are local quantities. Functional derivatives with respect to currents on different sites vanish.

The connected Green's functions making up the expansion of $\mathcal{F}[j,j^*]|_{J=0}$ are related to the Green's functions by a decomposition formula that can easily be derived by taking the functional derivatives of $\mathcal{Z}[j,j^*]|_{J=0}$ and comparing it with the same derivatives of $\ln \mathcal{Z}[j,j^*]|_{J=0}$. One will find that a Green's function of n variables (or more accurately: sets of variables $\{\mathrm{P},t,i\}$) decomposes into the corresponding cumulant with the same n variables plus all possible products of lower cumulants having altogether the same n variables again.

As we have set the hopping to zero, the unperturbed cumulants denoted by C_i can be expressed in terms of the unperturbed Green's functions $G^{(0)}$. Because of the $U(1)$-symmetry, these vanish for unequal numbers of creation and annihilation operators on each site which reduces the number of terms in the decomposition. For the 2-point functions, we have for example:

$$C_i^{\mathrm{P}_1\mathrm{P}_2}(t_1,t_2) = \delta_{ij} G_{ij}^{\mathrm{P}_1\mathrm{P}_2(0)}(t_1,t_2). \tag{4.12}$$

Apart from this, in the following we will need only one more decomposition:

$$\begin{aligned} C_i^{\mathrm{P}_1\mathrm{P}_2\mathrm{P}_3\mathrm{P}_4}(t_1,t_2;t_3,t_4) =& \delta_{ij}\delta_{jk}\delta_{kl} G_{ijkl}^{\mathrm{P}_1\mathrm{P}_2\mathrm{P}_3\mathrm{P}_4(0)}(t_1,t_2;t_3,t_4) \\ & - i C_i^{\mathrm{P}_1\mathrm{P}_3}(t_1,t_3) C_i^{\mathrm{P}_2\mathrm{P}_4}(t_2,t_4) - i C_i^{\mathrm{P}_1\mathrm{P}_4}(t_1,t_4) C_i^{\mathrm{P}_2\mathrm{P}_3}(t_2,t_3), \end{aligned} \tag{4.13}$$

where $G_{ijkl}^{\mathrm{P}_1\mathrm{P}_2\mathrm{P}_3\mathrm{P}_4,(0)}(t_1,t_2;t_3,t_4)$ was defined in Eq. (3.45). Note the prefactor i^{n+m-1} there which was included in the definitions (4.12) and (4.13). This explains the appearance of the factor i in front of the decompositions in Eq. (4.13).

4.5 Diagrammatic Rules

Now the expansion of the system can easily be depicted diagrammatically. To this end we make the following definitions:

- A cumulant $C_i^{\mathrm{P}_1\cdots\mathrm{P}_{2n}}(t_1,\cdots,t_{2n})$ is represented by a black circle with n entering legs and n

exiting legs. For example we have for $n = 1$:

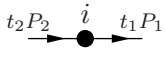

$$= C_i^{\mathrm{P}_1\mathrm{P}_2}(t_1, t_2). \tag{4.14}$$

- The currents $j_{i,\mathrm{P}_2}(t_2)$ or $j^*_{i,\mathrm{P}_1}(t_1)$ are represented by black squares with one leg, entering or exiting, respectively. As we can see in Eq. (4.10), each derivative with respect to a current on the backward path brings down a minus sign, so we include this sign into the definition of the graph:

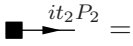

$$= \mathrm{P}_2 j_{i,\mathrm{P}_2}(t_2) \qquad , \qquad$$

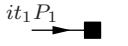

$$= \mathrm{P}_1 j^*_{i,\mathrm{P}_1}(t_1). \tag{4.15}$$

- Multiplying a cumulant with currents, integrating over the continuous variables, i.e. the time, and summing over discrete variables, i.e. site and path indices, is represented by combining the corresponding graphs. With this we obtain "closed" graphs with no indices, as for instance:

$$= \sum_{ij} \sum_{\mathrm{P}_1,\mathrm{P}_2} \mathrm{P}_1\mathrm{P}_2 \int_{-\infty}^{\infty} \mathrm{d}t_1 \int_{-\infty}^{\infty} \mathrm{d}t_2 \; \delta_{ij} C_i^{\mathrm{P}_1\mathrm{P}_2}(t_1, t_2) j^*_{i,\mathrm{P}_1}(t_1) j_{j,\mathrm{P}_2}(t_2). \tag{4.16}$$

This diagram makes up the expansion up to second order in the currents of a system without hopping.

When we now add a hopping term to the Hamiltonian and expand $\mathcal{F}[j, j^*](J)$ only in the currents, we get terms which are made up of *perturbed* cumulants, just like the expansion of $\mathcal{Z}[j, j^*](J)$ only in the currents in Eq. (4.7), was made up of *perturbed* Green's functions. These perturbed cumulants are not necessarily local and a decomposition can involve averages like $\langle \hat{\mathrm{a}}_{\mathrm{H}}(t) \rangle_0$ (which obviously are zero without hopping).

However, we still have to expand the time-evolution operator with respect to the hopping and after that, only the *unperturbed* cumulants will remain. These are local, but they can be linked to each other via a hopping.

If we want to see this explicitly, we can go back to Eq. (4.7) and replace the Green's functions there by the connected Green's functions. They are composed by various Green's functions. Next we expand the hopping. Then we get an expansion in terms of unperturbed Green's function. We re-write them in terms of unperturbed cumulants, and finally find in each order, what we already know from the linked-cluster theorem without any computation, namely that the weight of all the terms where at least one cumulant stays unlinked to the others, is zero.

- In our diagrammatic approach, we therefore have to add the possibility of linking cumulants by a hopping. This is done by an internal line between two cumulants. The respective times associated with the hoppings are always integrated and the path indices are always summed.

Associated with the path index is a prefactor $\pm$ of the hopping term. For instance we obtain:

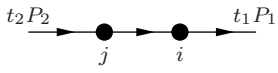

$$= \tilde{J}_{ij} \sum_{\mathrm{P}} \mathrm{P} \int_{-\infty}^{\infty} \mathrm{d}t \; C_i^{\mathrm{P}_1 \mathrm{P}}(t_1, t) C_j^{\mathrm{P}\mathrm{P}_2}(t, t_2) \tag{4.17}$$

Here we have defined the dimensionless matrix element $\tilde{J}_{ij} \equiv J_{ij}/J$ where J is the hopping strength. This will allow us a better bookkeeping at a later stage.

- For the whole expansion of $\mathcal{F}[j, j^*]$, we need the sum of all topologically nonequivalent connected diagrams. Each diagram must be closed. We still have to compare the diagram with Eq. (4.10) in order to get the right number of i and $\hbar$ prefactors. Finally, another prefactor called *symmetry factor* has to be taken into account.

The last point requires a further discussion: Let's pick one connected diagram. If we interchange two internal lines in the diagram, we might get either the same diagram representing the same decomposition or a similar diagram which, however, represents another term in the decomposition. The same is true when we interchange two entering or two exiting external lines or two site indices. If we assume that all these permutations lead to different terms, the prefactor $\frac{1}{(n!)(m!)^2}$ in the expansion (4.10) would be canceled in the diagrammatic scheme. In truth we now have overcounted all diagrams which appear repeatedly in the decomposition. To compensate this, we have to divide through the symmetry factor which is the number of times that one permutation of internal lines, entering or exiting lines or vertices gives the same diagram.

If there are, e.g., M external lines entering (or exiting) one vertex, any of the $M!$ permutations of those lines will lead to the same diagram. This is also true for M internal lines in the same direction. The third symmetry to be considered is the symmetry between equivalent vertices. Equivalent means that the number of any type of lines (entering, exiting, internal, external) is the same at these vertices. For M vertices with such a symmetry we would get a factor $M!$ as well. If we have any doubts with the symmetry factor, we can check it by writing down and counting all permutations in the decomposition.

4.6 Expansion in the MI Phase

As the number of n-point functions in the CTPF increases exponentially with every order, we will begin our problem slowly: We know that there is a phase transition, so the behavior of the gas should strongly depend on whether we are in the MI or the SF phase. Remember that in the latter phase, the $U(1)$-symmetry is broken and even in equilibrium the order fields differ from zero. For that reason we have to take into account terms of at least fourth order in the order parameter when we want to deal with the superfluid phase. The MI system, however, can be well described only by the knowledge of the 2-point function. Therefore, we will restrict ourselves at first to the MI case. When we have seen how the formalism works in this relatively easy case, it will be not too difficult to extend our considerations afterwards to the superfluid case.

This means, we now have to expand $\mathcal{F}[j, j^*](J)$ up to second order in the currents and to first order

in the hopping. We therefore denote our result $\mathcal{F}^{(2,1)}$. It reads

$$\mathcal{F}^{(2,1)}[j,j^*] = \frac{1}{\hbar^2}\Bigg\{ + \frac{J}{\hbar} \Bigg\}. \tag{4.18}$$

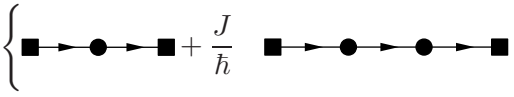

Note that the prefactor $-i$ from the definition of $\mathcal{F}$ in Eq. (3.59) and the i's coming from the expansion in Eq. (4.10) are killed by the prefactor in the definition of the Green's functions in Eq. (3.45).

We now have put a lot of work into finding an easy way of obtaining and writing down this expansion in a diagrammatic way. So it may seem strange to go back from these nice graphs to big formulas, but we still have to see how the Legendre transformation of this functional works in detail, so we are not yet at the end.

As we don't have to distinguish between the connected Green's functions and the Green's functions here due to $G_{ij}^{\mathrm{P_1P_2}(0)}(t_1,t_2) = \delta_{ij} G_{ij}^{\mathrm{P_1P_2}(0)}(t_1,t_2) = \ C_i^{\mathrm{P_1P_2}}(t_1,t_2)$, the kernel in Eq. (4.18) delivers us a formula for the first hopping-corrected contour-ordered Green's functions:

$$G_{ij}^{\mathrm{P_1P_2}(1)}(t_1,t_2) \equiv G_{ij}^{\mathrm{P_1P_2}(0)}(t_1,t_2) + \frac{J_{ij}}{\hbar} \sum_{\mathrm{P}} \mathrm{P} \int_{-\infty}^{\infty} \mathrm{d}t\ G_{ii}^{\mathrm{P_1P}(0)}(t_1,t) G_{jj}^{\mathrm{PP_2}(0)}(t,t_2). \tag{4.19}$$

We can interpret these Green's functions as the elements of a 2x2 matrix $\tilde{\boldsymbol{G}}_{ij}^{(1)}(t_1,t_2)$ like the one defined in Eq. (3.47). It acts on the currents which are now written as 2-component vectors. The corresponding signs $\mathrm{P}_{1,2}$ can be included in each vector by putting a minus sign in front of the lower component. We can then write:

$$\begin{aligned}
&\mathcal{F}^{(2,1)}[j,j^*] = \\
&\frac{1}{\hbar^2} \sum_{ij} \int_{-\infty}^{\infty} \mathrm{d}t_1 \int_{-\infty}^{\infty} \mathrm{d}t_2 \left\{ \left(j_{+,i}^*(t_1), -j_{-,i}^*(t_1) \right) \begin{pmatrix} G_{ij}^{++(1)}(t_1,t_2) & G_{ij}^{+-(1)}(t_1,t_2) \\ G_{ij}^{-+(1)}(t_1,t_2) & G_{ij}^{--(1)}(t_1,t_2) \end{pmatrix} \begin{pmatrix} j_{+,j}(t_2) \\ -j_{-,j}(t_2) \end{pmatrix} \right\} \\
&\equiv \frac{1}{\hbar^2} \sum_{ij} \int_{-\infty}^{\infty} \mathrm{d}t_1 \int_{-\infty}^{\infty} \mathrm{d}t_2\ \tilde{\boldsymbol{j}}_i^*(t_1) \tilde{\boldsymbol{G}}_{ij}^{(1)}(t_1,t_2) \tilde{\boldsymbol{j}}_j(t_2)
\end{aligned} \tag{4.20}$$

with the definition of the vector currents

$$\tilde{\boldsymbol{j}}_i(t) \equiv \begin{pmatrix} j_{+,i}(t) \\ -j_{-,i}(t) \end{pmatrix}, \qquad \tilde{\boldsymbol{j}}_i^*(t) \equiv \left(j_{i,+}^*(t), -j_{i,-}^*(t) \right). \tag{4.21}$$

Now we perform the Keldysh rotation (3.51), i.e. we insert $\mathbb{1} = QQ^{-1}$ in front and behind of the matrix. We then find the rotated currents $Q\boldsymbol{j}$ and $\boldsymbol{j}^* Q^{-1}$, according to (3.53):

$$\boldsymbol{j}_i(t) \equiv Q\tilde{\boldsymbol{j}}_i(t) = \begin{pmatrix} j_{\mathrm{q},i}(t) \\ j_{\mathrm{cl},i}(t) \end{pmatrix} = \frac{1}{\sqrt{2}} \begin{pmatrix} j_{+,i}(t) - j_{-,i}(t) \\ j_{+,i}(t) + j_{-,i}(t) \end{pmatrix}, \tag{4.22}$$

$$\boldsymbol{j}_i^*(t) \equiv \tilde{\boldsymbol{j}}_i^*(t) Q^{-1} = \left(j_{\mathrm{q},i}^*(t), j_{\mathrm{cl},i}^*(t) \right) = \frac{1}{\sqrt{2}} \left(j_{+,i}^*(t) - j_{-,i}^*(t),\ j_{+,i}^*(t) + j_{-,i}^*(t) \right). \tag{4.23}$$

The question now is whether the rotated matrix $Q\boldsymbol{G}_{ij}^{(1)}Q^{-1}$ really has the desired Keldysh structure

(3.55). Obviously, this is true for vanishing hopping $J_{ij} = 0$:

$$\begin{aligned}\mathcal{F}^{(2,1)}[j,j^*]\Big|_{J=0} &= \sum_{ij}\int_{-\infty}^{\infty}\mathrm{d}t_1\int_{-\infty}^{\infty}\mathrm{d}t_2\ \left(j^*_{\mathrm{q},i}(t_1), j^*_{\mathrm{cl},i}(t_1)\right)\begin{pmatrix} A^{(0)}_{ij}(t_1,t_2) & G^{\mathrm{R}(0)}_{ij}(t_1,t_2)\\ G^{\mathrm{A}(0)}_{ij},(t_1,t_2) & 0\end{pmatrix}\begin{pmatrix} j_{\mathrm{q},j}(t_2)\\ j_{\mathrm{cl},j}(t_2)\end{pmatrix}\\ &= \sum_{ij}\int_{-\infty}^{\infty}\mathrm{d}t_1\int_{-\infty}^{\infty}\mathrm{d}t_2\ \boldsymbol{j}^*_i(t_1)\boldsymbol{G}^{(0)}_{ij}(t_1,t_2)\boldsymbol{j}_j(t_2)\end{aligned} \tag{4.24}$$

Let us give, at this place, the explicit expressions for those unperturbed matrix elements which can be easily calculated from the definition Eq. (3.54) as we know the unperturbed eigenstates $|n_i\rangle$, given by the eigenvalue problem $\hat{\mathrm{H}}_{i,0}|n_i\rangle \equiv E_n|n_i\rangle$:

$$G^{\mathrm{R}(0)}_{ij}(t_1,t_2) = i\delta_{ij}\theta(t_1-t_2)\sum_{n=0}^{\infty}\frac{\mathrm{e}^{-\beta E_n}}{\mathcal{Z}^{(0)}}\left[(n+1)\mathrm{e}^{\frac{i}{\hbar}(E_{n+1}-E_n)(t_2-t_1)} - n\mathrm{e}^{\frac{i}{\hbar}(E_n-E_{n-1})(t_2-t_1)}\right], \tag{4.25}$$

$$G^{\mathrm{A}(0)}_{ij}(t_1,t_2) = -i\delta_{ij}\theta(t_2-t_1)\sum_{n=0}^{\infty}\frac{\mathrm{e}^{-\beta E_n}}{\mathcal{Z}^{(0)}}\left[(n+1)\mathrm{e}^{\frac{i}{\hbar}(E_{n+1}-E_n)(t_2-t_1)} - n\mathrm{e}^{\frac{i}{\hbar}(E_n-E_{n-1})(t_2-t_1)}\right], \tag{4.26}$$

$$A^{(0)}_{ij}(t_1,t_2) = i\delta_{ij}\sum_{n=0}^{\infty}\frac{\mathrm{e}^{-\beta E_n}}{\mathcal{Z}^{(0)}}\left[n\mathrm{e}^{\frac{i}{\hbar}(E_n-E_{n-1})(t_2-t_1)} + (n+1)\mathrm{e}^{\frac{i}{\hbar}(E_{n+1}-E_n)(t_2-t_1)}\right]. \tag{4.27}$$

Not surprisingly, the expressions in Eqs. (4.25)–(4.27) only depend on the time difference $t_1 - t_2$. This invariance under time translations is directly related to the conservation law of energy by the Noether theorem [74]. This general feature of time-independent Hamiltonians always allows us to eliminate one time argument of the Green's functions, e.g.:

$$G(t_1,t_2) = G(t_1-t_2,0). \tag{4.28}$$

But now let's go back to our actual problem and look at the Keldysh rotation of the perturbed matrix in Eq. (4.20). It reads explicitly:

$$\boldsymbol{G}^{(1)}_{ij} \equiv \frac{1}{2}\begin{pmatrix} G^{++(1)}_{ij} + G^{+-(1)}_{ij} + G^{-+(1)}_{ij} + G^{--(1)}_{ij} & G^{++(1)}_{ij} - G^{+-(1)}_{ij} + G^{-+(1)}_{ij} - G^{--(1)}_{ij}\\ G^{++(1)}_{ij} + G^{+-(1)}_{ij} - G^{-+(1)}_{ij} - G^{--(1)}_{ij} & G^{++(1)}_{ij} - G^{+-(1)}_{ij} - G^{-+(1)}_{ij} + G^{--(1)}_{ij}\end{pmatrix}. \tag{4.29}$$

The next step is straightforward, but a little bit lengthy: We have to insert the expression (4.19) into Eq. (4.29). The unperturbed part of each matrix element can immediately be separated into a matrix $\boldsymbol{G}^{(0)}_{ij}(t_1,t_2)$. The perturbed part of each Green's function consists of a sum of two products

$$\sum_{\mathrm{P}}\mathrm{P}\ G^{\mathrm{P}_1\mathrm{P}(0)}_{ii}(t_1,t)G^{\mathrm{P}\mathrm{P}_2(0)}_{jj}(t,t_2), \tag{4.30}$$

so in each matrix element we have in total 8 terms. But we can factorize them and then exploit the identity in Eq. (3.50) which then allows for a further factorization. With this we find, indeed, the vanishing of the lower right component in Eq. (4.29). Furthermore, with Eq. (3.54) we can express each off-diagonal element in terms of the corresponding off-diagonal element of the unperturbed matrix

and obtain:

$$G_{ij}^{\mathrm{R}(1)}(t_1,t_2) = G_{ij}^{\mathrm{R}(0)}(t_1,t_2) + \frac{J_{ij}}{\hbar}\int_{-\infty}^{\infty} \mathrm{d}t\; G_{ii}^{\mathrm{R}(0)}(t_1,t) G_{jj}^{\mathrm{R}(0)}(t,t_2), \tag{4.31}$$

$$G_{ij}^{\mathrm{A}(1)}(t_1,t_2) = G_{ij}^{\mathrm{A}(0)}(t_1,t_2) + \frac{J_{ij}}{\hbar}\int_{-\infty}^{\infty} \mathrm{d}t\; G_{ii}^{\mathrm{A}(0)}(t_1,t) G_{jj}^{\mathrm{A}(0)}(t,t_2). \tag{4.32}$$

This very nice scheme, which holds for the advanced and retarded Green's functions, does not work with the upper left element in Eq. (4.29). As we will later see, this is not a big problem, as this matrix element will not enter our equations of motion. Nevertheless, for the sake of completeness, we give the result here:

$$A_{ij}^{(1)}(t_1,t_2) = A_{ij}^{(0)}(t_1,t_2) + \frac{J_{ij}}{\hbar}\int_{-\infty}^{\infty} \mathrm{d}t\; \left(G_{ii}^{\mathrm{R}(0)}(t_1,t) A_{jj}^{(0)}(t,t_2) + A_{ii}^{(0)}(t_1,t) G_{jj}^{\mathrm{A}(0)}(t,t_2) \right). \tag{4.33}$$

Now we would like to write down the perturbed Green's function matrix (4.29) as a matrix which is built up of the unperturbed matrices. We could expect that the hopping correction is given as the product of two unperturbed matrices. But this turns out to be false. We find that the elements (4.31)–(4.33) are produced, when we interpose the Pauli matrix $\sigma^1 \equiv \begin{pmatrix} 0 & 1 \\ 1 & 0 \end{pmatrix}$ between the Green's functions [59], i.e.:

$$\boldsymbol{G}_{ij}^{(1)}(t_1,t_2) = \boldsymbol{G}_{ij}^{(0)}(t_1,t_2) + \frac{J_{ij}}{\hbar}\int_{-\infty}^{\infty} \mathrm{d}t\; \boldsymbol{G}_{ii}^{(0)}(t_1,t)\sigma^1 \boldsymbol{G}_{jj}^{(0)}(t,t_2). \tag{4.34}$$

Finally, we can bring the whole expansion (4.18) to the following form:

$$\begin{aligned}\mathcal{F}^{(2,1)}[j,j^*] &= \frac{1}{\hbar^2}\sum_{ij}\int_{-\infty}^{\infty}\mathrm{d}t_1\int_{-\infty}^{\infty}\mathrm{d}t_2\; \left(j_{\mathrm{q},i}^*(t_1), j_{\mathrm{cl},i}^*(t_1)\right) \begin{pmatrix} A_{ij}^{(1)}(t_1,t_2) & G_{ij}^{\mathrm{R}(1)}(t_1,t_2) \\ G_{ij}^{\mathrm{A}(1)}(t_1,t_2) & 0 \end{pmatrix} \begin{pmatrix} j_{\mathrm{q},j}(t_2) \\ j_{\mathrm{cl},j}(t_2) \end{pmatrix} \\ &= \frac{1}{\hbar^2}\sum_{ij}\int_{-\infty}^{\infty}\mathrm{d}t_1\int_{-\infty}^{\infty}\mathrm{d}t_2\; \boldsymbol{j}_i^*(t_1)\boldsymbol{G}_{ij}^{(1)}(t_1,t_2)\boldsymbol{j}_j(t_2).\end{aligned} \tag{4.35}$$

5 Effective Action in the MI Phase

In the previous section we expanded the generating functional of connected Green's functions $\mathcal{F}[j, j^*]$ up to second order in the currents j and j^*. These have only been a technical tool to break the $U(1)$-symmetry of the system. In the real physical system, however, they are zero. Therefore, we would like to replace them by a quantity being manifest in nature. As already mentioned, second-order phase transitions can be understood with the help of an order field. In the case of the transition from the MI to the SF phase, the condensate amplitude $\hbar\Psi_{i,\pm}(t) = \langle \hat{a}_{i,\pm}(t)\rangle_0$ and its complex conjugate $\hbar\Psi^*_{i,\pm}(t) = \langle \hat{a}^\dagger_{i,\pm}(t)\rangle_0$ are a good choice for an order field. Let us now see how we can find a functional of Ψ and Ψ^*, starting from $\mathcal{F}[j, j^*]$.

5.1 Legendre Transformation

The way to perform such a variable change, is the Legendre transformation. In this section, we want to show the general formalism for transforming the free energy into the effective action. As a result, we will see that we have to invert the Green's functions that we have found in the expansion of $\mathcal{F}[j, j^*]$ in Eq. (4.18). In our special case of a hopping expansion, the inversion scheme that we will apply for the hopping-perturbed function is the "heart" of the formalism, as it implicitly includes a resummation of the hopping diagrams. We will denote an own section to see how this works in detail. In the present section, however, we do not yet consider the hopping expansion, thus we are not restricted to a certain order in the hopping. Instead we concentrate on the expansion in the order fields, which are taken into account up to the second order.

From the definition of $\mathcal{F}[j, j^*]$ in Eqs. (3.57) and (3.59) we know that

$$\frac{\delta\mathcal{F}[\tilde{\boldsymbol{j}}, \tilde{\boldsymbol{j}}^*]}{\delta\tilde{\boldsymbol{j}}^*_i(t)} = \frac{1}{\hbar}\begin{pmatrix} \langle \hat{a}_{i,+}(t)\rangle_0 \\ \langle \hat{a}_{i,-}(t)\rangle_0 \end{pmatrix}, \tag{5.1}$$

where the functional derivative is defined according to Eq. (4.21) as

$$\frac{\delta}{\delta\tilde{\boldsymbol{j}}^*_i(t)} \equiv \begin{pmatrix} \frac{\delta}{\delta j^*_{+,i}(t)} \\ -\frac{\delta}{\delta j^*_{-,i}(t)} \end{pmatrix}. \tag{5.2}$$

We can exploit relation (5.1) to define the order parameter.

$$\tilde{\boldsymbol{\Psi}}_i(t) = \begin{pmatrix} \Psi_{i,+}(t) \\ \Psi_{i,-}(t) \end{pmatrix} \equiv \frac{\delta\mathcal{F}[\tilde{\boldsymbol{j}}, \tilde{\boldsymbol{j}}^*]}{\delta\tilde{\boldsymbol{j}}^*_i(t)}. \tag{5.3}$$

Note that from the definition (5.2), the backward component of $\tilde{\boldsymbol{\Psi}}$ does not have the usual minus

sign. The relation (5.3) means that $\tilde{\boldsymbol{j}}$ and $\tilde{\boldsymbol{\Psi}}$ are conjugate variables which motivates us to introduce a Legendre transformation. This will lead from the generating functional of the connected Green's functions to the generating functional of the one-particle irreducible Green's functions, i.e. the effective action $\Gamma[\tilde{\boldsymbol{\Psi}}, \tilde{\boldsymbol{\Psi}}^*]$. The transformation is given as usual by

$$\Gamma[\tilde{\boldsymbol{\Psi}}, \tilde{\boldsymbol{\Psi}}^*] \equiv \mathcal{F}\left[\tilde{\boldsymbol{j}}[\tilde{\boldsymbol{\Psi}}, \tilde{\boldsymbol{\Psi}}^*], \boldsymbol{j}^*[\tilde{\boldsymbol{\Psi}}, \tilde{\boldsymbol{\Psi}}^*]\right] - \sum_i \int_{-\infty}^{\infty} \mathrm{d}t \left(\tilde{\boldsymbol{j}}_i^*[\tilde{\boldsymbol{\Psi}}, \tilde{\boldsymbol{\Psi}}^*](t) \cdot \tilde{\boldsymbol{\Psi}}_i(t) + \tilde{\boldsymbol{\Psi}}_i^*(t) \cdot \tilde{\boldsymbol{j}}_i[\tilde{\boldsymbol{\Psi}}, \tilde{\boldsymbol{\Psi}}^*](t)\right). \quad (5.4)$$

To determine this quantity explicitly, we must express the currents $\tilde{\boldsymbol{j}}$ and $\tilde{\boldsymbol{j}}^*$ in terms of the order fields $\tilde{\boldsymbol{\Psi}}$ and $\tilde{\boldsymbol{\Psi}}^*$. We can do this by performing the functional derivative (5.3) in (4.35),

$$\tilde{\boldsymbol{\Psi}}_i(t_1) = \frac{1}{\hbar^2} \sum_j \int_{-\infty}^{\infty} \mathrm{d}t_2 \; \tilde{\boldsymbol{G}}_{ij}(t_1, t_2) \tilde{\boldsymbol{j}}_j(t_2), \quad (5.5)$$

with $\tilde{\boldsymbol{G}}_{ij}(t_1, t_2)$ being implicitly defined in Eq. (4.20). A subsequent inversion yields:

$$\tilde{\boldsymbol{j}}_i(t_1) = \hbar^2 \sum_j \int_{-\infty}^{\infty} \mathrm{d}t_2 \; \tilde{\boldsymbol{G}}_{ij}^{-1}(t_1, t_2) \tilde{\boldsymbol{\Psi}}_j(t_2). \quad (5.6)$$

Putting this into Eq. (5.4) gives us the effective action, with an index $(2, m)$ to stress that it comes from a second-order expansion in the fields, while the hopping order is (still) not specified:

$$\Gamma^{(2,m)}[\tilde{\boldsymbol{\Psi}}, \tilde{\boldsymbol{\Psi}}^*] = -\hbar^2 \sum_{ij} \int_{-\infty}^{\infty} \mathrm{d}t_1 \int_{-\infty}^{\infty} \mathrm{d}t_2 \; \tilde{\boldsymbol{\Psi}}_i^*(t_1) \tilde{\boldsymbol{G}}_{ij}^{-1}(t_1, t_2) \tilde{\boldsymbol{\Psi}}_j(t_2). \quad (5.7)$$

It is convenient to rotate the expressions on the right side of Eq. (5.4), leaving us with Γ as a functional of the rotated order fields $\boldsymbol{\Psi}_i(t)$. With the definition (5.3), we find

$$\boldsymbol{\Psi}_i(t) = Q \tilde{\boldsymbol{\Psi}}_i(t) = \begin{pmatrix} \Psi_{i,\mathrm{cl}}(t) \\ \Psi_{i,\mathrm{q}}(t) \end{pmatrix}, \quad \boldsymbol{\Psi}_i^*(t) = \tilde{\boldsymbol{\Psi}}_i^*(t) Q^{-1} = \left(\Psi_{i,\mathrm{cl}}^*(t), \Psi_{i,\mathrm{q}}^*(t)\right). \quad (5.8)$$

Note that the classical component is the one on top/on the left, which differs from the definition of $\boldsymbol{j}, \boldsymbol{j}^*$ in Eqs. (4.22) and (4.23). For the rotation of the matrix, we note

$$Q \tilde{\boldsymbol{G}}^{-1} Q^{-1} = Q^{-1} \tilde{\boldsymbol{G}}^{-1} Q = (Q^{-1} \tilde{\boldsymbol{G}} Q)^{-1} = \boldsymbol{G}^{-1}. \quad (5.9)$$

So we have to invert the matrix given in Eq. (4.35) which has the Keldysh structure from Eq. (3.55). This leads to:

$$\boldsymbol{G}_{ij}^{-1}(t_1, t_2) = \begin{pmatrix} 0 & \left[G_{ij}^{\mathrm{A}}(t_1, t_2)\right]^{-1} \\ \left[G_{ij}^{\mathrm{R}}(t_1, t_2)\right]^{-1} & \tilde{A}_{ij}(t_1, t_2) \end{pmatrix}. \quad (5.10)$$

In this matrix, the inverse functions of the advanced and the retarded Green's functions appear. The

entry in the third non-vanishing component is given by

$$\tilde{A}_{ij}(t_1,t_2) = -\sum_{k,l}\int_{-\infty}^{\infty}\mathrm{d}t\int_{-\infty}^{\infty}\mathrm{d}t'\left[G^{\mathrm{R}}_{ik}(t_1,t)\right]^{-1}A_{kl}(t,t')\left[G^{\mathrm{A}}_{lj}(t',t_2)\right]^{-1}. \tag{5.11}$$

The final result for the effective action in Keldysh space reads

$$\Gamma^{(2,m)}\left[\mathbf{\Psi},\mathbf{\Psi}^*\right] = -\hbar^2\sum_{i,j}\int_{-\infty}^{\infty}\mathrm{d}t_1\int_{-\infty}^{\infty}\mathrm{d}t_2\ \mathbf{\Psi}^*_i(t_1)\begin{pmatrix} 0 & \left[G^{\mathrm{A}}_{ij}(t_1,t_2)\right]^{-1} \\ \left[G^{\mathrm{R}}_{ij}(t_1,t_2)\right]^{-1} & \tilde{A}_{ij}(t_1,t_2)\end{pmatrix}\mathbf{\Psi}_j(t_2). \tag{5.12}$$

We note that this is always zero if $\Psi_{\mathrm{q}} = \Psi^*_{\mathrm{q}} = 0$, i.e. when the value of Ψ and Ψ^* do not depend whether time evolves forward or backward. Thus, we have an important normalization property of the effective action [75]:

$$\Gamma\left[\Psi_{\mathrm{cl}},\Psi^*_{\mathrm{cl}},\Psi_{\mathrm{q}}=0,\Psi^*_{\mathrm{q}}=0\right] = 0. \tag{5.13}$$

Now, the actual problem is the calculation of the matrix elements in Eq. (5.10). For the unperturbed system, this is a straightforward task. We only have to find the inverse of the unperturbed retarded/advanced Green's functions, which will be done in the next section. Afterwards, we will deal with a hopping-perturbed system. As already mentioned, the inversion there will work differently.

5.2 Frequency Space Green's Functions

To find the inverse functions, it is convenient to perform the Fourier transformation

$$f(\omega) = \int_{-\infty}^{\infty}\mathrm{d}t\ f(t)\mathrm{e}^{i\omega t} \tag{5.14}$$

for quantities related to annihilation operators and

$$f^*(\omega) = \int_{-\infty}^{\infty}\mathrm{d}t\ f^*(t)\mathrm{e}^{-i\omega t} \tag{5.15}$$

for its conjugates. The inverse relations read correspondingly

$$f(t) = \frac{1}{2\pi}\int_{-\infty}^{\infty}\mathrm{d}\omega\ f(\omega)\mathrm{e}^{-i\omega t}\quad,\quad f^*(t) = \frac{1}{2\pi}\int_{-\infty}^{\infty}\mathrm{d}\omega\ f^*(\omega)\mathrm{e}^{i\omega t}. \tag{5.16}$$

In particular, this transformation will turn out to be useful for a later resummation. We will see this at the end of this section when we take a look at the hopping-corrected Green's function. But let's begin with the inversion of the unperturbed retarded function defined in Eq. (4.25). To find its Fourier transform $G^{\mathrm{R}(0)}_{ij}(\omega_1,\omega_2)$, we use the integral representation of the step function:

$$\theta(t_1-t_2) = \lim_{\epsilon\to 0^+}\int_{-\infty}^{\infty}\frac{i/2\pi}{x+i\epsilon}\mathrm{e}^{-i(t_1-t_2)x}\mathrm{d}x. \tag{5.17}$$

In the following we will suppress the limit-symbol for economic reasons. The Dirac δ-function has the following Fourier representation

$$\delta(\omega_1-\omega_2)=\frac{1}{2\pi}\int_{-\infty}^{\infty}\mathrm{e}^{i(\omega_1-\omega_2)t}\,\mathrm{d}t. \tag{5.18}$$

Performing the substitution $t\equiv t_1-t_2$, we have

$$\begin{aligned}
&G_{ij}^{\mathrm{R}(0)}(\omega_1,\omega_2)=i\frac{\delta_{ij}}{\mathcal{Z}^{(0)}}\sum_{n=0}^{\infty}\mathrm{e}^{-\beta E_n}\int_{-\infty}^{\infty}\mathrm{d}t_1\;\mathrm{e}^{i(\omega_1-\omega_2)t_1}\int_{-\infty}^{\infty}\mathrm{d}t\;\mathrm{e}^{it\omega_2}\int_{-\infty}^{\infty}\mathrm{d}x\;\frac{i/2\pi}{x+i\epsilon}\;\mathrm{e}^{-itx}\\
&\times\left[(n+1)\mathrm{e}^{-\frac{i}{\hbar}(E_{n+1}-E_n)t}-n\;\mathrm{e}^{-\frac{i}{\hbar}(E_n-E_{n-1})t}\right]=\frac{-\delta_{ij}}{\mathcal{Z}^{(0)}}\sum_{n=0}^{\infty}\mathrm{e}^{-\beta E_n}\;\delta(\omega_2-\omega_1)\int_{-\infty}^{\infty}\frac{\mathrm{d}x}{x+i\epsilon}\int_{-\infty}^{\infty}\mathrm{d}t\\
&\times\left[(n+1)\mathrm{e}^{-\frac{i}{\hbar}(E_{n+1}-E_n-\hbar\omega_2+\hbar x)t}-n\mathrm{e}^{-\frac{i}{\hbar}(E_n-E_{n-1}-\hbar\omega_2+\hbar x)t}\right]=\frac{-2\pi\delta_{ij}}{\mathcal{Z}^{(0)}}\sum_{n=0}^{\infty}\mathrm{e}^{-\beta E_n}\delta(\omega_2-\omega_1)\\
&\times\int_{-\infty}^{\infty}\mathrm{d}x\left[(n+1)\frac{\delta\left(\frac{E_{n+1}-E_n}{\hbar}-\omega_2+x\right)}{x+i\epsilon}-n\frac{\delta\left(\frac{E_n-E_{n-1}}{\hbar}-\omega_2+x\right)}{x+i\epsilon}\right]\\
&=2\pi\delta_{ij}\delta(\omega_1-\omega_2)\frac{1}{\mathcal{Z}^{(0)}}\sum_{n=0}^{\infty}\mathrm{e}^{-\beta E_n}\left(\frac{n+1}{\frac{E_{n+1}-E_n}{\hbar}-\omega_2-i\epsilon}-\frac{n}{\frac{E_n-E_{n-1}}{\hbar}-\omega_2-i\epsilon}\right).
\end{aligned} \tag{5.19}$$

For practical reasons we define the function

$$g_{\mathrm{R}}(\omega)\equiv\frac{1}{\mathcal{Z}^{(0)}}\sum_{n=0}^{\infty}\mathrm{e}^{-\beta E_n}\left(\frac{n+1}{\frac{E_{n+1}-E_n}{\hbar}-\omega-i\epsilon}-\frac{n}{\frac{E_n-E_{n-1}}{\hbar}-\omega-i\epsilon}\right). \tag{5.20}$$

With this we can write compactly:

$$G_{ij}^{\mathrm{R}(0)}(\omega_1,\omega_2)=2\pi\delta_{ij}\delta(\omega_1-\omega_2)g_{\mathrm{R}}(\omega_1). \tag{5.21}$$

We see that the unperturbed function is diagonal in its spatial as well as in its temporal variables. So the inverse of it reads

$$\left[G_{ij}^{\mathrm{R}(0)}(\omega_1,\omega_2)\right]^{-1}=\frac{1}{2\pi}\delta_{ij}\delta(\omega_1-\omega_2)\frac{1}{g_{\mathrm{R}}(\omega_1)}. \tag{5.22}$$

Repeating the whole procedure for the advanced Green's function shows that it is nothing but the complex conjugate of (5.22):

$$G_{ij}^{\mathrm{A}(0)}(\omega_1,\omega_2)=2\pi\delta_{ij}\delta(\omega_1-\omega_2)g_{\mathrm{A}}(\omega_1). \tag{5.23}$$

with

$$g_{\mathrm{A}}(\omega)\equiv\frac{1}{\mathcal{Z}^{(0)}}\sum_{n=0}^{\infty}\mathrm{e}^{-\beta E_n}\left(\frac{n+1}{\frac{E_{n+1}-E_n}{\hbar}-\omega+i\epsilon}-\frac{n}{\frac{E_n-E_{n-1}}{\hbar}-\omega+i\epsilon}\right). \tag{5.24}$$

As in the case of the retarded function, this representation in Fourier space allows for an immediate inversion. For completeness, we still give the Fourier representation of the third non-vanishing matrix element A_{ij}:

$$\begin{aligned} A_{ij}(\omega_1,\omega_2) &= 2\pi\delta_{ij}\delta(\omega_1-\omega_2)\sum_{n=0}^{\infty}\mathrm{e}^{-\beta E_n}\left[n\delta(\omega_1-\omega_n)+(n+1)\delta(\omega_1-\omega_{n+1})\right] \\ &\equiv 2\pi\delta_{ij}\delta(\omega_1-\omega_2)a(\omega_1), \end{aligned} \tag{5.25}$$

where we have defined

$$\omega_n \equiv \frac{E_n - E_{n-1}}{\hbar}. \tag{5.26}$$

In Ref. [66] it is shown by a spectral analysis of the Green's functions that $A_{ij}(\omega_1,\omega_2)$ equals the dissipative part of the time-ordered Green's function. The whole Green's function matrix reads:

$$\boldsymbol{G}^{(0)}_{ij}(\omega_1,\omega_2) = 2\pi\delta_{ij}\delta(\omega_1-\omega_2)\begin{pmatrix} a(\omega_1) & g_{\mathrm{R}}(\omega_1) \\ g_{\mathrm{A}}(\omega_1) & 0 \end{pmatrix} \equiv 2\pi\delta(\omega_1-\omega_2)\boldsymbol{G}^{(0)}_{ij}(\omega_1). \tag{5.27}$$

We have already found the form of the inverse matrix function in Eq. (5.10). To write it down explicitly, we still have to take a look at the component $\tilde{A}_{ij}$. It is given in time space by Eq. (5.11) as a double temporal integral. In Fourier space, these integrals become trivial because of the frequency conservation. Thus we find

$$\tilde{A}_{ij}(\omega_1,\omega_2) = -\frac{1}{2\pi}\delta(\omega_1-\omega_2)\delta_{ij}\frac{a(\omega_1)}{g_{\mathrm{R}}(\omega_1)g_{\mathrm{A}}(\omega_1)} \equiv -\frac{1}{2\pi}\delta(\omega_1-\omega_2)\delta_{ij}\tilde{a}(\omega_1). \tag{5.28}$$

This allows for the following writing

$$\left[\boldsymbol{G}^{(0)}_{ij}(\omega_1,\omega_2)\right]^{-1} = \frac{1}{2\pi}\,\delta_{ij}\delta(\omega_1-\omega_2)\begin{pmatrix} 0 & 1/g_{\mathrm{A}}(\omega_1) \\ 1/g_{\mathrm{R}}(\omega_1) & \tilde{a}(\omega_1) \end{pmatrix} \equiv \frac{1}{2\pi}\delta(\omega_1-\omega_2)\left[\boldsymbol{G}^{(0)}_{ij}(\omega_1)\right]^{-1}. \tag{5.29}$$

Let us still take a look at the Fourier transform of the first hopping-corrected Green's function from Eq. (4.34), and the free energy from Eq. (4.35):

$$\begin{aligned} \hbar^2\mathcal{F}[j,j^*] &= \sum_{i,j}\int_{-\infty}^{\infty}\mathrm{d}t_1\int_{-\infty}^{\infty}\mathrm{d}t_2\;\boldsymbol{j}^*_i(t_1)\boldsymbol{G}^{(1)}_{ij}(t_1,t_2)\boldsymbol{j}_j(t_2) \qquad (5.30)\\ &= \sum_{i,j}\int_{-\infty}^{\infty}\mathrm{d}t_1\int_{-\infty}^{\infty}\mathrm{d}t_2\left\{\boldsymbol{j}^*_i(t_1)\boldsymbol{G}^{(0)}_{ij}(t_1,t_2)\boldsymbol{j}_j(t_2) + \frac{J_{ij}}{\hbar}\int_{-\infty}^{\infty}\mathrm{d}t\;\boldsymbol{j}^*_i(t_1)\boldsymbol{G}^{(0)}_{ii}(t_1,t)\sigma^1\boldsymbol{G}^{(0)}_{jj}(t,t_2)\boldsymbol{j}_j(t_2)\right\}. \end{aligned}$$

Using the Fourier representation of all quantities in Eq. (5.30) and doing the time integrations we obtain δ-functions, which can be integrated out. This leaves us with the following expression:

$$\int_{-\infty}^{\infty}\frac{\mathrm{d}\omega_1}{2\pi}\int_{-\infty}^{\infty}\frac{\mathrm{d}\omega_2}{2\pi}\left\{\boldsymbol{j}^*_i(\omega_1)\boldsymbol{G}^{(0)}_{ij}(\omega_1,\omega_2)\boldsymbol{j}_j(\omega_2) + \int_{-\infty}^{\infty}\frac{\mathrm{d}\omega}{2\pi}\frac{J_{ij}}{\hbar}\boldsymbol{j}^*_i(\omega_2)\boldsymbol{G}^{(0)}_{ii}(\omega_1,\omega)\sigma^1\boldsymbol{G}^{(0)}_{jj}(\omega,\omega_2)\boldsymbol{j}_j(\omega_2)\right\}. \tag{5.31}$$

Inserting Eq. (5.27) in Eq. (5.31), two frequency integrations become trivial. We get

$$\hbar^2 \mathcal{F}[j, j^*] = \int_{-\infty}^{\infty} \frac{\mathrm{d}\omega_1}{2\pi} \left\{ \boldsymbol{j}_i^*(\omega_1) \boldsymbol{G}_{ij}^{(0)}(\omega_1) \boldsymbol{j}_j(\omega_1) + \frac{J_{ij}}{\hbar} \boldsymbol{j}_i^*(\omega_2) \boldsymbol{G}_{ii}^{(0)}(\omega_1) \sigma^1 \boldsymbol{G}_{jj}^{(0)}(\omega_1) \boldsymbol{j}_j(\omega_1) \right\}. \tag{5.32}$$

This shows that we don't have to integrate over inner frequency variables in Fourier space. Instead, the hopping links two cumulants via a simple multiplication. The whole hopping-corrected Green's function can be directly taken from Eq. (5.32):

$$\boldsymbol{G}_{ij}^{(1)}(\omega_1) = \boldsymbol{G}_{ij}^{(0)}(\omega_1) + \frac{J_{ij}}{\hbar} \boldsymbol{G}_{ii}^{(0)}(\omega_1) \sigma^1 \boldsymbol{G}_{jj}^{(0)}(\omega_1), \tag{5.33}$$

or, if we want to keep both frequency variables:

$$\begin{aligned} \boldsymbol{G}_{ij}^{(1)}(\omega_1, \omega_2) &= \boldsymbol{G}_{ij}^{(0)}(\omega_1, \omega_2) + \int_{-\infty}^{\infty} \frac{\mathrm{d}\omega}{2\pi} \frac{J_{ij}}{\hbar} \boldsymbol{G}_{ii}^{(0)}(\omega_1, \omega) \sigma^1 \boldsymbol{G}_{jj}^{(0)}(\omega, \omega_2) \\ &= 2\pi\delta(\omega_1 - \omega_2) \left[\boldsymbol{G}_{ij}^{(0)}(\omega_1) + \frac{J_{ij}}{\hbar} \boldsymbol{G}_{ii}^{(0)}(\omega_1) \sigma^1 \boldsymbol{G}_{jj}^{(0)}(\omega_1) \right]. \end{aligned} \tag{5.34}$$

5.3 Resummation

We now want to consider explicitly a system with hopping. What is different then? The matrix in Eq. (5.12) still has the same form, but until now we have only found how to invert the unperturbed Green's functions. The perturbed matrix $\boldsymbol{G}_{ij}^{(1)}(t_1, t_2)$, however, is built up of the perturbed functions from Eqs. (4.31)–(4.33) which are not local. In the temporal variables, we proceed as before by diagonalizing these functions via a transformation into frequency space. For the spatial variables, however, we do not try an exact diagonalization, although this would be possible for a homogeneous system by performing another Fourier transformation into $\boldsymbol{k}$-space. But as we are doing a hopping expansion, we have a systematical reason to demand for the inverted Green's function that it has the form of a power series in the hopping as well. This motivates us to perform the inversion iteratively. We start with the equation

$$\sum_k \boldsymbol{G}_{ik}^{(1)}(\omega) \left[\boldsymbol{G}_{kj}^{(1)}(\omega) \right]^{-1} = \delta_{ij}. \tag{5.35}$$

Now, the iterative procedure works the following way: Instead of $\left[\boldsymbol{G}_{kj}^{(1)}(\omega) \right]^{-1}$, we plug into this equation the zeroth-order solution, i.e. $\left[\boldsymbol{G}_{kj}^{(0)}(\omega) \right]^{-1}$ from Eq. (5.29). The expression for $\boldsymbol{G}_{ik}^{(1)}(\omega)$ is given by Eq. (5.33). Then left side of Eq. (5.35) reads

$$\delta_{ij} + \frac{J_{ij}}{\hbar} \boldsymbol{G}_{ii}^{(0)}(\omega) \sigma^1. \tag{5.36}$$

We see that the second term, which is linear in J_{ij}, differs from the right side of Eq. (5.35). We subtract this term from $\left[\boldsymbol{G}_{kj}^{(0)}(\omega) \right]^{-1}$, which gives us a better approximation of $\left[\boldsymbol{G}_{kj}^{(1)}(\omega) \right]^{-1}$. Let us therefore define:

$$\left[\boldsymbol{G}_{ij}^{(1)}(\omega) \right]^{-1} \equiv \left[\boldsymbol{G}_{ij}^{(0)}(\omega) \right]^{-1} \left(\delta_{ij} - \frac{J_{ij}}{\hbar} \boldsymbol{G}_{ij}^{(0)}(\omega) \sigma^1 \right). \tag{5.37}$$

By re-inserting Eq. (5.37) in Eq. (5.35), we find that now the right side deviates from left side only by terms which are of second-order in J. To be consistent with our hopping expansion, these terms must be neglected. Although Eq. (5.37) is not the mathematically the inverse of Eq. (5.33), in a physical sense it is, since Eq. (5.33) approximates the full Green's function $\boldsymbol{G}$ and Eq. (5.37) approximates the inverse of it $\boldsymbol{G}^{-1}$.

From Eq. (5.37) we can directly read off the Green's function of two frequency variables. We must only note the prefactor $1/2\pi$ from Eq. (5.29):

$$\begin{aligned}\left[\boldsymbol{G}_{ij}^{(1)}(\omega_1,\omega_2)\right]^{-1} &= \frac{\delta(\omega_1-\omega_2)}{2\pi}\left[\boldsymbol{G}_{ij}^{(0)}(\omega_1)\right]^{-1}\left(\delta_{ij}-\frac{J_{ij}}{\hbar}\boldsymbol{G}_{ij}^{(0)}(\omega_1)\sigma^1\right)\\ &= \left[\boldsymbol{G}_{ij}^{(0)}(\omega_1,\omega_2)\right]^{-1}\left(\delta_{ij}-\frac{J_{ij}}{2\pi\hbar}\boldsymbol{G}_{ij}^{(0)}(\omega_1,\omega_2)\sigma^1\right).\end{aligned} \tag{5.38}$$

The second line of this equation shows us that the hopping has to be divided by 2π, when we express the inverse Green's function in terms of Green's functions of *two* frequency variables. The retarded and advanced components of this matrix read:

$$\left[G_{ij}^{\mathrm{R/A}(1)}(\omega_1,\omega_2)\right]^{-1} = \delta(\omega_1-\omega_2)\,\frac{1}{2\pi g_{\mathrm{R/A}}(\omega_1)}\left\{\delta_{ij}-g_{\mathrm{R/A}}(\omega_1)\frac{J_{ij}}{\hbar}\right\}. \tag{5.39}$$

Now we can get the explicit expression for the hopping-expanded effective action. We must insert Eq. (5.38) into the Fourier transform of Eq. (5.12) and find

$$\begin{aligned}\Gamma^{(2,1)}\left[\boldsymbol{\Psi},\boldsymbol{\Psi}^*\right] &= -\hbar^2\sum_{i,j}\int_{-\infty}^{\infty}\frac{\mathrm{d}\omega_1}{2\pi}\int_{-\infty}^{\infty}\frac{\mathrm{d}\omega_2}{2\pi}\;\boldsymbol{\Psi}_i^*(\omega_1)\left[\boldsymbol{G}_{ij}^{(1)}(\omega_1,\omega_2)\right]^{-1}\boldsymbol{\Psi}_j(\omega_2)\\ &= -\frac{\hbar^2}{(2\pi)^2}\sum_{i,j}\int_{-\infty}^{\infty}\frac{\mathrm{d}\omega_1}{2\pi}\;\boldsymbol{\Psi}_i^*(\omega_1)\left\{\left[\boldsymbol{G}_{ij}^{(0)}(\omega_1)\right]^{-1}-\frac{J_{ij}}{\hbar}\sigma^1\right\}\boldsymbol{\Psi}_j(\omega_1).\end{aligned} \tag{5.40}$$

The advantage of the inversion scheme applied above is the fact that a *resummation* is automatically made. Let us sketch what is meant by this by looking at the exact re-inversion of Eq. (5.37). To do this we must define the Fourier transformation into $\boldsymbol{k}$-space:

$$f_{\boldsymbol{k}} = \sum_i f_i \mathrm{e}^{-i\boldsymbol{k}\cdot\boldsymbol{r}_i}, \qquad f_{\boldsymbol{k}}^* = \sum_i f_i^* \mathrm{e}^{i\boldsymbol{k}\cdot\boldsymbol{r}_i} \tag{5.41}$$

$$f_i = \frac{1}{N_\mathrm{s}}\sum_{\boldsymbol{k}} f_{\boldsymbol{k}}\mathrm{e}^{i\boldsymbol{k}\cdot r_i}, \qquad f_i^* = \frac{1}{N_\mathrm{s}}\sum_{\boldsymbol{k}} f_{\boldsymbol{k}}^*\mathrm{e}^{-i\boldsymbol{k}\cdot r_i}. \tag{5.42}$$

Here both the index i and the coordinate $\boldsymbol{r}_i$ denote the position at a lattice site i, the total number of sites is denoted by N_s.

Assuming spatial homogeneity, we have $J_{ij} \to J_{\boldsymbol{k},\boldsymbol{k}'} = J_{\boldsymbol{k}}\delta_{\boldsymbol{k},\boldsymbol{k}'}$. With the δ-function in the frequencies and the Kronecker-δ in the wave vectors, we can define the Green's function as a function of only one frequency and one wave vector:

$$\left[\boldsymbol{G}^{(1)}(\boldsymbol{k},\omega)\right]^{-1} = \left[\boldsymbol{G}^{(0)}(\boldsymbol{k},\omega)\right]^{-1}\left\{1-\frac{J_{\boldsymbol{k}}}{\hbar}\boldsymbol{G}^{(0)}(\boldsymbol{k},\omega)\sigma^1\right\}, \tag{5.43}$$

which is immediately inverted:

$$\boldsymbol{G}^{(1)}(\boldsymbol{k},\omega) = \left\{1 - \frac{J_{\boldsymbol{k}}}{\hbar}\boldsymbol{G}^{(0)}(\boldsymbol{k},\omega)\sigma^1\right\}^{-1} \boldsymbol{G}^{(0)}(\boldsymbol{k},\omega). \tag{5.44}$$

The term in the brackets can be interpreted as a geometric sum:

$$\left\{1 - \frac{J_{\boldsymbol{k}}}{\hbar}\boldsymbol{G}^{(0)}(\boldsymbol{k},\omega)\sigma^1\right\}^{-1} = \sum_{m=0}^{\infty}\left(\frac{J_{\boldsymbol{k}}}{\hbar}\boldsymbol{G}^{(0)}(\boldsymbol{k},\omega)\sigma^1\right)^m. \tag{5.45}$$

This shows what is meant by resummation. Diagrammatically, this resummed Green's function is represented by the following chain diagram:

(5.46)

Although in our expansion of $\mathcal{F}$ given by Eq. (4.18), we had only considered the first two of the processes shown in the diagram above, our resummed Green's function includes all of them. If we did again an expansion of $\mathcal{F}$, but now took into account any of those longer chain diagrams, after performing the Legendre transform like done before, we would finally get the same result as in Eq. (5.37). The field-theoretical reason for this lies in the role of Γ as the generating functional of one-particle irreducible (OPI) Green's functions [14]. As all diagrams in (5.46) are constructed of one and the same OPI diagram, for the calculation of Γ it does not matter, how much of these diagram we take into account. We only need the first diagram (which is the OPI) and the second one, in order to have at least one non-local diagram seeding the resummation.

Our hope is that, although we started the expansion with the assumption of a small hopping, the resummation leads to equations which are even valid for larger hoppings.

5.4 Equations of Motion

Now let's have a look at the dynamics of the order fields. To find an equation of motion for them, we have to find the saddle points of $\Gamma^{(2,1)}$. For this we take the functional derivative of $\Gamma^{(2,1)}$ with respect to the order fields and set it equal to zero. For simplicity we do this in Fourier space, as we then have no integral over the time.

$$\frac{\delta\Gamma^{(2,1)}}{\delta\Psi^*_{i,\mathrm{q}}(\omega)} = \frac{-\hbar^2}{(2\pi)^2}\sum_j\left\{\left[G^{\mathrm{R}(1)}_{ij}(\omega)\right]^{-1}\Psi_{j,\mathrm{cl}}(\omega) + \tilde{A}^{(1)}_{ij}(\omega)\Psi_{j,\mathrm{q}}(\omega)\right\} = 0, \tag{5.47}$$

$$\frac{\delta\Gamma^{(2,1)}}{\delta\Psi^*_{i,\mathrm{cl}}(\omega)} = \frac{-\hbar^2}{(2\pi)^2}\sum_j\left[G^{\mathrm{A}(1)}_{ij}(\omega)\right]^{-1}\Psi_{j,\mathrm{q}}(\omega) = 0. \tag{5.48}$$

Taking the trivial solution of the last equation, $\Psi_{j,\mathrm{q}}(\omega) = 0$ on any site, the first equation reduces to

$$\sum_j \left[G_{ij}^{\mathrm{R}(1)}(\omega)\right]^{-1} \Psi_{j,\mathrm{cl}}(\omega) = 0. \tag{5.49}$$

This result states that, as long as we restrict ourselves on configurations with $\Psi_{\mathrm{q}} = 0$, the dynamics of a system is given by the retarded Green's function. For the complex conjugated field, we get a similar equation, but the advanced function will appear instead of the retarded one:

$$\frac{\delta\Gamma^{(2,1)}}{\delta\Psi_{i,\mathrm{q}}(\omega)} = \frac{-\hbar^2}{(2\pi)^2}\sum_j \left\{\Psi_{j,\mathrm{cl}}^*(\omega)\left[G_{ji}^{\mathrm{A}(1)}(\omega)\right]^{-1} + \Psi_{j,\mathrm{q}}^*(\omega)\tilde{A}_{ji}^{(1)}(\omega)\right\} = 0, \tag{5.50}$$

$$\frac{\delta\Gamma^{(2,1)}}{\delta\Psi_{i,\mathrm{cl}}(\omega)} = \frac{-\hbar^2}{(2\pi)^2}\sum_j \Psi_{j,\mathrm{q}}^*(\omega)\left[G_{ji}^{\mathrm{R}(1)}(\omega)\right]^{-1} = 0. \tag{5.51}$$

which now reduces to

$$\sum_j \Psi_{j,\mathrm{cl}}^*(\omega)\left[G_{ji}^{\mathrm{A}(1)}(\omega)\right]^{-1} = 0 \tag{5.52}$$

when $\Psi_{j,\mathrm{q}}^*(\omega) = 0$. This result agrees perfectly with the linear response theory, which is valid near equilibrium, where all the physics is given by the retarded/advanced Green's functions. We postpone the discussion of this equation to Chapter 7, where the spectra in the MI phase and the phase boundary between the MI and the SF are found from Eq. (5.49). Before we do that, we go beyond this phase boundary and extend our theory to the superfluid phase.

6 Effective Action in the SF Phase

According to Fig. 2.3, a superfluid system cannot be described by an effective action, which is quadratic in the order fields. It is crucial to take into account the next order, thus the expansion of Eq. (4.18) has to be extended up to fourth order in the currents.

6.1 Ψ^4 Expansion

With the diagrammatic rules given in Section 4.5, it is straightforward to write down the expansion of $\mathcal{F}$ up to fourth order in the currents diagrammatically:

$\mathcal{F}^{(4,1)}[j,j^*] = \frac{1}{\hbar^2}\Big\{$ 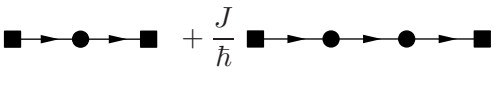 $+\frac{J}{\hbar}$ (6.1)

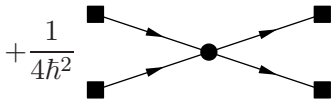 $+\frac{J}{2\hbar^3}\Big[$ 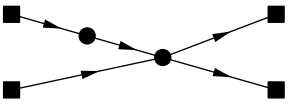 $+$ 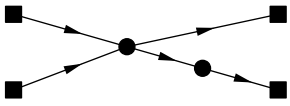 $\Big]\Big\}.$

The factor 1/2 in front of the last two terms comes from the symmetry of the diagrams. Either for the ingoing or for the outgoing lines, we have two possibilities of interchanging them without creating a new diagram. In the third diagram, both the ingoing and the outgoing lines have this symmetry, which gives us in total the prefactor 1/4.

In Eq. (6.1) a new cumulant with four legs appears, i.e. it depends on four time variables. Therefore, $2^4 = 16$ possibilities to distribute path indices $\pm$ exist. In the MI phase we were able to find a matrix representation for the $2^2 = 4$ cumulants in the second order. By a rotation of this matrix we could reduce the number of terms to only three. Now we will try a similar procedure again, but instead of a bilinear form, a fourth rank tensor must be rotated. The components of this tensor $C_i^{\mathrm{P}_1\mathrm{P}_2\mathrm{P}_3\mathrm{P}_4}(t_1,t_2;t_3,t_4)$ are given by Eq. (4.13). To save some space, we change the notation a little

bit by writing ${}_iC^{\mathrm{P_1P_4}}_{\mathrm{P_2P_3}}$ in the following. The product of this tensor with the currents can be written as

$$
\begin{aligned}
&{}_iC^{\mathrm{P_1P_4}}_{\mathrm{P_2P_3}} j^*_{i,\mathrm{P_1}}(t_1) j^*_{i,\mathrm{P_2}}(t_2) j_{i,\mathrm{P_3}}(t_3) j_{i,\mathrm{P_4}}(t_4) = \\
&= \tilde{\boldsymbol{j}}^*_i(t_1) \begin{pmatrix} \tilde{\boldsymbol{j}}^*_i(t_2) \begin{pmatrix} {}_iC^{++}_{++} & {}_iC^{++}_{+-} \\ {}_iC^{++}_{-+} & {}_iC^{++}_{--} \end{pmatrix} \tilde{\boldsymbol{j}}_i(t_3) & \tilde{\boldsymbol{j}}^*_i(t_2) \begin{pmatrix} {}_iC^{+-}_{++} & {}_iC^{+-}_{+-} \\ {}_iC^{+-}_{-+} & {}_iC^{+-}_{--} \end{pmatrix} \tilde{\boldsymbol{j}}_i(t_3) \\ \tilde{\boldsymbol{j}}^*_i(t_2) \begin{pmatrix} {}_iC^{-+}_{++} & {}_iC^{-+}_{+-} \\ {}_iC^{-+}_{-+} & {}_iC^{-+}_{--} \end{pmatrix} \tilde{\boldsymbol{j}}_i(t_3) & \tilde{\boldsymbol{j}}^*_i(t_2) \begin{pmatrix} {}_iC^{--}_{++} & {}_iC^{--}_{+-} \\ {}_iC^{--}_{-+} & {}_iC^{--}_{--} \end{pmatrix} \tilde{\boldsymbol{j}}_i(t_3) \end{pmatrix} \tilde{\boldsymbol{j}}_i(t_4)
\end{aligned} \tag{6.2}
$$

where the definition of the vector currents from Eq. (4.21) is applied.

This object can be Keldysh-rotated by rotating the sub-matrices as well as the overall matrix. In the new expression the currents $\tilde{\boldsymbol{j}}$ and $\tilde{\boldsymbol{j}}^*$ are replaced by $\boldsymbol{j}$ and $\boldsymbol{j}^*$ defined in Eqs. (4.22) and (4.23). The new cumulants are linear combinations of the 16 original ones from Eq. (6.2). These rotated cumulants are denoted by ${}_iC^{\mathrm{cl/q,cl/q}}_{\mathrm{cl/q,cl/q}}$. For an implicit definition of these cumulants, we write down the rotated equivalent of Eq. (6.2):

$$
\begin{aligned}
&\boldsymbol{j}^*_i(t_1) \begin{pmatrix} \boldsymbol{j}^*_i(t_2) \begin{pmatrix} {}_iC^{\mathrm{cl,cl}}_{\mathrm{cl,cl}} & {}_iC^{\mathrm{cl,cl}}_{\mathrm{cl,q}} \\ {}_iC^{\mathrm{cl,cl}}_{\mathrm{q,cl}} & {}_iC^{\mathrm{cl,cl}}_{\mathrm{q,q}} \end{pmatrix} \boldsymbol{j}_i(t_3) & \boldsymbol{j}^*_i(t_2) \begin{pmatrix} {}_iC^{\mathrm{cl,q}}_{\mathrm{cl,cl}} & {}_iC^{\mathrm{cl,q}}_{\mathrm{cl,q}} \\ {}_iC^{\mathrm{cl,q}}_{\mathrm{q,cl}} & {}_iC^{\mathrm{cl,q}}_{\mathrm{q,q}} \end{pmatrix} \boldsymbol{j}_i(t_3) \\ \boldsymbol{j}^*_i(t_2) \begin{pmatrix} {}_iC^{\mathrm{q,cl}}_{\mathrm{cl,cl}} & {}_iC^{\mathrm{q,cl}}_{\mathrm{cl,q}} \\ {}_iC^{\mathrm{q,cl}}_{\mathrm{q,cl}} & {}_iC^{\mathrm{q,cl}}_{\mathrm{q,q}} \end{pmatrix} \boldsymbol{j}_i(t_3) & \boldsymbol{j}^*_i(t_2) \begin{pmatrix} {}_iC^{\mathrm{q,q}}_{\mathrm{cl,cl}} & {}_iC^{\mathrm{q,q}}_{\mathrm{cl,q}} \\ {}_iC^{\mathrm{q,q}}_{\mathrm{q,cl}} & {}_iC^{\mathrm{q,q}}_{\mathrm{q,q}} \end{pmatrix} \boldsymbol{j}_i(t_3) \end{pmatrix} \boldsymbol{j}_i(t_4) \equiv \\
&\equiv \boldsymbol{j}^*_i(t_1) \boldsymbol{j}^*_i(t_2) \boldsymbol{C}^{(4)}_i(t_1, t_2; t_3, t_4) \boldsymbol{j}_i(t_3) \boldsymbol{j}_i(t_4).
\end{aligned} \tag{6.3}
$$

It might appear strange to call, for instance, the cumulant in the top left-hand corner ${}_iC^{\mathrm{cl,cl}}_{\mathrm{cl,cl}}$, although it is multiplied only with quantum components of the currents, but the meaning becomes clear, when we take a look at the origin of the cumulants: Inverting the relations (3.53), we can express the operators $\hat{\mathrm{a}}_\pm$ and currents $j_\pm$ in terms of operators $\hat{\mathrm{a}}_{\mathrm{q/cl}}$ and currents $j_{\mathrm{q/cl}}$. The generating functional $\mathcal{F}[j, j^*]$, given in Eq. (3.59) which is a functional of j_+, j_-, j^*_+, and j^*_-, can then be rewritten as a functional of the rotated currents $j_{\mathrm{cl}}, j_{\mathrm{q}}, j^*_{\mathrm{cl}}$, and j^*_{q}. Instead of terms like $j_+\hat{\mathrm{a}}_+ - j_-\hat{\mathrm{a}}_-$, we have $j_{\mathrm{q}}\hat{\mathrm{a}}_{\mathrm{cl}} + j_{\mathrm{cl}}\hat{\mathrm{a}}_{\mathrm{q}}$. Thus quantum currents mix with classical fields and vice versa. When we now expand this generating functional in terms of the rotated currents, we always get a classical operator in the cumulant, when a derivative with respect to a quantum current is taken, e.g. $\frac{\delta}{\delta j_{i,\mathrm{cl}}(t)} \hbar\mathcal{F}[\boldsymbol{j}, \boldsymbol{j}^*] = \langle \hat{\mathrm{a}}^\dagger_{i,\mathrm{q}}(t) \rangle$. Therefore we

have together with the decomposition formula from Eq. (4.13):

$$
\begin{aligned}
{}_iC^{\mathrm{cl,cl}}_{\mathrm{cl,cl}}(t_1,t_2;t_3,t_4) = i^3\Bigg\{&\left\langle \hat{\mathrm{T}}_\mathrm{c}\left\{\hat{\mathrm{a}}_{i,\mathrm{cl}}(t_1)\hat{\mathrm{a}}_{i,\mathrm{cl}}(t_2)\hat{\mathrm{a}}^\dagger_{i,\mathrm{cl}}(t_3)\hat{\mathrm{a}}^\dagger_{i,\mathrm{cl}}(t_4)\right\}\right\rangle_0 - \left\langle \hat{\mathrm{T}}_\mathrm{c}\left\{\hat{\mathrm{a}}_{i,\mathrm{cl}}(t_1)\hat{\mathrm{a}}^\dagger_{i,\mathrm{cl}}(t_3)\right\}\right\rangle_0 \\
&\times\left\langle \hat{\mathrm{T}}_\mathrm{c}\left\{\hat{\mathrm{a}}_{i,\mathrm{cl}}(t_2)\hat{\mathrm{a}}^\dagger_{i,\mathrm{cl}}(t_4)\right\}\right\rangle_0 - \left\langle \hat{\mathrm{T}}_\mathrm{c}\left\{\hat{\mathrm{a}}_{i,\mathrm{cl}}(t_1)\hat{\mathrm{a}}^\dagger_{i,\mathrm{cl}}(t_4)\right\}\right\rangle_0\left\langle \hat{\mathrm{T}}_\mathrm{c}\left\{\hat{\mathrm{a}}_{i,\mathrm{cl}}(t_2)\hat{\mathrm{a}}^\dagger_{i,\mathrm{cl}}(t_3)\right\}\right\rangle_0\Bigg\}. \qquad (6.4)
\end{aligned}
$$

The other cumulants in Eq. (6.3) are obtained in the same way. As for $n = 2$, the element in the right-down corner vanishes:

$$
\begin{aligned}
{}_iC^{\mathrm{q,q}}_{\mathrm{q,q}}(t_1,t_2;t_3,t_4) = i^3\Bigg\{&\left\langle \hat{\mathrm{T}}_\mathrm{c}\left\{\hat{\mathrm{a}}_{i,\mathrm{q}}(t_1)\hat{\mathrm{a}}_{i,\mathrm{q}}(t_2)\hat{\mathrm{a}}^\dagger_{i,\mathrm{q}}(t_3)\hat{\mathrm{a}}^\dagger_{i,\mathrm{q}}(t_4)\right\}\right\rangle_0 - \left\langle \hat{\mathrm{T}}_\mathrm{c}\left\{\hat{\mathrm{a}}_{i,\mathrm{q}}(t_1)\hat{\mathrm{a}}^\dagger_{i,\mathrm{q}}(t_3)\right\}\right\rangle_0 \\
&\times\left\langle \hat{\mathrm{T}}_\mathrm{c}\left\{\hat{\mathrm{a}}_{i,\mathrm{q}}(t_2)\hat{\mathrm{a}}^\dagger_{i,\mathrm{q}}(t_4)\right\}\right\rangle_0 - \left\langle \hat{\mathrm{T}}_\mathrm{c}\left\{\hat{\mathrm{a}}_{i,\mathrm{q}}(t_1)\hat{\mathrm{a}}^\dagger_{i,\mathrm{q}}(t_4)\right\}\right\rangle_0\left\langle \hat{\mathrm{T}}_\mathrm{c}\left\{\hat{\mathrm{a}}_{i,\mathrm{q}}(t_2)\hat{\mathrm{a}}^\dagger_{i,\mathrm{q}}(t_3)\right\}\right\rangle_0\Bigg\} = 0. \qquad (6.5)
\end{aligned}
$$

This guarantees the compliance of the normalization condition (5.13), since this cumulant is the only one which is not multiplied by quantum currents j_q, and thus this term wouldn't vanish by setting $j_\mathrm{q} = 0$. We can generalize the latter observation for any cumulant $C_{\mathrm{q}\cdots\mathrm{q}}$: These cumulants have to vanish in order to have Eq. (5.13) fulfilled [75]. The normalization condition (5.13) therefore is equivalent to

$$
C_{\mathrm{q}\cdots\mathrm{q}} = 0. \qquad (6.6)
$$

The proof of Eq. (6.6) is important and will be needed again at a later stage. We must show that any expectation value of quantum component operators $\left\langle \hat{\mathrm{T}}_\mathrm{c}\left\{\hat{\mathrm{a}}_{i,\mathrm{q}}(t_1)\cdots\hat{\mathrm{a}}^\dagger_{i,\mathrm{q}}(t_n)\right\}\right\rangle_0$ is zero. We therefore replace these operators by the operators in the $\pm$-basis according to the definition (3.53):

$$
2^{-n/2}\left\langle \hat{\mathrm{T}}_\mathrm{c}\left\{\left(\hat{\mathrm{a}}_{i,+}(t_1) - \hat{\mathrm{a}}_{i,+}(t_1)\right)\cdots\left(\hat{\mathrm{a}}^\dagger_{i,+}(t_n) - \hat{\mathrm{a}}^\dagger_{i,-}(t_n)\right)\right\}\right\rangle_0.
$$

Multiplying this out yields 2^n path-ordered terms. Now it is crucial to note that within a path-ordered product the position of the operator with the largest time does not depend on its path index. But this means that each ordered product appears twice, though with different signs. Thus, every term cancels out.

Instead of examining the other elements at this stage, let's continue with, in principal, the same procedure as in the MI phase and perform a Legendre transformation of $\mathcal{F}[j, j^*]$ in Eq. (6.1). Afterwards we will see which of the cumulants we really need to calculate. The definition for the Legendre transformation is the same as before, given in Eqs. (5.3) and (5.4), but to be more economic, we work in the {q,cl}-basis and in Fourier space from the beginning. As the Legendre transformation now requires a lot of bookkeeping, it is convenient to write it down diagrammatically. To this end, we

modify our previous definitions from Eqs. (4.14) and (4.15). The cumulant tensors are symbolized by

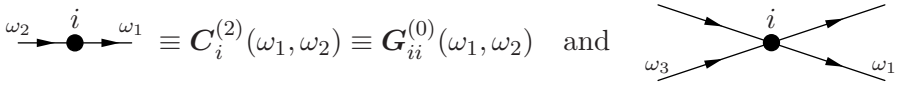

(6.7)

The vector currents are depicted by

(6.8)

If we now connect currents and cumulants with a closed line, we must integrate the corresponding frequency variable divided by 2π. When two cumulants are linked by a hopping, we additionally have to put the Pauli matrix σ^1 between the cumulants. Note that these re-definitions of the diagrams do not affect the expansion (6.1).

To do the Legendre transformation, we still must define symbols for the order fields and the inverse cumulants. We associate them with white squares and circles:

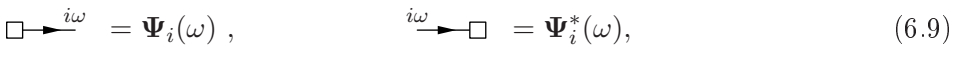

(6.9)

and

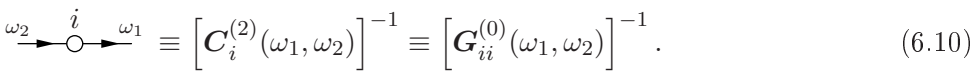

(6.10)

If we multiply a cumulant with its inverse, we get a δ-function in the frequencies and a Kronecker-δ in spatial variables, i.e.:

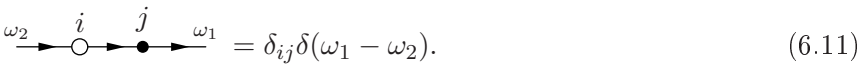

(6.11)

Note that the internal line between black and white cumulants does *not* represent a hopping, therefore it is not associated with the Pauli matrix σ^1.

Diagrammatically, Eq. (5.3) reads

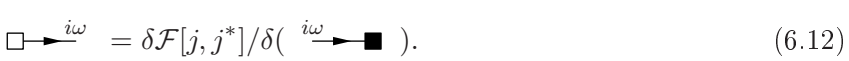

(6.12)

Such a diagrammatic derivative is performed by taking away the respective leg from all the graphs in $\mathcal{F}$. If there are graphs without such legs, they vanish completely. For graphs with more than one of

them, the usual product rule of differentiation has to be applied. We this we get from Eq. (6.1):

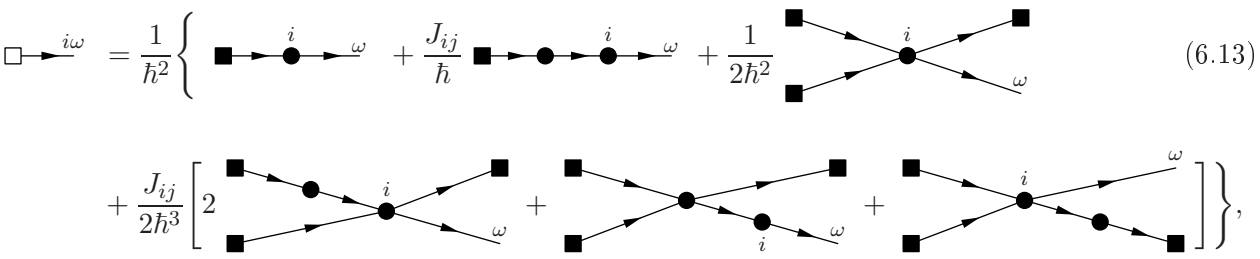

(6.13)

and a similar expression for the complex conjugate. Due to the derivative, there are some cumulants fixed to the site index i. Of course, currents which are directly linked to these cumulants must have the same site index. The site index of cumulants which are linked to them is summed, but such a link necessarily comes along with a hopping matrix element J_{ij} multiplying the whole diagram. In our case this restricts the summation to nearest neighbors.

Now Eq. (6.13) must be inverted iteratively, but now the iteration involves the hopping *and* the order fields. From our previous considerations in the Mott phase, we already know the solutions in the first hopping order and in second order in the fields, since we only have to insert Eq. (5.37) in the rotated and Fourier-transformed version of Eq. (5.6). In our diagrammatic notation this yields:

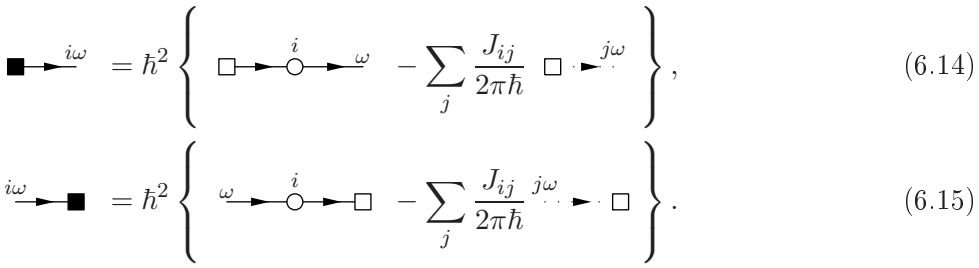

(6.14)

(6.15)

Here we have used a dotted line in order to mark the legs originally coming from a hopping process. They have to be distinguished from the others because of the σ^1 matrix which is multiplied by them.

Now we multiply Eq. (6.13) with $\overset{i\omega}{\longrightarrow\!\!\circ\!\!\longrightarrow}$ and insert Eqs. (6.14) and (6.15). We throw away all diagrams with a prefactor J^2 and are already at the end of the iteration, because any further step would give only terms which are of higher than fourth order in the fields. We now have

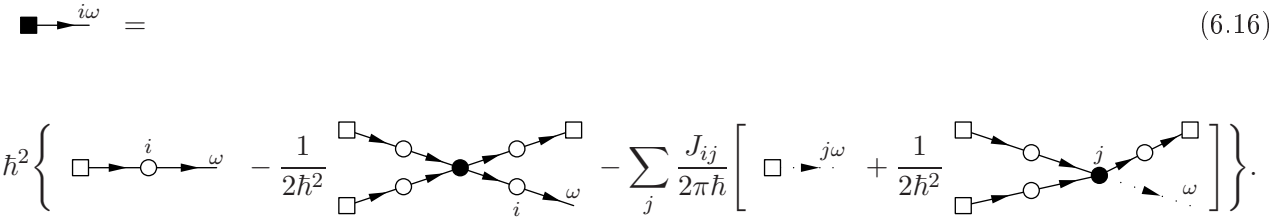

(6.16)

A similar expression exists for the complex conjugate of the order field. When we insert this into the equation for the effective action given by (5.4), we at first get a lot of diagrams. Of course, all diagrams with more than four order fields or of higher than linear hopping order are not taken into account.

We find that the diagrams with four legs and one hopping cancel. Thus the final result becomes very compact. Not surprisingly, it only contains the one-particle-irreducible diagrams:

$$\Gamma^{(4,1)} = -\hbar^2 \Bigg\{$$ 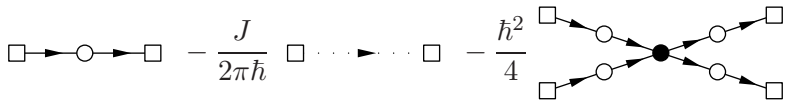 $$\Bigg\}. \tag{6.17}$$

Now we can replace the diagrams by its analytical analogues:

$$\begin{aligned}\Gamma^{(4,1)}[\boldsymbol{\Psi},\boldsymbol{\Psi}^*] = -\hbar^2 \Bigg\{ \sum_{i,j} \int_{-\infty}^{\infty} \frac{\mathrm{d}\omega_1}{2\pi} \int_{-\infty}^{\infty} \frac{\mathrm{d}\omega_3}{2\pi} \Bigg[\Bigg(\boldsymbol{\Psi}_i^*(\omega_1) \left[\boldsymbol{G}_{ii}^{(0)}(\omega_1)\right]^{-1} \boldsymbol{\Psi}_j(\omega_3) - \frac{J_{ij}}{\hbar} \boldsymbol{\Psi}_i^*(\omega_1)\sigma^1 \boldsymbol{\Psi}_i(\omega_3) \Bigg) \\ \times \frac{1}{2\pi}\delta(\omega_1-\omega_3) - \frac{\hbar^2}{4} \int_{-\infty}^{\infty} \frac{\mathrm{d}\omega_2}{2\pi} \int_{-\infty}^{\infty} \frac{\mathrm{d}\omega_4}{2\pi}\, \boldsymbol{\Psi}_i^*(\omega_1) \left[\boldsymbol{G}_{ii}^{(0)}(\omega_1)\right]^{-1} \boldsymbol{\Psi}_i^*(\omega_2) \left[\boldsymbol{G}_{ii}^{(0)}(\omega_2)\right]^{-1} \\ \times {}_i\boldsymbol{C}^4(\omega_1,\omega_2;\omega_3,\omega_4) \left[\boldsymbol{G}_{ii}^{(0)}(\omega_3)\right]^{-1} \boldsymbol{\Psi}_i(\omega_3) \left[\boldsymbol{G}_{ii}^{(0)}(\omega_4)\right]^{-1} \boldsymbol{\Psi}_i(\omega_4) \Bigg] \Bigg\}. \end{aligned} \tag{6.18}$$

6.2 Equations of Motion

Like before in the MI phase, we are especially interested in the equations of motion, which we get by taking the functional derivatives of $\Gamma^{(4,1)}[\boldsymbol{\Psi},\boldsymbol{\Psi}^*]$ from Eq. (6.18) with respect to the order fields. Again we choose the trivial solution for the quantum components of the order fields, $\Psi_\mathrm{q} = \Psi_\mathrm{q}^* = 0$, because we always want the backward fields having the same value as the forward ones. With this, the following two equations of motion are solved for arbitrary Ψ_cl and Ψ_cl^*:

$$\frac{\delta\Gamma}{\delta\Psi_{i,\mathrm{cl}}(\omega)} \stackrel{!}{=} 0, \tag{6.19}$$

$$\frac{\delta\Gamma}{\delta\Psi_{i,\mathrm{cl}}^*(\omega)} \stackrel{!}{=} 0. \tag{6.20}$$

In these derivatives, the only terms which do not include any quantum fields are the ones which contain the vanishing "all q"-cumulant. These terms, however, are zero because of the vanishing of this cumulant. Taking the derivatives with respect to a quantum component field yields another two equations of motion, which remain non-trivial under the condition $\Psi_\mathrm{q} = \Psi_\mathrm{q}^* = 0$:

$$\begin{aligned}\frac{\delta\Gamma[\boldsymbol{\Psi},\boldsymbol{\Psi}^*]}{\delta\Psi_{i,\mathrm{q}}(\omega)} = \frac{\hbar^2}{(2\pi)^3} \sum_j \Bigg\{ \Psi_{j,\mathrm{cl}}^*(\omega) \left(\frac{1}{g_\mathrm{A}(\omega)} - \frac{J_{ji}}{\hbar}\right) - \frac{\hbar^2}{4} \int_{-\infty}^{\infty}\mathrm{d}\omega_1 \int_{-\infty}^{\infty}\mathrm{d}\omega_2 \int_{-\infty}^{\infty}\mathrm{d}\omega_3 \\ \times \frac{1}{2\pi} \left[{}_jC_{\mathrm{q,q}}^{\mathrm{q,cl}}(\omega_1,\omega_2;\omega_3,\omega) \;+\; {}_jC_{\mathrm{q,cl}}^{\mathrm{q,q}}(\omega_1,\omega_2;\omega,\omega_3) \right] \frac{\Psi_{j,\mathrm{cl}}^*(\omega_1)\Psi_{j,\mathrm{cl}}^*(\omega_2)\Psi_{j,\mathrm{cl}}(\omega_3)}{g_\mathrm{A}(\omega_1)g_\mathrm{A}(\omega_2)g_\mathrm{R}(\omega_3)g_\mathrm{A}(\omega)} \Bigg\} \stackrel{!}{=} 0, \end{aligned} \tag{6.21}$$

$$\begin{aligned}\frac{\delta\Gamma[\boldsymbol{\Psi},\boldsymbol{\Psi}^*]}{\delta\Psi_{i,\mathrm{q}}^*(\omega)} = \frac{\hbar^2}{(2\pi)^3} \sum_j \Bigg\{ \Psi_{j,\mathrm{cl}}(\omega) \left(\frac{1}{g_\mathrm{R}(\omega)} - \frac{J_{ij}}{\hbar}\right) - \frac{\hbar^2}{4} \int_{-\infty}^{\infty}\mathrm{d}\omega_2 \int_{-\infty}^{\infty}\mathrm{d}\omega_3 \int_{-\infty}^{\infty}\mathrm{d}\omega_4 \\ \times \frac{1}{2\pi} \left[{}_jC_{\mathrm{q,q}}^{\mathrm{cl,q}}(\omega,\omega_2;\omega_3,\omega_4) \;+\; {}_jC_{\mathrm{cl,q}}^{\mathrm{q,q}}(\omega_2,\omega;\omega_3,\omega_4) \right] \frac{\Psi_{j,\mathrm{cl}}^*(\omega_2)\Psi_{j,\mathrm{cl}}(\omega_3)\Psi_{j,\mathrm{cl}}(\omega_4)}{g_\mathrm{R}(\omega)g_\mathrm{A}(\omega_2)g_\mathrm{R}(\omega_3)g_\mathrm{R}(\omega_4)} \Bigg\} \stackrel{!}{=} 0. \end{aligned} \tag{6.22}$$

Thus, only four of the fifteen non-vanishing elements in ${}_j\boldsymbol{C}^{(4)}$ determine the dynamics of the system as long as we assume the quantum component to be zero. These four cumulants ${}_jC^{\mathrm{cl,q}}_{\mathrm{q,q}}$, ${}_jC^{\mathrm{q,cl}}_{\mathrm{q,q}}$, ${}_jC^{\mathrm{q,q}}_{\mathrm{cl,q}}$, ${}_jC^{\mathrm{q,q}}_{\mathrm{q,cl}}$ require a closer examination.

6.2.1 The {q,q,q,cl} Cumulants

To simplify the notation, we will drop the site index of both the cumulants and the operators in this subsection.

- We first take a look at the relation of these cumulants to the Green's functions. According to Eq. (4.13), the decompositions are given by $C^{\mathrm{cl,q}}_{\mathrm{q,q}} = G^{\mathrm{cl,q}}_{\mathrm{q,q}} - iG^{\mathrm{cl,q}}G_{\mathrm{q,q}} - iG^{\mathrm{cl}}_{\mathrm{q}}G^{\mathrm{q}}_{\mathrm{q}}$. Both products of 2-point functions involve a {q,q} Green's function and therefore vanish. Thus any {q,q,q,cl} cumulant is identical to its corresponding Green's function. We have

$$C^{\mathrm{cl,q}}_{\mathrm{q,q}}(t_1,t_2;t_3,t_4) = -i\Big\langle \hat{\mathrm{T}}_{\mathrm{c}} \left\{ \hat{\mathrm{a}}_{\mathrm{cl}}(t_1)\hat{\mathrm{a}}_{\mathrm{q}}(t_2)\hat{\mathrm{a}}^{\dagger}_{\mathrm{q}}(t_3)\hat{\mathrm{a}}^{\dagger}_{\mathrm{q}}(t_4) \right\} \Big\rangle_0, \tag{6.23}$$

$$C^{\mathrm{q,q}}_{\mathrm{cl,q}}(t_1,t_2;t_3,t_4) = -i\Big\langle \hat{\mathrm{T}}_{\mathrm{c}} \left\{ \hat{\mathrm{a}}_{\mathrm{q}}(t_1)\hat{\mathrm{a}}_{\mathrm{cl}}(t_2)\hat{\mathrm{a}}^{\dagger}_{\mathrm{q}}(t_3)\hat{\mathrm{a}}^{\dagger}_{\mathrm{q}}(t_4) \right\} \Big\rangle_0, \tag{6.24}$$

$$C^{\mathrm{q,q}}_{\mathrm{q,cl}}(t_1,t_2;t_3,t_4) = -i\Big\langle \hat{\mathrm{T}}_{\mathrm{c}} \left\{ \hat{\mathrm{a}}_{\mathrm{q}}(t_1)\hat{\mathrm{a}}_{\mathrm{q}}(t_2)\hat{\mathrm{a}}^{\dagger}_{\mathrm{cl}}(t_3)\hat{\mathrm{a}}^{\dagger}_{\mathrm{q}}(t_4) \right\} \Big\rangle_0, \tag{6.25}$$

$$C^{\mathrm{q,cl}}_{\mathrm{q,q}}(t_1,t_2;t_3,t_4) = -i\Big\langle \hat{\mathrm{T}}_{\mathrm{c}} \left\{ \hat{\mathrm{a}}_{\mathrm{q}}(t_1)\hat{\mathrm{a}}_{\mathrm{q}}(t_2)\hat{\mathrm{a}}^{\dagger}_{\mathrm{q}}(t_3)\hat{\mathrm{a}}^{\dagger}_{\mathrm{cl}}(t_4) \right\} \Big\rangle_0. \tag{6.26}$$

- Second we note a quite obvious symmetry concerning the interchange of variables: We can change the time variables of two annihilation operators or of two creation operators if we change as well their indices {q,cl}. Note that, in general, we cannot do that with one annihilation and one creation operator. As a consequence of this we have

$$C^{\mathrm{cl,q}}_{\mathrm{q,q}}(t_1,t_2;t_3,t_4) = C^{\mathrm{q,q}}_{\mathrm{cl,q}}(t_2,t_1;t_3,t_4), \tag{6.27}$$

$$C^{\mathrm{q,cl}}_{\mathrm{q,q}}(t_1,t_2;t_3,t_4) = C^{\mathrm{q,q}}_{\mathrm{q,cl}}(t_1,t_2;t_4,t_3). \tag{6.28}$$

  This relation also holds in frequency space as can easily be seen by applying a Fourier transformation on these equations. Therefore the number of different cumulants in the equations of motion is reduced from four to two. Thus, in both equations (6.21) and (6.22), we can simply sum the cumulants:

$$C^{\mathrm{q,cl}}_{\mathrm{q,q}}(\omega_1,\omega_2;\omega_3,\omega) + C^{\mathrm{q,q}}_{\mathrm{q,cl}}(\omega_1,\omega_2;\omega,\omega_3) = 2C^{\mathrm{q,cl}}_{\mathrm{q,q}}(\omega_1,\omega_2;\omega_3,\omega), \tag{6.29}$$

$$C^{\mathrm{cl,q}}_{\mathrm{q,q}}(\omega,\omega_2;\omega_3,\omega_4) + C^{\mathrm{q,q}}_{\mathrm{cl,q}}(\omega_2,\omega;\omega_3,\omega_4) = 2C^{\mathrm{cl,q}}_{\mathrm{q,q}}(\omega,\omega_2;\omega_3,\omega_4). \tag{6.30}$$

- Finally we will show how these remaining two cumulants are related to each other by means of a complex conjugation. That there exists such a relation, is already obvious from the definitions (6.23)–(6.26), but we will show this explicitly via a long but helpful calculation.

To this end we introduce the short-hand notation $\big[\hat{a}_+ \pm \hat{a}_-\big](t_1) = \hat{a}_+(t_1) \pm \hat{a}_-(t_1)$ and use the definition from Eq. (3.53):

$$\begin{aligned} C^{\mathrm{cl,q}}_{\mathrm{q,q}}(t_1,t_2;t_3,t_4) &= \frac{-i}{4}\Big\langle \hat{\mathrm{T}}_{\mathrm{c}} \Big\{ \big[\hat{a}_+ + \hat{a}_-\big](t_1)\big[\hat{a}_+ - \hat{a}_-\big](t_2)\big[\hat{a}^\dagger_+ - \hat{a}^\dagger_-\big](t_3)\big[\hat{a}^\dagger_+ - \hat{a}^\dagger_-\big](t_4)\Big\}\Big\rangle_0 = \\ &\frac{-i}{4}\Big\langle \hat{\mathrm{T}}_{\mathrm{c}} \Big\{ \big[\hat{a}_+ - \hat{a}_- + 2\hat{a}_-\big](t_1)\big[\hat{a}_+ - \hat{a}_-\big](t_2)\big[\hat{a}^\dagger_+ - \hat{a}^\dagger_-\big](t_3)\big[\hat{a}^\dagger_+ - \hat{a}^\dagger_-\big](t_4)\Big\}\Big\rangle_0 = \\ &\frac{-i}{2}\Big\langle \hat{\mathrm{T}}_{\mathrm{c}} \Big\{ \hat{a}_-(t_1)\big[\hat{a}_+ - \hat{a}_-\big](t_2)\big[\hat{a}^\dagger_+ - \hat{a}^\dagger_-\big](t_3)\big[\hat{a}^\dagger_+ - \hat{a}^\dagger_-\big](t_4)\Big\}\Big\rangle_0 . \end{aligned} \tag{6.31}$$

For the last equality we have to split the expectation value of the second line into a sum of two expectation values and recognize that one of them vanishes, since it contains operators $\hat{a}_+ - \hat{a}_- \sim \hat{a}_{\mathrm{q}}$ only.

Now we must show the important relation

$$\Big\langle \hat{\mathrm{T}}_{\mathrm{c}} \Big\{ \hat{a}_-(t_1)\big[\hat{a}_+ - \hat{a}_-\big](t_2)\big[\hat{a}^\dagger_+ - \hat{a}^\dagger_-\big](t_3)\big[\hat{a}^\dagger_+ - \hat{a}^\dagger_-\big](t_4)\Big\}\Big\rangle_0 = 0 \qquad \text{if } t_1 \text{ is not the largest time.} \tag{6.32}$$

The proof of this is based on the same arguments as for the vanishing of the {q,q,q,q} cumulants given in Section 6.1. We must remember that the path order does not depend on the path index of the operator with the largest time. Since in Eq. (6.32) the operators at t_2, t_3, t_4 appear twice with different signs, all ordered products cancel if one of those times was the largest.

Note furthermore the symmetry in $t_3 \leftrightarrow t_4$. This allows to consider only three different time-orders $\theta(t_1-t_2)\theta(t_2-t_3)\theta(t_3-t_4)$, $\theta(t_1-t_3)\theta(t_3-t_2)\theta(t_2-t_4)$, and $\theta(t_1-t_3)\theta(t_3-t_4)\theta(t_4-t_2)$. Time-orders with $t_4 > t_3$ can directly be read from the ones given here by re-symmetrizing the result. We will denote this symmetrization by $\{\cdot\}_{t_3\leftrightarrow t_4}$. This saves space and reduces the computational task.

For a calculation of the expectation value in Eq. (6.32), we multiply out all the products yielding eight path-ordered terms. Then we consider each of the three relevant time-orders making use of Heaviside step functions $\theta(t-t')$. We then find for each time-order that the eight products can be expressed by a triple commutator. We therefore have:

$$\begin{aligned} C^{\mathrm{cl,q}}_{\mathrm{q,q}}(t_1,t_2;t_3,t_4) = \frac{-i}{2}\Bigg\{ &\theta(t_1-t_2)\theta(t_2-t_3)\theta(t_3-t_4)\Big\langle\Big[\Big[\Big[\hat{a}(t_1),\hat{a}(t_2)\Big],\hat{a}^\dagger(t_3)\Big],\hat{a}^\dagger(t_4)\Big]\Big\rangle_0 \\ &+\theta(t_1-t_3)\theta(t_3-t_2)\theta(t_2-t_4)\Big\langle\Big[\Big[\Big[\hat{a}(t_1),\hat{a}^\dagger(t_3)\Big],\hat{a}(t_2)\Big],\hat{a}^\dagger(t_4)\Big]\Big\rangle_0 \\ &+\theta(t_1-t_3)\theta(t_3-t_4)\theta(t_4-t_2)\Big\langle\Big[\Big[\Big[\hat{a}(t_1),\hat{a}^\dagger(t_3)\Big],\hat{a}^\dagger(t_4)\Big],\hat{a}(t_2)\Big]\Big\rangle_0\Bigg\}_{t_3\leftrightarrow t_4} . \end{aligned} \tag{6.33}$$

We note that this is almost identical to the usual definition of retarded n-point functions [55]. For convenience we introduce a factor 2 and define:

$$2C^{\mathrm{cl,q}}_{\mathrm{q,q}}(t_1,t_2;t_3,t_4) \equiv C^{\mathrm{R}}(t_1,t_2;t_3,t_4). \tag{6.34}$$

The other cumulant can be brought analogously to a similar form

$$C^{\mathrm{q,cl}}_{\mathrm{q,q}}(t_1,t_2;t_3,t_4) = \frac{-i}{2}\Bigg\{\theta(t_4-t_1)\theta(t_1-t_3)\theta(t_3-t_2)\left\langle\left[\left[\left[\hat{\mathrm{a}}^\dagger(t_4),\hat{\mathrm{a}}(t_1)\right],\hat{\mathrm{a}}^\dagger(t_3)\right],\hat{\mathrm{a}}(t_2)\right]\right\rangle_0 \tag{6.35}$$
$$+\theta(t_4-t_3)\theta(t_3-t_1)\theta(t_1-t_2)\left\langle\left[\left[\left[\hat{\mathrm{a}}^\dagger(t_4),\hat{\mathrm{a}}^\dagger(t_3)\right],\hat{\mathrm{a}}(t_1)\right],\hat{\mathrm{a}}(t_2)\right]\right\rangle_0$$
$$+\theta(t_4-t_1)\theta(t_1-t_2)\theta(t_2-t_3)\left\langle\left[\left[\left[\hat{\mathrm{a}}^\dagger(t_4),\hat{\mathrm{a}}(t_1)\right],\hat{\mathrm{a}}(t_2)\right],\hat{\mathrm{a}}^\dagger(t_3)\right]\right\rangle_0\Bigg\}_{t_1\leftrightarrow t_2}.$$

Coming back to the relation between this cumulant and the the cumulant from Eq. (6.33), we must recognize that $(\hat{\mathrm{A}}\hat{\mathrm{B}})^\dagger = \hat{\mathrm{B}}^\dagger\hat{\mathrm{A}}^\dagger$. Thus a complex conjugation acting on a commutator yields a minus sign, $[\hat{\mathrm{A}},\hat{\mathrm{B}}]^\dagger = -[\hat{\mathrm{A}}^\dagger,\hat{\mathrm{B}}^\dagger]$. Because of the factor $-i$ in Eq. (6.35) its complex conjugate will maintain the same sign. Therefore the only effect of a complex conjugation is an interchange of annihilation and creation operators. If we then change in addition the time variables $t_1 \leftrightarrow t_4,\ t_2 \leftrightarrow t_3$, we get back to the same expression as in Eq. (6.33). Therefore we have

$$\left(C^{\mathrm{q,cl}}_{\mathrm{q,q}}(t_4,t_3;t_2,t_1)\right)^* = C^{\mathrm{cl,q}}_{\mathrm{q,q}}(t_1,t_2;t_3,t_4). \tag{6.36}$$

Note that a similar relation holds for the 2-point functions. There we have

$$G^{\mathrm{R}}(t_1,t_2) = \left(G^{\mathrm{A}}(t_2,t_1)\right)^*. \tag{6.37}$$

In analogy we will call $2C^{\mathrm{q,cl}}_{\mathrm{q,q}}(t_1,t_2;t_3,t_4) \equiv C^{\mathrm{A}}(t_1,t_2;t_3,t_4)$ the advanced 4-point cumulant. What has to be done next, is to take either the retarded or the advanced function and calculate it. We are especially interested in its Fourier transform. This is a straightforward task very similar to the calculation for the 2-point function, but many different combinations have to be considered. Due to the length of this calculation, we put it into the appendix.

6.2.2 Equilibrium Configuration

Let's now come back to the equations of motion (6.21) and (6.22). Using the definition of the Fourier transformation into $\boldsymbol{k}$-space from Eq. (5.41), the summation over the site index can be eliminated from them. If we still make the equilibrium ansatz of a time-independent, homogeneous order field, i.e. $\Psi_{\boldsymbol{k},\mathrm{cl}}(\omega) = \Psi_{\mathrm{eq}}\delta_{\boldsymbol{k},\boldsymbol{0}}\delta(\omega)$, so that the ω-integrals become trivial. We have

$$2\pi\Psi^*_{\mathrm{eq}}\left(\frac{1}{g_{\mathrm{A}}(0)} - \frac{J_{\boldsymbol{0}}}{\hbar}\right) - \left[C^{\mathrm{q,cl}}_{\mathrm{q,q}}(0,0;0,0) + C^{\mathrm{q,q}}_{\mathrm{q,cl}}(0,0;0,0)\right]\frac{\hbar^2\Psi^*_{\mathrm{eq}}\Psi^*_{\mathrm{eq}}\Psi_{\mathrm{eq}}}{4g_{\mathrm{A}}(0)g_{\mathrm{A}}(0)g_{\mathrm{R}}(0)g_{\mathrm{A}}(0)} \stackrel{!}{=} 0, \tag{6.38}$$

$$2\pi\Psi_{\mathrm{eq}}\left(\frac{1}{g_{\mathrm{R}}(0)} - \frac{J_{\boldsymbol{0}}}{\hbar}\right) - \left[C^{\mathrm{cl,q}}_{\mathrm{q,q}}(0,0;0,0) + C^{\mathrm{q,q}}_{\mathrm{cl,q}}(0,0;0,0)\right]\frac{\hbar^2\Psi^*_{\mathrm{eq}}\Psi_{\mathrm{eq}}\Psi_{\mathrm{eq}}}{4g_{\mathrm{R}}(0)g_{\mathrm{A}}(0)g_{\mathrm{R}}(0)g_{\mathrm{R}}(0)} \stackrel{!}{=} 0. \tag{6.39}$$

From these equations, the equilibrium values of the order field Ψ_{eq} can be read off:

$$\hbar^2|\Psi_{\mathrm{eq}}|^2 = 2\pi\frac{4g_{\mathrm{A}}(0)g_{\mathrm{A}}(0)g_{\mathrm{R}}(0)g_{\mathrm{A}}(0)}{C^{\mathrm{q,cl}}_{\mathrm{q,q}}(0,0;0,0) + C^{\mathrm{q,q}}_{\mathrm{q,cl}}(0,0;0,0)}\left(\frac{1}{g_{\mathrm{A}}(0)} - \frac{J_{\boldsymbol{0}}}{\hbar}\right). \tag{6.40}$$

We note that all Green's functions become real in the limit $\omega \to 0$, which makes the right side of Eq. (6.40) real too, as it must be. The phase ϕ of the equilibrium order field can be chosen arbitrarily, so we set it to zero without loss of generality. Then the solution of the four equations of motion (6.19)–(6.22) in the stationary case reads:

$$\boldsymbol{\Psi}_{\boldsymbol{k},\mathrm{eq}}(\omega) = \begin{pmatrix} \Psi_{\mathrm{eq}} \\ 0 \end{pmatrix} \delta(\omega)\delta_{\boldsymbol{k},\boldsymbol{0}} \qquad \text{and} \qquad \boldsymbol{\Psi}^*_{\boldsymbol{k},\mathrm{eq}}(\omega) = (\Psi_{\mathrm{eq}},\ 0)\,\delta(\omega)\delta_{\boldsymbol{k},\boldsymbol{0}}. \tag{6.41}$$

It should be mentioned that in our basis, $\hbar\Psi_{\mathrm{cl}}$ is not the expectation value $\langle\hat{\mathrm{a}}\rangle$, but $(1/\sqrt{2})\langle\hat{\mathrm{a}}_+ + \hat{\mathrm{a}}_-\rangle = \sqrt{2}\langle\hat{\mathrm{a}}\rangle$.

6.2.3 Linearization of Equation of Motion

In the previous section we have found time-independent order fields in Eq. (6.41), which solve the equations of motion (6.19)–(6.22). But as one main goal is the description of the dynamics of the order parameter, we have to consider time-dependent solutions as well. The problem, however, is the fact that Γ from Eq. (6.18) contains non-local terms. The non-locality in space is associated with the Ψ^2 terms only. Given a homogeneous system, it can be handled by a Fourier transformation into the wave vector space. The non-locality in time, however, also concerns the Ψ^4 term, such that even in frequency space, three non-trivial integrals remain. One thing that helps us out, is a linearization of the equations of motion by assuming a configuration near equilibrium and Taylor expanding the effective action around this equilibrium position. Up to second order, all terms will then be local in Fourier space.

To do that expansion, we first refer to the normalization condition (5.13): Due to the vanishing of the "all q" components of the Green's functions, the whole effective action Γ vanishes, if the quantum fields are zero. Thus we have no zeroth order term. Furthermore, all first-order derivatives of Γ with respect to the fields evaluated at $\boldsymbol{\Psi}_{\mathrm{eq}}$ vanish according to Eqs. (6.38) and (6.39). So the only terms that we have to consider are the second derivatives. With the definitions $\Psi_{\mathrm{cl}}(\omega) \equiv \Psi_{\mathrm{cl}}(\omega) - \Psi_{\mathrm{eq}}$ and $\Psi_{\mathrm{q}}(\omega) \equiv \Psi_{\mathrm{q}}(\omega)$, the effective action reads

$$\begin{aligned}
&\Gamma[\Psi_{\mathrm{q}}, \Psi^*_{\mathrm{q}}, \Psi_{\mathrm{cl}}, \Psi^*_{\mathrm{cl}}] \approx \frac{1}{2}\sum_{ij}\int_{-\infty}^{\infty}\mathrm{d}\omega_1\int_{-\infty}^{\infty}\mathrm{d}\omega_2 \\
&\times\Bigg\{\frac{\delta^2\Gamma}{\delta\Psi_{i,\mathrm{cl}}(\omega_1)\delta\Psi^*_{j,\mathrm{q}}(\omega_2)}\bigg|_{\mathrm{eq}}\Psi^*_{j,\mathrm{q}}(\omega_2)\Psi_{i,\mathrm{cl}}(\omega_1) + \frac{\delta^2\Gamma}{\delta\Psi^*_{i,\mathrm{cl}}(\omega_1)\delta\Psi_{j,\mathrm{q}}(\omega_2)}\bigg|_{\mathrm{eq}}\Psi_{j,\mathrm{q}}(\omega_2)\Psi^*_{i,\mathrm{cl}}(\omega_1) \\
&+\frac{\delta^2\Gamma}{\delta\Psi_{i,\mathrm{cl}}(\omega_1)\delta\Psi_{j,\mathrm{q}}(\omega_2)}\bigg|_{\mathrm{eq}}\Psi_{j,\mathrm{q}}(\omega_2)\Psi_{i,\mathrm{cl}}(\omega_1) + \frac{\delta^2\Gamma}{\delta\Psi^*_{i,\mathrm{cl}}(\omega_1)\delta\Psi^*_{j,\mathrm{q}}(\omega_2)}\bigg|_{\mathrm{eq}}\Psi^*_{j,\mathrm{q}}(\omega_2)\Psi^*_{i,\mathrm{cl}}(\omega_1) \\
&+2\frac{\delta^2\Gamma}{\delta\Psi_{i,\mathrm{q}}(\omega_1)\delta\Psi_{j,\mathrm{q}}(\omega_2)}\bigg|_{\mathrm{eq}}\Psi_{j,\mathrm{q}}(\omega_2)\Psi_{i,\mathrm{q}}(\omega_1) + 2\frac{\delta^2\Gamma}{\delta\Psi^*_{i,\mathrm{q}}(\omega_1)\delta\Psi^*_{j,\mathrm{q}}(\omega_2)}\bigg|_{\mathrm{eq}}\Psi^*_{j,\mathrm{q}}(\omega_2)\Psi^*_{i,\mathrm{q}}(\omega_1) \\
&+2\frac{\delta^2\Gamma}{\delta\Psi_{i,\mathrm{q}}(\omega_1)\delta\Psi^*_{j,\mathrm{q}}(\omega_2)}\bigg|_{\mathrm{eq}}\Psi^*_{j,\mathrm{q}}(\omega_2)\Psi_{i,\mathrm{q}}(\omega_1) + 2\frac{\delta^2\Gamma}{\delta\Psi_{i,\mathrm{cl}}(\omega_1)\delta\Psi^*_{j,\mathrm{cl}}(\omega_2)}\bigg|_{\mathrm{eq}}\Psi^*_{j,\mathrm{cl}}(\omega_2)\Psi_{i,\mathrm{cl}}(\omega_1)
\end{aligned}$$

$$+2\frac{\delta^2\Gamma}{\delta\Psi_{i,\mathrm{cl}}(\omega_1)\delta\Psi_{j,\mathrm{cl}}(\omega_2)}\bigg|_{\mathrm{eq}}\Psi_{j,\mathrm{cl}}(\omega_2)\Psi_{i,\mathrm{cl}}(\omega_1)+2\frac{\delta^2\Gamma}{\delta\Psi^*_{i,\mathrm{cl}}(\omega_1)\delta\Psi^*_{j,\mathrm{cl}}(\omega_2)}\bigg|_{\mathrm{eq}}\Psi^*_{j,\mathrm{cl}}(\omega_2)\Psi^*_{i,\mathrm{cl}}(\omega_1)\Bigg\}. \tag{6.42}$$

The last six terms appear twice, as we have assumed the symmetry $i \leftrightarrow j$ of a homogeneous system in order to save writing space. Actually, this assumption is no restriction here, because we have written down these six terms only for completeness. The last three terms, however, vanish as a consequence of Eq. (5.13) and the other three terms are quadratic in quantum component fields. So when we derive the equations of motion from the expanded effective action in Eq. (6.42) and insert $\Psi_{\mathrm{q}} = \Psi^*_{\mathrm{q}} = 0$, also these terms do not contribute.

The remaining four terms are calculated straightforwardly. The first term reads

$$\begin{aligned}\frac{\delta^2\Gamma}{\delta\Psi_{i,\mathrm{cl}}(\omega_1)\delta\Psi^*_{j,\mathrm{q}}(\omega_2)}\bigg|_{\mathrm{eq}} &= \frac{\hbar^2}{(2\pi)^4}\Bigg\{\Big[\frac{1}{g_{\mathrm{R}}(\omega_1)}\delta_{ij}-\frac{J_{ij}}{\hbar}\Big]2\pi\delta(\omega_1-\omega_2)\\ &\quad-\frac{\hbar^2}{2}\left|\Psi_{\mathrm{eq}}\right|^2\frac{\delta_{ij}C^{\mathrm{R}}(\omega_2,0;0,\omega_1)}{g_{\mathrm{A}}(0)g_{\mathrm{R}}(0)g_{\mathrm{R}}(\omega_1)g_{\mathrm{R}}(\omega_2)}.\end{aligned} \tag{6.43}$$

Note that $C^{\mathrm{R}}(\omega_2,0;0,\omega_1)$ includes a function $\delta(\omega_1-\omega_2)$ as well. The second term with the derivative $\frac{\delta^2\Gamma}{\delta\Psi^*_{i,\mathrm{cl}}(\omega_1)\delta\Psi_{j,\mathrm{q}}(\omega_2)}\big|_{\mathrm{eq}}$ is the complex conjugate of Eq. (6.43), therefore we only have to interchange the advanced functions with the retarded ones. Still the derivative $\frac{\delta^2\Gamma}{\delta\Psi_{i,\mathrm{cl}}(\omega_1)\delta\Psi_{j,\mathrm{q}}(\omega_2)}\big|_{\mathrm{eq}}$ and its complex conjugate must be calculated. Thus, we have

$$\frac{\delta^2\Gamma}{\delta\Psi_{i,\mathrm{cl}}(\omega_1)\delta\Psi_{j,\mathrm{q}}(\omega_2)}\bigg|_{\mathrm{eq}} = -\frac{\hbar^4}{4(2\pi)^4}\left|\Psi_{\mathrm{eq}}\right|^2\frac{\delta_{ij}C^{\mathrm{R}}(\omega_1,\omega_2;0,0)}{g_{\mathrm{R}}(0)g_{\mathrm{R}}(0)g_{\mathrm{R}}(\omega_1)g_{\mathrm{A}}(\omega_2)}, \tag{6.44}$$

and its complex conjugated expression.

Now it is important to note that $C^{\mathrm{R}}(\omega_1,\omega_2;0,0) \sim \delta(\omega_1+\omega_2)$ in contrast to $C^{\mathrm{R}}(\omega_2,0;0,\omega_1) \sim \delta(\omega_1-\omega_2)$. The kernel of our Taylor expanded effective action from Eq. (6.42) therefore depends on one frequency variable only, but at some places this variable appears with a reversed sign. We must be careful with this sign, since neither the 2-point functions nor the 4-point functions are symmetric under a change of sign, i.e. $C^{\mathrm{R}}(\omega,0;0,\omega) \neq C^{\mathrm{R}}(-\omega,0;0,\omega)$. Nevertheless, we have $C^{\mathrm{R}}(\omega,-\omega;0,0) = C^{\mathrm{R}}(-\omega,\omega;0,0)$ according to Eq. (6.27).

Transforming the spatial variables into $\boldsymbol{k}$-space according to Eq. (5.14) yields a Kronecker-δ for translational invariant systems. Therefore the double sum $\sum_{ij}$ reduces to a single on $\sum_{\boldsymbol{k}}$. Similarly, the $\delta(\omega_1 \pm \omega_2)$-functions reduces the number of integrals from two to one. We can therefore write

$$\begin{aligned}\Gamma[\Psi_{\mathrm{q}},\Psi^*_{\mathrm{q}},\Psi_{\mathrm{cl}},\Psi^*_{\mathrm{cl}}] = \frac{1}{2}\sum_{\boldsymbol{k}}\int_{-\infty}^{\infty}\mathrm{d}\omega\Bigg\{&\frac{\delta^2\Gamma}{\delta\Psi_{\boldsymbol{k},\mathrm{cl}}(\omega)\delta\Psi^*_{\boldsymbol{k},\mathrm{q}}(\omega)}\bigg|_{\mathrm{eq}}\Psi^*_{\boldsymbol{k},\mathrm{q}}(\omega)\Psi_{\boldsymbol{k},\mathrm{cl}}(\omega)\\ &+\frac{\delta^2\Gamma}{\delta\Psi^*_{\boldsymbol{k},\mathrm{cl}}(\omega_1)\delta\Psi_{\boldsymbol{k},\mathrm{q}}(\omega)}\bigg|_{\mathrm{eq}}\Psi^*_{\boldsymbol{k},\mathrm{q}}(\omega_2)\Psi^*_{\boldsymbol{k},\mathrm{cl}}(\omega)+\frac{\delta^2\Gamma}{\delta\Psi_{\boldsymbol{k},\mathrm{cl}}(-\omega)\delta\Psi_{\boldsymbol{k},\mathrm{q}}(\omega)}\bigg|_{\mathrm{eq}}\Psi_{\boldsymbol{k},\mathrm{q}}(\omega)\Psi_{\boldsymbol{k},\mathrm{cl}}(-\omega)\\ &+\frac{\delta^2\Gamma}{\delta\Psi^*_{\boldsymbol{k},\mathrm{cl}}(-\omega)\delta\Psi^*_{\boldsymbol{k},\mathrm{q}}(\omega)}\bigg|_{\mathrm{eq}}\Psi^*_{\boldsymbol{k},\mathrm{q}}(\omega)\Psi^*_{\boldsymbol{k},\mathrm{cl}}(-\omega)+O(|\Psi_{\mathrm{q}}|^2)+O(|\Psi|^3)\Bigg\}.\end{aligned} \tag{6.45}$$

The remaining sum and integral are removed when taking the functional derivative. Then the two non-trivial equations of motion (6.21) and (6.22), which are integral equations, now appear as simple algebraic equations. Writing $\Psi_{\boldsymbol{k},\mathrm{cl}} \equiv \Psi$ and inserting Eqs. (6.43) and (6.44), we have

$$\begin{aligned}
0 \stackrel{!}{=} \frac{\delta\Gamma}{\delta\Psi_{\mathrm{q}}(\omega)} &= \frac{1}{2}\left\{ \left.\frac{\delta^2\Gamma}{\delta\Psi_{\boldsymbol{k},\mathrm{cl}}(\omega)\delta\Psi^*_{\boldsymbol{k},\mathrm{q}}(\omega)}\right|_{\mathrm{eq}} \Psi^*_{\boldsymbol{k},\mathrm{cl}}(\omega) + \left.\frac{\delta^2\Gamma}{\delta\Psi_{\boldsymbol{k},\mathrm{cl}}(-\omega)\delta\Psi_{\boldsymbol{k},\mathrm{q}}(\omega)}\right|_{\mathrm{eq}} \Psi_{\boldsymbol{k},\mathrm{cl}}(-\omega) \right\} \\
&= \frac{\hbar^2}{2(2\pi)^3}\left\{ \left[\frac{1}{g_{\mathrm{A}}(\omega)} - \frac{J_{\boldsymbol{k}}}{\hbar} - \frac{\hbar^2}{2}\left|\Psi_{\mathrm{eq}}\right|^2 \frac{C^{\mathrm{A}}(\omega,0;0,\omega)}{2\pi g_{\mathrm{R}}(0)g_{\mathrm{A}}(0)g_{\mathrm{A}}(\omega)g_{\mathrm{A}}(\omega)} \right] \Psi^*(\omega) \right. \\
&\quad \left. - \left[\frac{\hbar^2}{4}\left|\Psi_{\mathrm{eq}}\right|^2 \frac{C^{\mathrm{A}}(0,0;-\omega,\omega)}{2\pi g_{\mathrm{R}}(-\omega)g_{\mathrm{A}}(0)g_{\mathrm{A}}(\omega)g_{\mathrm{A}}(0)} \right] \Psi(-\omega) \right\},
\end{aligned} \tag{6.46}$$

and

$$\begin{aligned}
0 \stackrel{!}{=} \frac{\delta\Gamma}{\delta\Psi^*_{\mathrm{q}}(\omega)} &= \frac{1}{2}\left\{ \left.\frac{\delta^2\Gamma}{\delta\Psi^*_{\boldsymbol{k},\mathrm{cl}}(\omega)\delta\Psi_{\boldsymbol{k},\mathrm{q}}(\omega)}\right|_{\mathrm{eq}} \Psi_{\boldsymbol{k},\mathrm{cl}}(\omega) + \left.\frac{\delta^2\Gamma}{\delta\Psi^*_{\boldsymbol{k},\mathrm{cl}}(-\omega)\delta\Psi^*_{\boldsymbol{k},\mathrm{q}}(\omega)}\right|_{\mathrm{eq}} \Psi^*_{\boldsymbol{k},\mathrm{cl}}(-\omega) \right\} \\
&= \frac{\hbar^2}{2(2\pi)^3}\left\{ \left[\frac{1}{g_{\mathrm{R}}(\omega)} - \frac{J_{\boldsymbol{k}}}{\hbar} - \frac{\hbar^2}{2}\left|\Psi_{\mathrm{eq}}\right|^2 \frac{C^{\mathrm{R}}(\omega,0;0,\omega)}{2\pi g_{\mathrm{A}}(0)g_{\mathrm{R}}(0)g_{\mathrm{R}}(\omega)g_{\mathrm{R}}(\omega)} \right] \Psi(\omega) \right. \\
&\quad \left. - \left[\frac{\hbar^2}{4}\left|\Psi_{\mathrm{eq}}\right|^2 \frac{C^{\mathrm{R}}(\omega,-\omega;0,0)}{2\pi g_{\mathrm{A}}(-\omega)g_{\mathrm{R}}(0)g_{\mathrm{R}}(\omega)g_{\mathrm{R}}(0)} \right] \Psi^*(-\omega) \right\}.
\end{aligned} \tag{6.47}$$

With (6.36) we can check that one equation is the complex conjugate of the other. We will deal with the solution of these equations in the next chapter. For a compact reference to them, we introduce the following shorthand notations:

$$A(\omega,\boldsymbol{k})\Psi^*_{\boldsymbol{k}}(\omega) + B(\omega,\boldsymbol{k})\Psi_{\boldsymbol{k}}(-\omega) = 0, \tag{6.48}$$

$$A^*(\omega,\boldsymbol{k})\Psi_{\boldsymbol{k}}(\omega) + B^*(\omega,\boldsymbol{k})\Psi^*_{\boldsymbol{k}}(-\omega) = 0, \tag{6.49}$$

where A, B and its conjugates represent the different functional derivatives in Eqs. (6.46) and (6.47).

6.2.4 Superfluid Resummed Green's Function

With the linearization from the subsection above, we can find a 2-point function, which describes the correlations near equilibrium in the symmetry-broken phase. This function will be the superfluid analog of the resummed retarded function in the MI phase given by the inverse of Eq. (5.39). We will show that this superfluid retarded/advanced 2-point function can be completely constructed by the same terms A, A^*, B and B^*, which appear in Eqs. (6.48) and (6.49). Therefore, we need to know how to derive the retarded/advanced 2-point function from our generating functionals.

We begin with the functional $\mathcal{F}[j, j^*]$ defined in Eq. (3.59). However, we should not argue with the expansion from Eq. (4.35), where the relation between $\mathcal{F}$ and the retarded/advanced Green's functions is obvious, since this expansion is valid only for a system *without* broken symmetry. Then expectation values like $\langle\Psi_{\mathrm{cl}}\rangle$ which in principle may contribute to the Green's function are zero. Instead, we will stay more general and consider the source term specified in Eq. (4.5). There we still had worked in the

±-basis. Making use of the rotation matrix Q defined in Eq. (3.51), we transform it into the cl,q-basis:

$$\begin{aligned} j_{i,+}\hat{\mathrm{a}}^\dagger_{i_+} - j_{i,-}\hat{\mathrm{a}}^\dagger_{i,-} &= \left(\hat{\mathrm{a}}^\dagger_{i,+}, \hat{\mathrm{a}}^\dagger_{i,-}\right) \begin{pmatrix} j_{i,+} \\ -j_{i,-} \end{pmatrix} = \left(\hat{\mathrm{a}}^\dagger_{i,+}, \hat{\mathrm{a}}^\dagger_{i,-}\right) QQ \begin{pmatrix} j_{i,+} \\ -j_{i,-} \end{pmatrix} \\ &= \left(\hat{\mathrm{a}}^\dagger_{i,\mathrm{cl}}, \hat{\mathrm{a}}^\dagger_{i,\mathrm{q}}\right) \begin{pmatrix} j_{i,\mathrm{q}} \\ j_{i,\mathrm{cl}} \end{pmatrix} = j_{i,\mathrm{q}}\hat{\mathrm{a}}^\dagger_{i,\mathrm{cl}} + j_{i,\mathrm{cl}}\hat{\mathrm{a}}^\dagger_{i,\mathrm{q}}. \end{aligned} \tag{6.50}$$

Here the index i should be interpreted as a set of variables, including site index and time. Thus with a sum over this index, we denote at the same time a sum over the discrete variables and an integral over the continuous ones. Now we need the following relation:

$$\left\langle \hat{\mathrm{T}}_\mathrm{c}\left(\hat{\mathrm{a}}_{i,\mathrm{q}}\hat{\mathrm{a}}^\dagger_{j,\mathrm{cl}}\right)\right\rangle = \left\langle \hat{\mathrm{T}}\left(\hat{\mathrm{a}}_{i,+}\hat{\mathrm{a}}^\dagger_{j,-}\right) + \hat{\bar{T}}\left(\hat{\mathrm{a}}_{i,-}\hat{\mathrm{a}}^\dagger_{j,-}\right) - \hat{\mathrm{a}}_{i,-}\hat{\mathrm{a}}^\dagger_{j,+} - \hat{\mathrm{a}}^\dagger_{j,-}\hat{\mathrm{a}}_{i,+}\right\rangle = G^\mathrm{R}_{ij}. \tag{6.51}$$

The last equality is found by making use of the Heaviside step function. It can be used in order to substitute $\hat{\mathrm{T}}$ and $\hat{\bar{T}}$. Then it is easy to see that this is exactly the definition of the retarded Green's function given in Eq. (3.54). Similarly, we have $\langle \hat{\mathrm{T}}_\mathrm{c}\left(\hat{\mathrm{a}}_{i,\mathrm{cl}}\hat{\mathrm{a}}^\dagger_{j,\mathrm{q}}\right)\rangle = G^\mathrm{A}_{ij}$. From this we can see that

$$\frac{\delta^2\mathcal{F}[j,j^*]}{\delta j^*_{i,\mathrm{q}}\delta j_{j,\mathrm{cl}}}\Big|_{j=j^*=0} = G^\mathrm{A}_{ij} \qquad \text{and} \qquad \frac{\delta^2\mathcal{F}[j,j^*]}{\delta j^*_{i,\mathrm{cl}}\delta j_{j,\mathrm{q}}}\Big|_{j=j^*=0} = G^\mathrm{R}_{ij}. \tag{6.52}$$

We stress that these equations hold as long as $\langle\Psi_\mathrm{q}\rangle = 0$, since the derivatives decompose into vanishing products $\langle\hat{\mathrm{a}}_{i,\mathrm{cl}}\rangle\langle\hat{\mathrm{a}}_{j,\mathrm{q}}\rangle$. If we had to take derivatives with respect to two quantum sources, however, we still would get a decomposition term to Eq. (6.52). For the retarded/advanced Green's functions, however, this is not the case.

Now we have to find out how the second derivative of $\mathcal{F}[j,j^*]$ is related to the effective action $\Gamma[\Psi,\Psi^*]$. Making use of the product rule for functional derivatives, we find the following identity

$$\delta_{ij} = \frac{\delta j_{i,\mathrm{q}}}{\delta j_{j,\mathrm{q}}} = \sum_k \left(\frac{\delta j_{i,\mathrm{q}}}{\delta\Psi_{k,\mathrm{q}}}\frac{\delta\Psi_{k,\mathrm{q}}}{\delta j_{j,\mathrm{q}}} + \frac{\delta j_{i,\mathrm{q}}}{\delta\Psi^*_{k,\mathrm{q}}}\frac{\delta\Psi^*_{k,\mathrm{q}}}{\delta j_{j,\mathrm{q}}} + \frac{\delta j_{i,\mathrm{q}}}{\delta\Psi_{k,\mathrm{cl}}}\frac{\delta\Psi_{k,\mathrm{cl}}}{\delta j_{j,\mathrm{q}}} + \frac{\delta j_{i,\mathrm{q}}}{\delta\Psi^*_{k,\mathrm{cl}}}\frac{\delta\Psi^*_{k,\mathrm{cl}}}{\delta j_{j,\mathrm{q}}} \right) \tag{6.53}$$

With the definition of the Legendre transform in (5.3), we can express Ψ as the derivative of $\mathcal{F}$ with respect to j^*. In our basis, one must note that the derivative with respect to the quantum component of the currents brings down the classical component of the corresponding operator. Therefore we have, e.g.,

$$\Psi_{i,\mathrm{cl}} = \frac{\delta\mathcal{F}}{\delta j^*_{i,\mathrm{q}}}. \tag{6.54}$$

From (5.4), the inverse relations can be found:

$$j_{i,\mathrm{cl}} = \frac{\delta\Gamma}{\delta\Psi^*_{i,\mathrm{q}}}. \tag{6.55}$$

Inserting this in Eq. (6.53) yields

$$\delta_{ij} = \sum_k \Bigg(\frac{\delta^2\Gamma}{\delta\Psi_{k,\mathrm{q}}\delta\Psi^*_{i,\mathrm{cl}}} \frac{\delta^2\mathcal{F}}{\delta j_{j,\mathrm{q}}\delta j^*_{k,\mathrm{cl}}} + \frac{\delta^2\Gamma}{\delta\Psi_{k,\mathrm{cl}}\delta\Psi^*_{i,\mathrm{cl}}} \frac{\delta^2\mathcal{F}}{\delta j_{j,\mathrm{q}}\delta j^*_{k,\mathrm{q}}} + \frac{\delta^2\Gamma}{\delta\Psi^*_{k,\mathrm{q}}\delta\Psi^*_{i,\mathrm{cl}}} \frac{\delta^2\mathcal{F}}{\delta j_{j,\mathrm{q}}\delta j_{k,\mathrm{cl}}} + \frac{\delta^2\Gamma}{\delta\Psi^*_{k,\mathrm{cl}}\delta\Psi^*_{i,\mathrm{cl}}} \frac{\delta^2\mathcal{F}}{\delta j_{j,\mathrm{q}}\delta j_{k,\mathrm{q}}} \Bigg). \tag{6.56}$$

We should note that the second and the last term vanish when evaluated at $\Psi_\mathrm{q} = \Psi^*_\mathrm{q} = 0$, as they contain derivatives of Γ with respect to classical components only. In order to eliminate $\delta^2\mathcal{F}/(\delta j_{j,\mathrm{q}}\delta j_{k,\mathrm{cl}})$, we perform similar manipulations on another intrinsic equation, for instance:

$$0 = \frac{\delta j^*_{i,\mathrm{q}}}{\delta j_{j,\mathrm{q}}} = \sum_k \left(\frac{\delta^2\Gamma}{\delta\Psi_{k,\mathrm{q}}\delta\Psi_{i,\mathrm{cl}}} \frac{\delta^2\mathcal{F}}{\delta j_{j,\mathrm{q}}\delta j^*_{k,\mathrm{cl}}} + \frac{\delta^2\Gamma}{\delta\Psi^*_{k,\mathrm{q}}\delta\Psi_{i,\mathrm{cl}}} \frac{\delta^2\mathcal{F}}{\delta j_{j,\mathrm{q}}\delta j_{k,\mathrm{cl}}} \right). \tag{6.57}$$

Without the sum over k, we could directly inverse this equation and eliminate $\delta^2\mathcal{F}/(\delta j_{j,\mathrm{q}}\delta j_{k,\mathrm{cl}})$ from Eq. (6.56). We can get rid of this sum by the expansion which was used for the linearization of the equations of motion in the subsection above. Taking the expanded effective action from Eq. (6.45) and switching into Fourier space, Eqs. (6.56) and (6.57) appear without sum. But we have to take care with the sign of the frequencies, since the second derivatives with respect to two field or two conjugate fields imply a function $\delta(\omega + \omega')$, while the second derivatives with respect to one field and one conjugate field implies the function $\delta(\omega - \omega')$. Combining Eqs. (6.56) and (6.57), we can write:

$$\begin{aligned} 1 = &\frac{\delta^2\mathcal{F}}{\delta j_{\boldsymbol{k},\mathrm{q}}(\omega)\delta j^*_{\boldsymbol{k},\mathrm{cl}(\omega)}} \Bigg\{ \frac{\delta^2\Gamma}{\delta\Psi_{\boldsymbol{k},\mathrm{q}}(\omega)\delta\Psi^*_{\boldsymbol{k},\mathrm{cl}}(\omega)} - \left(\frac{\delta^2\Gamma}{\delta\Psi^*_{\boldsymbol{k},\mathrm{q}}(-\omega)\delta\Psi_{\boldsymbol{k},\mathrm{cl}}(-\omega)} \right)^{-1} \\ &\times \frac{\delta^2\Gamma}{\delta\Psi_{\boldsymbol{k},\mathrm{q}}(-\omega)\delta\Psi_{\boldsymbol{k},\mathrm{cl}}(\omega)} \frac{\delta^2\Gamma}{\delta\Psi^*_{\boldsymbol{k},\mathrm{q}}(\omega)\delta\Psi^*_{\boldsymbol{k},\mathrm{cl}}(-\omega)} \Bigg\}. \end{aligned} \tag{6.58}$$

According to Eq. (6.52), the first term can be interpreted as the Fourier transform of the retarded Green's function in the superfluid system, $G^\mathrm{R}_{\boldsymbol{k}}(\omega) = \sum_{ij} G^\mathrm{R}_{ij}(\omega) \exp\left[-i(\boldsymbol{r}_i - \boldsymbol{r}_j)\cdot\boldsymbol{k}\right]$, thus the term within the curly braces must be the inverse of it. Therefore we have

$$G^\mathrm{R}_{\boldsymbol{k}}(\omega) = \frac{\frac{\delta^2\Gamma}{\delta\Psi^*_{\boldsymbol{k},\mathrm{q}}(-\omega)\delta\Psi_{\boldsymbol{k},\mathrm{cl}}(-\omega)}}{\frac{\delta^2\Gamma}{\delta\Psi^*_{\boldsymbol{k},\mathrm{q}}(-\omega)\delta\Psi_{\boldsymbol{k},\mathrm{cl}}(-\omega)} \frac{\delta^2\Gamma}{\delta\Psi_{\boldsymbol{k},\mathrm{q}}(\omega)\delta\Psi^*_{\boldsymbol{k},\mathrm{cl}}(\omega)} - \frac{\delta^2\Gamma}{\delta\Psi_{\boldsymbol{k},\mathrm{q}}(-\omega)\delta\Psi_{\boldsymbol{k},\mathrm{cl}}(\omega)} \frac{\delta^2\Gamma}{\delta\Psi^*_{\boldsymbol{k},\mathrm{q}}(\omega)\delta\Psi^*_{\boldsymbol{k},\mathrm{cl}}(-\omega)}}, \tag{6.59}$$

and the complex conjugate expression for the retarded Green's function.

Now we should note that the equations of motion, (6.48) and (6.49) are solved, if

$$0 \stackrel{!}{=} A(-\omega,\boldsymbol{k})A^*(\omega,\boldsymbol{k}) - B^*(-\omega,\boldsymbol{k})B(\omega,\boldsymbol{k}). \tag{6.60}$$

This is exactly the denominator of the superfluid Green's function (6.59), i.e. the equations of motions are solved when the retarded/advanced Green's functions diverge.

7 Excitation Spectra

Up to now a lot of work has been done in order to derive a theory for the dynamics of bosons in optical lattices, but still we have said nothing about what is really going on in such systems. This will change in this chapter, since now we are in a position to calculate both the phase diagram and the excitation spectra. The spectra are given by a function $\omega(\boldsymbol{k})$ which relates the frequency of an excitation to its corresponding momentum. As already stated in the beginning, due to the Goldstone theorem we expect one gapless mode with $\omega(\boldsymbol{k}) \sim |\boldsymbol{k}|$ for small $|\boldsymbol{k}|$ in the superfluid phase. This expectation will be confirmed in this chapter, when we solve the equations of motion in the superfluid phase. Comparing our spectrum with the Bogoliubov result we will find a good agreement for weak interactions, but in contrast to that theory, our equations yield also a second solution, which is gapped and quadratic in $\boldsymbol{k}$. From the point of view of Bogoliubov theory, this finding is quite surprising. But if we consider the excitations in the Mott phase, such a mode seems to be necessary, since we find two kinds of MI excitations, too. Thus, again we start our calculations in the MI phase and present the SF calculations later. Of special interest is the behavior of the spectra near the phase boundary, where they are found to map onto each other. Moreover, critical exponents should quantitatively describe the system properties in this regime.

7.1 Spectra in the MI Phase

To see how things work, we first consider the easiest case, namely a system without hopping. Already this limit will give us some insight into the physics of the MI phase.

7.1.1 Zeroth Hopping Order

The MI equations of motion are given in Eq. (5.49). Setting $J = 0$ reduces the Green's function $G_{ij}^{\mathrm{R}(1)}$ to the unperturbed one, which is local. This leaves us with

$$\frac{1}{g_{\mathrm{R}}(\omega)} \Psi_{j,\mathrm{cl}}(\omega) = 0. \tag{7.1}$$

Using Eq. (5.20) the condition for non-trivial solutions therefore reads

$$\frac{1}{g_{\mathrm{R}}(\omega)} = \frac{\mathcal{Z}^{(0)}}{\sum_{n=0}^{\infty} \mathrm{e}^{-\beta E_n} \left(\frac{n+1}{\frac{E_{n+1}-E_n}{\hbar} - \omega - i\epsilon} - \frac{n}{\frac{E_n - E_{n-1}}{\hbar} - \omega - i\epsilon} \right)} = 0, \tag{7.2}$$

i.e. we must look for divergences in $g_{\mathrm{R}}(\omega)$. As this is a complex function, it would be helpful to have the real part separated from the imaginary part. This is done by multiplying both denominators in

Eq. (5.20) with their complex conjugates, leading to

$$g_{\mathrm{R}}(\omega) = \frac{1}{\mathcal{Z}^{(0)}} \sum_n \mathrm{e}^{-\beta E_n} \left[\frac{(n+1)(\Delta_{n+1} - \omega + i\epsilon)}{(\Delta_{n+1} - \omega)^2 + \epsilon^2} - \frac{n(\Delta_n - \omega + i\epsilon)}{(\Delta_n - \omega)^2 + \epsilon^2} \right] = \frac{-1}{\mathcal{Z}^{(0)}} \sum_{n=0}^{\infty} \mathrm{e}^{-\beta E_n} \times \left\{ \frac{(n+1)(\Delta_{n+1} - \omega)}{(\Delta_{n+1} - \omega)^2 + \epsilon^2} - \frac{n(\Delta_n - \omega)}{(\Delta_n - \omega)^2 + \epsilon^2} + i \left[\frac{(n+1)\epsilon}{(\Delta_{n+1} - \omega)^2 + \epsilon^2} - \frac{n\epsilon}{(\Delta_n - \omega)^2 + \epsilon^2} \right] \right\}, \tag{7.3}$$

where we have defined $\Delta_n \equiv \frac{E_n - E_{n-1}}{\hbar}$. With the identity

$$\lim_{\epsilon \to 0} \frac{\epsilon}{x^2 + \epsilon^2} = \pi \delta(x), \tag{7.4}$$

we can take the limit $\epsilon \to 0$. This gives us

$$g_{\mathrm{R}}(\omega) = \frac{1}{\mathcal{Z}^{(0)}} \sum_{n=0}^{\infty} \mathrm{e}^{-\beta E_n} \left(\frac{n+1}{\Delta_{n+1} - \omega} - \frac{n}{\Delta_n - \omega} + i\pi \Big[(n+1)\delta(\Delta_{n+1} - \omega) - n\delta(\Delta_n - \omega) \Big] \right) \tag{7.5}$$

We observe that a diverging term appears in the real part if

$$\omega = \Delta_n \quad \text{for any } n \in \mathbb{N}. \tag{7.6}$$

At these frequencies Δ_n, the argument of the δ-functions in the imaginary part becomes zero, too. Thus the imaginary part diverges as well. Therefore an order field $\Psi_j(\omega)$ being proportional to $\delta(\omega - \Delta_n)$ with arbitrary n solves the equation of motion. The general solution can be written as:

$$\Psi_{j,\mathrm{cl}}(\omega) = \sum_{n=1}^{\infty} A_n \delta(\omega - \Delta_n). \tag{7.7}$$

Note that this sum does not have a term with $n = 0$, since Eq. (7.5) does not diverge for $\omega = \Delta_0$. The coefficients A_n of this solution have to be chosen in accordance with the initial conditions. These coefficients still might depend on the site index and especially on temperature. We note that, although the temperature appears in the equation of motion, it influences the dynamics of the system only indirectly via the initial condition.

Going back to time space, we find

$$\Psi_{j,\mathrm{cl}}(t) = \int_{-\infty}^{\infty} \mathrm{d}\omega \sum_{n=1}^{\infty} A_n \delta(\omega - \Delta_n) \mathrm{e}^{-i\omega t} = \sum_{n=1}^{\infty} A_n \mathrm{e}^{-i\Delta_n t}. \tag{7.8}$$

Thus, the dynamics of the classical component of the order field consists of oscillations with the frequencies Δ_n. They correspond to the energies for changing the number of particles on a site by one.

We should note that the information about the excitation frequencies is contained in the real part as well as in the imaginary part of the retarded Green's function. This will help us a lot later in the calculation of the SF spectra. To see what kind of information is encoded in the retarded/advanced

Green's functions, we consider the following spectral representation [66] :

$$G^{\mathrm{R/A}}(\omega) = \int_{-\infty}^{\infty} \mathrm{d}\omega' \rho(\omega') \left(\frac{\mathcal{P}}{\omega - \omega'} \pm i\pi\delta(\omega - \omega') \right), \tag{7.9}$$

where $\mathcal{P}$ denotes the principal value of the integration across the singularity and $\rho(\omega)$ denotes the spectral function. This function does not only contain the excitation frequencies, but also information about their spectral weights, i.e. about how much of the total excitation energy is stored in each excitation. The spectral function obeys the so-called sum rule [66]:

$$\int_{-\infty}^{\infty} \mathrm{d}\omega \ \rho(\omega) = 1. \tag{7.10}$$

From the spectral representation in Eq. (7.9), we can further see that $\rho(\omega)$ can be obtained from the imaginary part of the advanced and retarded Green's function: $2\pi\rho(\omega) = G^{\mathrm{R}}(\omega) - G^{\mathrm{A}}(\omega) = 2\mathrm{Im}G^{\mathrm{R}}(\omega)$. In our case, we find from Eq. (7.5):

$$\rho(\omega) = \frac{-1}{\mathcal{Z}^{(0)}} \sum_{n=0}^{\infty} n\delta(\omega - \Delta_n) \left(\mathrm{e}^{-\beta E_n} - \mathrm{e}^{-\beta E_{n-1}} \right) = \frac{1}{\mathcal{Z}^{(0)}} \sum_{n=0}^{\infty} n\mathrm{e}^{-\beta E_n} \delta(\omega - \Delta_n) \left(\mathrm{e}^{\beta\Delta_n} - 1 \right). \tag{7.11}$$

Let us still check if this expression satisfies the sum rule. The ω-integration is trivial, so we immediately find

$$\int_{-\infty}^{\infty} \mathrm{d}\omega \ \rho(\omega) = \frac{1}{\mathcal{Z}^{(0)}} \sum_{n=0}^{\infty} n \left(\mathrm{e}^{-\beta E_n} - \mathrm{e}^{-\beta E_{n-1}} \right) = \frac{1}{\mathcal{Z}^{(0)}} \sum_{n=0}^{\infty} \mathrm{e}^{-\beta E_n} \left(n - n + 1 \right) = 1. \tag{7.12}$$

The transformation from the second to the third expression can be done by shifting the summation index in the second term. Then n is canceled from the sum and the whole expression reduces to 1.

Let's still investigate the zero-temperature limit of Eq. (7.2). Note that we have a Boltzmann sum of the form

$$\lim_{\beta\to\infty} \frac{1}{\mathcal{Z}} \sum_{m=0}^{\infty} \mathrm{e}^{-\beta E_m} f_m = \lim_{\beta\to\infty} \frac{\mathrm{e}^{-\beta E_n} \sum_{m=0}^{\infty} \mathrm{e}^{-\beta(E_m - E_n)} f_m}{\mathrm{e}^{-\beta E_n} \sum_{m=0}^{\infty} \mathrm{e}^{-\beta(E_m - E_n)}} = f_n, \tag{7.13}$$

where f_m is an arbitrary expression which does not depend on β and the summation index m denotes the occupation number. The final n in Eq. (7.13) now denotes the ground-state occupation number, i.e. a number which is fixed by μ/U [31]. For the last step, we need to note that with our standard Bose-Hubbard Hamiltonian from Eq. (2.1), degenerate ground-states can be excluded, so we have $E_m > E_n$ for any $m \neq n$, thus for $\beta \to \infty$ all terms in both sums become zero except the one with the ground-state occupation number n. The Green's function (7.2) then reduces to:

$$\frac{1}{g_{\mathrm{R}}(\omega)} = \left(\frac{n+1}{\omega_{n+1} - \omega + i\epsilon} - \frac{n}{\omega_n - \omega + i\epsilon} \right)^{-1} = 0. \tag{7.14}$$

This means that at $T = 0$, the system can be excited only at two frequencies which correspond to the creation of an additional particle or taking away one particle from the ground-state configuration. Taking away one particle can also be considered as the creation of a hole. This interpretation of the

two modes already gives us a good picture of the Mott-insulator physics, where the particle number per site is fixed and the system is excited by taking away or adding particles.

7.1.2 First Hopping Order

After having seen how the procedure of finding the spectra works for the quite easy case of a system without hopping, we can now go ahead and try the same for the case of much greater interest, the MI system with non-zero hopping. Let us first write down the equation of motion (5.49):

$$\left[G_{ij}^{\mathrm{R}(1)}(\omega)\right]^{-1}\Psi_{j,\mathrm{cl}}(\omega)=\sum_j\frac{1}{g_{\mathrm{R}}(\omega)}\left[\delta_{ij}-\frac{J_{ij}}{\hbar}g_{\mathrm{R}}(\omega)\right]\Psi_{j,\mathrm{cl}}(\omega)=0. \tag{7.15}$$

Here we have plugged in the inverse Green's function from Eq. (5.39), which is no longer local, since it contains the hopping matrix element J_{ij}. Thus it is advantageous to transform the equation into $\boldsymbol{k}$-space. Our solutions will then depend on a wave vector $\boldsymbol{k}$, and non-constant dispersion relations $\omega(\boldsymbol{k})$ should arise. With the assumption of spatial homogeneity, Eq. (7.15) is a convolution. Transforming into wave vector space yields

$$\frac{1}{g_{\mathrm{R}}(\omega)}\left[1-\frac{J_{\boldsymbol{k}}}{\hbar}g_{\mathrm{R}}(\omega)\right]\Psi_{\boldsymbol{k},\mathrm{cl}}(\omega)\stackrel{!}{=}0. \tag{7.16}$$

The condition for non-trivial solutions seems to be

$$1-\frac{J_{\boldsymbol{k}}}{\hbar}g_{\mathrm{R}}(\omega)=0, \tag{7.17}$$

where for a cubic lattice the hopping matrix J_{ij} from Eq. (2.16) transforms into $J_{\boldsymbol{k}}=2J[\cos(k_xa)+\cos(k_ya)+\cos(k_za)]$. But if we remember the form of $g_{\mathrm{R}}(\omega)$ given by Eq. (7.5), we see that we might have a problem with the imaginary part: Since 1 is a real number and $J_{\boldsymbol{k}}$ is real as well, the imaginary part, being non-zero for $\omega=\Delta_n$, cannot cancel. At these frequencies, the condition (7.17) cannot be fulfilled, which, however, does not mean that neither Eq. (7.16) is fulfilled.

Nevertheless, Eq. (7.17) can be used to calculate the phase boundary. In equilibrium the order field should be constant in time and space, as a homogeneous systems is assumed. The fields therefore should be of the form $\Psi_i(t)=\Psi_{i\mathrm{eq}}=\Psi_{\mathrm{eq}}$. After a Fourier transformation in the spatial and temporal variables, they read $\Psi_{\boldsymbol{k}}(\omega)=\Psi_{\mathrm{eq}}\delta_{\boldsymbol{k},\boldsymbol{0}}\delta(\omega)$. This ansatz might solve Eq. (7.17), because at $\omega=0$ the Green's function is real, and thus the problem with the imaginary part cannot occur. In equilibrium, the condition for a non-vanishing classical order field therefore reads

$$1-g_{\mathrm{R}}(0)\frac{J_{\boldsymbol{0}}}{\hbar}=0. \tag{7.18}$$

This equation determines the phase boundary in terms of a critical hopping parameter. Up to this critical value, the equilibrium order parameter must vanish in order to fulfill the equations of motion. For larger J, the order parameter might, for the first time, become finite, which means that the SF phase is reached. To go further, higher-order terms in Ψ must be taken into account. We have already done this in Chapter 6, where we found the equilibrium order field in Eq. (6.40). Inserting the critical

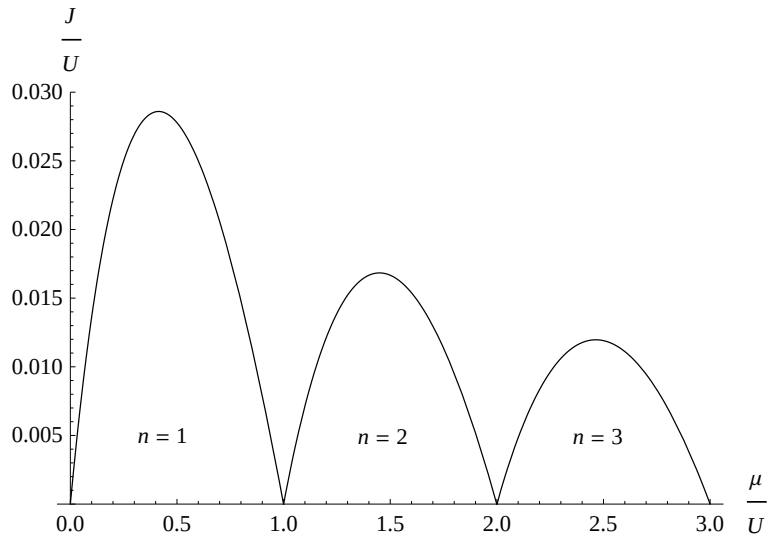

Figure 7.1: The phase boundary between the MI phase and the SF phase at T=0 shows lobes depending on the ground-state occupation number n.

parameters from Eq. (7.18) into Eq. (6.40), we find that Ψ_{eq} vanishes at the phase boundary.

For a hopping matrix like the one given in Eq. (2.16), we have $J_{\mathbf{0}} = zJ$, where $z = 2d$ denotes the coordination number, i.e. the number of nearest neighbors in a d-dimensional lattice. We therefore can directly determine the phase boundary $J_{\mathrm{PB}} = \frac{\hbar}{z g_{\mathrm{R}}(0)}$. One can divide both sides by the on-site interaction parameter U and thus gets the critical $J/U \equiv \tilde{J}$ as a function of the chemical potential $\mu/U \equiv \tilde{\mu}$. This function has a well-known lobe structure [31,36,69,73]. Its analytical expression reads

$$\frac{J_{\mathrm{PB}}}{U} = -\frac{(n-\tilde{\mu}-1)(n-\tilde{\mu})}{6(\tilde{\mu}+1)}. \tag{7.19}$$

The first three lobes are plotted in Fig. (7.1). The tips will turn out to be the physically most interesting part of the lobes. By setting the derivative of the lobe equation (7.19) with respect to $\tilde{\mu}$ equal to zero, we find the location of the lobe tips at

$$\tilde{\mu}_{\mathrm{cr}} = \sqrt{n(n+1)} - 1 \qquad \text{and} \qquad \tilde{J}_{\mathrm{cr}} = \frac{(\sqrt{n(n+1)} - n)(n - \sqrt{n(n+1)} + 1)}{6\sqrt{n(n+1)}} \tag{7.20}$$

This phase diagram agrees qualitatively with other theoretical predictions. It is exactly the same as the one obtained by mean-field theory [31]. However, in comparison with the most exact results, which are believed to be given by the Monte-Carlo data in Ref. [30], the $n = 1$ tip of our lobe is much too low. But in Ref. [69] it is shown for a similar hopping expansion that taking into account the second hopping order improves the result from about 20% error to 2% error. It is one great advantage of our perturbative approach, that it offers a way to go systematically beyond mean-field results, if this is desired. It should be mentioned, however, that calculating higher-order diagrams is a huge computational task. However, by making use of a computer algorithm, the effective potential of the system was calculated up to the 8th order [76,77]. In Ref. [76] it can be seen, how the calculated phase boundary gets closer to the Monte-Carlo data in each hopping order.

Coming back to the excitations of the system, we might be tempted to modify Eq. (7.17) and demand that only its real part vanishes, $\mathrm{Re}[1 - \frac{J_{\boldsymbol{k}}}{\hbar} g_{\mathrm{R}}(\omega)] = 0$. Then this formula is exactly the same as in Ref. [73], where the imaginary parts have been neglected from the beginning. A more convincing solution of this problem, however, is to take the resummed Green's functions as a whole and perform the limit $\epsilon \to 0$, instead of splitting it, as has been done in Eq. (7.17). Surely, taking the limit of the whole expression will be quite more complicated, but doing so is not only the more correct way, moreover we will get access to an additional information about the spectral weights.

From now on, it appears to be necessary to take the $\beta \to \infty$ limit for any analytical treatment. As the limit $\lim_{\beta\to\infty} g_{\mathrm{R}}(\omega)$ is well-defined by Eq. (7.14), we can take the limit for the resummed function $G^{\mathrm{R}(1)}(\omega)$ from Eq. (5.39) by taking $\lim_{\beta\to\infty} g_{\mathrm{R}}(\omega)$ wherever $g^{\mathrm{R}}(\omega)$ appears in Eq. (5.39). This leaves us with the following expression

$$G^{\mathrm{R}}_{\boldsymbol{k}}(\omega) = \frac{\frac{n-1}{\Delta_{n+1}-\omega-i\epsilon} - \frac{n}{\Delta_n-\omega-i\epsilon}}{1 - \frac{J_{\boldsymbol{k}}}{\hbar}\left(\frac{n-1}{\Delta_{n+1}-\omega-i\epsilon} - \frac{n}{\Delta_n-\omega-i\epsilon}\right)} \equiv \frac{a(\omega) - i\epsilon}{b_{\boldsymbol{k}}(\omega) - \epsilon^2 + i c_{\boldsymbol{k}}(\omega)}, \tag{7.21}$$

where the three functions a, b and c are defined as

$$a(\omega) = -\omega + (n+1)\Delta_n - n\Delta_{n+1}, \tag{7.22}$$

$$b_{\boldsymbol{k}}(\omega) = (\omega - \Delta_n)(\omega - \Delta_{n+1}) + \frac{J_{\boldsymbol{k}}}{\hbar}\left[\omega - (n+1)\Delta_n + n\Delta_{n+1}\right], \tag{7.23}$$

$$c_{\boldsymbol{k}}(\omega) = 2\omega + \frac{J_{\boldsymbol{k}}}{\hbar} - \Delta_n - \Delta n + 1. \tag{7.24}$$

Separating real and imaginary parts yields

$$G^{\mathrm{R}} = \frac{ab - \epsilon^2(a+c)}{b^2 + \epsilon^2(c^2 - 2b) + \epsilon^4} - i\frac{\epsilon(b - ac) - \epsilon^3}{b^2 + \epsilon^2(c^2 - 2b) + \epsilon^4}. \tag{7.25}$$

The limit $\epsilon \to 0$ can be taken immediately for the real part, yielding $\mathrm{Re}[G^{\mathrm{R}}_{\boldsymbol{k}}(\omega)] = \frac{a(\omega)}{b_{\boldsymbol{k}}(\omega)}$ with a divergence for $b_{\boldsymbol{k}}(\omega) = 0$, where we expect the excitation frequencies. For the imaginary part, we try to apply the formula (7.4) again by neglecting the term ϵ^3 in the numerator and the term ϵ^4 in the denominator. Without having a mathematical proof, we expect that in the limit $\epsilon \to 0$ they should not play a role. Then we have

$$\mathrm{Im}(G^{\mathrm{R}}) = -\pi\frac{b + ac}{c^2 - 2b}\delta\left(\sqrt{\frac{b^2}{c^2 - 2b}}\right). \tag{7.26}$$

This shows that the imaginary part is non-zero only for $b = 0$. We check that $c^2 - 2b \neq 0$ when $b = 0$, so we can take out the denominator from the δ-function according to the formula $\delta(kx) = \frac{1}{|k|}\delta(x)$. Furthermore we can set $b = 0$ in the term in front of the δ-function. Thus, the imaginary part reduces to:

$$\mathrm{Im}(G^{\mathrm{R}}) = -\pi\frac{ac \cdot |c|}{c^2}\ \delta(|b|). \tag{7.27}$$

We still employ the formula

$$\delta(f(x)) = \sum_i \frac{1}{|f'(x_i)|}\delta(x - x_i), \tag{7.28}$$

where the sum is over all x_i with $f(x_i) = 0$. Noting that Eq.(7.23) can be written as

$$b_{\boldsymbol{k}}(\omega) = [\omega - \Omega_+(\boldsymbol{k})]\,[\omega - \Omega_-(\boldsymbol{k})]\,, \tag{7.29}$$

with

$$\begin{aligned}\Omega_\pm(\boldsymbol{k}) =& \frac{1}{2}\Bigg(-\frac{J_{\boldsymbol{k}}}{\hbar} + \Delta_n + \Delta_{n+1} \\ &\pm \sqrt{\left[\frac{J_{\boldsymbol{k}}}{\hbar} - \Delta_n - \Delta_{n+1}\right]^2 - 4\left\{\frac{J_{\boldsymbol{k}}}{\hbar}\left[n\Delta_{n+1} - (n+1)\Delta_n\right] + \Delta_n\Delta_{n+1}\right\}}\Bigg),\end{aligned} \tag{7.30}$$

we get the result:

$$\begin{aligned}\mathrm{Im}[G^{\mathrm{R}}_{\boldsymbol{k}}(\omega)] =& -\pi\Bigg[\frac{|c_{\boldsymbol{k}}(\Omega_-(\boldsymbol{k}))|}{c_{\boldsymbol{k}}(\Omega_-(\boldsymbol{k}))}\frac{a(\Omega_-(\boldsymbol{k}))}{|\Omega_+(\boldsymbol{k}) - \Omega_-(\boldsymbol{k})|}\delta\left(\omega - \Omega_-(\boldsymbol{k})\right) \\ &+ \frac{|c_{\boldsymbol{k}}(\Omega_+(\boldsymbol{k}))|}{c_{\boldsymbol{k}}(\Omega_+(\boldsymbol{k}))}\frac{a(\Omega_+(\boldsymbol{k}))}{|\Omega_+(\boldsymbol{k}) - \Omega_-(\boldsymbol{k})|}\delta\left(\omega - \Omega_+(\boldsymbol{k})\right)\Bigg].\end{aligned} \tag{7.31}$$

Furthermore, checking that $\Omega_+(\boldsymbol{k}) \geq \Omega_-(\boldsymbol{k})$ and $|c_{\boldsymbol{k}}(\Omega_-(\boldsymbol{k}))|/c_{\boldsymbol{k}}(\Omega_-(\boldsymbol{k})) = -1$ while $|c_{\boldsymbol{k}}(\Omega_+(\boldsymbol{k}))|/c_{\boldsymbol{k}}(\Omega_+(\boldsymbol{k})) = +1$ for any $\boldsymbol{k}$, the whole expression reduces to

$$\mathrm{Im}(G^{\mathrm{R}}_{\boldsymbol{k}}(\omega)) = \pi\Big[\frac{a(\omega)}{\Omega_+(\boldsymbol{k}) - \omega}\delta\left(\omega - \Omega_-(\boldsymbol{k})\right) - \frac{a(\omega)}{\omega - \Omega_-(\boldsymbol{k})}\delta\left(\omega - \Omega_+(\boldsymbol{k})\right)\Big] = \pi\rho(\omega, \boldsymbol{k}). \tag{7.32}$$

Thus we have two dispersion modes $\Omega_+(\boldsymbol{k})$ and $\Omega_-(\boldsymbol{k})$ with the weights

$$w_\pm(\boldsymbol{k}) = -\frac{\pm a(\Omega_\pm(\boldsymbol{k}))}{\Omega_+(\boldsymbol{k}) - \Omega_-(\boldsymbol{k})}. \tag{7.33}$$

First we should check whether this result satisfies the sum rule (7.10). We find for any wave vector $\boldsymbol{k}$

$$\frac{1}{\pi}\int_{-\infty}^{\infty} \mathrm{d}\omega\ \mathrm{Im}(G^{\mathrm{R}}_{\boldsymbol{k}}(\omega)) = \frac{a(\Omega_-(\boldsymbol{k}))}{\Omega_+(\boldsymbol{k}) - \Omega_-(\boldsymbol{k})} - \frac{a(\Omega_+(\boldsymbol{k}))}{\Omega_+(\boldsymbol{k}) - \Omega_-(\boldsymbol{k})} = 1. \tag{7.34}$$

This is very encouraging, as it is not obvious from the beginning that the first-order approximation of the full Green's function fulfills this rule. Furthermore, this result justifies a posteriori the neglection of the higher ϵ-terms in Eq. (7.25).

The functions $\Omega_\pm(\boldsymbol{k})$ from Eq. (7.30) yield the pairs of frequencies and wave vectors, at which the real and the imaginary part of the Green's function diverge for $T = 0$, i.e. which solve the equation of motion (7.15). These dispersion relations are the same as in Ref. [73]. Inserting $\Delta_n = U(n-1) - \mu$

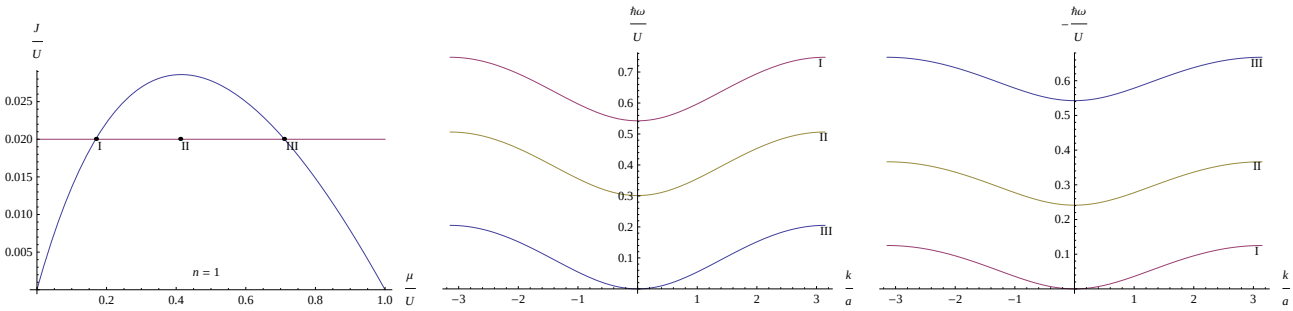

(a) phase boundary (b) particles (c) holes

Figure 7.2: Particle spectrum (b) and hole spectrum (c) of the first Mott lobe for three different μ/U at constant hopping J/U. Note the reversed sign of the ordinate in the hole spectrum.

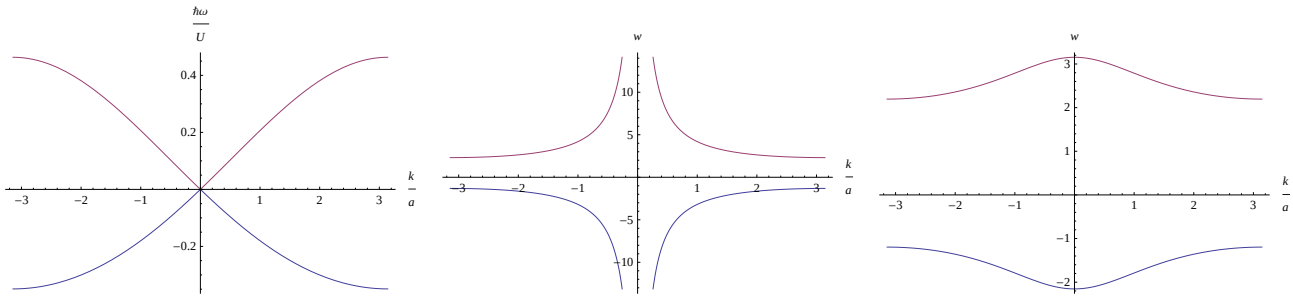

(a) Lobe tip spectrum (b) Spectral weights at tip (c) Spectral weights at $\frac{J}{U} = 0.02$

Figure 7.3: At the lobe tip the dispersion relation gets linear (a), and the spectral weights (b) diverge at $k = 0$. The spectral weights of the spectra from Fig. 7.2 are plotted in (c). Note that there is no μ-dependence.

into Eq. (7.30), we get

$$\Omega_{\pm}(\boldsymbol{k}) = \frac{1}{2\hbar}\left[U(2n-1) - 2\mu - J_{\boldsymbol{k}} \pm \sqrt{U^2 - 2J_{\boldsymbol{k}}U(2n+1) + J_{\boldsymbol{k}}^2}\right]. \tag{7.35}$$

The spectral weights $w_{\pm}(\boldsymbol{k})$ defined by Eq. (7.33) explicitly read

$$w_{\pm}(\boldsymbol{k}) = \frac{1}{2}\left(1 \pm \frac{U(1+2n) - J_{\boldsymbol{k}}}{\sqrt{U^2 - 2J_{\boldsymbol{k}}U(2n+1) + J_{\boldsymbol{k}}^2}}\right). \tag{7.36}$$

They do not depend on the chemical potential. At the tip of the lobe, both weights diverge at $\boldsymbol{k} = 0$, as can be found by inserting $\tilde{J}_{\mathrm{cr}}$ from Eq. (7.20) in Eq. (7.36).

To illustrate the result, we plot the spectra and their weights given by Eqs. (7.35) and (7.36). To this end we specialize the lattice dispersion $J_{\boldsymbol{k}} = 2J\sum_{i=1}^{d}\cos(k_i a)$ to the case of an excitation along one arbitrary lattice vector direction $k_i \equiv k$ in a three-dimensional lattice, i.e. the other components are set to zero. Then the lattice dispersion reads

$$J_k = 2J\left[2 + \cos(ka)\right]. \tag{7.37}$$

Qualitatively, it makes no difference, which direction we choose, so no interesting information is lost by this restriction to only one $\boldsymbol{k}$-component. The plotted spectra and their weights can be found in Figs. 7.2 and 7.3 for different parameters within the MI phase.

For small k, we still would like to bring the dispersion relations $\Omega_\pm(k)$ to the following form

$$\hbar\Omega_\pm(k) = \Delta_\pm + \frac{1}{2m_\pm}\hbar^2k^2 + O(k^4). \tag{7.38}$$

Then the gap of the spectrum is explicitly given by $\Delta_\pm$, and $m_\pm$ denotes the effective mass of the excitation. Such a form is achieved by a Taylor expansion of Eq. (7.35) in k. If we again choose $\boldsymbol{k} = (k, 0, 0)$, we find

$$\Delta_\pm = \frac{1}{2}\left(-6J - U + 2nU \pm \sqrt{36J^2 + U^2 - 12J(U + 2nU)} - 2\mu\right), \tag{7.39}$$

$$\frac{\hbar^2}{m_\pm} = J \pm \frac{J(-6J + U + 2nU)}{\sqrt{36J^2 + U^2 - 12J(U + 2nU)}}. \tag{7.40}$$

With this we can check that within all the Mott lobes, we have $\Delta_\pm \neq 0$, i.e. gapped excitations. It turns out that the masses of both branches have different shapes: We always have $m_- < 0$, while $m_+ > 0$. Furthermore, the branch with negative masses has negative energies, too, while the convex branch consists of positive energies. We therefore interpret the excitation of the Ω_--branch as holes, i.e. excitations created by taking away one particle with momentum $-k$. Correspondingly, Ω_+ is associated with particle excitations by adding one particle with momentum k. This interpretation can be checked by setting $J = 0$ in Eq. (7.39). We find that $\Delta_+ \to Un - \mu = \Delta_n$ corresponds to the energy needed for adding one particle to system without hopping, while $|\Delta_-| \to U(n-1) - \mu = \Delta_{n-1}$ is the energy needed for the creation of a hole.

For the creation of a particle and a hole at $\boldsymbol{k} = \boldsymbol{0}$, the energy difference between the two gaps has to be considered $E_{\text{pair}} = \Delta_+ - \Delta_- = \sqrt{36J^2 + U^2 - 12J(U + 2nU)}$. We find that this is exactly the width $W(n, \tilde{J})$ of the lobes [31]. To see that, we must invert Eq. (7.19), yielding:

$$\tilde{\mu}_{\text{PB}\pm} = \frac{1}{2}\left(-1 + 2n - 6\tilde{J} \pm \sqrt{1 - 12\tilde{J} - 24n\tilde{J} + 36\tilde{J}^2}\right), \tag{7.41}$$

from which follows the width of the lobe

$$W(n, \tilde{J}) = \mu_{\text{PB}+}(n, \tilde{J}) - \mu_{\text{PB}-}(n, \tilde{J}) = \sqrt{1 - 12\tilde{J} - 24n\tilde{J} + 36\tilde{J}^2} = \frac{\Delta_+ - \Delta_-}{U}. \tag{7.42}$$

The behavior becomes more interesting at the phase boundary: By evaluating $\Delta_\pm$ in Eq. (7.39) on the phase boundary given by Eq. (7.19), we find that the gap of the hole excitation vanishes in the interval $\tilde{\mu} \in (n-1, \sqrt{n(n+1)} - 1]$, i.e. on the left side of the lobe tip. The opposite is true for the particle excitation, where the gap vanishes in the interval $\tilde{\mu} \in [\sqrt{n(n+1)} - 1, n)$. At the tip of the lobe, which is characterized by Eq. (7.20), both modes become gap- and massless. This means that here and only here, we have an exact symmetry between particles and holes.

Since $1/m_\pm$ diverges at the lobe tips, Eq.(7.38) is not appropriate to describe the spectra there.

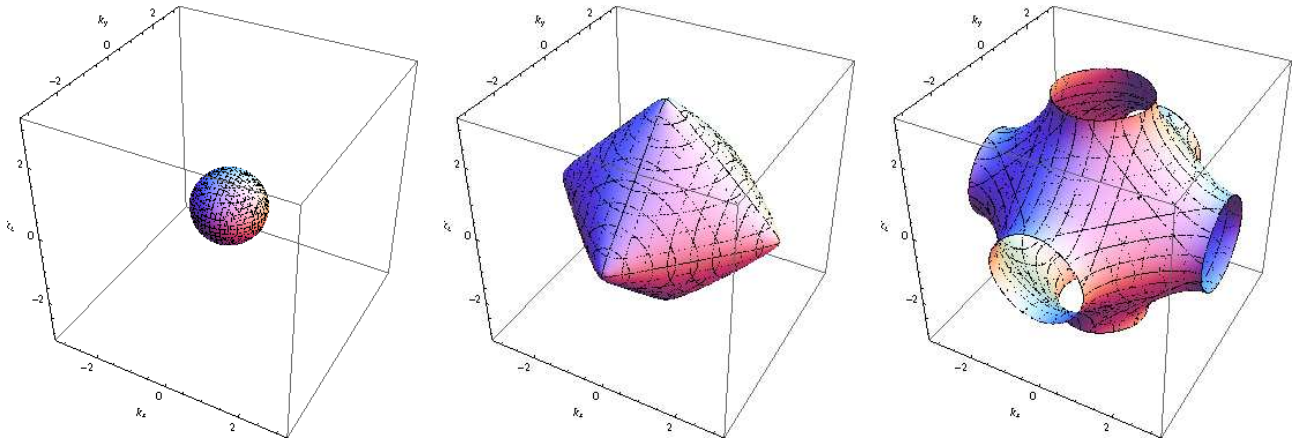

(a) $\frac{\hbar\omega}{U} = -0.28$ (b) $\frac{\hbar\omega}{U} = -0.37$ (c) $\frac{\hbar\omega}{U} = -0.40$

Figure 7.4: For three different energies, the surfaces of constant energy in $\boldsymbol{k}$-space are plotted. The parameters μ/U and J/U have been chosen as in Fig. 7.2 II. We consider hole excitations. When the excitation energy exceeds the gap, we get spherical surfaces as in a). For larger energies the sphere blows up, until the the upper bound of the energy band is reached. The isotropy gets lost and the symmetry of the lattice emerges, as can be seen in b). For even higher energies, no more excitations along the lattice directions exist, such that the constant energy surfaces look like in c).

Instead we find for small k

$$\hbar\Omega(k) = \pm U \frac{\sqrt{-2n^2 + \sqrt{n(1+n)} + 2n\left(-1 + \sqrt{n(1+n)}\right)}}{\sqrt{6}} k + O(k^2). \tag{7.43}$$

We will come back to the peculiarities at the tip in Section 7.3 when we discuss critical behavior.

One additional information that, in principle, could be extracted from the spectral function $\rho(\omega, \boldsymbol{k})$ is the density of states. It is given by a $\boldsymbol{k}$-integration of $\rho(\omega, \boldsymbol{k})$ over the first Brillouin zone. However, this integral turns out to be very complicated, because of the $\cos(k)$ and $\sqrt{\cos(k)}$ terms within the δ-function. So let's content ourselves with some plots of the constant energy surfaces in the $\boldsymbol{k}$-space shown in Fig. 7.4. There we see how the symmetry of the lattice emerges, when we increase the excitation energy.

7.2 Spectra in the SF Phase

The procedure to find the spectral function in the SF phase is exactly the same as before in the MI phase, i.e. we must take the Green's function, which now is given by Eq. (6.59), separate it in its real and its imaginary part and take the $\epsilon \to 0$ limit. But now, this limiting procedure turns out to be very complicated, as the lengthy 4-point cumulant enters the superfluid Green's function (6.59) at various places. It does not seem feasible to follow this way.

Instead we argue in the following way: The limiting procedure is different from setting $\epsilon = 0$ only for those frequencies where the Green's function diverges, i.e. at the resonance frequencies that we are looking for. But this also means that these frequencies can be found by setting $\epsilon = 0$ in Eq.

(6.59) instead of taking the limit. This immediately yields a real function of ω and $\boldsymbol{k}$. By finding its divergences, the excitation spectra are determined. Doing this, however, we loose all information about the spectral weights, which is encoded in the imaginary part of the Green's function.

Another way of finding the dispersion relations without making use of the Green's function is solving the equations of motion (6.46) and (6.47). Since the coefficients in these equations require a similar limiting procedure as the Green's function, we are confronted there with the same technical problem. But again we argue, that the real part is obtained by setting $\epsilon = 0$, while the $\epsilon \to 0$ limit would yield an imaginary part proportional to δ-functions coinciding with the divergences of the real parts. But as diverging coefficients do not solve the equations of motion, we will not consider these cases and restrict us to the case $\epsilon = 0$. We are then left with real coefficients only. In terms of Eqs. (6.48) and (6.49), this means that $A(\omega, \boldsymbol{k}) = A^*(\omega, \boldsymbol{k})$ and $B(\omega, \boldsymbol{k}) = B^*(\omega, \boldsymbol{k})$.

With the second equation of motion (6.49),

$$\Psi_{\boldsymbol{k}}(-\omega) = -\frac{B^*(-\omega, \boldsymbol{k})}{A^*(-\omega, \boldsymbol{k})}\Psi^*_{\boldsymbol{k}}(\omega), \tag{7.44}$$

we can eliminate one field from the first equation of motion (6.48), leading to

$$\left[A(\omega, \boldsymbol{k}) - B(\omega, \boldsymbol{k})\frac{B^*(-\omega, \boldsymbol{k})}{A^*(-\omega, \boldsymbol{k})}\right]\Psi^*_{\boldsymbol{k}}(\omega) = 0, \tag{7.45}$$

where all functional derivatives are evaluated at the equilibrium solution. The resonance condition for non-trivial solutions therefore reads:

$$\frac{\delta^2\Gamma}{\delta\Psi^*_{\boldsymbol{k},\mathrm{q}}(-\omega)\delta\Psi_{\boldsymbol{k},\mathrm{cl}}(-\omega)}\frac{\delta^2\Gamma}{\delta\Psi_{\boldsymbol{k},\mathrm{q}}(\omega)\delta\Psi^*_{\boldsymbol{k},\mathrm{cl}}(\omega)} - \frac{\delta^2\Gamma}{\delta\Psi^*_{\boldsymbol{k},\mathrm{q}}(-\omega)\delta\Psi^*_{\boldsymbol{k},\mathrm{cl}}(\omega)}\frac{\delta^2\Gamma}{\delta\Psi_{\boldsymbol{k},\mathrm{q}}(\omega)\delta\Psi_{\boldsymbol{k},\mathrm{cl}}(-\omega)} \stackrel{!}{=} 0. \tag{7.46}$$

This is the same as the equation one would obtain by looking for a vanishing denominator of the Green's function (6.59). The functional derivatives in Eq. (7.46) have already been taken in Eqs. (6.46) and (6.47). Eq. (7.46) represents an implicit equation for $\omega(\boldsymbol{k})$, but it is too complicated to be solved analytically. We will later discuss some expansions that we can make or limits that we can take in order to get analytic expressions, but at first we can take a look at solutions, which have been determined numerically. We make the following observations:

- Off the tip, we find all in all four SF dispersion branches. There are two branches with positive energy and two with negative energies. We find that the positive branches differ from the negative branches only by the sign. Remember that in the MI phase we had one mode with $\omega \geq 0$, that we interpreted as an excitation by adding one particle, and a second mode with $\omega \leq 0$, which was interpreted as an excitation by taking away one particle. But of course, in both cases, a positive energy is needed in order to excite the system. The different sign for the excitation frequency represents solely the fact that, when we add a particle, energy is collocated within the system, while energy is taken away from the system, when a hole is created. However, if we are interested in the excitation energy, we should rather consider $\hbar|\omega(k)|$ than $\hbar\omega(k)$. With this reasoning in mind we end up with two dispersion modes in the Mott phase and also two modes in the SF phase.

- One of the SF dispersion relation is gapped and quadratic for small k, the other SF mode is gapless and linear. For small k, we can therefore approximate both SF dispersion relations by

$$\omega_1(k) = \Delta + \frac{1}{2m}k^2 + \cdots , \tag{7.47}$$

$$\omega_2(k) = ck + \cdots , \tag{7.48}$$

  where Δ denotes the gap, m the effective mass of the massive excitations, and c the sound velocity of the massless mode.

- When we approach the phase boundary, the SF spectra become identical to the MI spectra. Depending on whether the chemical potential μ is smaller (larger) than at the top of the Mott lobe, the particle (hole) mode from the MI phase survives as a massive excitation in the SF phase.

To see this, we have plotted the two superfluid spectra (red), together with the particle/hole spectra in the MI phase (green) and the spectra at the phase boundary (blue) in the upper part of Fig. 7.5. The graph in the middle shows the situation around the tip of the first Mott lobe, on the left and right side we have plotted the spectra for smaller and larger μ. The latter resemble each other, but one must distinguish particle and hole excitations, in order to see the qualitative difference.

The mapping of the SF spectra onto the MI spectra becomes even clearer in the other plots of Fig. 7.5: In the second and the third row, the gap and the mass of each mode are plotted as a function of J/U. We see that off the tip the gapped SF mode ends up at the phase boundary with exactly the same gap as one of the MI modes. The same is true for its mass. The massless SF mode, however, gains mass near the phase boundary in a sudden, but continuous way. At the tip, both modes become mass- and gapless, no matter whether we come from the SF side or from the MI side. Finally the sound velocity of the massless SF mode is plotted in Fig. 7.5. While it remains finite at the tip of the lobe, it falls off continuously, if the phase boundary is approached off the tip.

Even without solving the resonance condition (7.46), we can show that our theory necessarily allows for this mapping: We only have to compare the retarded SF Green's function given by Eq. (6.59) with the retarded MI Green's function in Eq. (5.39). If we recognize that the equilibrium order field $|\Psi_{\mathrm{eq}}|^2$ given by Eq. (6.40) vanishes continuously, when the phase boundary is approached, it is easy to see that the SF Green's function reduces to the MI Green's function. Therefore it is a consequence of our Ginzburg-Landau ansatz that the phase transition takes a smooth course, as it should be in case of a second-order phase transition.

7.2.1 Interpretation of the Spectra

Still the question arises, how the SF modes can be interpreted. Therefore we should remember that the massless excitations are expected from many points of view:

- Already in the introduction we have stated that such a dispersion relation is crucial for the understanding of superfluidity [15,16].

- In Bogoliubov's approach to weakly interacting Bose gases, a linear spectrum is obtained as a consequence of the interactions [19].

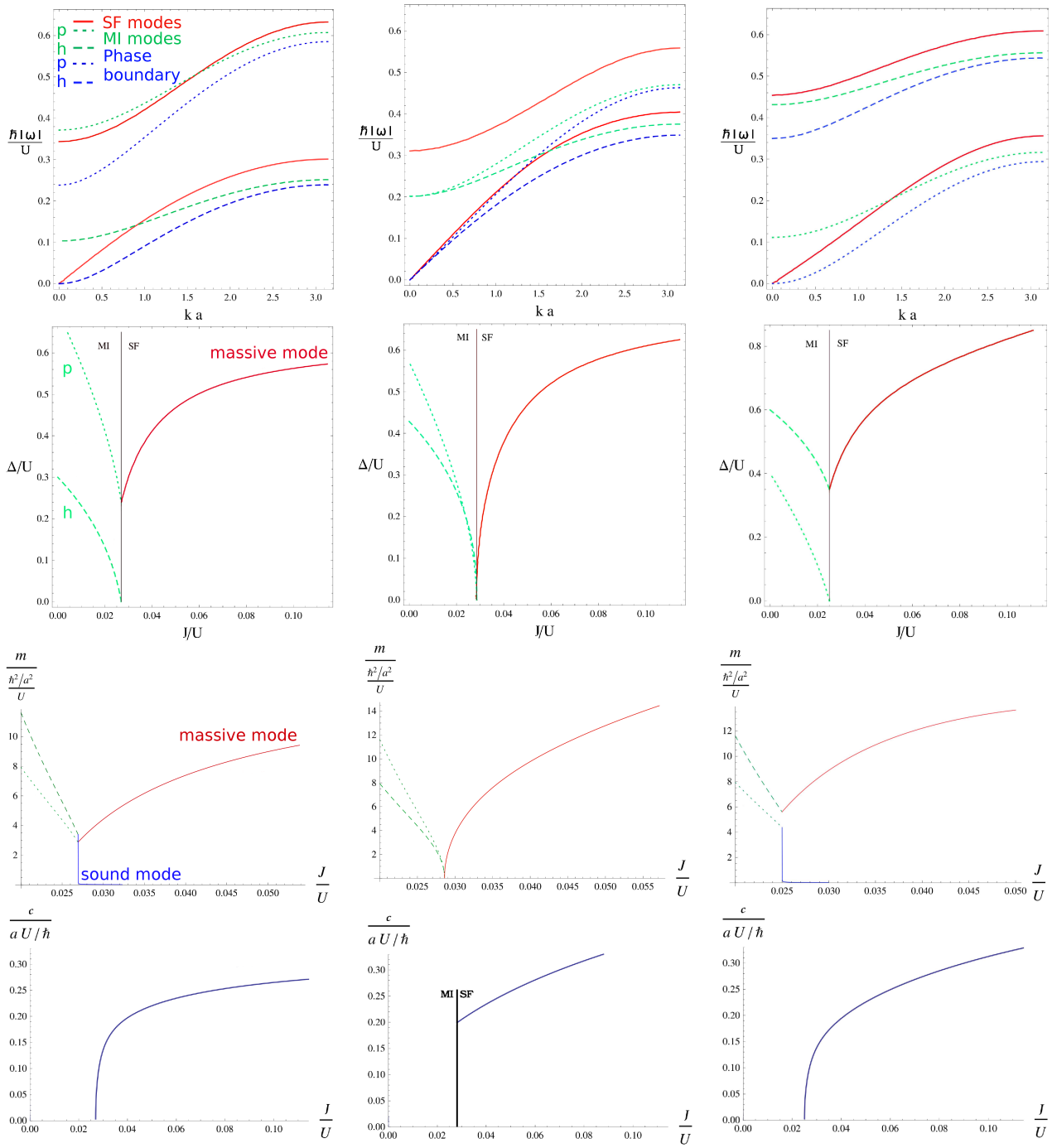

(a) $\tilde{\mu} = 0.3$ (b) $\tilde{\mu} = \sqrt{2} - 1$ (c) $\tilde{\mu} = 0.6$

Figure 7.5: The excitation spectra in both the MI and the SF phase are examined for three different $\tilde{\mu}$: The graphs in the middle consider the situation around the $n = 1$ lobe tip; Figs. (a) and (c) show the situation off the tip. The upper plots show the spectra $\omega(k)$ in the SF phase (red), at the phase boundary (blue) and in the MI phase (green). The MI excitations can be interpreted as particle modes (dotted lines) and hole modes (dashed lines). In the second and the third row we examine the gap Δ and the mass m of the excitations as functions of J/U. We find that the MI spectra map onto the SF spectra. The last row shows the sound velocity of the massless mode in the SF phase.

- In the light of symmetry-breaking, such a dispersion relation is expected from the Goldstone theorem [50].

In the ordered phase, the Landau free energy depicted in Fig. 2.3 is characterized by a minimum for a finite *absolute value* of the order parameter. In this picture, it is obvious that changing the phase of the order field should cost no energy. Thus, we would like to interpret the linear mode, at least for $\omega \to 0$, as a pure phase excitation. In this limit, the equations of motion (6.48) and (6.49) coincide:

$$A(0,\mathbf{0})\Psi_{\mathbf{0}}^{*}(0) + B(0,\mathbf{0})\Psi_{\mathbf{0}}(0) = 0, \tag{7.49}$$

Splitting the order field in its real and its imaginary part, we get the equations

$$[B(0,\mathbf{0}) - A(0,\mathbf{0})]\,\mathrm{Im}[\Psi_{\boldsymbol{k}}(0)] = 0, \tag{7.50}$$

$$[B(0,\mathbf{0}) + A(0,\mathbf{0})]\,\mathrm{Re}[\Psi_{\boldsymbol{k}}(0)] = 0. \tag{7.51}$$

Now we have to note that at $\omega = 0$ and $\boldsymbol{k} = \mathbf{0}$ the terms A and B get very simple, since $|\Psi_{\mathrm{eq}}|$ given by Eq. (6.40) cancels partially the functional derivatives. Thus we have

$$A(0,\mathbf{0}) = -\left(\frac{1}{g_{\mathrm{A}}(0)} - \frac{J_{\mathbf{0}}}{\hbar}\right) = B(0,\mathbf{0}). \tag{7.52}$$

But this means that Eq. (7.50) allows for non-trivial solutions, while Eq. (7.51) does not. Thus the excitations with $\omega = 0$ are purely imaginary, i.e. only the phase of the order field may change. Hence they must be interpreted as phase excitations in agreement with the picture of a wine-bottle shaped free-energy functional in Fig. 2.3.

Unfortunately, our argumentation holds only for the zero-energy case. For any other excitations on the massless branch and on the massive branch, we are not able to find such a unique classification.

To gain further insight, we rely on the results of other authors:

- In Ref. [78] a slave-boson method yields two modes very similar to ours. It is shown that within the sound mode, phase excitations are dominant leading to a density modulation of the system. Within the gapped mode, however, amplitude variations are much stronger than phase variations and the density stays constant within the gapped mode. This mode is interpreted as an interchange between condensate and non-condensate.

- In Ref. [79], both modes are further discussed from the point of view of a quantum phase model which is very similar to the superfluid regime of the BH model. Again, the sound mode is shown to reflect the phase degrees of freedom, while the gapped mode is interpreted as an amplitude mode.

- In Ref. [80] a random-phase approximation does not only find two, but several modes. Amongst them, a second gapped mode appears, which is symmetrical in energy to the gapped mode arising from the MI spectra. Remember that our theory has yielded such a mode as well, but we have argued that only the absolute value of the excitation energy has a physical meaning. In Ref. [80], however, the authors calculate the spectral weights of each mode and find that the mirrored mode has zero strength.

Concerning the sound mode, all cited publications claim good agreement with the excitation spectrum predicted by Bogoliubov theory which is considered to describe very well the sound mode excitations. Also the experimental data presented in Ref. [25] confirms this. More questionable, however, is the gapped mode, since neither does Bogoliubov's theory predict such an excitation nor has there yet been any experimental detection.

From our point of view, however, it is quite natural to have a gapped mode in the SF phase, since we have seen that it directly takes up one of the MI mode. If we look at the weight of this mode at the phase boundary, we find from Fig. 7.3(c) in agreement with Ref. [80], that it is of the same order as the gapless mode. Thus this mode must be present also in the SF phase. Unfortunately, we have not been able to calculate the weights within the SF phase, so we cannot exclude that the weight of the gapped mode decays very fast, when we go away from the lobe. In Ref. [78], the weight is calculated at $J = 1.2\ J_\mathrm{c}$ above the tip. Here, the authors find that it becomes significant only for large k.

This might be one reason for the failure of the experimental detection, but Ref. [78] still gives another argument: Due to missing density modulations in the gapped mode, it is not sensitive to Bragg spectroscopy. We can try to understand this by considering the physical situation at the phase boundary: Depending on the position on the lobe, it still costs some energy Δ to create a particle (hole), while the creation of a hole (particle) is for free. If we simultaneously create a particle and a hole, we have to pay this amount of energy Δ. Obviously, we have not changed the local density, but the local density of particle/hole pairs has increased. It is proportional to $|\Psi_{i,\mathrm{cl}}|^2 \sim \langle \hat{\mathrm{a}}_i \rangle \langle \hat{\mathrm{a}}_i^\dagger \rangle$. Thus it seems to make sense interpreting the gapped mode as an amplitude mode at constant density.

Refs. [78,79] therefore propose measurements via lattice modulation. Since $|\Psi_\mathrm{eq}|$ is a function of J and U, an exchange between condensed and non-condensed particles should be stimulated via a modulation of those two parameters. This technique has already been applied by the group of T. Esslinger [81] and indeed a finite energy absorption has been found. This can probably be interpreted as a first experimental evidence of the gapped mode.

7.2.2 Sound Mode

In this section, we will further analyze the SF sound mode. Before we discuss our own results, we briefly sketch the way, how this mode is described within the Bogoliubov approximation.

Bogoliubov Spectrum

The Bogoliubov approach [19] as well as the Gross-Pitaevskii (GP) approach [82,83] on cold bosonic gases is based on the idea that due to weak interactions the bosonic operators $\hat{\mathrm{a}}_i$ and $\hat{\mathrm{a}}_i^\dagger$ can be replaced by their c-number classical expectation values ϕ_i and ϕ_i^*. Bogoliubov's approach still considers quantum fluctuations $\hat{\tilde{a}}_i$, i.e. $\hat{\mathrm{a}}_i = \phi_i + \hat{\tilde{a}}_i$ and $\hat{\mathrm{a}}_i^\dagger = \phi_i^* + \hat{\tilde{a}}_i^\dagger$.

Within in the GP ansatz, the Bose-Hubbard HHamiltonian from Eq. (2.1) takes the following classical form [84]

$$H_\mathrm{GP} = \sum_i \left(-J \sum_{j \in \mathrm{n.n.}} \phi_i^* \phi_j - \mu |\phi_i|^2 - \frac{U}{2} |\phi_i|^4 \right), \tag{7.53}$$

leading to the equation of motion

$$i\hbar\frac{\partial\phi_i}{\partial t} = -\sum_j J_{ij}\phi_j - \mu\phi_i - U\phi_i|\phi_i|^2. \tag{7.54}$$

Assuming a homogeneous condensate, i.e. $\phi_i = \phi$, and neglecting third and higher order fluctuation terms, the Bogoliubov approach for the BH model [28,80] yields the Hamilton operator

$$\begin{aligned}\hat{\mathrm{H}}_{\mathrm{B}} = \sum_i \Bigg\{ &\frac{U}{2}|\phi|^4 - \mu|\phi|^2 - 6J|\phi|^2 + \left[\hat{\tilde{a}}_i^\dagger\left(|\phi|^2 U - \mu - 6J\right)\phi + \mathrm{h.c.}\right] \\ &+ \frac{U}{2}\left(\phi^2\hat{\tilde{a}}_i^{\dagger 2} + 4|\phi|^2\hat{\tilde{a}}_i^\dagger\hat{\tilde{a}}_i + \phi^{*2}\hat{\tilde{a}}_i^2\right) - \mu\hat{\tilde{a}}_i^\dagger\hat{\tilde{a}}_i\Bigg\} - J\sum_{\langle i,j\rangle}\hat{\tilde{a}}_i^\dagger\hat{\tilde{a}}_j.\end{aligned} \tag{7.55}$$

The energy is minimized by setting the first order fluctuation terms to zero, $U|\phi|^2 - \mu - 6J = 0$. The solution of this equation is also the solution of the time-independent, homogeneous GP equation. We therefore denote it by ϕ_{GP}:

$$\phi_{\mathrm{GP}} = \sqrt{\frac{\mu + 6J}{U}}. \tag{7.56}$$

A transformation into $\boldsymbol{k}$-space according to Eq. (5.41) yields

$$\hat{\mathrm{H}}_{\mathrm{B}} = N\left(-6J - \mu + \frac{U}{2}n_0\right)n_0 + \sum_{\boldsymbol{k}}\left(-J_{\boldsymbol{k}} - \mu\right)\hat{\tilde{a}}_{\boldsymbol{k}}^\dagger\hat{\tilde{a}}_{\boldsymbol{k}} + \frac{U}{2}n_0\sum_{\boldsymbol{k}}\left(\hat{\tilde{a}}_{\boldsymbol{k}}\hat{\tilde{a}}_{-\boldsymbol{k}} + 4\hat{\tilde{a}}_{\boldsymbol{k}}^\dagger\hat{\tilde{a}}_{\boldsymbol{k}} + \hat{\tilde{a}}_{-\boldsymbol{k}}^\dagger\hat{\tilde{a}}_{\boldsymbol{k}}^\dagger\right), \tag{7.57}$$

where $n_0 = |\phi_{\mathrm{GP}}|^2$. Using the bosonic commutation rule $[\hat{\tilde{a}}_{\boldsymbol{k}}, \hat{\tilde{a}}_{\boldsymbol{k}}^\dagger] = 1$, this Hamiltonian can be diagonalized by the so-called Bogoliubov transformation

$$\begin{pmatrix}\hat{\tilde{a}}_{\boldsymbol{k}} \\ \hat{\tilde{a}}_{\boldsymbol{k}}^\dagger\end{pmatrix} = \begin{pmatrix}u_{\boldsymbol{k}}\hat{\mathrm{b}}_{\boldsymbol{k}} + v_{-\boldsymbol{k}}^*\hat{\mathrm{b}}_{-\boldsymbol{k}}^\dagger \\ u_{-\boldsymbol{k}}^*\hat{\mathrm{b}}_{-\boldsymbol{k}}^\dagger + v_{\boldsymbol{k}}\hat{\mathrm{b}}_{\boldsymbol{k}}^\dagger\end{pmatrix}. \tag{7.58}$$

Here the normalization $|u_{\boldsymbol{k}}|^2 - |v_{-\boldsymbol{k}}|^2 = 1$ guarantees the bosonic character of the new operators $\hat{\mathrm{b}}_{\boldsymbol{k}}$ and $\hat{\mathrm{b}}_{\boldsymbol{k}}^\dagger$. After this transformation the Hamiltonian reads

$$\hat{\mathrm{H}}_{\mathrm{B}} = -\frac{U}{2}n_0^2 N + \frac{1}{2}\sum_{\boldsymbol{k}}\left(\hbar\omega_{\boldsymbol{k}} - Un_0 - \epsilon_{\boldsymbol{k}}\right) + \sum_{\boldsymbol{k}}\hbar\omega_{\boldsymbol{k}}\hat{\mathrm{b}}_{\boldsymbol{k}}^\dagger\hat{\mathrm{b}}_{\boldsymbol{k}}, \tag{7.59}$$

where $\epsilon_{\boldsymbol{k}}$ denotes the free dispersion

$$\epsilon_{\boldsymbol{k}} = 2J\left(3 - \sum_{\nu=1}^{3}\cos\left(k_\nu a\right)\right) = 4J\sum_{\nu=1}^{3}\sin^2\left(\frac{k_\nu a}{2}\right), \tag{7.60}$$

while the Bogoliubov dispersion is given by

$$\hbar\omega_{\boldsymbol{k}} = \sqrt{\epsilon_{\boldsymbol{k}}^2 + 2Un_0\epsilon_{\boldsymbol{k}}}. \tag{7.61}$$

Furthermore, one finds for the Bogoliubov parameters

$$|v_{\boldsymbol{k}}|^2 = |u_{\boldsymbol{k}}|^2 - 1 = \frac{1}{2}\left(\frac{\epsilon_{\boldsymbol{k}} + Un_0}{\hbar\omega_{\boldsymbol{k}}} - 1\right). \tag{7.62}$$

A self-consistency check can be made by calculating the total particle number $n(\boldsymbol{k}) = n_0\delta_{\boldsymbol{k},\boldsymbol{0}} + |v_{-\boldsymbol{k}}|^2$. Since in the Gross-Pitaevskii limit, n_0 already equals the total particle number, the Bogoliubov approach is good as long as $|v_{-\boldsymbol{k}}|$ is small.

In the next subsection, we will compare our spectrum with the Bogoliubov spectrum given by Eq. (7.61). For small k, this function can be linearized, and we can extract a sound velocity from Eq. (7.61). It is given by

$$\frac{c}{a/\hbar} = \sqrt{2J(\mu + 6J)}. \tag{7.63}$$

But now let's see how good our theory agrees with these famous results.

Sound Mode from Effective Action

Because of the complicated ω-dependence in the resonance condition (7.45), we have been at first content with a numerical solution plotted in Fig. 7.5. But as the sound mode is gapless for $|\boldsymbol{k}| = 0$, its small-k behavior can be well approximated, if we Taylor expand the equations of motion in ω and $\boldsymbol{k}$ around $\omega = 0$ and $|\boldsymbol{k}| = 0$. In that case the resonance condition (7.45) becomes analytically solvable. For more simplicity we choose without loss of generality $\boldsymbol{k} = (k, 0, 0)$ again and get:

$$\alpha_1(n,\mu,J,U)k^2 + \alpha_2(n,\mu,J,U)\omega^2 + \alpha_3(n,\mu,J,U)k^2\omega^2 + O(\omega^3) + O(k^2) = 0, \tag{7.64}$$

where the coefficients α_i are complicated functions, which we do not want to write down explicitly. As long as α_1 and α_2 have non-zero values, the solution of (7.64) yields a non-zero sound velocity

$$c(n,\mu,J,U) = \sqrt{-\frac{\alpha_1(n,\mu,J,U)}{\alpha_2(n,\mu,J,U)}}. \tag{7.65}$$

We can reduce the number of variables by measuring all energies in units of U, i.e. $\tilde{J} = J/U$ and $\tilde{\mu} = \mu/U$. We then define the dimensionless quantity

$$\tilde{c}(n,\tilde{\mu},\tilde{J}) = \frac{c(n,\mu,J,U)}{aU/\hbar}. \tag{7.66}$$

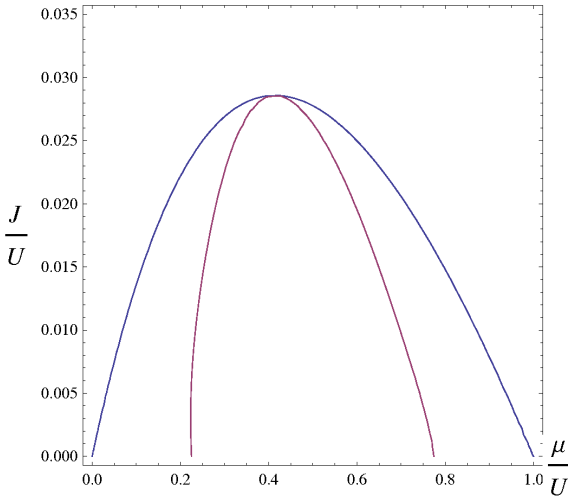

(a) Coefficients $\alpha_1 = 0$ and $\alpha_2 = 0$ from Eq. (7.64).

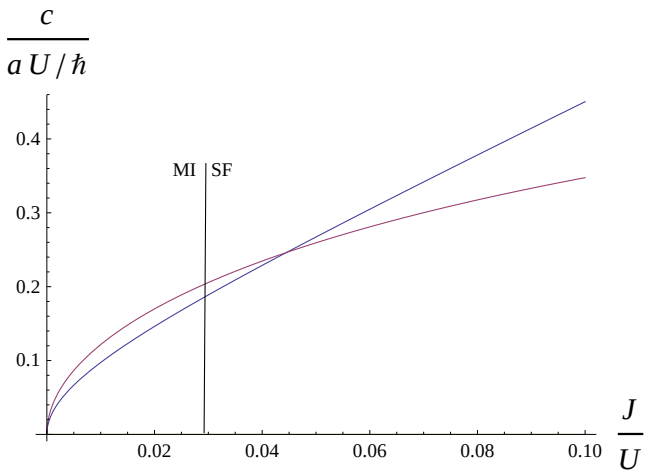

(b) Sound velocity

Figure 7.6: (a) In the figure on the left-hand side the coefficients in Eq. (7.64) are investigated: On the blue line which lies completely on the Mott lobe, we have $\alpha_1(1, \mu, J, U) = 0$. On the purple line lying within the Mott lobe and hitting the lobe at its tip, we have $\alpha_2(1, \mu, J, U) = 0$. (b) The sound velocity c obtained within our approach (purple) is compared to the Bogoliubov prediction (blue) from Eq. (7.63) for a fixed $\mu/U = \sqrt{2} - 1$.

This function is plotted for $n = 1$ and constant $\tilde{\mu}$ in the right part of Fig. 7.5. Its explicit expression for $n = 1$ reads

$$\begin{aligned}\tilde{c}(1,\tilde{\mu},\tilde{J}) = \Big[\Big(\tilde{J}\tilde{\mu}^2(1+\tilde{\mu})^3(3-2\tilde{\mu})\big(-3+8\tilde{\mu}-10\tilde{\mu}^2+4\tilde{\mu}^3+\tilde{\mu}^4\big)^2\big((\tilde{\mu}-1)\tilde{\mu}+6\tilde{J}(1+\tilde{\mu})\big)\Big)\Big/ \\ \Big(36\tilde{J}(1-\tilde{\mu})^3\tilde{\mu}^3(-27+108\tilde{\mu}+9\tilde{\mu}^2-92\tilde{\mu}^3+3\tilde{\mu}^4-24\tilde{\mu}^5+7\tilde{\mu}^6)-(-1+\tilde{\mu})^3\tilde{\mu}^3 \\ (27-135\tilde{\mu}+36\tilde{\mu}^2+172\tilde{\mu}^3-210\tilde{\mu}^4+294\tilde{\mu}^5-196\tilde{\mu}^6+60\tilde{\mu}^7+15\tilde{\mu}^8+\tilde{\mu}^9)+18\tilde{J}^2(1+\tilde{\mu})^2 \\ (27-270\tilde{\mu}+1359\tilde{\mu}^2-3860\tilde{\mu}^3+5950\tilde{\mu}^4-4512\tilde{\mu}^5+1198\tilde{\mu}^6+100\tilde{\mu}^7+135\tilde{\mu}^8-66\tilde{\mu}^9+3\tilde{\mu}^{10})\Big)\Big]^{1/2}.\end{aligned} \tag{7.67}$$

For general n the expression becomes much more lengthy, so we don't give it here.

From Fig. 7.5 we suppose that the sound velocity vanishes at the phase boundary except for the lobe tip. Now we are able to see this explicitly by examining the roots of α_1 and α_2 in Fig. 7.6(a). It can be seen that the sound velocity becomes zero on the whole lobe except at the tip, where both coefficients α_1 and α_2 become zero resulting in a finite sound velocity.

For a comparison with Eq. (7.63) from the Bogoliubov theory, we have plotted $\tilde{c}(1, \tilde{\mu}, \tilde{J})$ for fixed $\tilde{\mu} = \sqrt{2} - 1$ in Fig. 7.6(b) together with the Bogoliubov prediction. At first sight the agreement does not seem pretty good, as for large J/U the Bogoliubov result diverges, while our result tends to a constant value. But nevertheless, we should look at what happens, when U decreases independently from J, as a crucial assumption in the derivation of the Bogoliubov spectrum was the weakness of interactions.

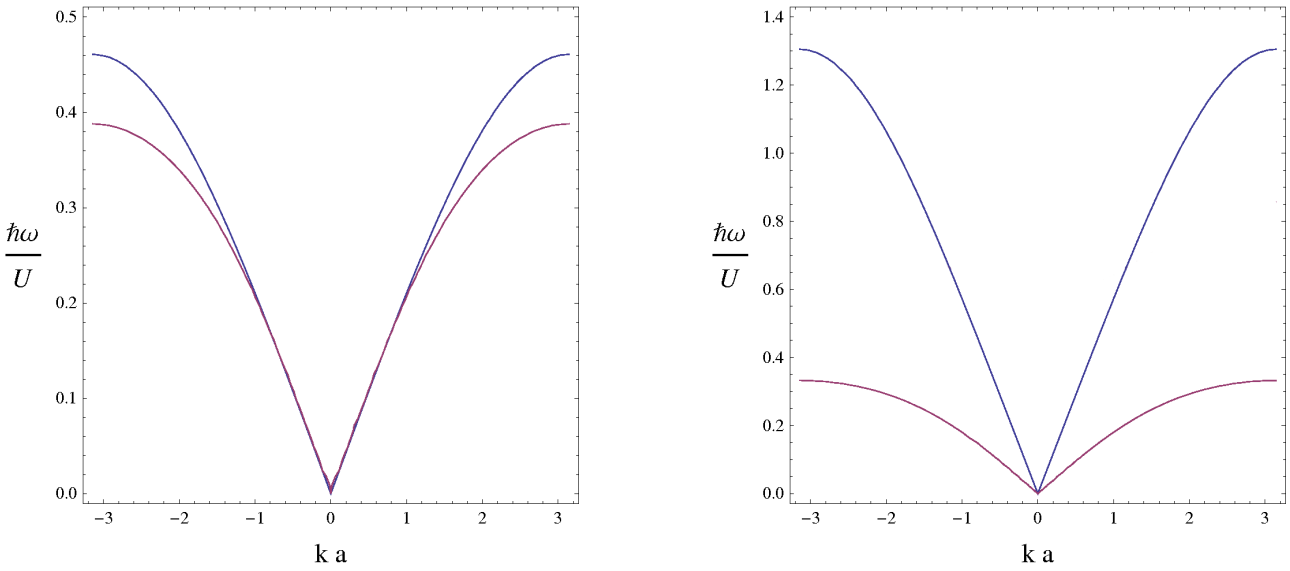

(a) $\frac{J}{U} = 0.04, \frac{\mu}{U} = 0.34$ (b) $\frac{J}{U} = 0.15, \frac{\mu}{U} = 0.22$

Figure 7.7: Bogoliubov spectrum (blue) versus sound mode predicted by Eq. (7.45) (purple): In both plots (a) and (b), the parameter $J/U, \mu/U$ are chosen such that $n \approx 1$ according to Ref. [70]. While the system in (a) is close to the phase boundary, in (b) it is deep in the SF phase.

We therefore expand our result from (7.64) in U yielding

$$\frac{c}{a/\hbar} = \sqrt{2J(6J+\mu)} + \frac{J\left[216J^3(1+2n) - 6J(1+2n)\mu^2 - (1+6n)\mu^3 + 36J^2(\mu+2n\mu)\right]}{2\sqrt{2}\mu^3\sqrt{J(6J+\mu)}}U + O(U^2). \tag{7.68}$$

In zeroth interaction order, we thus obtain the Bogoliubov result. This means that our theory, which we started as a small J expansion, yields the same result as a theory for small U in the asymptotic limit $U \to 0$. As this is a quite remarkable finding, we are going to study this in more details.

First we check, if only the sound velocity or even the whole spectrum of our theory coincides with the Bogoliubov result in the weak interaction limit. Therefore, we make a Taylor expansion in U of the resonance condition (7.45). To zeroth order we get

$$\hbar^2\omega(\boldsymbol{k})^2 = 4J\sum_{\nu=1}^{3}\sin^2\left(\frac{k_\nu a}{2}\right)\left[4J\sum_{\nu=1}^{3}\sin^2\left(\frac{k_\nu a}{2}\right) + 2(\mu+6J)\right]. \tag{7.69}$$

This is exactly the result from Eq. (7.61) obtained in the Bogoliubov approximation with a Gross-Pitaevskii order field (7.56). In Fig. 7.7 we compare this spectrum with the numerical solution of the full resonance condition. We find that in the left picture the agreement of both spectra is quite good. Only for large k, our dispersion relation is flattened a little bit. Deeper in the SF phase, however, our spectrum strongly deviates from this result.

We are thus confronted with the somehow strange result, that we have a perfect agreement with Bogoliubov for small U, but not for large J/U. So we take a look on the first-order term in Eq. (7.68).

Here we have an asymptotic J^3 behavior. This means that the influence of this first-order correction gets bigger, when we are deep in the SF phase. Unfortunately, in this regime the Bogoliubov result is supposed to be very good. This is surely a limitation of our theory. But as we started our perturbation theory in the Mott phase with an expansion for small J, we shouldn't expect too much. We have good reasons to believe that at the onset of superfluidity our corrections to the Bogoliubov spectrum are relevant. A strong evidence for that is the fact that $c(n, \mu, U, J)$ vanishes at the phase boundary with the exception of the lobe tips.

A final answer to the question, whether our result corrects the Bogoliubov spectrum near the phase boundary, can only be given by experiment. The sound mode of bosons in optical lattice was recently measured by the group of K. Sengstock [25]. This data is shown in Fig. 1.5 in the Introduction. A quantitative comparison with our results, however, is not possible, since in the experimental setup the atoms are confined by an additional harmonic trap. To describe this situation theoretically, one must introduce a chemical potential μ_i which depends on the lattice site. Thus the assumption of homogeneity, which was made in the derivation of our spectra, is no longer fulfilled. But qualitatively we can see from Fig. 1.5, that the experimental spectrum agrees well with the Bogoliubov spectrum for small k, but for large k, it is flattened a little bit. This is also the case for our result as shown in Fig. 7.7.

7.2.3 Gapped Mode

We now have seen that our results are identical to Bogoliubov's predictions, if we truncate the equation of motion (7.45) in zeroth interaction order yielding Eq. (7.69). This equation does not allow for a gapped mode. We find, however, that a gapped mode arises, if we take into account higher orders in U. This mode must therefore be considered as a phenomenon, which is caused by strong interactions.

Expanding Eq. (7.45) up first-order in U, however, still turns out to be too crude, as the effective masses of the excitations have the wrong sign compared to the numerical solution shown in Fig. 7.5. Since this solution yields $m \sim 1/\sqrt{U}$, these masses get big for small U. Then the wrong sign does not play an important role, because the dispersion relation becomes very flat. In the limit $U \to 0$, we get $\hbar\omega(\boldsymbol{k}) = 2\mu$. By comparing this with our numerical solutions, this can be considered a reasonable approximation.

Now we should note that μ is a paramter used in our theoretical description, but not being fixed in the real system. There the particle number is given and we have to choose μ in such a way that the particle number is reproduced. As one can best see from Eq. (7.56) for the condensate density deep in the SF phase, a vanishing interaction parameter U demands for a vanishing chemical potential μ, if the density is to be maintained constant. Thus we see again, that this mode has to disappear in the limit $U \to 0$.

Further analysis of the gapped mode turns out to be very difficult. For the gapless mode, a Taylor expansion around $\omega = 0$ and $k = 0$ was possible. But solutions with $\omega \neq 0$ cannot be properly described in such a limit. So we really seem to be reliant on the numerical results. We will extend them a little bit further in the next section, where the critical properties are discussed.

7.3 Critical Behavior

The fact that the system behaves differently at the lobe tip than on the rest of the lobe requires some further considerations. It has already been argued by Weichman *et al.* [31] that such a difference must occur. Their argument is based on the fact that, while the particle number per lattice site is quantized to integer numbers in the MI phase, in the SF phase it is not. Thus a transition into the SF phase in general comes along with a change of the density. Only at the tip of the lobe, the phase boundary is hit by a superfluid $n = \text{const.}$ curve, thus only there a transition *without* a density change is possible. So while on the whole lobe except at its tip the phase transition is driven by an addition or subtraction of particles, on the tip of the lobe it is the increase of the hopping parameter J, which smoothly drives the system into the SF phase. This explains the different critical behavior.

7.3.1 Some Scaling Ideas

To examine this behavior a little bit closer, we should first state the concept of critical theories [14,34,85]: When a system undergoes a phase transition, some of its properties are supposed to be *universal*. That means that they depend on the behavior of the system under scaling transformations rather than on microscopic details. Systems which behave equally under the same scaling transformations belong to the same *universality class*, which means that their universal properties can be described by the same *critical exponents* in the vicinity of the phase transition. Scaling transformations might act on any relevant quantity within the theory, for example on time and length scales, i.e.:

$$x \to x\mathrm{e}^{-\nu} \tag{7.70}$$

$$t \to t\mathrm{e}^{-z\nu}. \tag{7.71}$$

To see, if a system is invariant under such a transformation, we have to look at its Lagrangian. A crucial role plays the *dynamic critical exponent* z. It gives the ratio of the scaling factors for time and space. It is clear that the scaling for a Lorentz-invariant Lagrangian, for instance, must have $z = 1$. Such a scaling leaves velocities invariant and the corresponding systems have a relativistic excitation spectrum $\hbar\omega(\boldsymbol{k}) = \sqrt{\Delta^2 + c^2\boldsymbol{k}^2}$. Galilei-invariant systems have $z = 2$ and their spectrum is quadratic in $\boldsymbol{k}$.

Another interesting property concerning the excitation spectra near the phase boundary is the behavior of an energy gap Δ. We have seen that within the BH model, the gap vanishes at least for one mode, when the phase boundary is approached. This can be described by the power law:

$$\Delta \sim (J - J_{\mathrm{PB}})^a, \tag{7.72}$$

where again the exponent a is universal. As energy scales with the inverse of the scaling for time, we have $a = z\nu$.

Coming back to the BH model, the scaling behavior on the tip of lobe should be different of the rest of the phase boundary. This can be seen by writing down the Lagrangian for a continuum quantum

field theory of the Bose-Hubbard system [34]:

$$\mathcal{L} = K_1 \Psi^* \frac{\partial \Psi}{\partial t} + K_2 \left| \frac{\partial \Psi}{\partial t} \right|^2 + K_3 |\nabla \Psi|^2 + (\lambda_2/2) |\Psi|^2 + (\lambda_4/4!) |\Psi|^4 , \tag{7.73}$$

where the K's and λ's are parameters depending on the system parameter μ, U and J. Investigating K_1, it is found in Ref. [34] that $K_1 = 0$ at the tips of the lobes, resulting in a Lorentz-invariant scaling theory with $z = 1$, whereas $z = 2$ holds elsewhere. The universality class of the transition at the tip is often referred to as the XY-model in $d+1$ dimensions or the $O(2)$ quantum rotor model. For this theory the mean-field value of the critical exponent $z\nu$ is found to be $1/2$ [31], thus $\nu = 1/2$ in mean-field. Outside the tip, the systems belongs to the universality class of dilute Bose gases with $z\nu = 1$, so again we have the mean-field exponent ν=1/2.

7.3.2 Critical Exponents

From the point of view presented in the subsection above, the linear shape of the dispersion relation at the tips, in contrast to the quadratic shape elsewhere on the lobe, is a consequence of the different dynamic critical exponents. Let us still see which critical exponents $z\nu$ are produced by our theory.

We have the theoretical tools to study the critical exponents on both sides of the phase boundary. Due to their universality, they of course must be the same on both sides [85]. And while we can calculate $z\nu$ analytically in the MI phase, numerical methods must be applied on the SF phase. Nevertheless, we are going to examine $z\nu$ in both phases in order to check our theory. Furthermore, in the SF phase we can go through the lobe tip either at constant density or at constant hopping, which should yield different exponents.

Approaching the Phase Boundary from the MI phase

The MI phase approach to the tip has already been graphically investigated in Ref. [73] which is based on the same retarded Green's function as ours. Here we will extend the study of the critical exponents to the whole phase boundary. In the MI phase this can be done analytically.

The gap is given by Eq. (7.35), when we set $\boldsymbol{k} = \mathbf{0}$: $\Delta(U, \mu, J) \equiv \hbar\Omega_{\pm}(\mathbf{0})$. Of course we have to choose the dispersion relation with a vanishing gap, i.e. a hole spectrum for $\mu < \mu_{\text{tip}}$ and the particle spectrum otherwise.

Next we invert the equation for the phase boundary (7.19). For more simplicity, we restrict ourselves to the first Mott lobe $n = 1$:

$$\tilde{\mu}_{\text{PB}_{1,2}} = \frac{1}{2} \left(1 - 6\tilde{J}_{\text{PB}} \pm \sqrt{1 - 36\tilde{J}_{\text{PB}} + 36\tilde{J}_{\text{PB}}^2} \right), \tag{7.74}$$

where $\tilde{\mu}_{\text{PB}}$ and $\tilde{J}_{\text{PB}}$ denote the chemical potential and the hopping at the phase boundary measured in units of U. We have two solutions, as the lobe is hit twice by $J = \text{const.} < J_{\text{tip}}$.

Now we insert $\tilde{\mu}_{\text{PB}_{1,2}}$ in Δ which leaves us with the following expression:

$$\tilde{\Delta}(\tilde{\mu}, \tilde{J}) \equiv \frac{\Delta(U, \mu, J)}{U} = 3(\tilde{J}_{\text{PB}} - \tilde{J}) \pm \left(\sqrt{1 - 36\tilde{J}_{\text{PB}} + 36\tilde{J}_{\text{PB}}^2} - \sqrt{1 - 36\tilde{J} + 36\tilde{J}^2} \right). \tag{7.75}$$

Note that this is still a function of $\tilde{\mu}$, since $\tilde{J}_{\mathrm{PB}}$ depends on $\tilde{\mu}$. If we now fix μ, we can find out how the gap behaves, when the phase boundary is approached. We still have to replace $J = J_{\mathrm{PB}} - j$. We then have

$$\tilde{\Delta}(\tilde{\mu}, \tilde{j}) = 3\tilde{j} \pm \left(\sqrt{1 - 36\tilde{J}_{\mathrm{PB}} + 36\tilde{J}_{\mathrm{PB}}^2} - \sqrt{1 - 36\tilde{J}_{\mathrm{PB}} + 36\tilde{J}_{\mathrm{PB}}^2 - 36\tilde{j} - 72\tilde{J}_{\mathrm{PB}}\tilde{j} + 36\tilde{j}^2} \right). \quad (7.76)$$

For $\tilde{\mu} = \sqrt{2} - 1$ the phase boundary is hit at the tip. There we have $\tilde{J}_{\mathrm{PB}} = 1/2 - \sqrt{2}/3$ and hence $\sqrt{1 - 36\tilde{J}_{\mathrm{PB}} + 36\tilde{J}_{\mathrm{PB}}^2} = 0$. Thus the gap reads

$$\tilde{\Delta}(\tilde{\mu}_{\mathrm{tip}}, \tilde{j}) = 3\tilde{j} \pm \sqrt{24\sqrt{2}\tilde{j} + 36\tilde{j}^2}. \quad (7.77)$$

As $\tilde{j}$ vanishes at the phase boundary, the behavior near criticality is given by the lowest order in $\tilde{j}$, i.e. we have the result

$$\tilde{\Delta}(\tilde{\mu}_{\mathrm{tip}}, \tilde{j}) \sim \sqrt{j}. \quad (7.78)$$

This means that the critical exponent is $z\nu = 1/2$.

For all other μ, there remains a non-zero term $1 - 36\tilde{J}_{\mathrm{PB}} + 36\tilde{J}_{\mathrm{PB}}^2$ under the square root. This means that the gap is not proportional to $\sqrt{j}$, but to j. With a Taylor expansion in j, we get:

$$\tilde{\Delta}(\tilde{\mu}, \tilde{j}) \approx \left(3 \pm \frac{36 - 72\tilde{J}_{\mathrm{PB}}}{2\sqrt{1 - 36\tilde{J}_{\mathrm{PB}} + 36\tilde{J}_{\mathrm{PB}}^2}} \right) j. \quad (7.79)$$

Hence we have $z\nu = 1$ in agreement with Ref. [31].

Approaching the Phase Boundary from the SF Phase

At the tip of the lobe the gap of the SF gapped mode vanishes, so we can also determine the critical exponent for it on this side of the phase transition. Here we have the possibility either to approach the tip along the line of constant density or along a tangent to the phase boundary with constant hopping parameter $\tilde{J}$. As we have seen in the MI phase, this difference should concern the critical exponents, so we investigate both cases separately.

For a study at constant density we need to know the average particle number $\overline{n}$ in the SF phase as a function of $\tilde{\mu}$ and $\tilde{J}$. Obtaining this information within our theory is complicated, so we revert to a thermodynamic effective action theory in imaginary time [70]. There the derivative of the effective action with respect to μ directly yields $\overline{n}$. It is found that $\overline{n}$ =const along a line hitting the lobe tip, but without being parallel to the $\tilde{J}$ axis. The latter has been assumed by Weichman *et al.* [31], but due to the bosonic commutation relations, the BH model has, different than the fermionic Hubbard model, no particle/hole symmetry.

In Fig. 7.8(a) we plot the gap along $\overline{n} = 1$. Noting the double-logarithmic axes, we can extract the critical exponent from this graph: $z\nu = 0.5$. We also investigated $z\nu$ for constant $\tilde{\mu} = \sqrt{2} - 1$ and found the same value $z\nu = 0.5$, i.e. it makes no quantitative difference if we use the $\overline{n}$ =const line

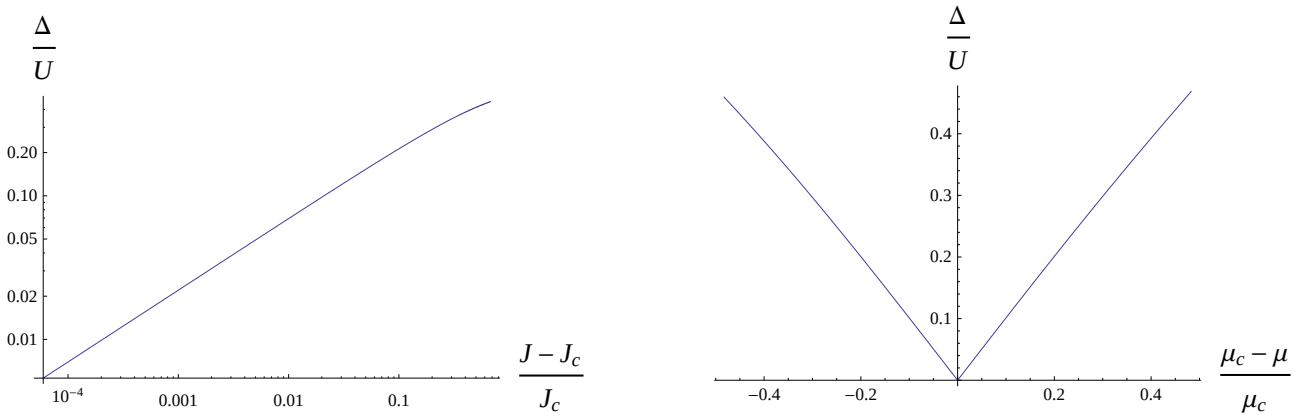

(a) $\overline{n} = \text{const.}$ (b) $J = \text{const.}$

Figure 7.8: The gap Δ is examined, when the tip of the $n = 1$ Mott lobe is approached from the SF phase at constant $\overline{n}$ (a) or at constant J (b). The linear shape in (b) corresponds to a critical exponent $z\nu = 1$, while in (a) a double-logarithmic plot is used yielding $z\nu = 0.5$

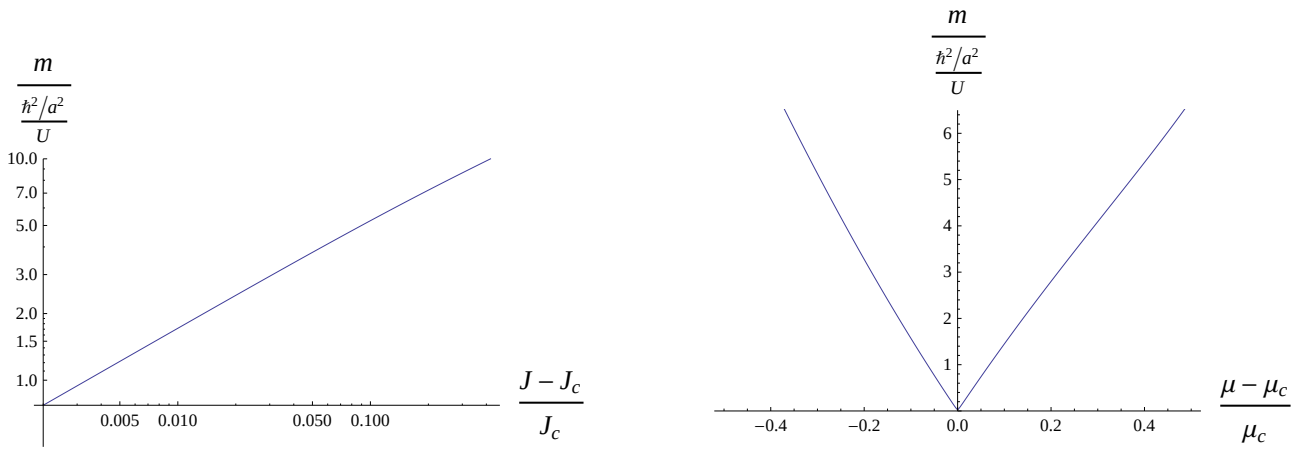

(a) $\overline{n} = \text{const.} = 1$ (b) $J = \text{const.} = J_c$

Figure 7.9: The effective mass m at tip of the $n = 1$ Mott confirms the exponents from Fig. 7.8.

from Ref. [70] or the one from Ref. [31]. Comparing this result with the critical exponents in the MI phase, we find that they are the same on both sides of the phase transition, as it has to be.

If we approach the tip of the lobe at constant J/U, the situation looks completely different. It is shown in Fig. 7.8(b). We find that $\Delta \sim \mu - \mu_c$, i.e $z\nu = 1$. Thus a transition tangent to the phase boundary has the same critical exponent $z\nu$ as a transition off the lobe. But since $z = 1$ at the tip, also the exponent ν must be 1 for the tangent transition in agreement with Ref. [31].

Another quantity that vanishes at the tip of the lobe is the effective mass of the excitations. As we have $z = 1$ at the multicritical point, masses have to scale like energies, thus we expect the same critical exponents as for the gap. In Fig. 7.9(a) we plot our result for constant $\overline{n}$. Noting the double-logarithmic scale of the axis, we find $z\nu = 0.5$. For constant J, the masses decrease linearly with $\mu - \mu_c$ as shown in Fig. 7.9(b). We therefore have $z\nu = 1$. Thus, both cases are consistent with the results found for the gap Δ.

8 Relation to other Theories

In this final chapter we would like to point out the relation of our effective action theory to the theory of Gross-Pitaevskii sketched in Section 7.2.2 and to a similar approach as ours, though in imaginary time [70].

8.1 Gross-Pitaevskii Equation

We have already seen that the sound mode becomes the Bogoliubov spectrum in the limit $U \to 0$. We want to take this up and consider the Green's functions in this limit. At finite temperature the structure of $G^{\mathrm{R/A}}(\omega_1, \omega_2)$ and $C^{\mathrm{R/A}}(\omega_1, \omega_2; \omega_3, \omega_4)$ can be taken from Eqs. (5.20) and (A.15):

$$G^{\mathrm{R/A}}(\omega_1, \omega_2) = \frac{1}{\mathcal{Z}^{(0)}} \sum_{n=0}^{\infty} \mathrm{e}^{\beta E_n} \overline{g_n}(\omega_1, \omega_2), \tag{8.1}$$

$$C^{\mathrm{R/A}}(\omega_1, \omega_2; \omega_3, \omega_4) = \frac{1}{\mathcal{Z}^{(0)}} \sum_{n=0}^{\infty} \mathrm{e}^{\beta E_n} \overline{C_n}(\omega_1, \omega_2; \omega_3, \omega_4). \tag{8.2}$$

We must note that the kernels $\overline{g_n}$ and $\overline{C_n}$ as well as the unperturbed energies E_n and the partition function $\mathcal{Z}^{(0)}$ depend on the interaction U and must be taken into account, when we expand in U. In the lowest, non-trivial interaction order, these functions read:

$$G_{\mathrm{R/A}}(\omega_1, \omega_2) = -2\pi \frac{1}{\mu + \omega} \delta(\omega_1 - \omega_2) + O(U) \tag{8.3}$$

$$C^{\mathrm{R/A}}(\omega_1, \omega_2; \omega_3, \omega_4) = -2\pi \frac{2U}{(\mu + \omega_1)(\mu + \omega_2)(\mu + \omega_3)(\mu + \omega_4)} \delta(\omega_1 + \omega_2 - \omega_3 - \omega_4) + O(U^2). \tag{8.4}$$

In this limit the Green's functions do not depend on temperature, since the kernels $\overline{g_n}$ and $\overline{C_n}$ do not depend on n. Thus, the temperature-dependence from the exponential can be canceled by the temperature-dependence of the partition function. Any higher-order terms, however, are not independent from the temperature.

In the previous chapter, we have made the limit $U \to 0$ at $T = 0$. Actually, this has not been correct, since at zero temperature the Green's functions reduce to one single $\overline{g_n}$ or $\overline{C_n}$, respectively. Then n is the ground-state occupation number. But we know that this is a function of μ/U, thus it would be affected by $U \to 0$. At finite temperature, however, we do not have to worry about that, since n is a summation index.

The small U expansion of the equilibrium order field Ψ_{eq} from Eq. (6.40) yields

$$(\hbar |\Psi_{\mathrm{eq}}|)^2 = 2 \frac{6J + \mu}{U} + O(U^0), \tag{8.5}$$

which is, apart from the factor 2, identical to the Gross-Pitaevskii field in Eq. (7.56). This factor is due to our definition of classical and quantum components $\hbar\Psi_{\mathrm{cl}} = \sqrt{2}\langle\hat{\mathrm{a}}\rangle$.

Eq. (8.5) shows that the order field diverges for small U with $U^{-1/2}$. We should note that there are terms of different order in Ψ in the equation of motions (6.21) and (6.22): the term with $G_{\mathrm{R/A}}(\omega_1, \omega_2)$ is multiplied with only one field, while the term with $C^{\mathrm{R/A}}(\omega_1, \omega_2; \omega_3, \omega_4)$ is multiplied with three fields. To have the same order in U for all the terms, we truncate the U-expansion of $G_{\mathrm{R/A}}$ in zeroth order, while for $C^{\mathrm{R/A}}$ it is truncated only in first order. The equation of motion (6.21) then reads

$$0 \stackrel{!}{=} \sum_j \Big\{ \left[(-\hbar\omega - \mu)\,\delta_{ij} - J_{ij}\right] \psi^*_{j,\mathrm{cl}}(\omega) + \frac{\hbar^2}{2} U \delta_{ij} \int_{-\infty}^{\infty} \mathrm{d}\omega_2 \int_{-\infty}^{\infty} \mathrm{d}\omega_3 \int_{-\infty}^{\infty} \mathrm{d}\omega_4 \\ \times \delta(\omega + \omega_2 - \omega_3 - \omega_4) \psi_{i,\mathrm{cl}}(\omega_2) \psi^*_{i,\mathrm{cl}}(\omega_3) \psi^*_{i,\mathrm{cl}}(\omega_4) \Big\}. \tag{8.6}$$

This is the Fourier transform of the Gross-Pitaevskii equation given in (7.54). The factor $1/2$ in front of U comes again from the definition of $\hbar\Psi_{\mathrm{cl}}$ as $\sqrt{2}\langle\hat{\mathrm{a}}\rangle$. The fact that our theory produces the GP limit, is a nice crosscheck of our results.

8.2 Effective Action in Imaginary Time

Another possible check of our theory is the comparison with the ITF approach in Ref. [70]. Instead of defining the generating functional $\mathcal{Z}$ by an integration along the real-time axis, an integration from $t = 0$ to $t = -i\hbar\beta$ is used there. Thus, this formalism is, *at first*, a pure thermodynamical theory without any significance for real-time dynamics. Nevertheless a comparison of both formalisms is possible, as in thermal equilibrium it should play no role, which integration path is chosen, since both can be related to each other via an analytic continuation.

In order to throw some light on the relationship between those two formalisms, we first realize that both encode all information within the corresponding Green's functions: In the ITF, these are the time-ordered n-point functions defined by Eq. (3.28). In the CTPF, we have 2^n path-ordered n-point functions defined by Eq. (3.45). Making the assumption $\Psi_{\mathrm{q}} = 0$, we found that only a few linear combinations of them are necessary to describe the dynamics of the system. We named these functions the advanced/retarded functions, see Eqs. (4.31) and (6.34). So they should be compared with their imaginary-time analogs. To do that, we set $\epsilon = 0$ in the retarded/advanced function from the CTPF and replace the real and continuous frequency variable ω by the discrete Matsubara frequency $i\omega_m = i\pi m/(\hbar\beta)$ or vice versa, where $m \in \mathbb{N}$.

- For $n = 2$, we find that the retarded n-point function from the CTPF is exactly the same as the thermal Green's function from the ITF given in Ref. [70].
- For $n = 4$, however, a discrepancy appears. The thermal 4-point function from Ref. [70] differs

from the retarded function $C^{\mathrm{R}}(\omega_1,\omega_2;\omega_3,\omega_4)$ given in Eq. (A.15) by the following term:

$$\frac{1}{\mathcal{Z}^{(0)}}\sum_{n=0}^{\infty}\mathrm{e}^{-\beta E_n}\Bigg\{\delta_{\omega_{m2},\omega_{m4}}\Big(\frac{(n+1)^2}{(E_{n+1}-E_n-i\omega_{m1})(E_{n+1}-E_n-i\omega_{m2})} + \frac{n^2}{(E_n-E_{n-1}-i\omega_{m1})(E_n-E_{n-1}-i\omega_{m4})} - \frac{n(n+1)}{(E_n-E_{n-1}-i\omega_{m1})(E_{n+1}-E_n-i\omega_{m4})} - \frac{n(n+1)}{(E_n-E_{n-1}-i\omega_{m4})(E_{n+1}-E_n-i\omega_{m1})}\Big)\Bigg\}_{\omega_{m1}\leftrightarrow\omega_{m2}}. \tag{8.7}$$

At this place we should remember that $C^{\mathrm{R}}(\omega_1,\omega_2;\omega_3,\omega_4)$ is the retarded Green's function and at the same time the *retarded* connected Green's function. Since the retarded/advanced functions have the form $\left\langle \hat{\mathrm{T}}_{\mathrm{c}}\left\{\hat{\mathrm{a}}_{\mathrm{q}}^{\dagger}\hat{\mathrm{a}}_{\mathrm{q}}^{\dagger}\hat{\mathrm{a}}_{\mathrm{q}}\hat{\mathrm{a}}_{\mathrm{cl}}\right\}\right\rangle_0$, any decomposition consists of an expectation value $\left\langle \hat{\mathrm{T}}_{\mathrm{c}}\left\{\hat{\mathrm{a}}_{\mathrm{q}}^{\dagger}\hat{\mathrm{a}}_{\mathrm{q}}\right\}\right\rangle_0$ according to Eq. (4.13). Due to the fact that this expectation value is built up of quantum component operators only, it must vanish, as we have proved in Section 6.1. Thus the retarded/advanced Green's functions are equal to the corresponding retarded/advanced connected Green's functions.

For the thermal Green's function this is not the case. The *connected* Green's function contains the following additional decomposition term:

$$-\Big\{\delta_{\omega_{m2},\omega_{m4}}g_2(\omega_{m1})g_2(\omega_{m2})\Big\}_{\omega_{m1}\leftrightarrow\omega_{m2}}. \tag{8.8}$$

Now we note that for $\beta\to\infty$ the expressions (8.7) and (8.8) cancel each other, thus the connected 4-point functions become the same in both formalisms.

Noting that the equation of motions (6.21) and (6.22) are structurally identical to the equation of motion obtained in the ITF, the accordance of the connected Green's functions means identical results concerning on the one hand the equilibrium order field Ψ_{eq} and on the other hand the dynamics of the system. This saves us for $T=0$.

Unfortunately, for finite temperature the expressions (8.7) and (8.8) do *not* cancel, and thus the equations of motion in both formalisms are no longer the same. We wouldn't be concerned with that, if this discrepancy affected only the dynamics of the system, since it is far from obvious that the analytic continuation $\omega_m\to i\omega+\epsilon$ in the thermal Green's function yields the right real-time function [55–57,66,86,87]. Due to the definition of the Matsubara frequencies (3.33), we for example have an ambiguity concerning factors $\mathrm{e}^{i\beta\omega_{\mathrm{m}}}=1$, with which we could multiply the ITF Green's functions without changing their value. For real, continuous frequencies, however, these terms would not be equal to 1 any longer. But even without making an analytic continuation, we can compare both formalisms by restricting ourselves to equilibrium predictions. We find discrepancies concerning the static solution for the order field from Eq. (6.40). To obtain this time-independent quantity, all frequencies are set to zero. Then the ITF produces a unique result, which is confirmed by Ref. [36]. Thus we have to suppose that our equilibrium field has the wrong temperature dependence.

Another problem, which seems to be closely related to this one, concerns thermodynamic quantities like the free energy, which contains useful information about the occupation number n or the compressibility κ. In the ITF, the free energy is directly given by the generating functional $\mathcal{F}[j,j^*]$ which must be evaluated at $j=j^*=0$. Then n and κ can immediately be gained by derivations of $\mathcal{F}$ with

respect to the chemical potential μ. Evaluated at $j = j^* = 0$, it is the same as the effective action Γ evaluated at equilibrium [70]. We therefore have in the ITF:

$$\langle n \rangle = -\frac{1}{N} \frac{\partial \Gamma}{\partial \mu}\bigg|_{\psi=\psi_{\mathrm{eq}}}, \tag{8.9}$$

$$\kappa = -\frac{1}{N} \frac{\partial^2 \Gamma}{\partial \mu^2}\bigg|_{\psi=\psi_{\mathrm{eq}}}. \tag{8.10}$$

In the CTPF, however, the assumption $\Psi_{\mathrm{q}} = 0$ automatically yields $\mathcal{F} = \Gamma = 0$. Thus the functional $\mathcal{F}$ cannot be interpreted as the free energy, neither can we derive $\langle n \rangle$ or κ from Γ. So the question arises, whether this thermodynamic information is contained at all in the CTPF. From the point of view of the equations of motion, it might be possible to drop the assumption $\Psi_{\mathrm{q}} = 0$, but since $\Psi_{\mathrm{q}} \sim \left(\langle \hat{\mathrm{a}}_+^\dagger \rangle - \langle \hat{\mathrm{a}}_-^\dagger \rangle \right)$ this would be an unphysical solution, as long as the forward and the backward paths are identical.

If we take again a look at the integration contours shown in Fig. 3.1, we see that the contour in b), which ends at a finite time $t - i\hbar\beta$, certainly encodes the same statistical information as the ITF and allows for an interpretation of $\mathcal{Z}$ as the thermodynamic partition function. Our approach, however, integrates along the contour depicted in Fig. 3.1c). Here the integration along the imaginary-time axis, which is responsible for the thermal averaging, is neglected. We justified this with the fact that all what happens at finite real times, is infinitely far away from the imaginary part of the contour, which has been pushed into the infinite past [59,60]. For a theory in thermal equilibrium, however, it now seems crucial to include this part. Since in an equilibrium situation, energy is conserved during the whole time-evolution, it must make a difference, whether we start with the perturbed or the unperturbed system at a given temperature β. A similar argument against the neglection of the imaginary part is given by Refs. [56,88], where different contours are discussed to resolve this problem. Ref. [89] proposes to deal with equilibrium situations by shifting the backward path from t to $t - i\hbar\beta$. It requires further studies to find out whether such a contour really resolves the discrepancies between the CTPF and the ITF.

9 Summary and Outlook

Finally, we would like to summarize our main results and point out the open questions that we are still left with. The goal has been the derivation of a real-time Ginzburg-Landau theory of order fields to describe the MI-SF quantum phase transition undergone by a bosonic system in an optical lattice. The basic models, which have guided us, have been presented in Chapter 2.

To construct a Ginzburg-Landau functional, we have chosen a Green's function formalism presented in Chapter 3. Since it is difficult to extract real-time information from the thermal Green's functions [55,56], the technique of contour-ordered Green's functions defined in Section 3.4 has been applied. However, 2^n n-point functions exist in this formalism, thus the Keldysh rotation [66] introduced in Section 3.5 is a useful simplification, since in this basis always one n-point function becomes zero. The general proof of this can be found in Section 6.1. Furthermore, the Keldysh rotation introduces, amongst others, the retarded/advanced Green's functions, which are more physical than the contour-ordered Green's functions. This can be seen in Sections 5.4 and 6.2, where the dynamic equations of the system are exclusively given by the retarded/advanced functions [75].

In Chapter 4 we have expanded a free-energy-like functional of symmetry-breaking sources simultaneously in the currents and in the hopping parameter. Since the currents have been defined as conjugate variables of the order fields, expanding in them prepares the Ginzburg-Landau functional where, in view of a proper description of the phase transition, the dependence on the fields can be truncated in fourth order [14]. The hopping expansion is physically justified for large dimensions due to the scaling behavior of the problem [68].

In Sections 4.3 – 4.5 we have shown that, due to the linked-cluster theorem [71,72], this expansion can be directly written down diagrammatically. The building blocks of the expansion are the cumulants of the system *without hopping*, which can straightforwardly be calculated. Up to second order in the currents and first order in the hopping, this expansion is performed in Section 4.6. There we have used the "old" basis of contour-ordered functions and performed the Keldysh rotation afterwards. This careful procedure has shown that in the Keldysh basis, the Pauli matrix σ^1 must be put in between two Green's function matrices in order to correctly describe a hopping process [59].

In Chapter 5 we have Legendre transformed the functional from Section 4.6. This transformation yields the effective action, which serves as a Ginzburg-Landau functional, since the artificial currents are replaced by physical order fields Ψ and Ψ^* which can be identified with the expectation values of the annihilation/creation operators [69,70]. Furthermore, it resums the Green's function as is shown in detail in Section 5.3. The resummation allows for good results even for a larger hopping parameter. In second order in the currents, however, the approach is restricted to the MI phase, thus we had to repeat the procedure from Sections 4.6 and 5.1 in order to get the higher-order terms. This is done in Section 6.1, where we work in the Keldysh basis and in frequency space from the beginning. The final functional $\Gamma[\Psi, \Psi^*]$ is given in Eq. (6.18). From this functional, we get the equations of motions

(6.21) and (6.22), which yield the equilibrium order field in Eq. (6.40). To solve the equations of motion in the dynamic case, we have linearized them around the equilibrium result in Section 6.2.3. In this linear approximation, we have also been able to derive a SF retarded Green's function from the effective action, which is given by Eq. (6.59).

With this theoretical groundwork we are well equipped to tackle the actual goal of our thesis, namely to find concrete results about the dynamic behavior of the system. This work is done in Chapter 7, where we have found the phase boundary as well as the respective excitation spectra in both the Mott-insulator and the superfluid phase. For simplicity, we have restricted ourselves to $T = 0$. The result for the phase boundary shown in Fig. 7.1 is identical with the mean-field result [31], but we could go beyond it by including higher-order hopping terms [69]. This is one big advantage of our systematic perturbation expansion. In the MI phase, we have been able to find analytic expressions for the spectra and their weights given by Eqs. (7.35) and (7.36). These are the usual particle/hole excitations predicted by mean-field theory [73].

In Section 7.2 we have first solved numerically the equations of motion in the SF phase. This yielded two excitation branches, where one has the linear shape expected from Bogoliubov theory [28], while the other one is gapped and quadratic. We have analyzed the gap, the mass, and the sound velocity of these spectra and found that they perfectly map onto the MI spectra. All this information is contained in Fig. 7.5. We have shown that this mapping is a natural consequence of our Ginzburg-Landau ansatz. Then an analytic result for the sound velocity has been obtained in Eq. (7.67) by a Taylor expansion of the equations of motion for small ω. In the limit $U \to 0$, the gapless spectrum gets identical to the Bogoliubov spectrum, whereas the gapped mode disappears. Unlike the Bogoliubov approximation, our approach is also able to describe the behavior in the vicinity of the phase boundary. Therefore we have analyzed the critical exponents in Section 7.3 and reproduced the mean-field results from Ref. [31].

As already mentioned, the results from Chapter 7 could still be improved by including higher-order hopping terms. But even in the first order, which we have examined here, the SF equations of motion are so complicated that not all the information, which is contained, could be extracted. This concerns especially the spectral weights, which could give some hints for the heavily discussed SF gapped mode [78–80]. For the interpretation of this mode, which has few experimental evidence [81], it would also be helpful to get more information about the character of this excitation.

The sound mode, however, has been recently measured via Bragg spectroscopy [25], thus we must try to compare our result with the experimental data. To this end we must check the influence of the additional harmonic trap in the experimental setup. The theoretical problem with such a trap is, that spatial homogeneity has been crucial in our derivation of the equations of motion. It could be considered, for instance, within a Thomas-Fermi approximation [42].

Instead of comparing our results with experiments, we have pointed out the relation of our approach to other theories on the problem. In Section 8.1 we have shown that for $U \to 0$ our equations of motion become identical to the Gross-Pitaevskii equation. Thus, although we have started the perturbation expansion from the strong-coupling limit, we are able to extract the right weak-coupling limit. This has not been achieved before, as the following citation from the recently published book "Ultracold Quantum Fields" by H. Stoof *et al.* [90] may demonstrate: "*Although these* [the weak- and the strong

coupling limit] *should be smoothly connected to each other, at present it is not known how to formulate a mean-field theory that interpolates between these two extremes.*"

In Section 8.2, our results have been compared with an effective action theory in imaginary time from Ref. [70]. They perfectly agree for $T = 0$. For finite temperature, however, a disagreement in the 4-point function has been found.

Certainly the main force in future works must be put into the failure of our theory in thermoequilibrium, which arose very unexpectedly. We therefore have to check, whether a different contour is able to circumvent this problem. We suspect that an integration contour like in Fig. 3.1b), which contains an imaginary part from t to $t - i\hbar\beta$, is able to describe the equilibrium situation properly [60,88]. Unfortunately, many feasible properties of the Keldysh contour, which have been used in this thesis, do not hold for such a contour, so this theory would have to start from the very beginning.

Although we believe that out of equilibrium the Keldysh contour is appropriate to describe the system, we first have to check, how to handle the equilibrium situation, before we can go on and apply the theory to non-equilibrium situations as for example in collapse and revival experiments [41]. The situation found there could then be described by a Bose-Hubbard Hamiltonian where the parameters depend on time. Certainly, the CTPF would come out on top in such a problem, since the ITF would no longer be applicable. In such a time-dependent system, however, neither frequency is conserved at the vertices nor a linearization of the equation of motions around equilibrium is possible. Thus we would end up with multiple integral equations and would rely on new methods of solving them.

A CTPF 4-Point Function

Here we show how to calculate the retarded 4-point function as defined in Eqs. (6.33) and (6.34) and its Fourier transform. We suppose that $t_3 > t_4$, which reduces the number of time-orders that have to be considered to only three. To compensate this restriction, we will have to symmetrize the expression in these variables at the end of the calculation.

Writing out the triple commutator in Eq. (6.33) yields eight operator products for each time-order. The expectation values of these products can directly be read from the definition of the creation and annihilation operators:

$$\hat{\mathrm{a}}|n\rangle = \sqrt{n}|n-1\rangle, \quad \hat{\mathrm{a}}^\dagger|n\rangle = \sqrt{n+1}|n+1\rangle. \tag{A.1}$$

We have

$$\begin{aligned} C^{\mathrm{R}}(t_1,t_2;t_3,t_4) = -i\sum_n^\infty \frac{\mathrm{e}^{-\beta E_n}}{\mathcal{Z}^{(0)}}\Big\{&\theta(t_1-t_2)\theta(t_2-t_3)\theta(t_3-t_4)\ A_n + \\ &\theta(t_1-t_3)\theta(t_3-t_4)\theta(t_4-t_2)\ B_n + \theta(t_1-t_3)\theta(t_3-t_2)\theta(t_2-t_4)\ C_n\Big\}_{t_3\leftrightarrow t_4}, \end{aligned} \tag{A.2}$$

where the respective coefficients are given by

$$\begin{aligned} A_n \equiv\ & (n+1)(n+2)\exp\left[\frac{i}{\hbar}\Big(t_4(E_{n+1}-E_n)+t_3(E_{n+2}-E_{n+1})+t_2(E_{n+1}-E_{n+2})+t_1(E_n-E_{n+1})\Big)\right] \\ & -(n+1)(n+2)\exp\left[\frac{i}{\hbar}\Big(t_4(E_{n+1}-E_n)+t_3(E_{n+2}-E_{n+1})+t_1(E_{n+1}-E_{n+2})+t_2(E_n-E_{n+1})\Big)\right] \\ & +n(n-1)\exp\left[\frac{i}{\hbar}\Big(t_4(E_n-E_{n-1})+t_3(E_{n-1}-E_{n-2})+t_2(E_{n-1}-E_n)+t_1(E_{n-2}-E_{n-1})\Big)\right] \\ & -n(n-1)\exp\left[\frac{i}{\hbar}\Big(t_1(E_{n-1}-E_n)+t_2(E_{n-2}-E_{n-1})+t_3(E_{n-1}-E_{n-2})+t_4(E_n-E_{n-1})\Big)\right] \\ & +n(n+1)\exp\left[\frac{i}{\hbar}\Big(t_4(E_{n+1}-E_n)+t_1(E_n-E_{n+1})+t_2(E_{n-1}-E_n)+t_3(E_n-E_{n-1})\Big)\right] \\ & -n(n+1)\exp\left[\frac{i}{\hbar}\Big(t_4(E_{n+1}-E_n)+t_2(E_n-E_{n+1})+t_1(E_{n-1}-E_n)+t_3(E_n-E_{n-1})\Big)\right] \\ & +n(n+1)\exp\left[\frac{i}{\hbar}\Big(t_3(E_{n+1}-E_n)+t_1(E_n-E_{n+1})+t_2(E_{n-1}-E_n)+t_4(E_n-E_{n-1})\Big)\right] \\ & -n(n+1)\exp\left[\frac{i}{\hbar}\Big(t_3(E_{n+1}-E_n)+t_2(E_n-E_{n+1})+t_1(E_{n-1}-E_n)+t_4(E_n-E_{n-1})\Big)\right], \end{aligned} \tag{A.3}$$

$$
\begin{aligned}
B_n \equiv\ & n(n+1)\exp\left[\frac{i}{\hbar}\Big(t_2(E_{n-1}-E_n)+t_4(E_n-E_{n-1})+t_3(E_{n+1}-E_n)+t_1(E_n-E_{n+1})\Big)\right] \\
& - n(n+1)\exp\left[\frac{i}{\hbar}\Big(t_1(E_{n-1}-E_n)+t_3(E_n-E_{n-1})+t_4(E_{n+1}-E_n)+t_2(E_n-E_{n+1})\Big)\right] \\
& + n(n-1)\exp\left[\frac{i}{\hbar}\Big(t_2(E_{n-1}-E_n)+t_1(E_{n-2}-E_{n-1})+t_3(E_{n-1}-E_{n-2})+t_4(E_n-E_{n-1})\Big)\right] \\
& - (n+2)(n+1)\exp\left[\frac{i}{\hbar}\Big(t_4(E_{n+1}-E_n)+t_3(E_{n+2}-E_{n+1})+t_1(E_{n+1}-E_{n+2})+t_2(E_n-E_{n+1})\Big)\right] \\
& + 2(n+1)^2\exp\left[\frac{i}{\hbar}\Big(t_4(E_{n+1}-E_n)+t_1(E_n-E_{n+1})+t_3(E_{n+1}-E_n)+t_2(E_n-E_{n+1})\Big)\right] \\
& - 2n^2\exp\left[\frac{i}{\hbar}\Big(t_2(E_{n-1}-E_n)+t_3(E_n-E_{n-1})+t_1(E_{n-1}-E_n)+t_4(E_n-E_{n-1})\Big)\right], \qquad \text{(A.4)}
\end{aligned}
$$

$$
\begin{aligned}
C_n \equiv\ & n(n-1)\exp\left[\frac{i}{\hbar}\Big(t_2(E_{n-1}-E_n)+t_1(E_{n-2}-E_{n-1})+t_3(E_{n-1}-E_{n-2})+t_4(E_n-E_{n-1})\Big)\right] \\
& + n(n+1)\exp\left[\frac{i}{\hbar}\Big(t_3(E_{n+1}-E_n)+t_1(E_n-E_{n+1})+t_2(E_{n-1}-E_n)+t_4(E_n-E_{n-1})\Big)\right] \\
& - (n+2)(n+1)\exp\left[\frac{i}{\hbar}\Big(t_4(E_{n+1}-E_n)+t_3(E_{n+2}-E_{n+1})+t_1(E_{n+1}-E_{n+2})+t_4(E_n-E_{n+1})\Big)\right] \\
& - n(n+1)\exp\left[\frac{i}{\hbar}\Big(t_4(E_{n+1}-E_n)+t_2(E_n-E_{n+1})+t_1(E_{n-1}-E_n)+t_3(E_n-E_{n-1})\Big)\right] \\
& + 2(n+1)^2\exp\left[\frac{i}{\hbar}\Big(t_4(E_{n+1}-E_n)+t_2(E_n-E_{n+1})+t_3(E_{n+1}-E_n)+t_1(E_n-E_{n+1})\Big)\right] \\
& - 2n^2\exp\left[\frac{i}{\hbar}\Big(t_1(E_{n-1}-E_n)+t_3(E_n-E_{n-1})+t_2(E_{n-1}-E_n)+t_4(E_n-E_{n-1})\Big)\right]. \qquad \text{(A.5)}
\end{aligned}
$$

The substitution $\tilde{t}_i = t_i - t_4$ cancels one time argument in the expressions. Now we perform the Fourier transformation. It can be done in exactly the same way as in Section 5.2, where we transformed the 2-point function. For each step function we insert its Fourier representation from Eq. (5.17), yielding δ-functions that can easily be integrated out. Since the variable t_4 could be canceled, the Fourier transformation in this variable simply gives $2\pi\delta(\omega_1+\omega_2-\omega_3-\omega_4)$ guaranteeing frequency conservation. We therefore introduce the notation

$$
\theta(t_1-t_2)\theta(t_2-t_3)\theta(t_3-t_4)A_n \to -i2\pi\delta(\omega_1+\omega_2-\omega_3-\omega_4)\ a_n, \qquad \text{(A.6)}
$$

and similarly for B_n and C_n. The coefficients a_n, b_n, and c_n are given by

$$\begin{aligned}
a_n \equiv & \frac{(n+2)(n+1)}{(E_n - E_{n+1} + \omega_1 + i\epsilon_1)(E_n - E_{n+2} + \omega_1 + \omega_2 + i\epsilon_2)(E_n - E_{n+1} + \omega_1 + \omega_2 - \omega_3 + i\epsilon_3)} \\
& - \frac{(n+2)(n+1)}{(E_{n+1} - E_{n+2} + \omega_1 + i\epsilon_1)(E_n - E_{n+2} + \omega_1 + \omega_2 + i\epsilon_2)(E_n - E_{n+1} + \omega_1 + \omega_2 - \omega_3 + i\epsilon_3)} \\
& + \frac{n(n-1)}{(E_{n-2} - E_{n-1} + \omega_1 + i\epsilon_1)(E_{n-2} - E_n + \omega_1 + \omega_2 + i\epsilon_2)(E_{n-1} - E_n + \omega_1 + \omega_2 - \omega_3 + i\epsilon_3)} \\
& - \frac{n(n-1)}{(E_{n-1} - E_n + \omega_1 + i\epsilon_1)(E_{n-2} - E_n + \omega_1 + \omega_2 + i\epsilon_2)(E_{n-1} - E_n + \omega_1 + \omega_2 - \omega_3 + i\epsilon_3)} \\
& + \frac{n(n+1)}{(E_n - E_{n+1} + \omega_1 + i\epsilon_1)(E_{n-1} - E_{n+1} + \omega_1 + \omega_2 + i\epsilon_2)(E_n - E_{n+1} + \omega_1 + \omega_2 - \omega_3 + i\epsilon_3)} \\
& - \frac{n(n+1)}{(E_{n-1} - E_n + \omega_1 + i\epsilon_1)(E_{n-1} - E_{n+1} + \omega_1 + \omega_2 + i\epsilon_2)(E_n - E_{n+1} + \omega_1 + \omega_2 - \omega_3 + i\epsilon_3)} \\
& + \frac{n(n+1)}{(E_n - E_{n+1} + \omega_1 + i\epsilon_1)(E_{n-1} - E_{n+1} + \omega_1 + \omega_2 + i\epsilon_2)(E_{n-1} - E_n + \omega_1 + \omega_2 - \omega_3 + i\epsilon_3)} \\
& - \frac{n(n+1)}{(E_{n-1} - E_n + \omega_1 + i\epsilon_1)(E_{n-1} - E_{n+1} + \omega_1 + \omega_2 + i\epsilon_2)(E_{n-1} - E_n + \omega_1 + \omega_2 - \omega_3 + i\epsilon_3)},
\end{aligned} \tag{A.7}$$

$$\begin{aligned}
b_n \equiv & \frac{-n(n+1)}{(E_n - E_{n+1} + \omega_1 + i\epsilon_1)(\omega_1 - \omega_3 + i\epsilon_2)(E_{n-1} - E_n + \omega_2 + i\epsilon_3)} \\
& - \frac{-n(n+1)}{(E_{n-1} - E_n + \omega_1 + i\epsilon_1)(\omega_1 - \omega_3 + i\epsilon_2)(E_n - E_{n+1} + \omega_2 + i\epsilon_3)} \\
& + \frac{-n(n-1)}{(E_{n-2} - E_{n-1} + \omega_1 + i\epsilon_1)(\omega_1 - \omega_3 + i\epsilon_2)(E_{n-1} - E_n + \omega_2 + i\epsilon_3)} \\
& - \frac{-(n+2)(n+1)}{(E_{n+1} - E_{n+2} + \omega_1 + i\epsilon_1)(\omega_1 - \omega_3 + i\epsilon_2)(E_n - E_{n+1} + \omega_2 + i\epsilon_3)} \\
& + \frac{-2(n+1)^2}{(E_n - E_{n+1} + \omega_1 + i\epsilon_1)(\omega_1 - \omega_3 + i\epsilon_2)(E_n - E_{n+1} + \omega_2 + i\epsilon_3)} \\
& - \frac{2n^2}{(E_{n-1} - E_n + \omega_1 + i\epsilon_1)(\omega_1 - \omega_3 + i\epsilon_2)(E_{n-1} - E_n + \omega_2 + i\epsilon_3)},
\end{aligned} \tag{A.8}$$

$$
\begin{aligned}
c_n \equiv & \frac{n(n+1)}{(E_n - E_{n+1} + \omega_1 + i\epsilon_1)(\omega_1 - \omega_3 + i\epsilon_2)(E_{n-1} - E_n + \omega_1 + \omega_2 - \omega_3 + i\epsilon_3)} \\
& - \frac{n(n+1)}{(E_{n-1} - E_n + \omega_1 + i\epsilon_1)(\omega_1 - \omega_3 + i\epsilon_2)(E_n - E_{n+1} + \omega_1 + \omega_2 - \omega_3 + i\epsilon_3)} \\
& + \frac{n(n-1)}{(E_{n-2} - E_{n-1} + \omega_1 + i\epsilon_1)(\omega_1 - \omega_3 + i\epsilon_2)(E_{n-1} - E_n + \omega_1 + \omega_2 - \omega_3 + i\epsilon_3)} \\
& - \frac{(n+2)(n+1)}{(E_{n+1} - E_{n+2} + \omega_1 + i\epsilon_1)(\omega_1 - \omega_3 + i\epsilon_2)(E_n - E_{n+1} + \omega_1 + \omega_2 - \omega_3 + i\epsilon_3)} \\
& + \frac{2(n+1)^2}{(E_n - E_{n+1} + \omega_1 + i\epsilon_1)(\omega_1 - \omega_3 + i\epsilon_2)(E_n - E_{n+1} + \omega_1 + \omega_2 - \omega_3 + i\epsilon_3)} \\
& - \frac{-2n^2}{(E_{n-1} - E_n + \omega_1 + i\epsilon_1)(\omega_1 - \omega_3 + i\epsilon_2)(E_{n-1} - E_n + \omega_1 + \omega_2 - \omega_3 + i\epsilon_3)}.
\end{aligned} \tag{A.9}
$$

To take the limit $i\epsilon \to 0$, we note that all terms look like

$$
\frac{1}{(x + i\epsilon_1)(y + i\epsilon_2)(z + i\epsilon_3)}. \tag{A.10}
$$

Applying Eq. (7.4) subsequently for each ϵ_i leaves us with

$$
\left[\frac{1}{x} - i\pi\delta(x)\right]\left[\frac{1}{y} - i\pi\delta(y)\right]\left[\frac{1}{z} - i\pi\delta(z)\right]. \tag{A.11}
$$

Thus, divergences of the real part occur, when $xyz = 0$. In this case, the diverging term $\frac{1}{xyz}$ interferes with δ-functions, but they do not affect the asymptotic behavior of the real part close to these divergences. In the imaginary part, however, the δ-functions play the crucial role, since it is only non-zero as long as $xyz \neq 0$.

But in Section 7.2 we have argued that the dynamic behavior can be extracted from the real part alone, and thus we can neglect the δ-functions in the following. The only thing that remains to be done now, is to join all terms from a_n, b_n and c_n, in order to get a compact expression.

First we note that each term in b_n has a "partner" in c_n. Then we take a look at the terms in a_n, which are proportional to $n(n+1)$. Two of the four terms read

$$
\begin{aligned}
& \frac{+1}{(E_n - E_{n+1} + \omega_1)(E_n - E_{n+1} + \omega_1 + \omega_2 - \omega_3)(E_{n-1} - E_{n+1} + \omega_1 + \omega_2)} + \\
& \frac{+1}{(E_n - E_{n+1} + \omega_1)(E_{n-1} - E_n + \omega_1 + \omega_2 - \omega_3)(E_{n-1} - E_{n+1} + \omega_1 + \omega_2)}.
\end{aligned} \tag{A.12}
$$

Now we mustn't forget the symmetrization that has to be performed in $\omega_3 \leftrightarrow \omega_4$. Then the first term in (A.12) plus the symmetrization of the second term can be combined to

$$
\frac{(E_{n-1} - E_{n+1} + 2\omega_1 + 2\omega_2 - \omega_3 - \omega_4)}{(E_n - E_{n+1} + \omega_1)(E_n - E_{n+1} + \omega_1 + \omega_2 - \omega_3)(E_{n-1} - E_n + \omega_1 + \omega_2 - \omega_4)(E_{n-1} - E_{n+1} + \omega_1 + \omega_2)}. \tag{A.13}
$$

Still noting the frequency conservation, $\omega_1 + \omega_2 - \omega_3 - \omega_4 = 0$, we get

$$\frac{1}{(E_n - E_{n+1} + \omega_1)(E_n - E_{n+1} + \omega_3)(E_{n-1} - E_n + \omega_4)}. \tag{A.14}$$

Finally we combine everything and write:

$$\begin{aligned}
&\text{Re } C^{\text{R}}(\omega_1, \omega_2; \omega_3, \omega_4) = -2\pi\delta(\omega_1 + \omega_2 - \omega_3 - \omega_4) \sum_{n=0}^{\infty} \frac{\mathrm{e}^{-\beta E_n}}{\mathcal{Z}^{(0)}} \\
&\times \left\{ \frac{n(n+1)}{(E_n - E_{n-1} - \omega_1)(E_{n+1} - E_n - \omega_4)} \left(\frac{1}{E_n - E_{n-1} - \omega_3} - \frac{1}{E_{n+1} - E_n - \omega_2} \right) \right. \\
&+ \frac{n(n+1)}{(E_n - E_{n-1} - \omega_3)(E_{n+1} - E_n - \omega_1)} \left(\frac{1}{E_n - E_{n-1} - \omega_2} - \frac{1}{E_{n+1} - E_n - \omega_4} \right) \\
&+ \frac{-(n+2)(n+1)}{(E_{n+1} - E_n - \omega_4)(E_{n+2} - E_n - \omega_1 - \omega_2)} \left(\frac{1}{E_{n+1} - E_n - \omega_1} + \frac{1}{E_{n+1} - E_n - \omega_2} \right) \\
&+ \frac{n(n-1)}{(E_n - E_{n-1} - \omega_4)(E_n - E_{n-2} - \omega_1 - \omega_2)} \left(\frac{1}{E_n - E_{n-1} - \omega_1} + \frac{1}{E_n - E_{n-1} - \omega_2} \right) \\
&+ \frac{2(n+1)^2}{(E_{n+1} - E_n - \omega_1)(E_{n+1} - E_n - \omega_2)(E_{n+1} - E_n - \omega_4)} \\
&\left. + \frac{-2n^2}{(E_n - E_{n-1} - \omega_1)(E_n - E_{n-1} - \omega_2)(E_n - E_{n-1} - \omega_4)} \right\}_{\omega_3 \leftrightarrow \omega_4,\ \omega_2 \leftrightarrow \omega_1}.
\end{aligned} \tag{A.15}$$

We checked this result by comparing it with the ITF Green's function in Section 8.2. Agreement is found for $T = 0$.

Bibliography

[1] Greiner, M., Mandel, O., Esslinger, T., Hänsch, T. W., and Bloch, I. Quantum Phase Transition From a Superfluid to a Mott Insulator in a Gas of Ultracold Atoms. *Nature* **415**, 39 (2002).

[2] Kapitza, P. Viscosity of Liquid Helium below the λ-Point. *Nature* **141**, 74 (1938).

[3] Allen, J. and Misener, A. Flow of Liquid Helium II. *Nature* **141**, 75 (1938).

[4] Kleinert, H. *Gauge Fields in Condensed Matter Vol. I.* World Scientific (1989).

[5] Wilks, J. *The Properties of Liquid and Solid Helium.* Clarendon Press (1967).

[6] London, F. The λ-Phenomenon of Liquid Helium and the Bose-Einstein Degeneracy. *Nature* **141**, 643 (1938).

[7] Bose, S. N. Plancks Gesetz und Lichtquantenhypothese. *Z. Phys.* **26**, 178 (1924).

[8] Einstein, A. Quantentheorie des Einatomigen Idealen Gases. *Sitzungsberichte der Preußischen Akademie der Wissenschaften* **1**, 3 (1925).

[9] Tisza, L. Transport Phenomena in Helium II. *Nature* **141**, 913 (1938).

[10] Andronikashvili, E. L. Direct Observation of Two Kinds of Motion in Helium II. *J. Phys. (Moscow)* **10**, 201 (1946).

[11] Penrose, O. and Onsager, L. Bose-Einstein Condensation and Liquid Helium. *Phys. Rev.* **104**, 576 (1956).

[12] Lipa, J. A., Nissen, J. A., Stricker, D. A., Swanson, D. R., and Chui, T. C. P. Specific Heat of Liquid Helium in Zero Gravity very near the λ-Point. *Phys. Rev. B* **68**, 174518 (2003).

[13] Kleinert, H. Critical Exponents from Seven-Loop Strong-Coupling ϕ^4 Theory in Three Dimensions. *Phys. Rev. D* **60**, 085001 (1999).

[14] Kleinert, H. and Schulte-Frohlinde, V. *Critical Properties of* Φ^4*-Theories.* World Scientific (2001).

[15] Landau, L. The Theory of Superfluidity of Helium II. *J. Phys. (Moscow)* **5**, 71 (1941).

[16] Landau, L. On the Theory of Superfluidity of Helium II. *J. Phys. (Moscow)* **11**, 91 (1947).

[17] Schwabl, F. *Statistische Mechanik.* Springer (2006).

[18] Ellis, T., Jewell, C. I., and McClintock, P. V. E. Measurement of the Landau Velocity in He II. *Phys. Lett. A* **78**, 358 (1980).

[19] Bogoliubov, N. N. On the Theory of Superfluidity. *J. Phys. (Moscow)* **11**, 23 (1947).

[20] Anderson, M. H., Ensher, J. R., Matthews, M. R., Weiman, C. E., and Cornell, E. A. Observation of Bose-Einstein Condensation in a Dilute Atomic Vapor. *Science* **269**, 198 (1995).

[21] Davis, K. B., Mewes, M.-O., Andrews, M. R., van Druten, N. J., Durfee, D. S., Krun, D. M., and Ketterle, W. Bose-Einstein Condensation in a Gas of Sodium Atoms. *Phys. Rev. Lett.* **75**, 3969 (1995).

[22] Henshaw, D. G. and Woods, A. D. Modes of Atomic Motions in Liquid Helium by Inelastic Scattering of Neutrons. *Phys. Rev.* **121**, 1266 (1961).

[23] Stenger, J., Inouye, S., Chikkatur, A. P., Stamper-Kurn, D. M., Pritchard, D. E., and Ketterle, W. Bragg Spectroscopy of a Bose-Einstein Condensate. *Phys. Rev. Lett.* **82**, 4569 (1999).

[24] Kozuma, M., Deng, L., Hagley, E. W., Wen, J., Lutwak, R., Helmerson, K., Rolston, S. L., and Phillips, W. D. Coherent Splitting of Bose-Einstein Condensed Atoms with Optically Induced Bragg Diffraction. *Phys. Rev. Lett.* **82**, 871 (1999).

[25] Ernst, P. T., Götze, S., Krauser, J. S., Pyka, K., Lühmann, D.-S., Pfannkuche, D., and Sengstock, K. Momentum-Resolved Bragg Spectroscopy in Optical Lattices. `arXiv:0908.4242v1` .

[26] Clement, D., Fabbri, N., Fallani, L., Fort, C., and Inguscio, M. Exploring Correlated 1D Bose Gases from the Superfluid to the Mott-Insulator State by Inelastic Light Scattering. *Phys. Rev. Lett.* **102**, 155301 (2009).

[27] Ozeri, R., Katz, N., Steinhauer, J., and Davidson, N. Colloquium: Bulk Bogoliubov excitations in a Bose-Einstein condensate. *Rev. Mod. Phys.* **77**, 187 (2005).

[28] van Oosten, D., van der Straten, P., and Stoof, H. T. C. Quantum Phases in an Optical Lattice. *Phys. Rev. A* **63**, 053601 (2001).

[29] Freericks, J. K. and Monien, H. Strong-coupling Expansions for the Pure and Disordered Bose-Hubbard Model. *Phys. Rev. B* **53**, 2691 (1996).

[30] Capogrosso-Sansone, B., Prokof'ev, N. V., and Svistunov, B. V. Phase Diagram and Thermodynamics of the Three-Dimensional Bose-Hubbard Model. *Phys. Rev. B* **75**, 134302 (2007).

[31] Fisher, M. P. A., Weichman, P. B., Grinstein, G., and Fisher, D. S. Boson Localization and the Superfluid-Insulator Transition. *Phys. Rev. B* **40**, 546 (1989).

[32] Jaksch, D., Bruder, C., Cirac, J. I., Gardiner, C. W., and Zoller, P. Cold Bosonic Atoms in Optical Lattices. *Phys. Rev. Lett.* **81**, 3108 (1998).

[33] Binney, J., Dowrick, N., Fisher, A., and Newman, M. *The Theory of Critical Phenomena.* Oxford University Press (1993).

[34] Sachdev, S. *Quantum Phase Transitions.* Cambridge University Press (1999).

[35] Tiesinga, E., Verhaar, B. J., and Stoof, H. T. C. Threshold and Resonance Phenomena in Ultracold Ground-State Collisions. *Phys. Rev. A* **47**, 4114 (1993).

[36] Hoffmann, A. Bosonen im optischen Gitter. Master's thesis, FU Berlin, `http://www.physik.fu-berlin.de/~pelster/Theses/hoffmann.pdf` (2007).

[37] Ashcroft, N. W. and Mermin, N. D. *Solid State Physics.* Saunders College Publishing (1976).

[38] Hoffmann, A. and Pelster, A. Visibility of Cold Atomic Gases in Optical Lattices for Finite Temperatures. *Phys. Rev. A* **79**, 053623 (2009).

[39] Czycholl, G. *Theoretische Festkörperphysik.* Springer (2008).

[40] Meixner, J. *Mathieusche Funktionen und Sphäroidfunktionen.* Springer (1954).

[41] Greiner, M., Mandel, O., Hänsch, T., and Bloch, I. Collapse and Revival of the Matter Wave Field of a Bose-Einstein Condensate. *Nature* **419**, 51 (2002).

[42] dos Santos, F. E. A. Collapse and Revival in Bosonic Optical Lattices. In preparation.

[43] Diener, R. B., Zhou, Q., Zhai, H., and Ho, T. L. Criterion for Bosonic Superfluidity in an Optical Lattice. *Phys. Rev. Lett.* **98** (2007).

[44] Scarola, V. W. and Das Sarma, S. Quantum Phases of the Extended Bose-Hubbard Hamiltonian: Possibility of a Supersolid State of Cold Atoms in Optical Lattices. *Phys. Rev. Lett.* **95**, 033003 (2005).

[45] Lühmann, D.-S., Bongs, K., Sengstock, K., and Pfannkuche, D. Self-Trapping of Bosons and Fermions in Optical Lattices. *Phys. Rev. Lett.* **101**, 050402 (2008).

[46] Best, T., Will, S., Schneider, U., Hackermüller, L., van Oosten, D., Bloch, I., and Lühmann, D.-S. Role of Interactions in ^{87}Rb-^{40}K Bose-Fermi Mixtures in a 3D Optical Lattice. *Phys. Rev. Lett.* **102**, 030408 (2009).

[47] Gerbier, F., Widera, A., Fölling, S., Mandel, O., Gericke, T., and Bloch, I. Phase Coherence of an Atomic Mott Insulator. *Phys. Rev. Lett.* **95**, 050404 (2005).

[48] Sakurai, J. J. *Modern Quantum Mechanics.* San Fu Tuan (1993).

[49] Huang, K. *Quantum Field Theory.* (1998).

[50] Goldstone, J. and Salam, A. and Weinberg, S. Broken symmetries. *Phys. Rev.* **127**, 965 (1962).

[51] Nambu, Y. Quasi-Particles and Gauge Invariance in the Theory of Superconductivity. *Phys. Rev.* **117**, 648 (1960).

[52] Gell-Mann, M. and Low, F. Bound States in Quantum Field Theory. *Phys. Rev.* **84**, 350 (1951).

[53] Kadanoff, L. P. and Baym, G. *Quantum Statistical Mechanics: Green's Function Methods in Equilibrium and Non-Equilibrium Problems.* W.A. Benjamin (1962).

[54] Abrikosov, A. A., Gorkov, L. P., and Dzyaloshinksi, I. E. *Methods of Quantum Field Theory in Statistical Physics.* Dover Publications (1976).

[55] Kobes, R. Correspondence between Imaginary-Time and Real-Time Finite-Temperature Field Theory. *Phys. Rev. D* **42**, 562 (1990).

[56] Evans, T. S. N-point Finite Temperature Expectation Values at Real Times. *Nucl. Phys. B* **374**, 340 (1992).

[57] Guerin, F. Retarded-advanced N-point Green Functions in Thermal Field Theories. *Nucl. Phys. B* **432**, 281 (1994).

[58] Schwinger, J. Brownian Motion of a Quantum Oscillator. *J. Math. Phys.* **2**, 407 (1961).

[59] Rammer, J. and Smith, H. Quantum Field-Theoretical Methods in Transport Theory of Metals. *Rev. Mod. Phys.* **58**, 323 (1986).

[60] Mills, R. *Propagators for Many-Particle Systems.* Gordon and Breach (1969).

[61] Brouwer, P. Theory of Many-Particle Systems. Lecture notes for P654, Cornell University, (2005).

[62] Keldysh, L. V. Diagram Technique for Nonequilibriun Processes. *Sov. Phys. JETP* **20**, 1018 (1965).

[63] Kamenev, A. Many-body Theory of Non-equilibrium Systems. `arXiv:cond-mat/0412296v2` (2005).

[64] van Eijck, M. A., Kobes, R., and van Weert, C. G. Transformations of Real-Time Finite-Temperature Feynman Rules. *Phys. Rev. D* **50**, 4097 (1994).

[65] Kadanoff, L. P. and Baym, G. *Quantum Statistical Mechanics.* Benjamin (1962).

[66] Kleinert, H. *Path Integrals in Quantum Mechanics, Statistics and Polymer Physics.* World Scientific (2009).

[67] Negele, J. W. and Orland, H. *Quantum Many-Particle Systems.* Addison-Wesley Publishing Company (1988).

[68] Byczuk, K. and Vollhardt, D. Correlated Bosons on a Lattice: Dynamical Mean-Field Theory for Bose-Einstein Condensed and Normal Phases. *Phys. Rev. B* **77**, 235106 (2008).

[69] dos Santos, F. E. A. and Pelster, A. Quantum Phase Diagram of Bosons in Optical Lattices. *Phys. Rev. A* **79**, 013614 (2009).

[70] Bradlyn, B., dos Santos, F. E. A., and Pelster, A. Effective Action Approach for Quantum Phase Transitions in Bosonic Lattices. *Phys. Rev. A* **79**, 013615 (2009).

[71] Gelfand, M., Singh, R. R. P., and Huse, D. A. Perturbation Expansions for Quantum Many-Body Systems. *J. Stat. Phys.* **59**, 1093 (1990).

[72] Metzner, W. Linked-Cluster Expansion Around the Atomic Limit of the Hubbard Model. *Phys. Rev. B* **43**, 8549 (1991).

[73] Ohliger, M. Thermodynamic Properties of Spinor Bosons in Optical Lattices. Master's thesis, FU Berlin, `http://www.physik.fu-berlin.de/~pelster/Theses/ohliger.pdf` (2007).

[74] Goldstein, H. and Poole, C. P. *Classical Mechanics.* Addison Wesley (2001).

[75] Chou, K., Su, Z., Hao, B., and Yu, L. Equilibrium and Nonquilibrium Formalisms Made Unified. *Phys. Rep.* **118**, 1 (1985).

[76] Teichmann, N., Hinrichs, D., Holthaus, M., and Eckardt, A. Bose-Hubbard Phase Diagram with Arbitrary Integer Filling. *Phys. Rev. B* **79**, 100503 (2009).

[77] Teichmann, N., Hinrichs, D., Holthaus, M., and Eckardt, A. Process-Chain Approach to the Bose-Hubbard Model: Ground-State Properties and Phase Diagram. *Phys. Rev. B* **79**, 224515 (2009).

[78] Huber, S. D., Altman, E., Buchler, H. P., and Blatter, G. Dynamical Properties of Ultracold Bosons in an Optical Lattice. *Phys. Rev. B* **75**, 085106 (2007).

[79] Huber, S. D., Theiler, B., Altman, E., and Blatter, G. Amplitude Mode in the Quantum Phase Model. *Phys. Rev. Lett.* **100**, 050404 (2008).

[80] Menotti, C. and Trivedi, N. Spectral Weight Redistribution in Strongly Correlated Bosons in Optical Lattices. *Phys. Rev. B* **77**, 235120 (2008).

[81] Stöferle, T., Moritz, H., Schori, C., Köhl, M., and Esslinger, T. Transition from a Strongly Interacting 1D Superfluid to a Mott Insulator. *Phys. Rev. Lett.* **92**, 130403 (2004).

[82] Gross, E. P. Structure of a Quantized Vortex in Boson Systems. *Nuovo Cimento* **20**, 454 (1961).

[83] Pitaevskii, L. P. Vortex Lines in an Imperfect Bose Gas. *Sov. Phys. JETP* **13**, 451 (1961).

[84] Polkovnikov, A., Sachdev, S., and Girvin, S. M. Nonequilibrium Gross-Pitaevskii Dynamics of Boson Lattice Models. *Phys. Rev. A* **66**, 053607 (2002).

[85] Zinn-Justin, J. *Quantum Field Theory and Critical Phenomena.* Oxford University Press, (2002).

[86] Guerin, F. Four-Point Functions in Keldysh Basis. `arXiv:hep-ph//0105313v1` .

[87] Aurenche, P. and Becherrawy, T. A Comparison of the Real-Time and the Imaginary-Time Formalisms of Finite-Temperature Field Theory for 2,3, and 4-Point Green functions. *Nucl. Phys. B* **379**, 259 (1992).

[88] Evans, T. S. New Time Contour for Equilibrium Real-Time Thermal Field Theories. *Phys. Rev. D* **47**, R4196 (1993).

[89] Jakobs, S. G., Pletyukhov, M., and Schoeller, H. Properties of Multi-Particle Green and Vertex Functions within Keldysh Formalism, (2009).

[90] Stoof, H. T. C., Gubbels, K. B., and Dickerscheid, D. B. M. *Ultracold Quantum Fields*. Springer (2009).

Acknowledgements

Now that this thesis is finished, let me take a look back on the past year. It was a really nice time, so I am much obliged to the people in Professor Kleinert's group who guaranteed the friendly working atmosphere. What I have accomplished in the last 12 months is due to their intensive help.

Thus I express my gratitude to the head of the group, Prof. Dr. Dr. h.c. mult. Hagen Kleinert, for the affiliation. It has always been a great pleasure to be present at those lunches when he explained the universe on a piece of napkin. Unfortunately, these napkins did not substitute his books.

I am also very obliged to Priv.-Doz. Dr. Axel Pelster who supervised this thesis. He gave me the ideas to start my work; when I got stuck he was the doctor to be consulted; and unlike most doctors he took the time to find diseases, even when the patient felt alright. Thus what emerged, in many respects is due to him. Beyond that, Dr. Pelster made sure that I did not stay restricted on my particular subject by organizing various interesting events like the New Year's Meeting or the Summer School in Munich. I am really grateful for that.

Many thanks go to Ednilson Santos for inducting me into calculational methods, teaching me numerous tricks and patiently answering so many questions. The discussions with him have always been very instructive to me.

Not only due to direct neighborhood, but also because of their fantastic cooperativeness Aristeu Lima and Victor Bezerra have permanently been exposed to my questions. Their help saved me the time that I have lost chatting with them in the office. *Obrigado*!

Always open has been the door of Dr. Jürgen Dietel's and Dr. Flavio Nogueira's office. It is a good place both to celebrate breakthroughs and to complain their failure. And the physical problems I could discuss with them did not only concern my thesis, but also teeth, ears etc.

Balance has also been guaranteed by the other present and former students in the group, Markus Düttmann, Walja Korolevski, Oliver Gabel, Nathalie Pfitzinger and Jochen Brüggemann. For helpful critics and corrections I would like to thank my predecessor Matthias Ohliger.

Special thanks go to my parents for their diverse support on the long way and to Joseane giving me a good excuse for not being in Berlin.